Nuclear magnetic resonance spectroscopy of Vinylidenefluoride polymers.

Philip Wormald

NUCLEAR MAGNETIC RESONANCE SPECTROSCOPY OF VINYLIDENEFLUORIDE POLYMERS

By

Philip Wormald B.Sc.

A thesis submitted in partial fulfilment of the requirements for the degree of

Doctor of Philosophy

Department of Chemistry

University of Durham

2005

Memorandum

The research presented in this thesis has been carried out at the Department of Chemistry of the University of Durham and the University of Durham Industrial Research Laboratory between October 1999 and December 2004. It is the original work of the author unless stated otherwise. None of this work has been submitted for any other degree.

CHARACTERISATION OF POLYVINYLIDENEFLUORIDE AND A VINYLIDENEFLUORIDE TELOMER BY NUCLEAR MAGNETIC RESONANCE

Abstract

High-resolution solid- and solution state NMR techniques have been applied in the study of a Semi crystalline fluoropolymer Poly(vinylidienfluoride) (PVDF) and a vinylidienfluoride telomer. The application of standard solution-state experiments with high power decoupling and two-dimensional techniques has provided a greater understanding of the structure of these two fluoropolymers. Specifically, Cosy and Tocsy experiments gave information on signals normally related to end groups and to previously unidentified structures, which suggest the presence of at least a second major structure. ^{19}F solid-state Magic Angle Spinning Nuclear Magnetic Resonance (MAS-NMR) using relaxation filters in pulse sequences, has revealed fundamental differences relating to morphology and structure. The location of reverse units in the amorphous and crystalline domains is investigated by fluorine $T_{1\rho}$ filtered Radio Frequency Driven Recoupling (RFDR) and spin-diffusion experiments. These experiments proved that the reverse units are dominant in the amorphous phase, yet could have association with rigid species. Furthermore, signals generally associated with crystalline domains are not homogenic in character. The presence of a highly mobile species was detected and investigated using the delayed acquisition technique and T_2 measurements. This showed the possibility of end-group signal in the spectral region normally associated with reverse groups. Furthermore, proton $T_{1\rho}$ measurements of nascent and annealed PVDF, recorded at variable temperature are related to molecular motion and debated with respect to the effect of spin diffusion on populations. The relationship between thermal events and thermal history of PVDF and its effect on molecular motion is debated.

Acknowledgements

I would like to thank mainly two people whom, during this thesis have given me a great deal of help.

Doctor David Apperley at the EPSRC solid-state NMR service at the University of Durham whom I worked with for 4 years whose expert knowledge as a NMR spectroscopist and manager has given me a great deal of the knowledge I have today.

My supervisor Professor R.K Harris for his guidance and expertise throughout my time in Durham.

Furthermore I would like to thank Dr Tomas Braeuniger of the NMR research group at Durham for his friendship and numerous discussions at the Three Swans and continued collaboration in MQMAS NMR.

I would also like to express my gratitude to M. Smith at the University of St Andrews for her help in setting up the solution-state NMR machine, fixing things and acquiring the solution-state NMR spectra. Also, Dr Alan Kenwright at the University of Durham for his contribution to the discussion on proton relaxation.

Abbreviations used in this thesis.

B Magnetic induction field

B_0 Magnetic induction field of the spectrometer

B_1, B_2....Radiofrequency magnetic induction field associated with υ_1, υ_2

$\hat{I}$ spin quantum number (components $\hat{I}_x$ $\hat{I}_y$ $\hat{I}_z$)

$\hat{I}_+$, $\hat{I}_-$ raising and lowering spin operator

μ Magnetic dipole moment (μ_z along B_0)

γ Gyromagnetic ratio

υ The strength of an rf magnetic field, expressed in angular frequency units.

υ_1, Frequency of observing rf magnetic field

υ_2 Frequency of irradiating rf magnetic field

ω_1, ω_2 as for υ_1 and υ_2 but in rad s^{-1}

σ Shielding constant, subscripts $\perp$ and $\|$ give the axially symmetric case

T_1 Spin-lattice (longitudinal) relaxation time of nucleus

T_2 Spin-Spin (transverse) relaxation time of nucleus

$T_{1\rho}$ Spin-lattice relaxation time of nucleus in the frame of reference rotating in B_1

δ_x Chemical shift of the nucleus X usually given in ppm

Cp Heat capacity

$\overline{DP}_{ncum}$ The average cumulated degree of polymerisation

t_p Duration of RF pulse

Contents

CHAPTER 1

1.1 Introduction.

Vinylidenefluoride polymers have a polymer chain of -$[CH_2\text{-}CF_2]_n$- monomers. Dependent on the synthetic pathway, about 5% of these monomers are 'so called reverse units' -$[CH_2\text{-}CH_2\text{-}CF_2\text{-}CF_2]$-. The amount of reverse unit has been shown to have a significant effect on the crystalline form of PVDF. Other major properties are due to the van der Waals radius (0.135 nm) of the fluorine atom, which is only slightly larger than that of hydrogen (0.12 nm) and forms highly polar bonds. A combination of this polarity and higher levels of structure in poly (vinylidenefluoride) influences the piezo- and pyro-electric properties of this polymer. It is this property and a combination of high thermal stability, chemical inertness, low water absorption, low dielectric constant, good weather-ability and resistance to ageing, that makes PVDF and related fluoro-polymers of interest in many applications in aeronautics, engineering, optics and microelectronics.

Work over the past 40 years has reveled the structure of several crystalline forms and chain defects. There does however, remain several questions, pertaining to the nature of chain-end groups and/branching. Only a few works have been published in respects to these issues and furthermore, no complete NMR investigation, conducted on one and the same PVDF sample was found in the literature. This is important as different types of PVDF have different thermal history, which has been shown to affect the results of various spectral methodologies such as differential scanning calorimetry (DSC). Also, no complete NMR investigation on low molecular weight VDF was available. NMR of these low molecular weight compounds could give indications to the type of end-group or branch point formed, depending on the synthetic pathway. Certainly no combination of solution and solid-state NMR on these two types of fluoropolymers has been applied. A full investigation would be the use of two-dimensional homo and heteronuclear methodologies in solution-state NMR to assign signals and their spin systems. High-resolution solid-state NMR spectra of these polymers to verify the range of mobilities and crystalline domains, is also of interest. The effect of molecular weight and mobile units could show

NMR spectroscopy of ^{19}F is favourable due its 100% abundance, high magnetogyric ratio, which is second only to protons and its spin quantum number of ½. Furthermore, it has a receptivity of 84% of that for protons and a chemical shift range similar to that of ^{13}C. So these properties of fluorine convey very agreeable sensitivity in the NMR experiment. In contrast, its high magnetic moment γ, and its natural abundance imply that dipolar interactions (homo and hetero nuclear) are probably strong. However, the combination of fast MAS and proton decoupling, have been shown to result in well-resolved ^{19}F spectra for several solid fluorinated polymers. In this thesis we use these magnetic properties of the fluorine nuclei and apply solid- and solution-state NMR technology to define the morphological and structural characteristics of a poly (vinylidenefluoride), PVDF, with the trade name Kynar 301F.

The above-mentioned properties make ^{19}F solid-state magic-angle spinning NMR an important technique for the characterisation of fluoropolymer morphology, as discussed in articles by Harris and co-workers.

Nuclear magnetic resonance (NMR) spectroscopy of the solid-state has developed into a powerful analytical tool for the determination of morphology, especially in polymers. In NMR spectroscopy certain interactions are present. The effects of these interactions differ depending on whether the experiment is run in the solid or solution-state. Such interactions include:

1) Shielding
2) Homonuclear dipolar coupling
3) Heteronuclear dipolar coupling

The shielding of nuclei is an effect of the external magnetic field, which causes the circulation of electrons and creates a local magnetic field at the nucleus. For nuclei in molecules this either augments or opposes the external field. Thus the electronic structure of the molecule influences the size of the shielding. The resonance frequency of a nucleus is therefore characteristic of its environment. Rapid tumbling of the molecules in a solution averages out any orientation dependency to the external field and produces a narrow line at a position known as the isotropic chemical shift. In the spectra of a powdered solid all orientations, with respect to the external field, of a given site are present. When local symmetry is less than cubic these orientations have different resonance frequencies. This leads to a broad line shape.

The source of the dipolar interaction lies in the position of two nuclei in relation to each other, their associated magnetic fields, and the orientation of each nucleus to the static

magnetic field. If these nuclei are in solution and tumbling, the dipolar coupling will not produce observable splitting because although they have finite value at any instance in time, the couplings are averaged to zero on the NMR time scale due to the isotropic tumbling of the molecule. However, their relative positions in space will alter, and the local field of one nucleus will fluctuate, if at an appropriate rate, this can induce relaxation.

In solid state NMR this molecular tumbling is not present and therefore the dipolar interaction is anisotropic: dependent on the orientation of the internuclear vector of the dipole pair with regard to the static magnetic field and thus in powder systems, a broad line shape is generated. Further discussion on dipolar and chemical shift interactions in solids can be found under sections 1.3.5 and 1.3.6 respectively.

In powder systems, the line shapes for dilute spins are termed inhomogeneous and result from the superposition of many narrow lines. As stated above, the position of these lines in the spectrum depend on the relative orientation of the magnetic field and the principal axis system of the relevant interaction. In systems of abundant spins, homonuclear dipolar interactions often dominate and homogeneous lines are observed, giving static proton spectra, which can have a line width of up to 80 kHz.

Several techniques are available to decrease the effects of such interactions and produce a resolved spectrum:

1) Magic-angle spinning (MAS) [1]. To fully average interactions with the use of MAS it is a necessity that the spin-rate be greater than the magnitude of the static line width. Where this is not the case for inhomogeneously broadened lines, the line shape is broken up into a relatively narrow isotropic line (or lines) and spinning sidebands, where the intensities depend upon the principal components of the relevant interaction tensor. For homogeneously broadened lines, the spinning speed needs to be greater than the full static line width in order to achieve narrowing. This may mean that spinning rates in excess of 60 kHz are needed; unfortunately this is technically demanding and commercially unavailable.

2) High-power decoupling. The basic need for the decoupling of an abundant spin such as protons from carbon is to take out the interactions between the nuclei that complicate the spectra as in solution state NMR, or broaden the signal as in solid state NMR. The differences between these two techniques are approached below under the section, line-narrowing techniques 1.3.7.

Problems can also arise in solid-state NMR spectroscopy of other strongly coupled spins, for example when ^{19}F is observed in fluoropolymer systems. For polymeric materials, the major contributing factor to the static line shape is the dipolar interaction, whether it is H-H or H-F in systems containing fluorine. For materials with a diverse

morphology, such as semi crystalline polymers, spectral interpretation is even more complicated. However the application of relaxation filters and pulse sequences incorporating dipolar recoupling and spin diffusion offers the possibility of extracting information on morphology and the structure of the individual phases. A more detail description of this methodology will be offered in chapter 2.

The observation of magnetic resonance relaxation of nuclei and its temperature dependence can be used to reveal information about molecular motion. It is the morphological phases and molecular motions, along with the nature of the fluorine line shapes that form the topic of this thesis.

1.2 Thesis overview

This thesis reports work done on a part time basis at the department of chemistry university of Durham and the university of Durham Industrial Research Laboratory (UDIRL).

This thesis describes a morphological study, by NMR, of the semi-crystalline fluoropolymer, poly (vinylidenefluoride) (PVDF), and the effects of aging on molecular motion and thermal transitions. Solution-state ^{19}F NMR was used to establish chemical shifts, fluorine connectivity and reverse-unit content. This information was then used to aid chemical shift assignment of the solid-state spectra. Relaxation filter experiments and a dipolar recoupling experiment gave information related to the solid-state morphology. A spectrum from the crystalline component showing the trans-gauche configuration was obtained, along with spectra showing signals from the amorphous phase, reverse units and mobile units.

The effect of annealing PVDF was investigated using variable temperature proton relaxation and Differential Scanning Calorimetry (DSC). Earlier NMR relaxation work on PVDF from the literature is compared with the new results and the nature of the inter-phase region is debated with regard to molecular motion and thermal transitions.

For comparison a vinylidenefluoride (VDF) telomer, of significantly lower molecular weight than PVDF was examined. Solution-state ^{19}F NMR was used to establish chemical shifts, connectivity and reverse-unit content, and the nature of a highly mobile species, also detected in PVDF, is examined using two-dimensional solution-state spectroscopy. Furthermore, the application of high power decoupling at 500 MHz gave superior resolution enabling the determination of new features in the spectra and a more though investigation than previously performed. Relaxation filters were used to determine the solid-state structure with regards to the crystalline and amorphous phases.

1.3 THEORY OF NMR

All magnetic nuclei have an intrinsic angular momentum (or spin) quantized in units of $\hbar(=h/2\pi)$. Its magnitude is: spin angular momentum $=\left[I(I+1)\right]^{1/2}\hbar$, where I is the spin quantum number and can have the values of 0, 1/2, 1, 3/2,..... The vector quantity of the spin angular momentum ***I*** (vector), has 2 I+1 projections on an arbitrary axis such as $I_z = m\hbar$, where m is the magnetic quantum number having integral steps between +I and - I.

The magnetic moment of a nucleus μ is directly proportional to ***I*** according to $\mu=\gamma I$ where γ is the gyromagnetic ratio. With no magnetic field present, all 2 I+1 orientations of a spin-I nucleus have the same energy. However, when placed in a magnetic field this degeneracy is removed and the magnetic moment μ has an energy $E=-\mu\cdot\mathbf{B}$, where **B** is the magnetic field experienced by the nucleus; this is called the Zeeman effect. In a strong field the quantization axis is now defined with the field direction and $E=-\mu_z B$. The energies of the 2 I+1 states for the spin-I nucleus are equally spaced and separated by an energy gap $\hbar\gamma B$. The selection rule $\Delta m = \pm 1$ gives the allowed transitions, which are between adjacent energy levels. Thus the resonance condition is $\Delta E = h\nu = \hbar\gamma B$ and the frequency ν of electromagnetic radiation is $\nu = \gamma B/2\pi$.

1.3.1: FRAME OF REFERENCE

In a sample containing a large number of identical spins, the total bulk magnetisation (**M**) precesses about the external magnetic field of magnitude B_0, with the angular frequency $(\omega_0) = -\gamma\,\mathbf{B}_0$, as in figure 1.1 this is the laboratory frame.

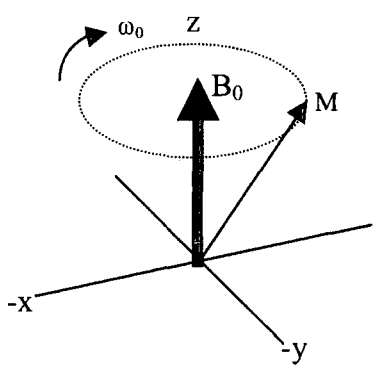

Figure 1.1 Laboratory reference frame, where **M** precesses around the field direction B_0.

If a weak radio frequency is applied, a magnetic field $\mathbf{B_1}$ with an angular frequency of ω_{rf}, can be considered to rotate in the x y plane about the z-axis. In the rotating frame reference system the axis system rotates with $\mathbf{B_1}$, so that there is an effective field B_{eff}. This means that the field $\mathbf{B_1}$, would appear to be stationary in the rotating frame with M precessing around $\mathbf{B}_{eff}$ figure 1.2. For further explanation on the rotating frame see (Harris R.K, Hore P in bok review)

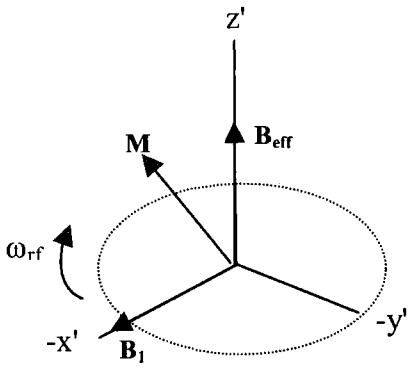

Figure 1.2. The rotating frame of reference. The difference between the angular frequencies of the laboratory and rotating frame $\Omega = \omega_0-\omega_{rf}$ represents the offset frequency of the reference and the effective field is $B_{eff}= (\omega_0-\omega_{rf})/\gamma$.

The concept of the rotating frame is convenient because we do not need to evaluate time- dependent magnetic fields.

In a simple pulsed NMR experiment the displacement of the spin system from its initial state of equilibrium along B_0 is made by applying a rf pulse (B_1) along the x' axis of the rotating frame, with the transmitter frequency ω_{rf} set close to ω_0. A pulse of a duration t_p causes precession through the z y plane at an angular frequency of γB_1. The angle of this rotation β is defined $\beta= \gamma B_1 t_p$ (figure 1.3). When the pulse is turned off, the return to equilibrium (relaxation) may be monitored.

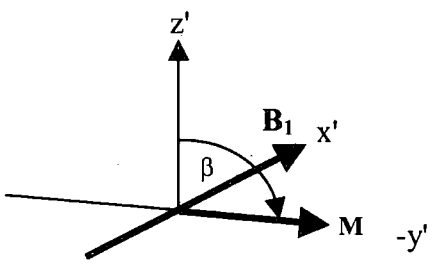

Figure 1.3. This shows the representation of the effect on magnetisation by an applied radio frequency pulse of strength B_1 and duration t_p such that the pulse angle β is 90°.

1.3.2: RELAXATION

When the pulse described above is turned off, the spin system starts to return to equilibrium.

Two types of process describe the return to equilibrium:

1) Spin-lattice relaxation, describing the return to equilibrium along the z-axis

2) Transverse relaxation, (or spin-spin), describing the rate of relaxation in the x y plane.

These motions are described by the Bloch equations:

$$\frac{dM_x(t)}{dt} = M_y(t)\gamma B_0 \qquad \text{Equation 1}$$

$$\frac{dM_y(t)}{dt} = -M_x(t)\gamma B_0 \qquad \text{Equation 2}$$

$$\frac{dM_z(t)}{dt} = 0 \qquad \text{Equation 3}$$

where $M_z(t)$ is the magnetisation along the z-axis at time t. $M_y(t)$ is the magnetisation in the y' plane at time t.

1.3.3: DYNAMICS OF SOLID-STATE NMR

During a NMR experiment the spins may experience electric and magnetic fields from the spectrometer and from their environments. The interactions with the static field and the rf pulse are termed external interactions. However, the nucleus may experience a number of internal interactions as a result of its environment in the sample. Possible internal interactions are summarised in figure 1.4. For this work, spin-rotation and quadrupolar interactions can be ignored

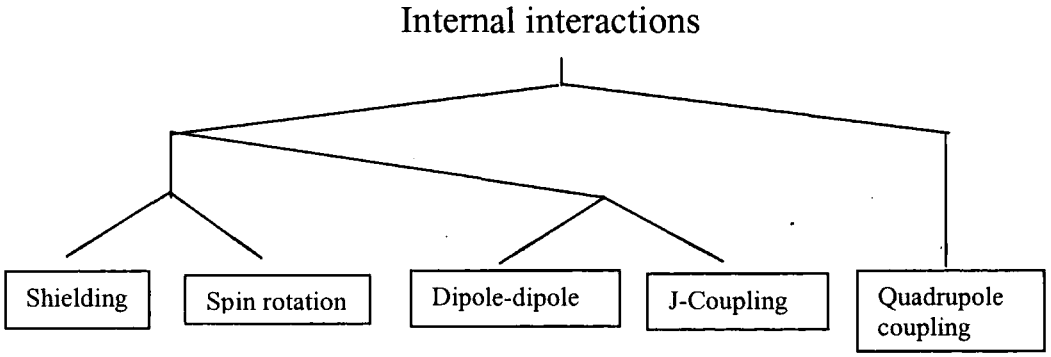

Figure 1.4. Schematic overview of the internal interactions that effect NMR spectra.

1.3.4: DIPOLE-DIPOLE COUPLING

A spinning nucleus acts as a small magnet and therefore generates a magnetic field, figure 1.5. For a nucleus with the magnetic moment μ at an angle α to the B_0 field and a distance r between two nuclei (the nucleus at point a will generate a field at the nucleus at point b) the situation is:

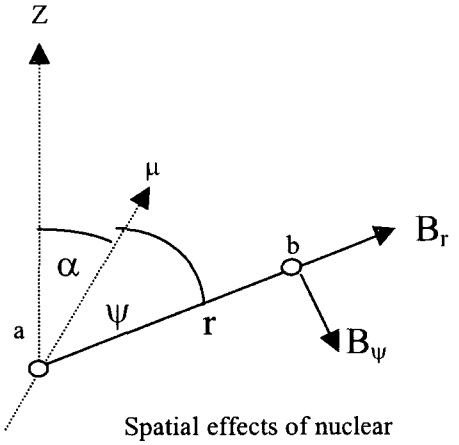

Spatial effects of nuclear magnetic moments

$$B_r = \frac{\mu_0 2\mu}{4\pi r^3}\cos\psi \qquad \text{Equation 4}$$

$$B\psi = \frac{\mu_0 \mu}{4\pi r^3}\sin\psi \qquad \text{Equation 5}$$

Figure 1.5. The magnitude of the dipolar field for a nucleus is dependent on the distance r to a neighbouring nucleus, μ_0 is the permeability of vacuum.

Figure 1.6 a shows a nucleus k, affected by the local field of its neighbor j by a direct through-space interaction.

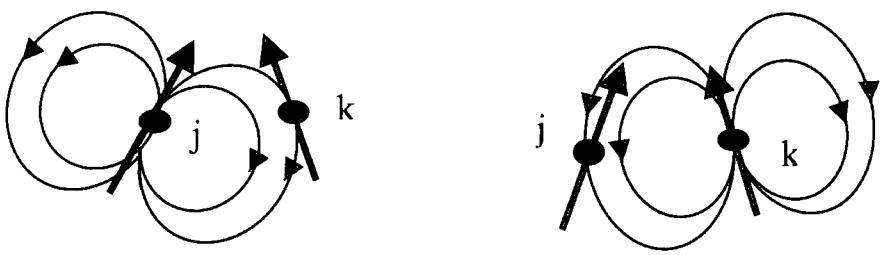

Figure 1.6. Two point dipoles and how their magnetic fields influence each other.

In the same manner the local field of k affects j (figure 1.6b). The energy between the two-point dipoles μ_j and μ_k where r is the distance between μ_j and μ_k is given by.

$$E = \left\{ \frac{\mu_j \cdot \mu_k}{r^3} - 3\frac{(\mu_j \cdot r)(\mu_k \cdot r)}{r^5} \right\} \frac{\mu_0}{4\pi} \qquad \text{Equation 6}$$

The resonance frequency of X in a pair of heteronuclear AX spins is determined by the net field in the Z component direction generated by A and the splitting is proportional to this field and the gyromagnetic ratio of X. The factor $\frac{\gamma_j \gamma_k \hbar^2}{r^3} \frac{\mu_0}{4\pi}$ is the dipolar-coupling constant (R) of the two spins. The measurement of the dipole-dipole coupling is useful for molecular studies giving inter and intra nuclear distances and therefore the geometry of the molecule. Where heteronuclear dipolar splitting = $R\left(3\cos^2\Theta_{jk}-1\right)$

and homonuclear dipolar splitting = $3/2R\left(\cos^2\Theta_{jk}-1\right)$ Equation 7

The term 3/2 arises due to mixing of the $\alpha_A\beta_X$ and $\beta_A\alpha_X$ spin states; otherwise the same general principals apply to both homo and hetero nuclear coupling.

The angle Θ_{jk} is described by the vector joining the spins and the external magnetic field B_0.

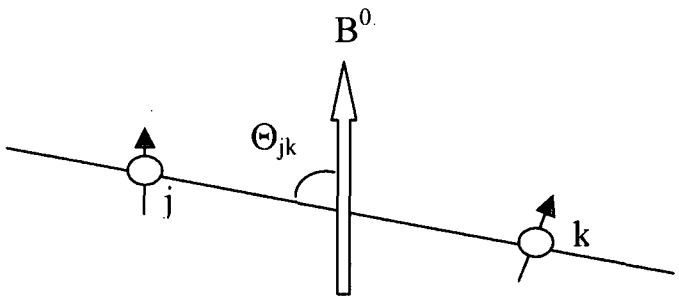

Figure 1.7 Definition of the vector describing the relationship between two spins and the magnetic field

In solids, dipolar interactions are not averaged as in solution NMR where molecules in liquids rotate quickly and a rapid change in the axis and speed of orientation takes place. If the frequency of these changes is greater than the dipolar interaction then spectra do not usually contain any dipolar splitting.

The situation is also more complicated in spectra of powder samples where for an AX spin system each pair of spins has a unique value of θ but the distribution is random. The spectrum is the sum of the single crystal spectrum for θ, between 0° and 90°. The

addition of these spectra gives the line shape shown in figure 1.8 known as the dipolar powder pattern.

Both homo and heteronuclear dipolar coupling are orientation dependent through Θ_{jk} (figure 1.8). Spins aligned parallel to the external field have $\Theta_{jk}=0$. Spins perpendicular to the field have ($\Theta_{jk}= \pi/2$). This means that $3\cos^2\Theta_{jk}-1=0$ for

$$\Theta_{jk} = \cos^{-1}(1/\sqrt{3}) = 54.75 \qquad \text{Equation 8}$$

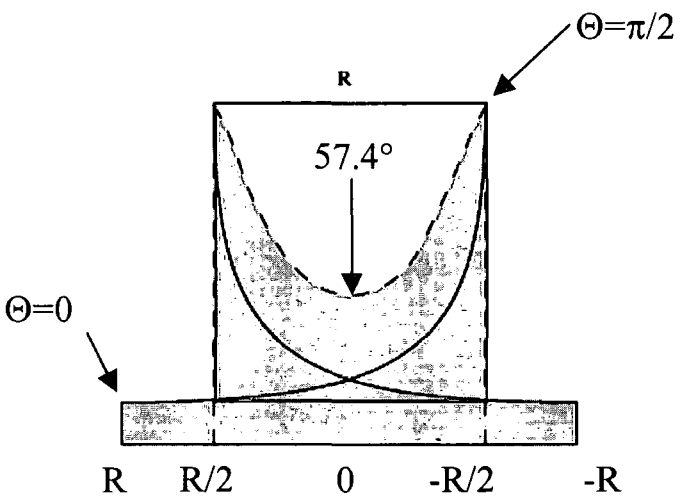

Figure 1.8 Hypothetical representation of the orientation dependency of a heteronuclear AX spin system showing the two lines for the A and X splitting along with the total pattern in gray, where R is the dipolar coupling constant.

and the doublet splitting decreases to zero at $\theta=54.7°$, the so-called magic angle (see line narrowing techniques).

1.3.5: CHEMICAL SHIFT AND SHIELDING

The NMR frequency of a nucleus in a molecule is determined principally by its gyromagnetic ratio γ and the strength of the magnetic field B that it experiences.

$$\nu=\frac{\gamma B}{2\pi} \qquad \text{Equation 9}$$

Not all nuclei of the same species, for example protons, have the same resonance frequency. This is due to the position of the nucleus in the molecule and thereby the local electron distribution. This effect is known as the chemical shift.

The chemical shift arises because the external field B_0 causes electrons to circulate within their molecular orbitals. This induced motion generates a small magnetic field $\mathbf{B}^{induced}$. The nucleus is thus shielded from the external field B_0 by its surrounding electrons. The nucleus then experiences a magnetic field **B**, which is slightly smaller than the external field and the proportionality constant for the induced field σ, is called the shielding constant (equation 10).

$$B=B_0-B^{induced}=B_0(1-\sigma) \qquad \text{Equation 10}$$

Thus the resonance frequency ν of a nucleus becomes:

$$\nu=\left|\frac{\gamma_j}{2\pi}\right|B_0(1-\sigma) \qquad \text{Equation 11}$$

The strength of the induced current is directly proportional to the applied field
The linear dependence of the induced field on the applied field may be written:

$$B^{induced}=\sigma\times B_0 \qquad \text{Equation 12}$$

Where σ represents a 3×3 matrix called the shielding tensor giving:

$$\begin{pmatrix} B_x^{induced} \\ B_y^{induced} \\ B_z^{induced} \end{pmatrix}=\begin{pmatrix} \sigma_{xx} & \sigma_{xy} & \sigma_{xz} \\ \sigma_{yx} & \sigma_{yy} & \sigma_{yz} \\ \sigma_{zx} & \sigma_{zy} & \sigma_{zz} \end{pmatrix}\times\begin{pmatrix} 0 \\ 0 \\ B_0 \end{pmatrix} \qquad \text{Equation 13}$$

Which then evaluates to:

$$\begin{pmatrix} B_x^{induced} \\ B_y^{induced} \\ B_z^{induced} \end{pmatrix}=\begin{pmatrix} \sigma_{xz}B_0 \\ \sigma_{yz}B_0 \\ \sigma_{zz}B_0 \end{pmatrix} \qquad \text{Equation 14}$$

Therefore the magnitude and direction of the induced field at a given site depends on both the orientation of the molecule to the applied field and the location of a nucleus in

the molecule. Here the notation σ_{xz} signifies the component of the induced field in the x direction when the external field is in the z direction.

If all molecules in the rigid lattice of a single crystal have the same angle of orientation they also have the same chemical shift, figure 1.7. If the crystal is rotated the shift will change.

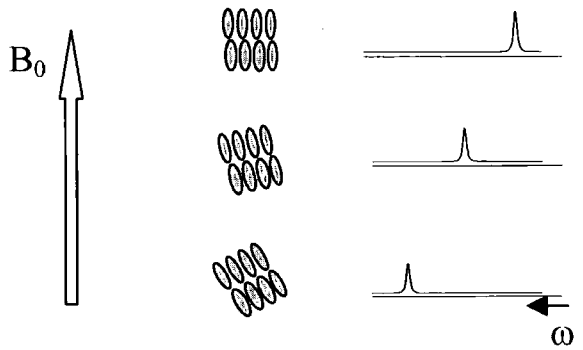

Figure 1.9 The chemical shift for a sample is highly dependent upon its orientation to the B_0 field. Different orientations result in a change in the chemical shift.

For a powder sample containing many crystals with different orientations, the array of chemical shifts contributes to a broadband shape (figure 1.8).

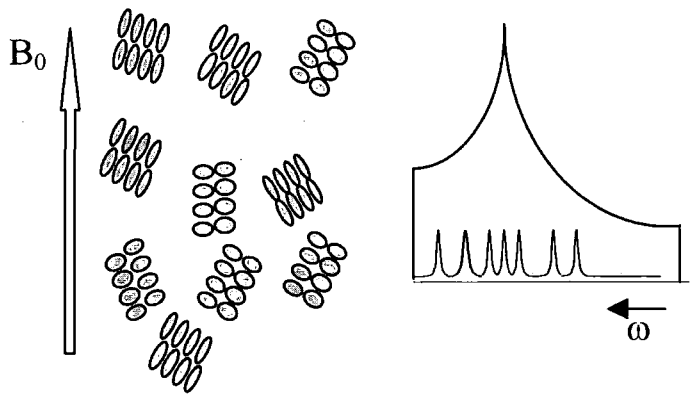

Figure 1.10. For a powder sample the many orientations result in a broad line-shape made up of many individual chemical shifts.

The shielding tensor is usually assumed to be symmetric, i.e. $\sigma_{xy}= \sigma_{yx}$. The terms $\sigma_{xx},\sigma_{yy},\sigma_{zz}$ in the equations below are the principal components of the tensor and give information on :

- The isotropic average $\sigma_j^{iso}=\frac{1}{3}(\sigma_{xx}+\sigma_{yy}+\sigma_{zz})$ Equation 15

- The anisotropy $\Delta\sigma = \sigma_{zz} - \frac{1}{2}(\sigma_{yy} + \sigma_{xx})$ Equation 16

- The asymmetry $\eta = \frac{(\sigma_{yy} - \sigma_{xx})}{\frac{2}{3}\Delta\sigma}$ Equation 17

The chemical shift tensor (always referred to a reference) is given by:

$\delta_{iso} = \sigma_{ref} - \sigma_{iso}$, $\Delta\delta = -\Delta\sigma$ and $\eta_\delta = \eta_\sigma$.

This means that the shielding produced is anisotropic in character. The shielding will have different values if, say, a molecular symmetry axis is perpendicular $\perp$ or parallel $\parallel$ to the B_0 field, figure 1.11.

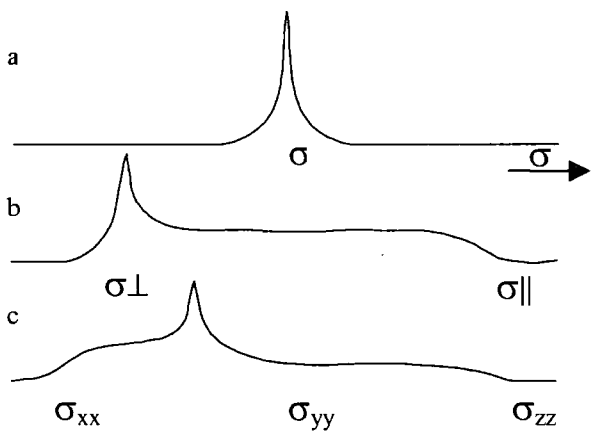

Figure 1.11. Powder patterns caused by shielding anisotropy for sites with (a) cubic symmetry, (b) axial symmetry and (c) lower symmetry.

Where the symmetry is axial at an angle θ to B_0

$$\sigma_{zz} = -\frac{1}{3}(\sigma_\perp + 2\sigma_\parallel) + \frac{1}{3}(3\cos^2\Theta - 1)(\sigma_\perp - \sigma_\parallel) \quad \text{Equation 18}$$

Here the term $\frac{1}{3}(\sigma_\perp + 2\sigma_\parallel)$ is the isotropic average and $(\sigma_\perp - \sigma_\parallel)$ is the anisotropy.

1.3.6 LINE-NARROWING TECHNIQUES

As shown in section 1.3.5, the dipolar interaction and the shielding anisotropy (1.3.6) have an orientation dependency with the magnetic field B_0 scaled by the term, $3\cos^2\theta$-1. For a powder sample all values of Θ exist at random with respect to the magnetic field B_0 figure (1.10); this gives a powder pattern with substantial dipolar broadening and/or shielding anisotropy (figure 11).

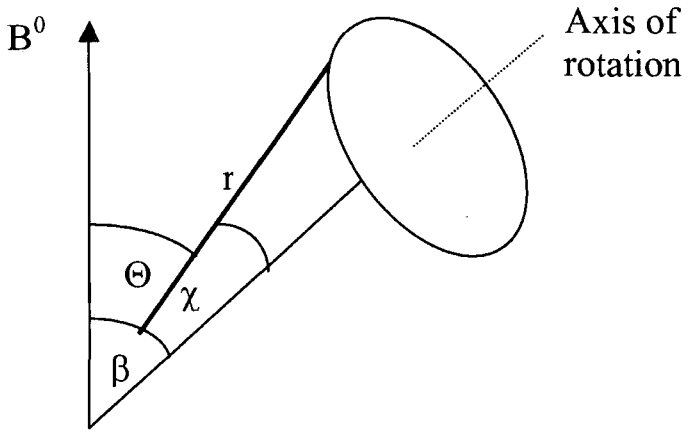

Figure 1.12. Macroscopic sample rotation at the angle β to the applied field B_0. The geometric relationships involved in the magic angle rotation.

The rotation of the sample (figure 1.12) around an axis β to B_0, describing a conical path for the inter-nuclear distance r and/or shielding tensor axis, allows us to determine the average of $(3\cos^2\Theta - 1)$ through

$$< 3\cos^2\Theta - 1 >= \frac{1}{2}(3\cos^2\beta - 1)(3\cos^2\chi - 1) \quad \text{Equation 19}$$

The parameter χ is fixed for a rigid solid but behaves as Θ for a powder i.e. takes all possible values. The term $\frac{1}{2}(3\cos^2\beta - 1)$ acts as a scaling factor. For β=54.7°, $\cos\beta = \frac{1}{\sqrt{3}}$

and the term $\frac{1}{2}(3\cos^2\beta - 1)$ =0, and shielding anisotropy is eliminated, giving increased resolution. This is termed "magic angle spinning" and applies to both the homonuclear and heteronuclear dipolar cases. The solution β=54.7° is called the magic angle. MAS averages out all anisotropic interactions described by second-rank tensors, thus eliminating anisotropic broadening and revealing structural information in the isotropic shift

1.3.7: DECOUPLING

Decoupling is implemented by the application of a second rf pulse at the frequency of the nuclei to be irradiated, i.e. protons. The decoupling is homonuclear, if the decoupled and observed nuclei are the same and heteronuclear if they are different.

In solution state spectroscopy decoupling is generally applied with two goals in mind; either the selective decoupling of a single resonance to identify its coupled partner(s) or non-

selective (broadband) decoupling of one nuclide to enhance and simplify the spectrum of a different nuclide (for example C-{H} or F-{H} couplings), by the removal of scalar spin-spin coupling.

This method facilitates the observation of a spatially dilute nucleus in the presence of an abundant spin network (heteronuclear decoupling).

To acquire proton decoupled spectra in the solution state the most common method is broadband decoupling during acquisition of carbon spectra. This removes ^{13}C-^{1}H couplings thus simplifying the spectra and increasing the signal intensity. Furthermore the saturation of the protons during decoupling provides further signal enhancement due to the nuclear Overhauser effect (NOE). The application of gated, inverse-gated and power-gated decoupling facilitates the acquisition of spectra with or without NOE and none or varying degrees of scalar coupling.

In ^{13}C-{^{1}H} solid-state studies the abundant spins are decoupled by a strong and continuous radio-frequency field. However other heteronuclear decoupling methods such as TPPM (two-pulse phase modulated) and SPINAL-64 have been applied with good results. To achieve homo nuclear decoupling multiple pulse sequences have been developed using specifically designed cycles of many pulses repeated many times with stroboscopic observation of the magnetisation, such as CRAMPS (combined rotation and multiple-pulse sequences) and BLEW24.

As described above, broad signals observed in solid-state NMR spectra arise mainly because of heteronuclear and homonuclear dipolar interactions and shielding anisotropy.

As stated earlier, broadening cause by dipolar interactions cannot be fully removed by MAS, but broadening arising from the shielding anisotropy requires only moderate rates of MAS. The effect of the shielding anisotropy may be seen in the spectrum as satellites called spinning sidebands. The anisotropy is in the order of 3 kHz, which increases with an increase in B_0. MAS at achievable rates, allows us to "spin out" the anisotropy and combined with a certain decoupling regime, results in an increase in spectral resolution.

1.3.8. CROSS POLARIZATION

For dilute spins ^{13}C, relaxation times make acquiring solid-state spectra difficult, giving poor sensitivity. The use of the cross polarisation technique in this circumstance gives spectra with improved intensity. Here the source of the ^{13}C magnetisation is the ^{1}H spins and is made possible when the Hartmann-Hahn match condition is met.

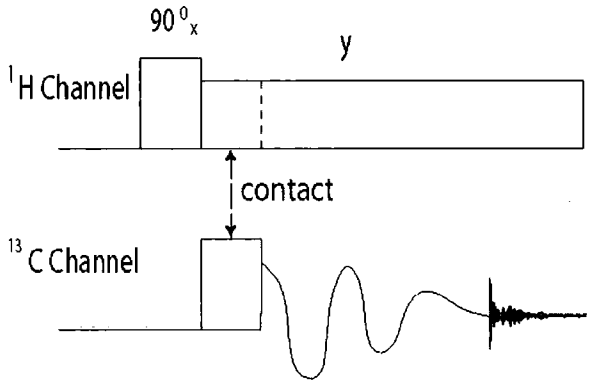

Figure 1.13 The cross polarisation pulse sequence. A 90° is applied in the proton channel and then a spin-lock. The magnetisation is increased on the carbon channel until the Hartmann-hahn match is achieved and a transfer of magnetisation can take place.

Firstly a 90^0 pulse is applied to the proton channel that is then spin locked in the y direction (figure 1.13). Then a pulse is applied to the ^{13}C channel and its power adjusted so as to meet the requirements of the following condition, where the transfer of magnetisation takes place in the rotating frame:

$$\gamma_H B_{1H} = \gamma_C B_{1C}$$

This means that the rotating frames of reference for the nuclei have the same precession rates and energies so that a transfer of energy is induced through the dipolar hamiltonian flip-flop term.

This transfer of energy gives a common spin temperature for the two species. The enhanced magnetisation of the carbons $\frac{\gamma_H}{\gamma_C} \sim 4$ can then be monitored by the free induction decay (FID). The system is now dependent on T_1H, which is shorter than that of the carbons and results in a spectrum with increased intensity. The same procedure can be used on any abundant spin such as ^{19}F for cross polarisation to a dilute spin. However, nearly all spectra in this thesis have been acquired with direct polarisation with the exception of the measurement of ^1H relaxation rates via proton to fluorine cross-polarisation to compare signal intensities.

1.4: EXPERIMENTAL

Solid-state spectra were recorded by direct ^{19}F polarisation, with ^1H decoupling, using a dual channel Varian INOVA spectrometer, operating at 299.95 MHz for ^1H and 282.21 MHz for ^{19}F, with a Doty XC5 $^1H/^{19}F$ probe. The spectral reference was a replacement sample of C_6F_6 ($\delta_F = -166.4$ ppm with respect to the $CFCl_3$). The ^1H decoupling was also used during

referencing so that corrections for the Bloch-Siegert shift [18] are not required. With decoupling the signal moves to a lower frequency with a difference of ~1.5 ppm for the spectrometer used. All spectra were recorded with a spin rate of 14 kHz. The probe temperature was calibrated by the methanol method [19]. Spinning at 14 kHz with a bearing gas supply at 20 °C gave a sample temperature of 60 °C. Silicon nitride rotors were used on all samples, with Vespel drive caps to avoid any fluorine background signal. The sample volume was restricted to 70 μl to increase rf homogeneity. The spectra showing the effect of fast MAS (chapter 3) on the line shape of 19F and ^{1}H were recorded with no decoupling on a 500 MHz Varian Infinity plus spectrometer, operating at 499.75 MHz for ^{1}H and 470.18 MHz for ^{19}F, using a Varian T3 2.5 mm probe.

The following parameters were used: a pulse duration of 3.6 μs ($\pi/2$) was used for ^{19}F, with a proton decoupling field during acquisition equivalent to 85 kHz and a 2 s recycle delay. Discrimination of the crystalline domains of PVDF was achieved with a pre-acquisition fluorine spin-lock time at a field equivalent to 80 kHz. The pulse sequences for domain selectivity used in the solid state are shown in figure 1.14 and appendix (ii) along with relevant parameters. A more detailed description of the domain selection is given in chapter 2. For the ^{1}H variable temperature measurements, a Varian static probe was use to measure proton spin-lattice relaxation times, using a saturation recovery pulse sequence. The signal was recorded for 8 different values of τ ranging from 0.2 to 32 seconds.

A variable spin lock pulse was used for $T_{1\rho}$ (H) measurements with a spin-lock power of 2.0 mT, 49 values of τ were acquired ranging from 40 μs to 40 ms. Both T_1 and $T_{1\rho}$ measurements were made using a $\pi/2$ pulse of 1.8 μs. Data were analysed in terms of a two-component fit to an exponential decay by least-squares fitting of the peak intensities using Sigma Plot® 4.0 software.

The solution-state spectra of PVDF were recorded at 22°C on a 500 MHz Varian Inova spectrometer, operating at 499.75 MHz for ^{1}H and 470.18 MHz for ^{19}F. The solvent was dimethylsulfoxide-d_6 (DMSO-d_6) and chemical shifts are quoted relative to the signal for a replacement sample of $CFCl_3$.

The ^{1}H-coupled ^{19}F COSY spectrum of PVDF in DMSO-d_6 at 22°C was recorded using a 90° pulse of 15 μs with a 2 s recycle delay and 512 increments.

The solution-state spectra of the VDF telomer were recorded at 22°C on a 500 MHz Bruker Avance spectrometer, operating at 499.75 MHz for ^{1}H and 470.18 MHz for ^{19}F. The solvent was dimethylsulfoxide-d_6 (DMSO-d_6) and chemical shifts are quoted relative to the signal for a replacement sample of $CFCl_3$.

The ^{19}F COSY spectrum of PVDF in DMSO-d_6 at 22°C was recorded using a 90° pulse of 15 μs with a 2 s recycle delay and 512 increments. All pulse programs, acquisition and

processing parameters for solution and solid-state spectra are given in Appendix (i) and (ii) respectively. Solution-state pulse programs were provided as standard bruker sequences. Solid-state pulse sequences were standard pulse programs modified for fluorine detection or written. Examples of these solid-state sequences are shown below.

1.4.1 SOLID STATE PULSE SEQUENCES

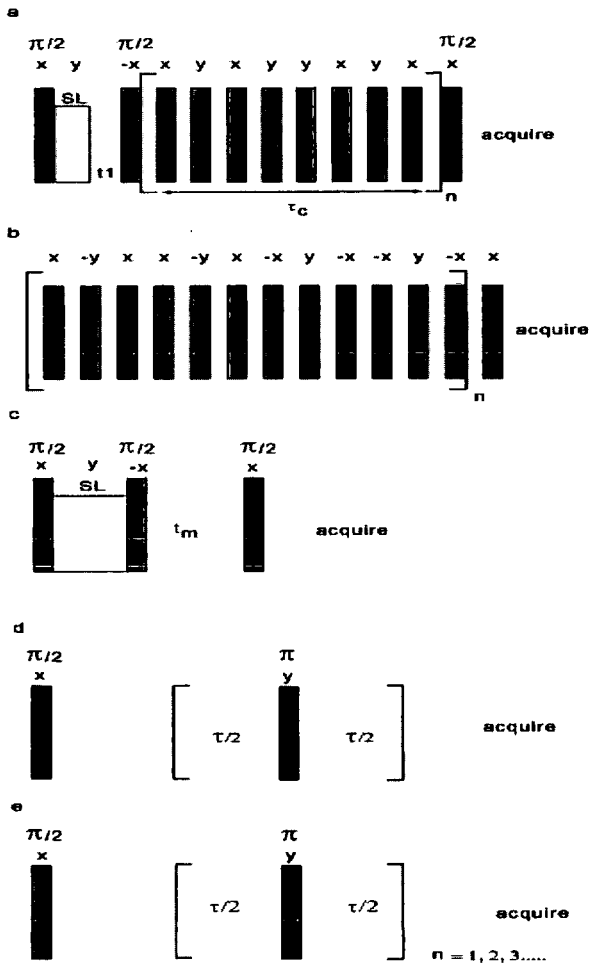

Figure1.14 Major solid-state pulse sequences (with phases) used in this work. From top to bottom: (a) RFDR with $T_{1\rho}(F)$ relaxation filter, τ_c=RFDR mixing, looped *n* times, t1=evolution time, SL=spin locking; (b) Dipolar filter, looped *n* times (n=16); (c) The Goldman-shen spin diffusion experiment with $T_{1\rho}(F)$ relaxation filter. SL=spin-locking; (d) Direct polarization with delayed acquisition $\tau/2$ = 4ms; (e) Carr-Purcell-Meiboom-Gill experiment where the echo pulse is repeated n time before acquisition and is then incremented. The pulse programs are given in appendix (i).

Figure 1.14a shows the RFDR pulse sequence with a spin lock pulse for pre-selection of the crystalline component. This is followed by an evolution period t1 during which the chemical shift evolution takes place. A 90° pulse with a –x phase positions the selected magnetisation along the z-axis. A train of eight 180° pulses which are rotor synchronised and applied during a time period τ_C, recouple the dipole- dipole interaction. This is repeated seven times (n=7), before a 90° observation pulse is applied. Rotor synchronisation is achieved by a delay between the 180° pulses being set to the inverse of the rotor speed minus the pulse duration. The result is a 2D spectrum with off-diagonal peaks showing connectivity of the signals due to their dipole-dipole interaction.

The dipolar filter experiment (figure1.14b) suppresses the strong dipole-dipole interactions, typically within the crystalline component, by a series of 12, 90° pulses repeated n times. The degree of suppression is regulated by the number n = 2, 4, 16 etc. This results in a spectrum of the amorphous component. The Goldman – Shen experiment is used to determine spin-diffusion and thereby domain size (figure1.14c). A spin-lock experiment is applied to pre-select the crystalline component, followed by a –x pulse which places the magnetisation along the z-axis. The spin diffusion of this component is allowed for varying values of τ_m and then the signal is recorded after an observation pulse.

The single-pulse delayed acquisition experiment (figure1.14d) was carried out with a spin echo to refocus heteronuclear inhomogeneities. The acquisition delay $\tau/2$ was 4 ms and optimised to sample T_2 and therefore give a spectrum of mobile units.

The Carr-Purcell-Meiboom Gill sequence consists of a 90° pulse followed by a 180° pulse (figure1.14e), which gives a single echo. An incremented delay $\tau/2$ precedes and follows the 180° pulse. This is repeated by incrementing n = 1, 2, 3 in a loop wise fashion. The decay in signal intensities provides a measurement of the T_2 relaxation time for the signals.

1.4.2 DSC

A Perkin-Elmer Pyris 1 DSC with external Nitrogen cryofill and a working temperature range from -180 °C to 260 °C was used for thermal analysis. The calibration was made using cyclohexane (87°C) and indium (156.0°C). All samples were enclosed in aluminium pans and weighed. Measurements were taken with a first heat cycle from -100°C to 200°C with a heating rate of 10°C/min. Then quenching from 200°C to -100°C at 50°C/min. The temperature is then held at -100°C before the second heat cycle starts from -100°C to 200°C with a heating rate of 10°C/min. Pyris Thermal Analysis software for Windows version 3.52 was used for instrument control and data analysis.

1.4.3 Sample preparation and characterisation

PVDF

The nascent powder sample was α-PVDF (Kynar 301 F), supplied by Atofina, France, with a molecular weight of 1×10^6 D (given by suppliers), reverse unit content of 4.7 % by NMR, crystallinity of ~28% [20,21], and melting point of 158 °C by DSC. For the proton relaxation measurements (chapter 4) the nascent α-PVDF was annealed at 200 °C for 1 hour and then left to stand at 20°C for 24 hours before DSC and NMR measurements were taken. Half of the initial annealed sample was left to stand for 240 hours before DSC and NMR measurements were taken.

VDF Telomer

The synthesis of this fluorinated telomer was made at the laboratory of Dr B. Ameduri at the Laboratoire de Chimie Appliquée, Ecole Nationale Supérieure de Montpellier.
The reaction of VDF with the telogen MeOH was carried out in a 160-mL Hastelloy (HC-276) autoclave equipped with inlet and outlet valves, a manometer and a rupture disc, with 1.050 g of the initiator (tert-butyl peroxide) and 52 g of methanol. The autoclave was then cooled, degassed and pressurised with 20 bar of nitrogen to check eventual leaks.
Three vacuum (20 mm Hg) / nitrogen cycles were made to expel oxygen and 20.0 g of VDF was then introduced in the autoclave. The autoclave was heated to 142°C for 5 hrs. An increase in pressure from 3 to 48 bars is observed and then a fall of pressure to 22 bars. After the reaction, the autoclave was placed in an ice bath for 30 minutes and 8.8 g of un-reacted VDF was progressively released. After opening of the autoclave, a phase separation was observed and after precipitating the heavier phase from pentane a white powder was obtained. No specific preparation was necessary for any other samples, as these were commercial products.

Chapter 2

Solution-state spectroscopy of PVDF

2.1 Introduction to ^{19}F Solution state Spectroscopy PVDF

The literature shows only a few detailed investigations of PVDF by ^{19}F and ^{1}H solution-state NMR [1, 2, 3, 4]. Relating them to similar fluorine shifts of the low molecular weight VDF compounds [2] has identified the shifts of specific fluorines in PVDF. Many of these works have aimed to identify chain end groups, branching and the degree of reverse units with reported chemical shifts around –107 and –114 ppm for CF_2-CH_3 and CH_2-CF_2H respectively. Although an obvious methodology, which would aid in the solution of these questions, would be to perform two-dimensional ^{19}F and ^{1}H correlation spectroscopy, such reports are sparse in the literature. Katoh et.al [1] performed ^{19}F J-correlated spectroscopy with broad band ^{1}H decoupling on PVDF; interestingly no ^{19}F chemical shifts related to chain end groups were reported in these one and two-dimensional experiments. It is also strange that the authors state that they report the results of a ^{19}F-^{1}H J correlated two-dimensional technique of PVDF developed in their laboratory. However, no spectra or results of such an experiment are reported in that paper, nor is there any later amendment. A 2D J-correlated spectrum of PVDF has been reported by Cais [4] where the connectivity of signals showing regiospecificty (-CH2-CF2-) and reverse units (-CH2-CH2-CF2-CF2-) are discussed, but no reference is made to the structure of end groups except that they were too weak to be detected. Furthermore, in a later work by Herman et al. [2] the effect of molecular weight and chain end groups on the crystal forms of PVDF oligomers is reported. A comparison between the ^{19}F spectra of the three VDF oligomers and PVDF showed no signals related to chain end groups for PVDF. The lack of signal from chain end groups in PVDF in these works could be due to the degree of polymerisation. However, using ^{19}F correlated spectroscopy, Pianca et al. [4] reported ^{19}F coupling for signals at –107.8 and –114.3 ppm for low molecular weight PVDF and assigned them to end groups - CH_2-CF_2-CF_2-CH_3. Inspection of their spectrum does not, however, show any off diagonal peaks confirming this assignment.

It was therefore of interest to evaluate the microstructure of our high molecular weight PVDF by solution-state NMR techniques including ^{19}F-^{1}H and ^{19}F-^{19}F J correlated two-dimensional spectroscopy to assign specific groups, particularly the chain end groups.

The preparation of samples for solution state spectroscopy was made by dissolving aliquots of PVDF in 1ml of DMSO in NMR tubes. All pulse programs used for solution state spectroscopy were of standard sequences and the parameters are given under appendix (i).

2.2 ^{19}F Solution state Spectroscopy PVDF

The proton coupled and proton decoupled ^{19}F spectrum of our sample of α PVDF in solution in DMSO at 22°C is illustrated in figures 2.1 and 2.2 respectively.

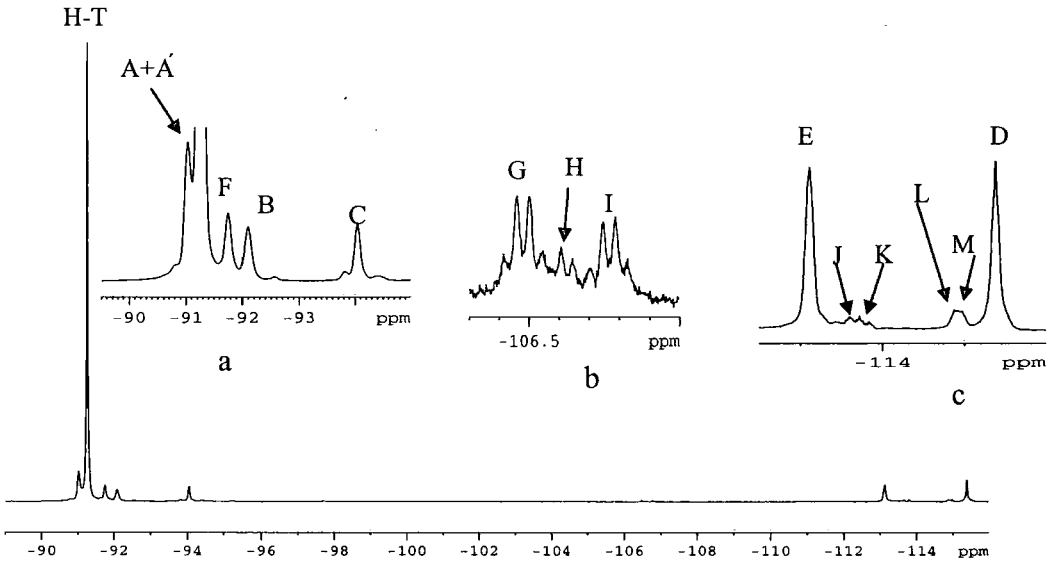

Figure 2.1 The coupled ^{19}F spectrum of our sample of α PVDF in solution in DMSO at 22°C with expansions a (main chain region), b (chain end groups, and c (reverse units and chain end groups).

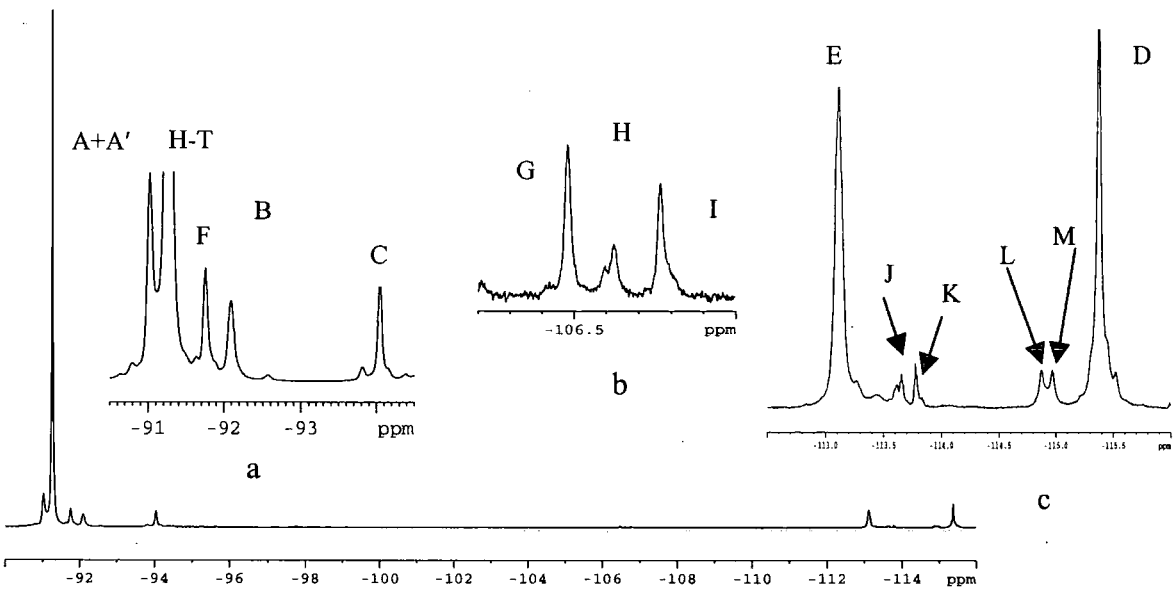

Figure 2.2 The ^{19}F proton-decoupled spectrum of α PVDF in solution in DMSO at 22°C with expansion a (main chain region), b (chain end groups), and c (reverse units).

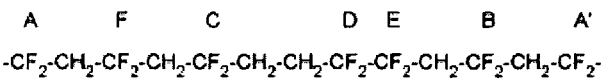

Figure 2.3 The ^{19}F assignment of signals for α PVDF around the reverse unit.

The most intense peak in the ^{19}F solution-state spectrum is from CF_2 groups of regular $(CF_2CH_2)_n$ chains remote from any reverse units (E and D) and labelled HT in figures 2.1. and 2.2. Figure 2.3 shows part of a polymer chain around a reverse unit, together with the lettering to distinguish the various fluorine sites. The spectrum is similar to those illustrated in the literature [see specifically ref. 5], although care should be taken when comparing chemical shifts, as they are sensitive to the solvent used, concentration and temperature [6-10]. Assignments are indicated in figures 2.1 and 2.2 and the chemical shifts are shown in Table 1.

δ_F/ppm (solution)	Relative Intensity	Assignment
-90.02	1.22	A and A'
-91.25	19.01	Main chain CF_2
-91.75	0.66	F
-92.09	0.47	B
-94.05	0.64	C
-106.48	0.06	G
-106.62	0.02	H
-106.77	0.04	I
-113.11	0.70	E
-113.65	0.07	J
-113.78	0.09	K
-114.87 d 19 Hz	0.08	L
-114.97 d 19 Hz	0.08	M
-115.35	0.87	D

Table 1 Chemical shifts and assignments for the ^{19}F spectra of PVDF in solution in DMSO-d_6 at 22°C

Other minor peaks, at $\delta_F = -106$ to -107 ppm (figure 2.1 b and 2.2 b), have been attributed to end-groups, branches or oligomeric species etc. [2, 4, 5, 8, 9]. From figures 2.1 b the signals at $\delta_F = -106$ to -107 (G, H, and I) show $^{19}F - ^{1}H$ coupling. However the proton-decoupled spectrum (figure 2.2 b) shows that the signal G and I are singlets whereas H contains more than one signal. Also, a pair of small signals seen at ~114.6 ppm (J and K) is generally accepted as arising from chain end units, though spectra in the literature confirming this for PVDF are sparse. The signals arising from CF_2H type end-groups (~-114 ppm, J, K L and M) are broad and unresolved (figure 2.1 c). However the proton decoupled spectrum (figure 2.2 c) of this region shows a doublet for the signals L and M ~-114.9 ppm with a 43 Hz $^{3}J_{F\text{-}F}$ coupling. The signals ~-113.78 ppm, J and K, were more resolved in the decoupled spectrum but still complex. Therefore it was of interest to investigate these signals in order to establish end group-content and signals associated with them. Integration of the peaks E and D gave a reverse-group content of 5.5%, calculated by the method of Russo [10].

$$\text{Reverse units (\%)} = \left[\frac{1}{2}(E+D+L)/100 \times TOTAL\right]$$

Where

$$TOTAL = (A=A') + (H\text{-}T) + F = B+C+G+H+I+J+K$$

2.3 ^{19}F correlation Spectroscopy of PVDF

The next step was to establish ^{19}F -^{19}F-connectivity using correlated spectroscopy. The observed cross-peaks are generally consistent with earlier two-dimensional work [1, 4]. Figures 2.4a and 2.4b show the ^{1}H-coupled ^{19}F COSY spectrum of PVDF where three- and four-bond J-coupling effects are observed but no longer-range (^{5}J) couplings are detected. For example, the signal B couples to E but not to D. There is correlation between the two reverse signals D and E, but the lack of a strong correlation between D and any other signal confirms the position of D in the reverse unit (figure 2.4a). Again this shows that no ^{5}J coupling exists, as then D would bond to C.

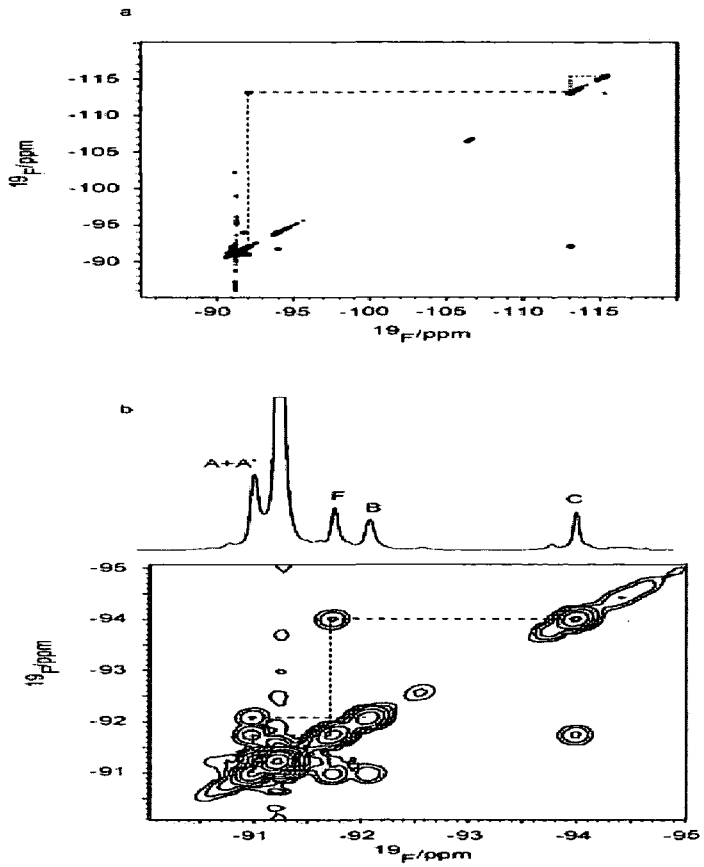

Figure 2.4a and 2.4b. The COSY spectrum of PVDF in DMSO-d_6 at 22°C, figure 2.4a (above), showing the connectivity between the signals B, D and E. Figure 2.4 b shows an enlargement of the main chain region. Note that F and C are correlated (on the same side of the reverse units) whilst B is not coupled to either. Also, B and F correlate to the same peak A+A'.

Furthermore, the signal B correlates to E in the reverse unit. It can also be seen in figure 2.4b that B correlates to a peak to high frequency of that for the main-chain units A+A', as does the F signal. Therefore A+A' form a composite peak, with cross-peaks to the signals at both –91.75 (F) and –92.09 ppm (B) and twice the intensity of these peaks. Thus the assignment made by Katoh et al. [1] to the CF_2 group can now be extended with the CF_2 group labelled A'. The spectra therefore show signals for 7 CF_2 groups around the reverse-unit position in the chain (figure 2.4b). With regard to the minor signals in the spectra, no off-diagonal correlations between signals around -106 to -107 ppm and any other signal in the spectrum were detected, implying that the relevant fluorines are remote from any other fluorine atoms.

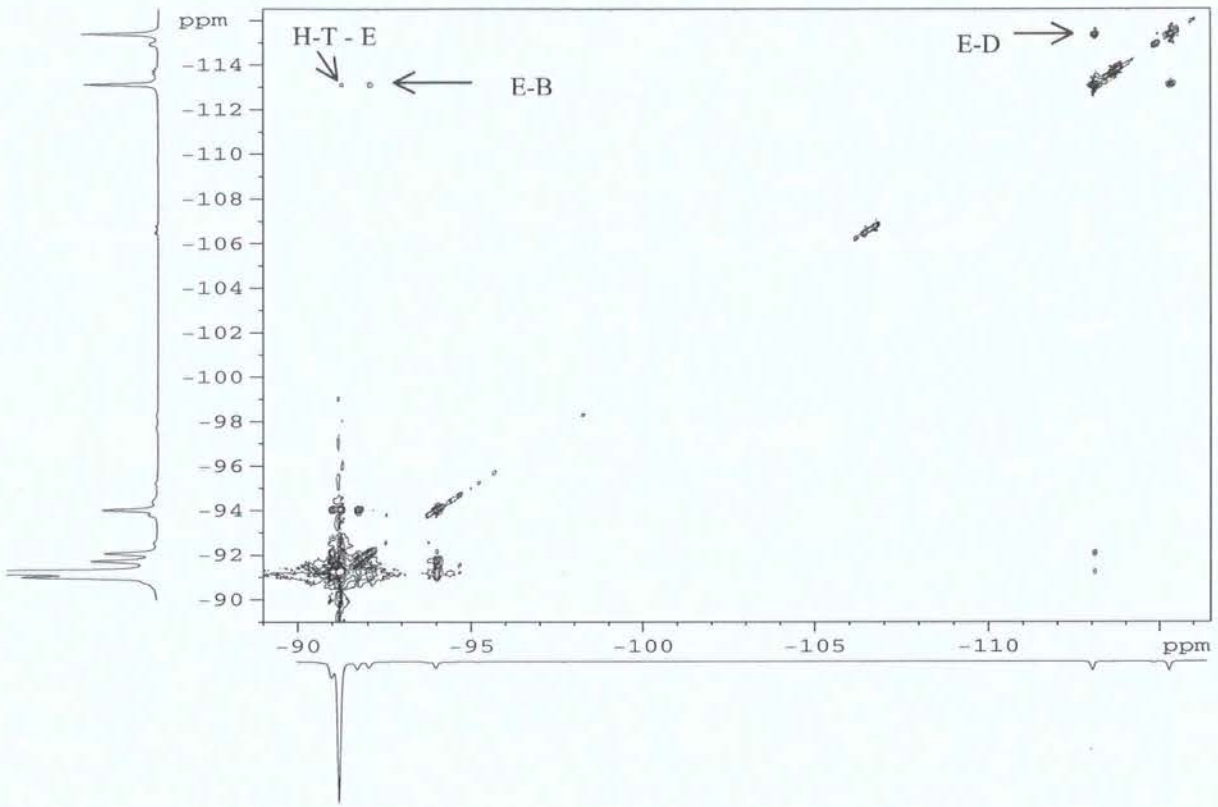

Figure 2.5 The 19F TOCSY experiment of PVDF in DMSO-d_6 at 22°C

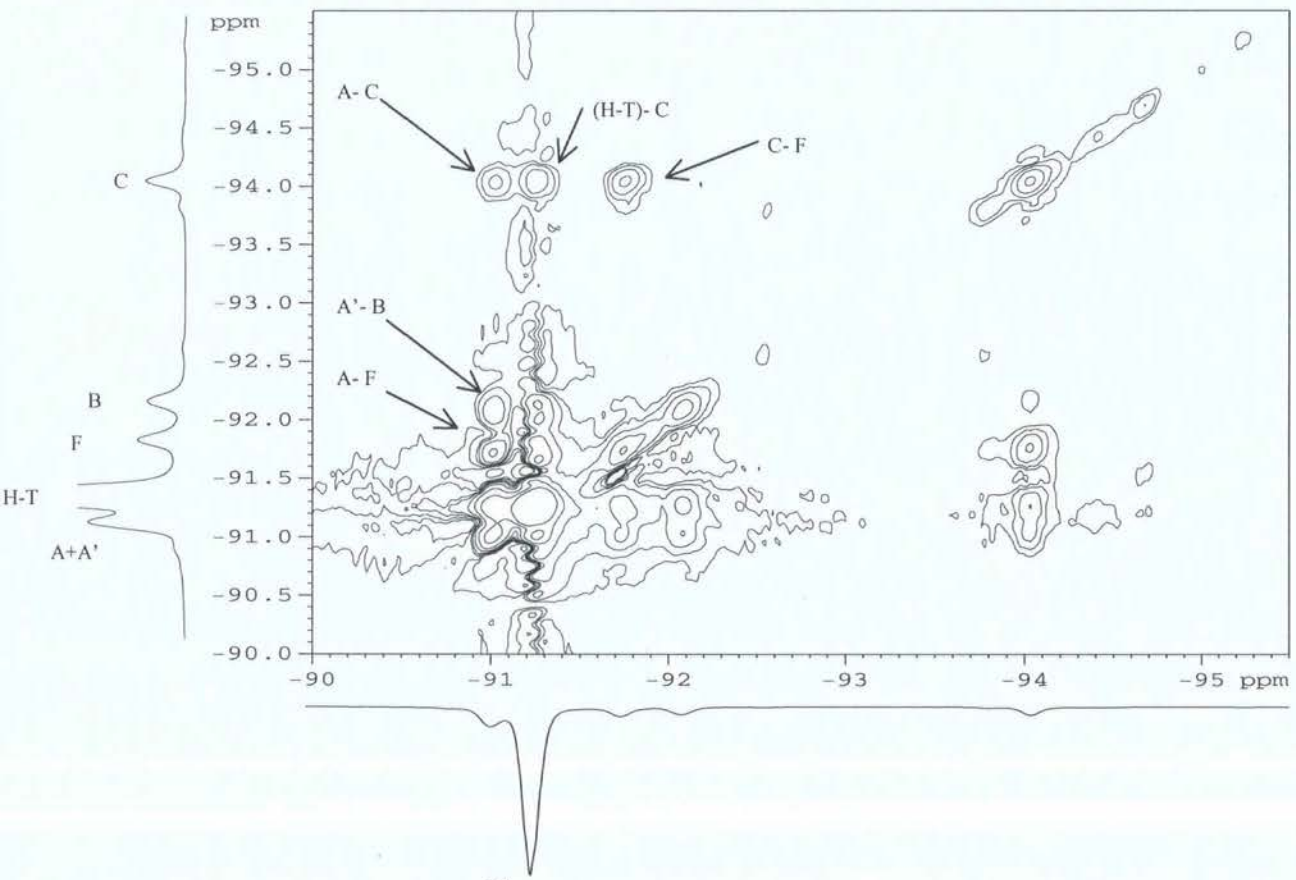

Figure 2.6 Expansion of ^{19}F TOCSY of PVDF in DMSO-d_6 at 22°C

To further investigate the structure of PVDF, total correlation spectroscopy (TOCSY) was used. As in the COSY experiment this gives homonuclear correlation based on scalar couplings, but also correlation between spins within the same spin system even if they have no coupling to each other. As the COSY experiment showed no coupling for the signals at ~-106 to -107 ppm, the TOCSY experiment could provide information on the spin system of these signals i.e. which spin system there belong to. Chemical shifts are listed in table 1. In figure 2.5 the reverse unit signal E, shares the same spin system as B and D, verifying the COSY assignments of these signals. It also shows that E correlates with the main chain (H-T). However the signal D still only correlates to E, which would mean that it is only shares the same spin system with E. Although several mixing times ranging from 20-80 ms were tried, no other off diagonal intensity was observed from this signal. From figure 2.6 it is clear that the signal A+A', which only showed coupling to the main chain (H-T) and F in the COSY spectrum, gives off diagonal intensities to F, B and C and therefore has a shared spin system with A-F, A-C and C-F. This verifies the composite nature of the A+Á signal, with B showing coupling to A' and E. Correlation for the signals ~ -106 to –107 ppm were not observed in either the COSY or TOCSY experiments. The same is also true for the signals J, K, L, and M.

This differs from the work by Pianca et al. [4], since these authors proposed end-groups of the type $CH_3CF_2CF_2CH_2$ for the peaks near – 107 ppm. It is worthy of note that they were dealing with low molar mass PVDF, whereas our samples have high molar mass. Our results suggest the assignment of the -106 to -107 ppm peak to branching points, such as $-CH_2CF_2CH(CF_2CH_2-)CF_2CH_2-$, which has been previously deduced [4, 11, 12] by use of empirical rules for chemical shifts. They could also arise from impurities from the mode of synthesis.

2.4. ^{1}H Solution-state Spectroscopy

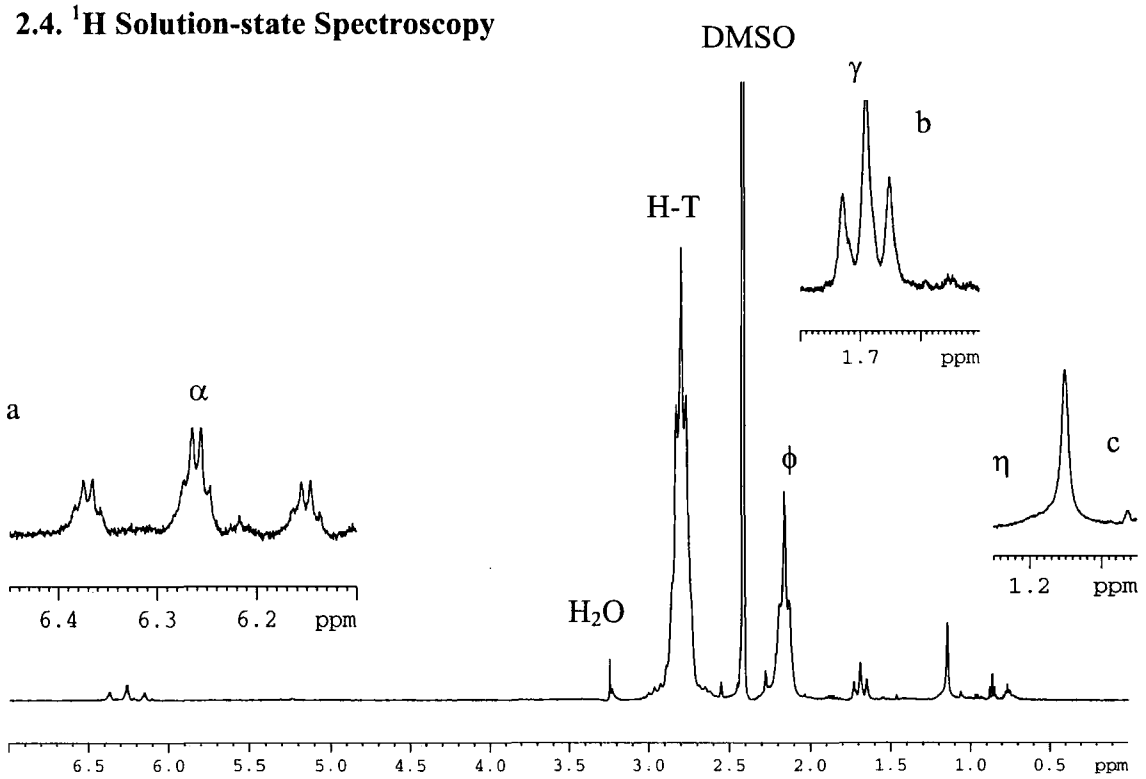

Figure 2.7 The ^{1}H spectrum of PVDF with a water pre-saturation pulse in DMSO-d_6 at 22°C

The fluorine-coupled proton spectrum of PVDF is shown in figure 2.7 with assignments in table 3. Major signals show a triplet of quartets for the $-CF_2H$ end group at 6.26 ppm with 4.5 Hz $^3J_{H-H}$ and a 55.5 Hz $^2J_{H-F}$, figure 2.8 a. The main chain CH_2-CF_2 (H-T) gives a quintet at 2.8 ppm with 16 Hz $^3J_{H-F}$ coupling [13, 14, but it is not first order and the signal contains further coupling which is not resolved. The triplet at 2.26 ppm which is assigned to CF_2-CH_2-CH_2-CF_2 of the reverse units. This signal seems to be somewhat intense and is accidentally degenerate. A further triplet is seen at 1.69 ppm (figure 2.7b) with a 19Hz $^3J_{H-F}$ which could be CH_3-CF_2- end groups. To simplify the spectrum and verify fluorine to proton coupling, a ^{19}F decoupled proton spectrum was acquired and is shown in figure 2.8.

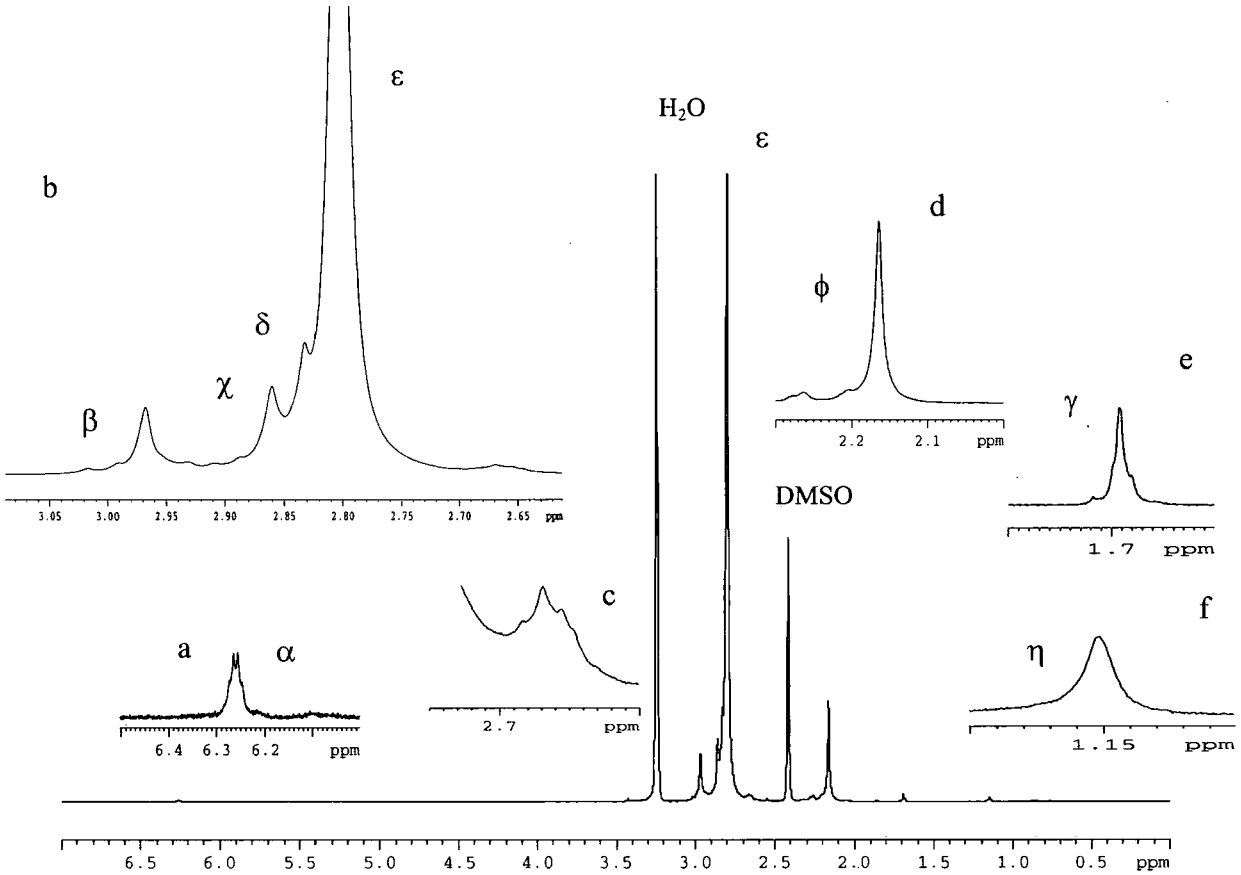

Figure 2.8 The ^{1}H Fluorine decoupled spectrum of PVDF in DMSO-d_6 at 22°C with expansion a-f. Greek letters are the proton assignments in table 2.

The triplet of quartets now only shows one quartet at 6.26 ppm, figure 2.8a. We know from our own experiments on VDF (chapter 4) that a triplet of triplets with the same coupling values and chemical shift represents a CH_2-CF_2H end group. This would mean that the signal here could represent a CH_3-CF_2H molecule, which would have to be present as an occlusion compound in solid PVDF. This would, however, be highly unlikely as this molecule would be very volatile having a boiling point of –25 °C. Furthermore no connectivity was seen in the COSY experiment figure 2.4 though it should be noted that these signal are very low in intensity. The peak at 3.33 ppm is the H_2O signal, which was suppressed in figure 2.7.The region around 3.0 ppm is now more resolved due to the fluorine decoupling and shows signals at 2.98 (α), 2.87 (χ) and 2.83 (δ) ppm, figure 2.7b. Figure 2.8c shows a signal at 2.67 ppm but this is still unresolved and no assignment is made here. The main chain CH_2-CF_2 is now a singlet (at 2.80 ppm), as is the signal for the reverse unit at 2.16 ppm. Figure 2.9 e shows a multiplet at 1.69 ppm tentatively assigned to end chain CF_2-CH_3. The signal at 1.15 ppm, which is a singlet in both proton spectra, is identified in the literature [13] as tert-

butyl alcohol and is probably the reactant product of tert-butyl-peroxide used as the radical initator. The alcohol proton has a chemical shift similar to that of the main chain

δ_H/ppm (solution)		Assignment and coupling constants in Hz
6.26	t q	$^3J_{H-H}$ 4.27 $^2J_{H-F}$ 54.7
3.25	s	H_2O
2.80	t	$^3J_{H-F}$ 15 CH_2-CF_2
2.67	quintet	$^3J_{H-F}$ 1.92 not assigned
2.42	quintet	DMSO-d_6
2.16	t	$^3J_{H-F}$ 15 CH_2-CH_2
1.69	t	$^3J_{H-F}$ 19 CF_2-CH_3
1.15	s	$(CH_3)_3$-COH
0.86	t	$^3J_{H-H}$ 7.5 CH_2-CH_3
0.77	m	Not assigned

Table 2 The ^1H (^{19}F coupled) chemical shifts of PVDF in DMSO-d_6 at 22°C. Multiplicities are q=quartet t=triplet, d=doublet, s=singlet and m=multiplet.

δ_H/ppm (solution)		Assignment and coupling constants in Hz
6.26	q	α $^3J_{H-H}$ 4.27 –CF_2H
3.25	s	H_2O
2.98	s	β D-E-CH_2-B
2.87	s	χ B-CH_2-A'
2.83	s	δ F-CH_2-C
2.80	s	ε CH_2-CF_2 Main chain
2.67	quintet	Unresolved and not assigned
2.42	quintet	DMSO-d_6
2.16	s	ϕ CH_2-CH_2 Reverse units
1.69	m	γ CF_2-CH_3
1.15	s	η $(CH_3)_3$-COH
0.86	t	ι $^3J_{H-H}$ 7.5 CH_2-CH_3
0.77	m	Not assigned

Table 3 The ^1H (^{19}F decoupled) chemical shifts of PVDF in DMSO-d_6 at 22°C. Multiplicities are q=quartet t=triplet, d=dubblet, s=singlet and m=multiplet. A, B, C, D, E, F refer to CF_2 assignments figure 4

protons and only a signal intensity of 1/9 of the tert-butyl CH_3 protons and would therefore not be observerd.The signal at 0.86 ppm (ι) is a triplet in both the fluorine coupled and decoupled proton spectra and is assigned to CH_2-CH_3 end groups. The corresponding CH_2 is not seen probably due to overlap and low intensity. A multiplet is seen at 0.77 ppm but no further information could be extracted from this signal.

2.5 Heteronuclear ^{19}F-^{1}H spectroscopy.

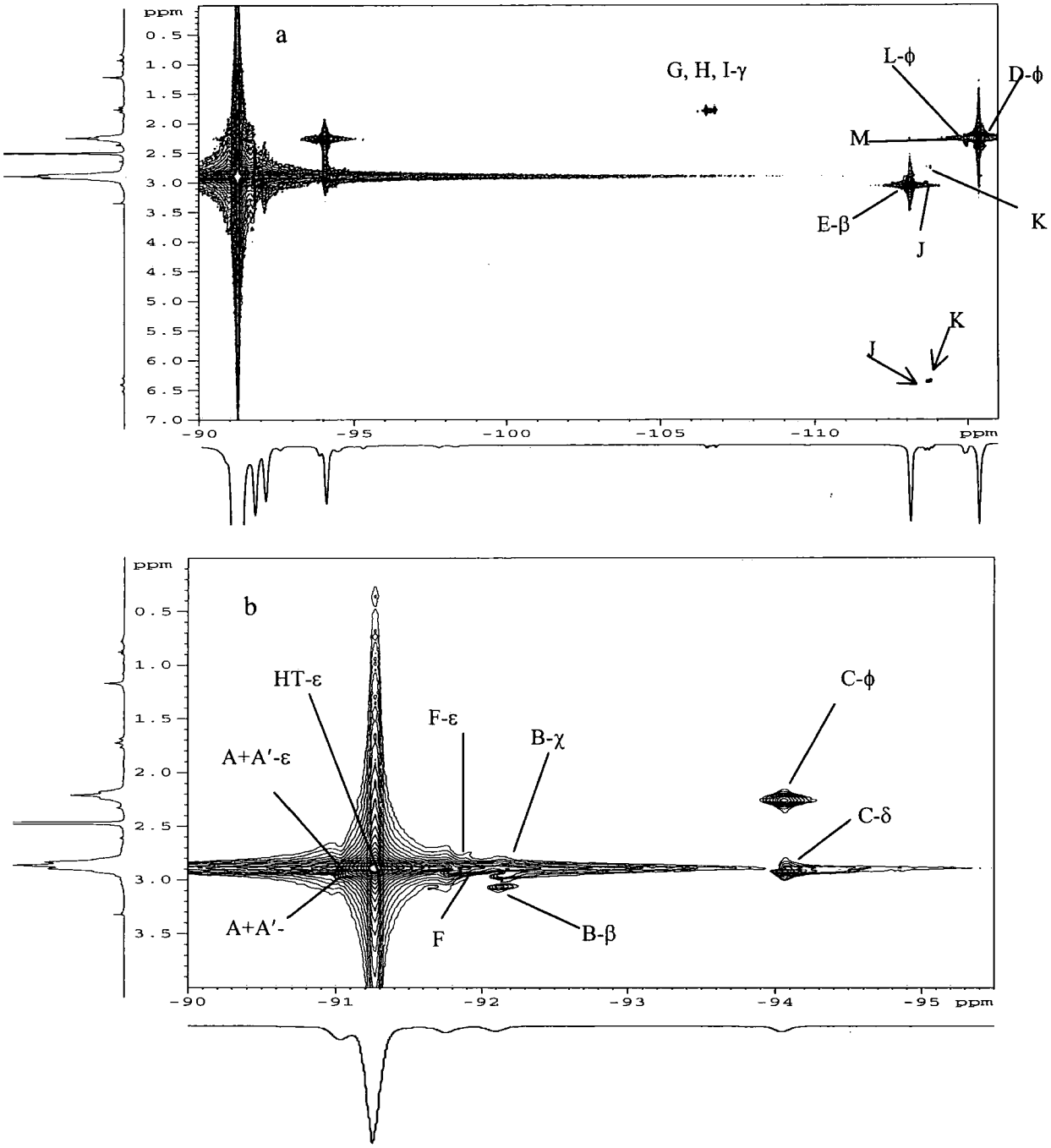

Figure 2.9 The ^{19}F-^{1}H Heteronuclear-correlated spectrum of PVDF in DMSO-d_6 at 22°C (a) and expansion (b)

Figure 2.9a and 2.b show the result of the heteronuclear ^{19}F-^{1}H correlation experiment. Here the ^{19}F-^{1}H coupling has been specifically selected to 30 Hz by arraying the mixing time. A typical $^{3}J_{FH}$ is ~17Hz (trans) and ~6 Hz (cis). The information retrieved shows which proton correlates to which fluorine. Table 3 shows the correlation, with chemical shifts and the ^{19}F – ^{1}H coupling constants from the one-dimensional spectra figures 2.2, 2.8 and table 2. Hence, a proton signal can be assigned to a specific fluorine signal.

δ_F/ppm (solution)		δ_H/ppm (solution)	Assignment
-90.02	A+A'	2.81 ε and 2.87 χ	$-CH_2-CF_2-$ main chain
-91.25	H-T	2.81 ε	$-CH_2-CF_2-$ main chain
-91.76	F	2.81 ε and 2.83 δ	$-CH_2-CF_2-$ main chain
-92.09	B	2.98 β and 2.87 χ	$-CF_2-CH_2-CF_2-CH_2-CF_2-$
-94.05	C	2.83 δ and 2.16 ϕ	$-CF_2-CH_2-CF_2-$ CH_2-CH_2-
-106.48	G	1.69 γ	$-CF_2-CH_3$
-106.62	H	1.69 γ	$-CF_2-CH_3$
-106.77	I	1.69 γ	$-CF_2-CH_3$
-113.11	E	2.98 β	CH_2- $CH_2-CF_2-CF_2-CH_2$
-113.66	J	6.26 α and 2.92	Not assigned
-113.78	K	6.26 α and 2.67	Not assigned
-114.87	L	2.16 ϕ	Not assigned
-114.97	M	2.24	Not assigned
-115.39	D	2.16 ϕ	$-CH_2-CH_2-CF_2-CF_2-CH_2$

Table 3 ^1H and ^{19}F chemical shift correlation of PVDF in DMSO-d_6 at 22°C from the heteronuclear correlation spectrum figure 2.9. Proton and fluorine chemical shift values are from the decoupled spectra figures 2.8 and 2.3 respectively and assignments are in bold characters.

The ^{19}F signals A+A', H-T, and F all show correlation to the main chain CH_2 proton at 2.81 ppm. The ^{19}F signal B at –92.09ppm correlates to two proton signals at 2.98 and 2.87 ppm. The signal E at –113.11 also correlates to the proton signal at 2.98 ppm.
The signal C correlates to the reverse unit CH_2 at 2.16 ppm, as does the signal D, and to adjacent protons at 2.83 ppm verifying the position of the reverse unit $-CH_2-CH_2-$. The signals J and K have chemical shift values normally attributed to chain end groups show correlation to the same chain end proton signals, a triplet of quartets at 6.26 ppm. However J has further coupling to a proton signal at 2.92 ppm whereas K couples to a proton signal at 2.67 ppm in the proton spectra figure 2.9 c, both unresolved. The fact that these two fluorine shifts, typical of chain end groups also correlate to the same protons, the triplet of quartets at 6.26 ppm, suggests that several very similar chain-end groups could be present. Although I have assigned the signal at 0.86 ppm (ι) to $-CH_2-CH_3$ from the literature a few comments should be made on this point. No correlation

was seen for these protons in the HETCOR experiment, but there was correlation in the proton COSY with the singlet at 1.15ppm. Furthermore, proton spectra repeated at weekly intervals showed that both of these signals decreased in intensity over time. It would therefore seem that this is signal from a volatile compound or a there is a reaction taking place.

The information from the HETCOR experiment allows the assignment of the fluorine-decoupled proton spectrum figure 2.8 and table 2. The structure of the reverse unit could now be assigned with regard to both proton and fluorine chemical shifts.

2.6. Summary of solution NMR of PVDF

The high molecular weight sample of PVDF has been studied by ^{1}H and ^{19}F solution-state NMR using standard one-dimensional spectroscopy and two-dimensional techniques (COSY, TOCSY and HETCOR). The average cumulated degree of polymerisation ($\overline{DP}_{ncum}$) of PVDF was evaluated by calculating the relevant intensities of the polymer chain backbone signals and the end group at 6.26 ppm from the ^{1}H proton spectrum [15]. For PVDF this gave a $\overline{DP}_{ncum}$ =117, because of the fact that the precise nature of these signals are unknown this value should not be taken as an accurate representation. The integration of the peaks E and D in the ^{19}F spectrum gave a reverse-group content of 5.5%. The structure was identified by chemical shifts, coupling constants and by referring to literature values [1-10]. The proton spectra showed the characteristic normal ($-CF_2-\mathbf{CH_2}-CF_2-$) units at 2.8 ppm and the reverse units ($-CF_2-\mathbf{CH_2}-\mathbf{CH_2}-CF_2-\ CF_2-$) at 2.16 ppm. Both signals were triplets with a 15 Hz $^{3}J_{F-H}$ coupling, which are in agreement with previous work (14). The corresponding structure is found in the ^{19}F spectra (figures 2.2 and 2.3) with signals at –91.25 (H-T) and –113.11 (E) and –115.35 ppm (D) representing ($-CH_2-\mathbf{CF_2}-CH_2-$), ($-CF_2-CH_2-CH_2-CF_2-\ \mathbf{CF_2}-$) and ($-CF_2-CH_2-CH_2-\mathbf{CF_2}-\ CF_2-$) respectively.

The ^{19}F signals at –113.87 (L) and –114.97 (M) ppm in figure 2.2 show as multiples but in the ^{1}H-decoupled spectrum (figure 2.3) as two broad singlets. From the HETCOR experiment (figure 10 a) the signal (L) correlated to a proton resonance at 2.16 ppm, typical of reverse units, and (M) to a proton signal at 2.24 ppm. Furthermore, no coupling for these signals was evident to any other species in the COSY or the TOCSY experiments showing that they were not related to the same spin system as the major signals. They were therefore judged not to be related to the main structure of PVDF.

The signals in the –106 to -107 ppm region, G and I, both gave a quartet whereas the signal H is a poorly defined multiplet (figure 2.2). In the proton-decoupled spectrum

(figure 2.3) G and I gave singlets and H a broad signal. We have earlier (16) proposed the assignment of these signals to branch points. However there were all found to correlate to a triplet in the proton spectrum at 1.69 ppm (γ), with a ^{1}H-^{19}F coupling constant of 19 Hz and identified as arising from CF_2-CH_3 end-groups. No ^{19}F coupling was evident in the COSY or TOCSY, spectra suggesting that these end-groups may be remote from any other main chain fluorine groups. The findings of Pianca et.al [4], who reported ^{19}F coupling for signals at –107.8 and –114.3 ppm for low molecular weight PVDF (though not evident in the reported spectra) and assigned them to end-groups - CH_2-CF_2-CF_2-CH_3, are not verified here for high molecular weight PVDF, as ^{19}F-^{19}F coupling would be expected for this species.

All fluorine signals A, Á B, C (figure 2.2 and 2.3) related to the main chain showed $^{3}J_{HF}$ 15Hz coupling (table 2). The position of C at –94.05 ppm, assigned to CF_2 groups adjacent to the reverse unit, is verified in the HETCOR spectrum (figure 2.9 b) as it correlates to protons at 2.16 and 2.84 ppm, arising from reverse and main-chain protons respectively (table 3). The ^{19}F signal B at –92.09ppm is seen to correlate at a proton shift at 2.87 ppm. From the above information the following structural entities of PVDF were deduced.

ε A ε F δ C ϕ ϕ D E β B χ Á ε
-CH_2-CF_2-CH_2-CF_2-CH_2-CF_2-CH_2-CH_2-CF_2-CF_2-CH_2-CF_2-CH_2- CF_2-CH_2-

-CF_2-CH_3 -CH_2-CH_3

Figure 2.10 Suggestion **for** structural units of main chain PVDF and end-groups from the solution-state NMR data.

References

[1] Katoh E, Ogura. K, Ando. I, Polym I, 12, 1994, 1352

[2] Herman, Toshiyuki. U, Astushi. K, Susumu. U, Takeshi. K, Norimasa. O, Polymer 38, 1997, 167.

[3] Pianca M, Barchiesi. E, Esposto. G, Radice S, Fluorine Chem, 95, 1999, 71.

[4] Cais R, Kometani J.M, Macromolecules, 18, 1985, 1354.

[5] Ferguson RC, Brame Ir. EG, Phys Chem, 83, 1979, 1397

[6] Cais RE, Sloane NIA. Polymer, 24, 1983, 179.

[7] Cais RE, Kometani 1M. Macromolecules, 17, 1984, 1887

[8] Ferguson RC, Ovenall DW. Polym Prepr ACS Polym Chern, 25, 1984, 340

[9] Lutringer G, Meurer B, Weill G. Polymer, 32, 1990, 884.

[10] Russo S, Behari I, Chengji S, Pianca M, Barchiesi E, Moggi G. Polymer, 34, 1993,

651

[11] Yu H, Mil, Ni H. Chin I Microwave Radiofreq Spectrosc, 1, 1984, 372.

[12] Murascheva YeM, Shasbkov AS, Dontsov AA. Polym Sci USSR, 23, 1981, 711.

[13] M. Duc, B. Ameduri, B. Boutevin, M. Kharroubi, and J-M. Sage, Macromol. Chem. Phys. 199 (1998) 1271.

[14] Balague J, Ameduri B, Boutevin B, Caporiccio G. J. Fluor. Chem, 70, 1995, 215-223

[15] Saint-Loup R, Ameduri B, J. Fluor. Chem. 116, 20002, 27-34

[16]P. Wormald, D.C. Apperley, F. Beaume, and R.K. Harris, Polymer. 44 (2003) 643.

Chapter 3

Solid-state NMR of PVDF

3.1 Review of ^{19}F Solid-State NMR and PVDF.

Poly(vinylidenefluoride) crystallises into four polymorphs, α, β, γ and δ, depending upon the thermal treatment administered. The unit cell of the lattice of α PVDF consists of two chains in the tg+ tg- conformation. The electric dipole components are mutually antiparallel and therefore neutralise each other; hence it exhibits non-polar behaviour. A polar analogue to α PVDF is δ PVDF, which has a tttg+ tttg- conformation and is formed by the application of a high electric field [1]. This involves the rotation of every second chain by 180° about the chain axis whereby their dipole moments point in the same direction. The most highly polar phase is the β phase. Its unit cell consists of two all-trans chains packed with their dipole moments pointing in the same direction figure 3.1.

Studies by X-ray diffraction and solid-state nuclear magnetic resonance (NMR) spectroscopy [2, 3] have shown that when thermally treated and drawn, a blend of the α and β phases is inevitable. Transitions between polymorphs have been studied by a combination of differential scanning calorimetry (DSC), infrared spectroscopy and X-ray diffraction techniques [4, 5]. These experiments showed that the α to β transition was most efficient between 70 and 90 °C during drawing. The majority of researchers have concentrated their attention on the β polymorph because of its piezo- and pyro-electrical properties, giving subsequent industrial usage. However, these properties are affected by the presence of regiodefective, so-called reverse units (see below). Lovinger, showed that the sample temperature and the mole percentage of the reverse units were fundamental to the α/β ratio and thereby the physical properties of the material [6].

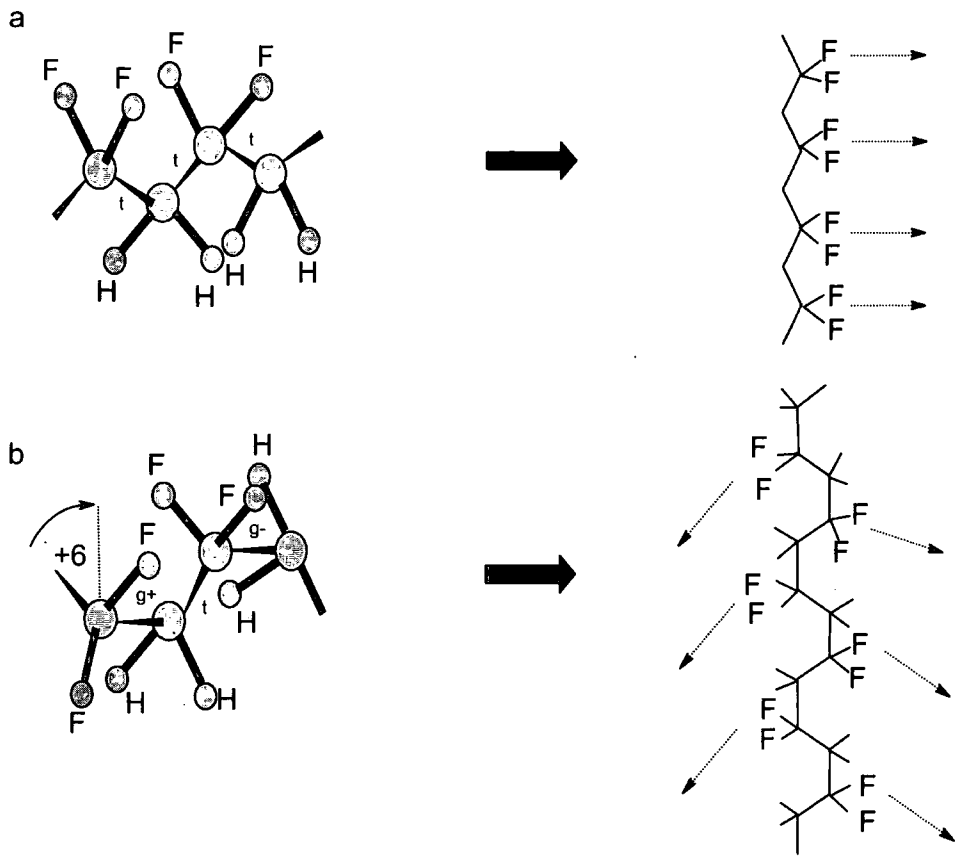

Figure 3.1 Schematic representation of the chain segments of the most common crystalline chain formations in PVDF: a, ttt (all trans) and b, g^+tg^- conformation. The arrows in the diagram on the far right indicate projections of the $-CF_2$ dipole directions in planes defined by the carbon backbone. The g^+tg^- conformation has dipole moments perpendicular and parallel to the chain axis, while the trans conformation has all dipoles normal to the molecular axis.

Solid-state magic-angle spinning NMR has been shown to be an important technique for the characterisation of polymer morphology [7]. Holstein et al. showed that solid-state ^{19}F NMR together with high-power ^1H decoupling gives increased chemical shift resolution for PVDF [8]. Differences in relaxation behaviour of the crystalline and amorphous phases were used to edit the spectrum, thus revealing important details about the morphology of the material. In a later work from the same group [9] these differences in relaxation behaviour were utilised for domain selection in spin-diffusion experiments. The measurement of domain sizes and their dependence on the contact time during cross-polarisation MAS experiments incorporating relaxation filters was compared and found to be in agreement with static domain size measurements [9, 10, 11]. Ando et al. [12] have also used solid-state NMR to study PVDF, putting emphasis on understanding the cross-polarization behaviour between two abundant spin systems.

Scheler [13] proved that magic-angle spinning at 35 kHz effectively suppressed heteronuclear (H, F) dipolar interactions without the need for proton decoupling. He also used radio frequency driven recoupling (RFDR) [14] with high-speed magic-angle spinning and showed that the reverse units had a spin exchange with the amorphous region. No exchange between the crystalline and reverse units was detected, nor between signals for the two reverse units, suggesting that these bands originate from different types of fluorines which are separated in space. Su and Tzou [15] also applied fast MAS ^{19}F NMR to PVDF.

Effects of the thermal history of a polymer and the role of the interface regions or crystal surfaces form a highly debated question in polymer material chemistry.

These phenomena are observed in PVDF by differential scanning calorimetry and will be discussed in chapter 6.

3.2 Solid-state spectra of PVDF

To reference the spectra, a rotor insert was filled with liquid C_6F_6 and inserted in to a silica nitride rotor with vespel drive and end caps. No spinning was applied and the probe was then tuned. It should be noted here that the pre-probe filters were purpose built by Goss electronics to provide sufficient separation between the fluorine and proton frequencies. A spectral width of 100 kHz and recycle time of 1 second was used to acquire a spectrum of C_6F_6. The pulse duration was then arrayed and the value for a 90° pulse established. The single ^{19}F resonance line of C_6F_6 is referenced as –166.4 ppm relative to the signal for $CFCl_3$. Silica nitride rotors were packed with PVDF and sealed with a vespel drive tip and end cap. The spinning speed was set to 14 kHz and both the fluorine and proton channels were tuned.

The 90° pulse was then re-established for the solid PVDF (see section 1:4) and the recycle delay time arrayed to establish the condition for maximum signal. Typically 128 acquisitions were collected.

The direct-polarisation ^{19}F $\{^1H\}$ solid-state NMR spectrum of Kynar 301F is shown in figure 2.5 and the chemical shifts are summarised in Table 2. A proton – fluorine cross polarisation (CP) experiment was undertaken in order to compare signal intensities with the direct polarisation (DP). As no advantage in signal intensity or spectral resolution was recorded and the direct polarisation spectra are quantitative, the direct polarisation experiment was used through out the ensuing investigation. A proton-decoupling field of

85 kHz was used to remove most, if not all, of the effects from heteronuclear (H, F) coupling [10].

The signal in the solid-state spectrum of PVDF at –91.2 ppm is at a comparable position to the solution state signal at –91.26 ppm, figure 2.2, and is therefore assigned to the main polymer chain in the amorphous domain, along with the chemical shifts for the reverse units R1 and R2 at –113.8 ppm and –114.9 ppm respectively.

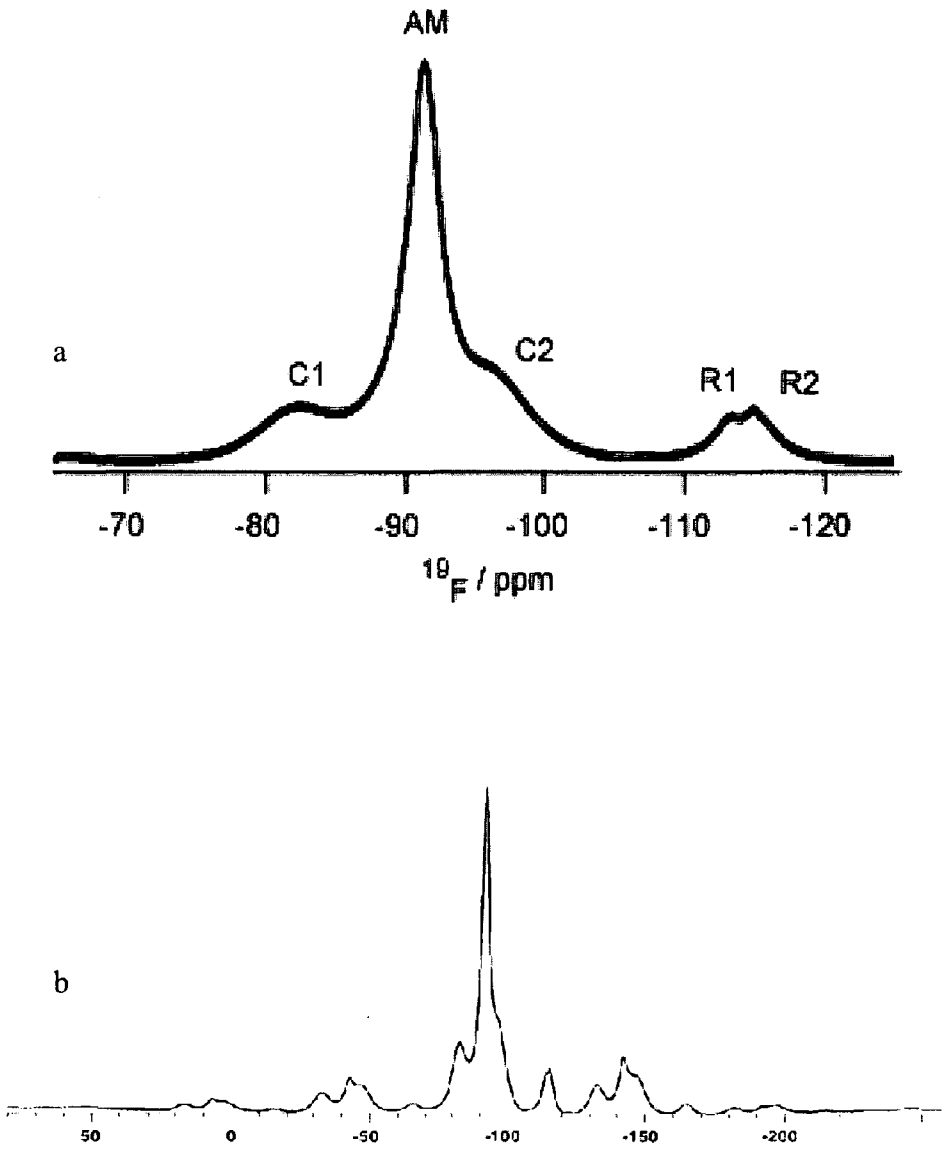

Figure 3.2 (a) The solid-state proton-decoupled ^{19}F direct polarization MAS spectrum of PVDF recorded at 14 kHz spin rate. The crystalline signals are labelled C1 and C2, along with a signal from the amorphous region AM, and the reverse units R1 and R2. (b) shows the full spectrum of PVDF with spinning sidebands at 8kHz ^{19}F-^{19}F dipolar strength.

δ_F/ppm (solid)	Assignment
-82.1	Crystalline domains
-91.2	Amorphous domains
-95.6	Crystalline domains
~-107	Chain branching?
-113.8	Reverse unit
-114.9	Reverse unit
~-115	$-CH_2CF_2H$ end groups?

Table 1 The chemical shifts of PVDF from the solid-state proton-decoupled ^{19}F direct polarization MAS spectrum of PVDF recorded at 14 kHz spin rate, figure 3.3.

The main difference between the solution and solid-state spectra, apart from the resolution, is the introduction of two broad signals belonging to the crystalline domain at –82.1 and 95.6 ppm. The difference in the chemical shift of these signals lies in the fluorine gauche (-82.1 ppm) and trans (–95.6 ppm) configuration in α PVDF. From the spectrum in figure 3.2a it can be seen that these two crystalline signals C1 and C2 (at –82.1 and –95.6 ppm respectively) have different signal intensities. However, the increase in the signal intensity of the trans signal is probably due to signals from the CF_2 units in close proximity to the reverse units such as F, B and C seen in chapter 2 figure 2.1 and figure 2.2, which all have similar chemical shifts to the trans signal, yet different from the main chain CF_2 chemical shift at –91.2 ppm. The R1 (–113.8 ppm) and R2 (–114.9 ppm) signals are assigned to reverse units, and direct integration of the whole solid-state DP spectrum (including spinning sidebands) gives the combined intensity of these signals as 9.3 %, implying a reverse-unit content of 4.7% (compared to a value of 5.5% obtained from solution-state NMR spectra in chapter 2).

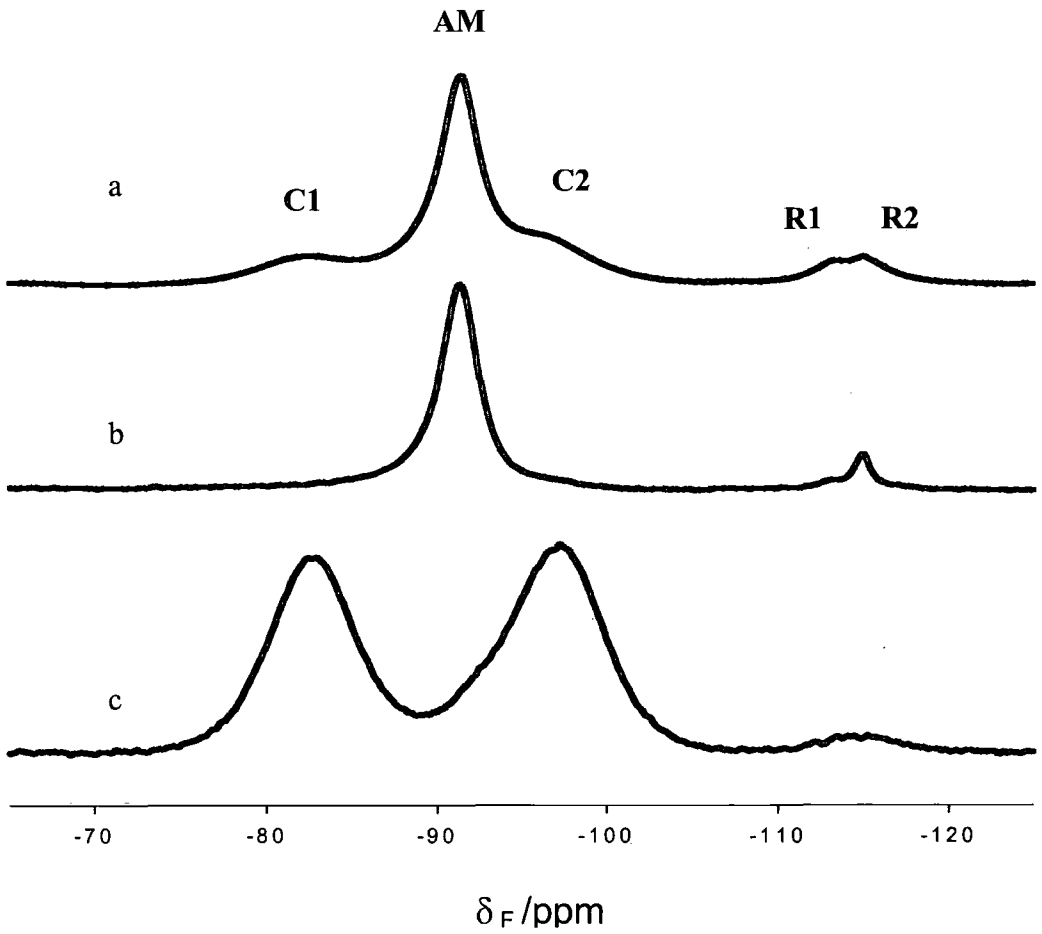

Figure 3.3 ^{19}F direct polarisation spectra of PVDF recorded at 60°C (a) direct polarisation; (b) direct polarisation with dipolar filter; and (c) direct polarisation with 25 ms spin lock.

A dipolar filter [15] suppresses signals from strongly dipolar-coupled species (figure 3.3 b). It is, therefore, expected to remove signals originating from relatively rigid material (i.e. crystalline domains). In this experiment all fluorine dipolar-coupling interactions are converged. If the time between the pulses is long (7-20 μs), the averaging is not effective for large dipolar interactions, i.e. rigid domains, and the magnetisation of the corresponding fluorines then relaxes. The remaining magnetisation belongs to fluorines with small dipolar interactions as a result of partial averaging due to high molecular mobility, i.e. the amorphous domain. The set up for this experiment is made by arraying the number of loops (n), which regulates the extent of suppression of the dipolar interaction selecting the signal. Figure 3.2b shows the result of such an experiment. The

signals C1 and C2 are suppressed and are therefore assigned to the crystalline material of α PVDF in accordance with the literature [1, 6, 9]. The remaining intense signal at –92.1 ppm is confirmed as being associated with the amorphous material, in which sufficient molecular motion results in partial averaging of the dipolar coupling. The behaviour of the R1 and R2 signals in this experiment proved to be complex.

Fast MAS should, in principle, remove the ^{19}F-^{19}F homonuclear dipolar coupling. However, the spin rate used here does not do that completely, as the dipolar filter would probably then not have any effect. The result of a $T_{1\rho}$ experiment is shown in figure 3.3 c, were a single spin-lock time of 25 ms was used and a spectrum of the rigid domain acquired. The fluorine gauche (-82.1 ppm) and trans (–95.6 ppm) configuration in α PVDF is seen and that these two crystalline signals C1 and C2 now have equal intensities.

3.3. Relaxation, motion and morphology.

As explained in section 1.3 there are two distinct relaxation processes describing the return to equilibrium of magnetisation after a radio frequency pulse: one via the lattice, T_1, and the second by transverse relaxation, T_2. By applying the appropriate pulse sequences, the decay or growth of the signal can be measured.

To measure T_1, the spins are disturbed from thermal equilibrium and then monitored during their return to thermal equilibrium. The inverse-recovery sequence, (180°-τ- 90°) inverts the spin population with a 180° pulse. The magnetisation vector now aligned in the –z-axis will return to the z-axis towards the x-y plane at a rate dictated by T_1. As magnetisation cannot de detected in the z –axis the recovery is monitored by placing the vector in the x-y plane using a 90° pulse after a period τ. Repetition of the experiment with increasing values of τ allows observation of the spins relaxation behaviour. When τ is sufficiently long ($\tau_\infty = 5T_1$) complete relaxation is achieved between the pulses and maximum positive signal is recorded.

However the spin-lattice relaxation can be measured in the rotating frame and is then called $T_{1\rho}$. Here a $(\pi/2)_x$ pulse is applied followed by a spin lock pulse (see section 1.4). This second pulse of a given power and duration (τ), locks the magnetisation along the y-axis in the rotating frame (B_{1y}). During this spin-lock time dephasing of magnetisation takes place. If the duration of the spin-lock time is varied, between 0.03 to 40 ms in this

case, spectra containing signals of specific components can be recorded and the decay measured. The spin-lattice relaxation in the rotating frame is often exponential according to $M_y(\tau) = M_0 \exp(-\tau/T_{1\rho})$. In this manner the $T_{1\rho}$ can be measured for all components of the spectrum, table 5.

The effect of the strength of this spin-locking field is seen in figure 3.4, which shows how increasing B_{1y} influences the $T_{1\rho}$ relaxation values of the components in PVDF. In figure 3.4, an increase in the $T_{1\rho}$ (F) value is seen for all components as the B_{1y} field increases from 30 kHz to ~70 kHz. Above 70 kHz, a separation in the relaxation times of the crystalline, the amorphous and reverse unit components are seen. A substantial separation is reached around 80 kHz. This is due to the difference in the $T_{1\rho}$ of the crystalline and amorphous regions and reflects their molecular mobility's, the crystalline regions being more rigid than the amorphous region. On the basis of these observations a spin-lock field was applied at 80 kHz in later work, giving ample differentiation in the relaxation times of these components.

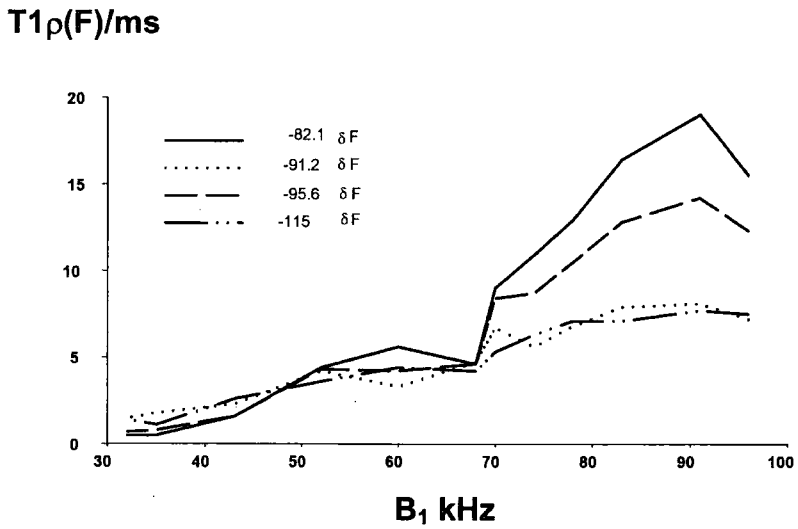

Figure 3.3 The effect of increasing B_1 field on the relaxation rates of the individual ^{19}F spectral components of PVDF.

The Carr-Purcell-Meiboom-Gill (CPMG) pulse sequence was used to measure T_2 relaxation, which gives information on the low frequency motion of the polymer. This measurement is, however, not as simplistic as it may seem. The problem with measuring the T_2 relaxation is that it is inhomogeneous. The free induction decay consists of contributions of spins precessing at different frequencies, which destroys phase-

coherence. This is caused by spin-spin relaxation through intra or inter-molecular magnetic fields and also inhomogeneity in the B_0 field. Furthermore, T_2 is strongly dependent on the MAS frequency since it relates to linewidths. As the width of the NMR signal is dependent on these factors it is of interest to separate them. This separation is achieved by the CPMG sequence, which is shown in chapter 1 diagram 1.14 e. In this pulse sequence a 90° pulse is followed by a spin echo (180° pulse) with a varying time delay τ. The decay of the signal intensity of the echo is then measured and the rate of decay calculated. The purpose of the spin echo is to refocus the dephasing of spins due to sample inhomogeneities.

Another simple method, which can be used to measure the long time transverse relaxation time is the direct polarisation delayed acquisition (DPDA) [20] pulse sequence. Here a delay of 4 ms between a 90° pulse and acquisition gives signals from highly mobile species with long T_2 relaxation. Varying the acquisition delay allows measurement of the signal decay in a similar manner to the CPMG experiment and gave similar results as would be expected.

So what is the point of measuring these relaxation parameters for a polymer? The reason is that structural and motional information can be obtained due to the fact that different domains and structural entities have different relaxation timescales.

These above three different types of relaxation (T_1, $T1_\rho$ and T_2) provide specific information about structure and motional dynamics of the material and allow utilisation of pulse programs incorporating relaxation filters. The main difference in the information retrieved is that the frequencies of molecular motion (MHz for T_1, kHz for $T_{1\rho}$ and low-frequency motion from T_2) are probed on different timescales. Typical time scales are T_1 = seconds to days, giving information on bulk magnetisation, $T_{1\rho}$ = milliseconds which gives relaxation in the rotating frame and can be used to select molecular domains by spin-locking and T_2 micro to milliseconds giving information on mobility and amorphous domains. The pathway for relaxation in solids is usually dictated by the dipole-dipole interaction between spins, which is greater in more rigid domains than mobile domains.

3.4. Results of the relaxation measurements.

The T_1 relaxation for PVDF was measured by the inverse recovery-method and assuming exponential relaxation. Here the growth of $M_z(t)$ is monitored by varying the time τ

between the two pulses. Typical values were τ =2, 4, 8,16, 32, 64, 128 and 256 seconds and T_1 calculated according to equation 1 and shown in table 3.

$$M_z(t) = M_0\left[1 - 2\exp(-\tau / T_1)\right] \quad \text{Equation 1}$$

The T_1 values were calculated using Varian software 6.1. Values were T_1(H) = 0.51 s and T_1 (F) ranged from 0.57 s to 0.63 s for the various fluorine sites, in each case measured at 60°C directly by inversion-recovery (with fluorine decoupling in the former case and with proton decoupling in the latter, but only during acquisition time) see table 2. The danger of overheating the probe prevented decoupling being applied during the recovery time τ. However it should be noted that in these circumstances the relaxation may not, in principle, be single exponential.

	T (°C)	C1	AM	C2	R1	R2
T_1(F) (s)	60	0.63	0.57	N/A	0.59	0.59
$T_{1\rho}$(H) (ms)	60	14	7.1	13	7.1	6.9
$T_{1\rho}$(F) (ms)	60	9.5	3.5	N/A	4.1	4.6
	100	6.2	2.9	5.0	3.2	6.2
T_1(H) (s)	60	0.51				

Table 2 Relaxation measurements of T_1(F) by inversion recovery, $T_{1\rho}$(H) by cross-polarisation H→F with delayed contact time and proton decoupling during acquisition (only), $T_{1\rho}$(F) by direct-polarisation with varied spin-lock times and H decoupling during acquisition (only), and T_1(H) by inversion recovery. All values result from fitting to a single-exponential decay and should be considered as average values. N/A = signal not resolved, [a] average over all protons in the sample

All relaxation analyses of $T_{1\rho}$ and T_2 were performed by least squares fitting of the peak intensities $SS = \sum_{i=1}^{n} w_i(y_i - \hat{y}_i)^2$ using the Marquardt-Levenberg algorithm with subsequent fitting to the following equations:

$$y = y_0 + ae^{-bx} \quad \text{One-component fit}$$

$$y = y_0 + ae^{-bx} + ce^{-dx} \quad \text{Two-component fit}$$

where a and c are the populations of that component and b and d are the inverse of the component's $T_{1\rho}$ values. The validity of the fitted model was judged by the Predicted

Residual Error Sum of Squares (PRESS), the Durbin-Watson statistic (DWS) and regression value R. The PRESS value is a gauge of how well a regression model predicts new data. The smaller the PRESS statistic, the better the predictive ability of the model. The Durbin-Watson statistic is a measure of correlation between the residuals. If the residuals are not correlated, the Durbin-Watson statistic will be 2; the more this value differs from 2, the greater the likelihood that the residuals are correlated.
Regression assumes that the residuals are independent of each other; the Durbin-Watson test is used to check this assumption. Then the Durbin-Watson value should not deviate from 2 by more than 0.50, that is below 1.50 or above 2.50. Typical values were PRESS=1.9, DWS=1.8 and R =0.99916. See appendix IV for explanation of statistical parameters.
Signal intensities from the CPMG experiment and subsequent analysis gave a satisfactory two-component fit (table 3) for the AM and R1/R2 signals, in agreement with the lineshape analysis of the same signals (see table 6). Fitting these signal intensities to more than two components did not result in a substantial increase in the statistical validity.
The measurement of peak heights (following CP from ^{1}H) under MAS, with a variable-duration spin-lock field equivalent to 80 kHz shows that the C1/C2 and AM signals for our sample have different $T_{1\rho}(F)$ values: 9.5 ms for C1 and 3.5 ms for AM.
Deconvolution of the peaks could have been used as an alternative method of evaluation here, however due to the complexity of the lineshape a conclusive analysis by this methodology was difficult to obtain.
Previously published $T_{1\rho}(F)$ values were 20 and 8 ms (at 35°C) for C1 and AM respectively [8, 9] with a spin-lock field equivalent to 88 kHz. This discrepancy in $T_{1\rho}(F)$ relaxation times probably arises not only because of the differences in the spin-lock fields and temperatures, but also because of variations between the materials such as crystallinity and thermal history [17]. It has been shown that polymer relaxation properties, as monitored by dielectric spectroscopy and dynamic mechanical analysis [18, 19, 20] are sensitive to reverse-unit content as well as to the degree of crystallinity.

A $T_{1\rho}(F)$ spin-lock experiment consisting of a 90° pulse followed by a spin-lock pulse of 25 ms duration should give a spectrum favouring signals from that component (C1/C2) of the sample with the long $T_{1\rho}(F)$, as is seen in Figure 3.3 c. It should be noted that this spectrum has a very low absolute intensity (of the order of 5% of the total intensity in the

direct-polarisation spectrum) because the spin-lock time is more than twice as long as the longer of the two values of $T_{1\rho}(F)$. Some intensity is retained in the R1/R2 region.

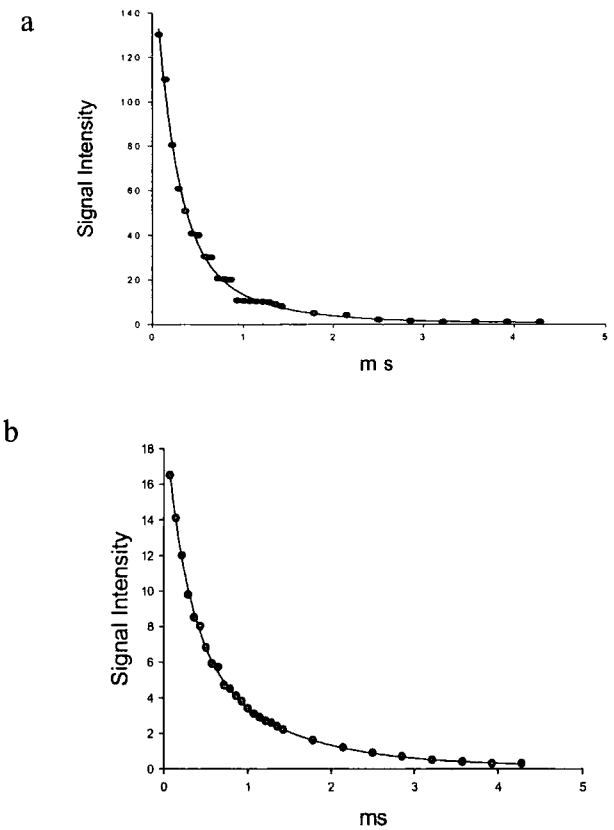

Figure 3.5 Exponential decay curves of the ^{19}F direct polarization CPMG spectra of PVDF recorded at 60°C the amorphous (a) and the anomalous signal decay (b), both fitted to a two-component decay function.

T_2 Components fitted ms	Amorphous Peak	Anomalous peak
One T_2 component	0.32 ms	0.50 ms
Two T_2 components	0.22 ms and 0.78 ms	0.26 ms and 1.1 ms

Table 3 The results of T_2 exponential decay analysis from the CPMG experiment of PVDF at 60°C.

3.5. Decomposition of the spectra

ppm	Linewidth/Hz	% of component
-115.2(R2)	1055	11
-113.1 (R1)	429	0.7
-96.7 (C2)	1917	22
-91.4 (AM)	758	48
-91.1 (X)	1876	8
-82.2 (C1)	1754	11

Table 4 Decomposition data of the ^{19}F direct polarization spectra of PVDF figure 3.3 a.

In principle, decomposition of the direct-polarisation spectrum (figure 3.3a) should give information on the relative intensities of the phases present in the material. However, the apparent complexity of the line shapes and the number of signals potentially present in the spectrum (including sidebands shown in figure 3.2b) mean that conclusive data are difficult to obtain. Nevertheless, numerous attempts at decomposition using Gaussian, Lorentzian and a combination of both lineshapes, suggested that two Lorentzian lines of different widths (758 and 1876 Hz at 60°C) but at the same chemical shift, best represent the intense AM signal whereas Gaussian lines of 1754 Hz and 1917 Hz for the C1 and C2 signals respectively are appropriate for these crystalline lines (table 4). The treatment of the amorphous band as two signals may be an over simplification, but it is at least mathematically convenient and, moreover, suggests that the amorphous material probably exhibits a range of motilities and includes some relatively rigid material. That the lineshape analysis gives a greater percent for C2 than C1 probably is due to the contribution of signals (F, B, and C, see chapter 2 table 1) originating from fluorine in the vicinity of the reverse units.

Decomposition of the entire spectrum in a similar manner, including sidebands, suggests that crystalline α PVDF may account for as little as 30% of the sample, which is in agreement with the value of 28% crystallinity calculated from DSC measurements (see chapter 6 table 1).

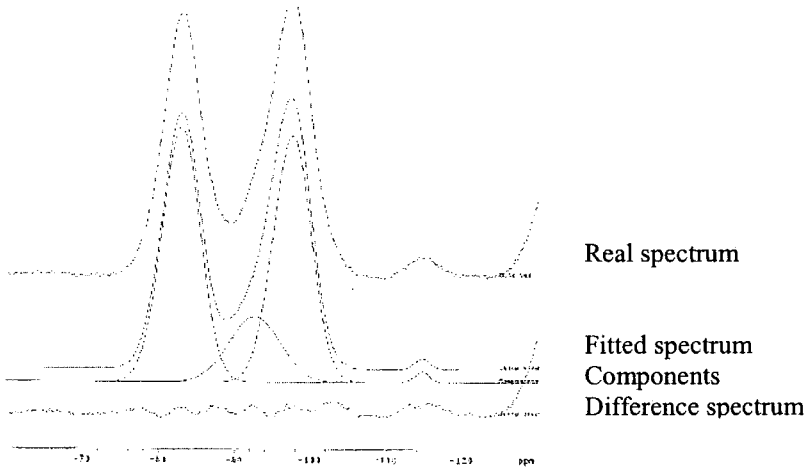

Figure 3.6 Decomposition of the ^{19}F direct polarization spectra of PVDF recorded at 60°C with 25 ms spin lock. The top spectrum is the actual spectrum, underneath is the fitted spectrum and then the individual components. The difference spectrum shows how good the fitted spectrum is compared to the real spectrum.

ppm	Linewidth/Hz	% of component
-114.8 (R1/R2)	672	0.7
-97.5 (C2)	1689	41.5
-92.6	1622	14.9
-82.8 (C1)	1656	42.9

Table 5 The results of the deconvolution of the ^{19}F direct polarisation spectra of PVDF recorded at 60°C with 25 ms spin lock.

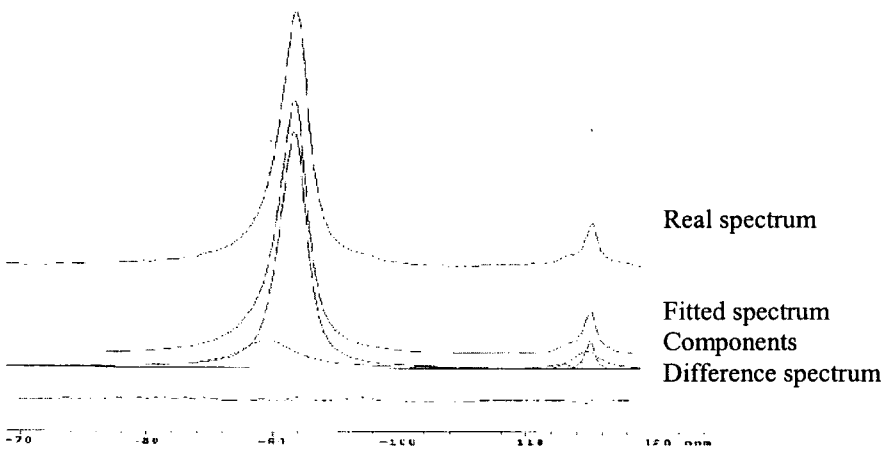

Figure 3.7 Decomposition of the ^{19}F direct polarisation spectra of PVDF recorded at 60°C with a dipolar filter. The top spectrum is the actual spectrum, underneath is the fitted spectrum and then the individual components. The line above the ppm scale shows the difference between real and fitted spectra.

ppm	Linewidth/Hz	% of component
-114.9 (R1/R2)	252	2.7
-114.7 (R1/R2)	700	5.8
-113.0(R1/R2)	309	0.6
-91.4(AM)	709	71.5
-89.5 (X)	1520	19.4

Table 6 The results of decomposition of the ^{19}F direct polarisation dipolar filtered spectra of PVDF figure 3.7.

The results of the decomposition of the spin lock experiment, figure 3.6, show similar line widths to the full DP experiment for C1 and C2 and with nearly equal intensities of the two components as would be expected. The are only slight discrepancies between the chemical shifts of the C1 and C2 signals compared to the DP experiment in which contributions from more mobile species are probable. There is also a rigid component at –92.6 ppm with a similar linewidth to the C1 and C2 components (table 4). This component is also seen in the decomposition of the direct polarisation experiment at –91.1 ppm, again with a comparable linewidth. This strongly suggests that the amorphous signal at ~ –91.2 ppm has a contribution from a signal related to a rigid domain. Furthermore a signal at –114.8 ppm indicates that the crystalline region at least has an association with a small amount of reverse units.

Decomposition of the dipolar-filtered spectrum, figure 3.7, shows a rigid component at –89.5 ppm with a similar linewidth to the C1 and C2 components (tables 4 and 6). This is also in agreement with the linewidth of the rigid component at –92.6 ppm from the spin-lock experiment (table 5) though one would not expect a rigid component to be present from this experiment. It would seem that the amorphous AM signal has contributions from components of varying mobilities as neither the dipolar or spin-lock experiments eliminate this component and therefore could be representative of an intermediate phase. Decomposition of the reverse region of the dipolar-filtered spectrum gave major contributions from the signal at –114.7 ppm and the anomalous signal at –114.9 ppm. Although the linewidths are what would be expected of mobile components, less than that of the rigid components, the decomposition of two signals related to the reverse units R1 and R2 and so obvious in the solution spectra (chapter 2 figure 2.2) did not prove

possible. The dipolar filter spectrum of this region is dominated by the R2 or anomalous signal. It would seem that although, the rigid components are suppressed by the dipolar filter, an array of mobilities complicates the analysis. The results of the lineshape analysis for the dipolar filter spectrum are, however, broadly in agreement with the results of the there T_2 relaxation decay curves (table 3). Both methods of analysis show two-component behaviour for the amorphous (AM) and the reverse (R2) signals.

3.6. Variable temperature results

Recently, Su and Tzou [21] investigated the effects of fast MAS at 20, 30 and 35 kHz at "ambient temperature" and concluded that effective suppression of ^{1}H, ^{19}F dipolar coupling in α PVDF was reached by a spin rate of 35 kHz. They obtained chemical shift tensor components from spinning sideband intensities, but apparently they did not consider how interplay of the shielding and dipolar tensors might have influenced the detailed distribution of intensities in the spinning sideband manifolds.

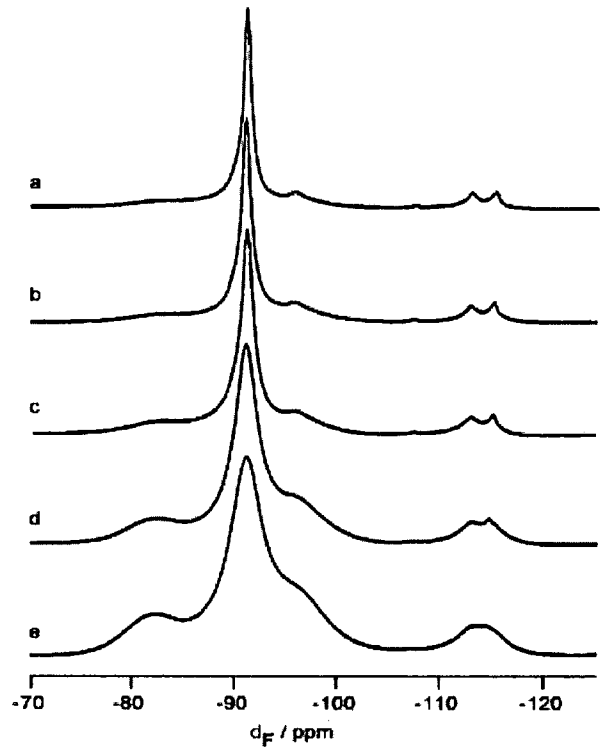

Figure 3.8 shows the effect on the spectrum of our sample of a variation in controlled temperature at a constant spin rate of 14 kHz (but not on a constant vertical scale). Direct polarisation ^{19}F NMR spectra of PVDF recorded at (a) 120°C (b) 110 °C (c) 100°C (d) 60 °C (e) 20°C. The spin rate was 14kHz.

A significant decrease in the AM signal line width is seen at elevated temperatures, which causes the C1 and C2 signals to be relatively less prominent. The AM half-height linewidth drops by a factor of ca. 2 from 60°C (860 Hz, figure 3.8d) to 100°C (430 Hz, Figure 3.8 c). A similar increase in resolution would be seen if an increase in temperature accompanied fast MAS in the experiments of references [13] and [21]. With no temperature control, the sample temperature at a spin rate of 35 kHz is likely to have been around 65°C [22]. It is therefore possible that a combination of spin-rate and sample heating was responsible for part of the increased resolution at high spin-rates observed by Su and Tzou. Such effects have recently been reported in detail by Brus [23], who showed that sample heating up to a difference of 58 K could be seen and that MAS-induced heating could effect the determination of the isotropic, anisotropy and asymmetry parameters of the shielding tensor. It would seem that temperature control and accurate temperature calibration are required if reliable results are to be produced. The values of $T_{1\rho}(F)$ for peaks C1 and AM at 100°C (6.2 and 2.9 ms respectively) are somewhat lower than at 60°C.

3.7. The minor signals in the spectra

The signals at –113.8 and –114.9 ppm have been assigned [1, 8] to adjacent CF_2 fluorines in the same type of reverse unit as recognised from the solution-state spectrum, chapter 2 figures 2.1 and 2.2 [19, 16], and these have been shown [9] to be mostly associated with the amorphous domains. Our measurements agree, in general, with this conclusion. Thus, at 60°C, $T_{1\rho}(H)$ values for signals R1 and R2 are 7.1 and 6.9 ms respectively (compared to 7.1 ms for AM and 14.0 ms for C1). Similarly, $T_{1\rho}(F)$ values are 4.1 and 4.6 ms for R1 and R2 respectively (3.5 ms for AM and 9.5 ms for C1).

However, there is evidence from a number of solid-state experiments (see below), which suggests the situation in this region of the spectrum is more complex. Thus it is apparent from Figure 3.3b that the reverse-unit signal R1 at –113.8 ppm is suppressed to some extent, along with C1 and C2, by the dipolar filter experiment. This suggests that it may be in some way associated with rigid regions, at least in small part, in contrast to conclusions in the literature [3,8,9] on other PVDF samples. Figure 3.3c shows that in the $T_{1\rho}(F)$-filtered spectrum of the material a broad signal can still be seen in the region corresponding to R1 and R2, again suggesting that there may be some contribution associated with rigid regions. The intensity of the R_1 and R_2 signals in the $T_{1\rho}(F)$ filtered

spectrum (Figure 3.3 c) is 1.4% of the intensity in that region in the unfiltered spectrum. If the entire R1/R2 signal has a $T_{1\rho}(F)$ in common with the amorphous component of the sample (3.5 ms) we would expect only 0.3% of the original signal to be present in the $T_{1\rho}(F)$ filtered spectrum. Thus this residual signal at ca. –114 ppm must have a similar $T_{1\rho}(F)$ to that of the C1/C2 peaks, confirming that it must be closely associated with rigid/crystalline material (i.e. probably at the interface between crystalline and amorphous domains).

However, Figure 3.3 b appears to show an enhancement of signal R2 with respect to the AM peak. There is other evidence for a diversity of behaviour in the R1/R2 region. In order to investigate this anomaly further, we obtained a series of ^{19}F spectra at 100°C following spin-locking for various times.

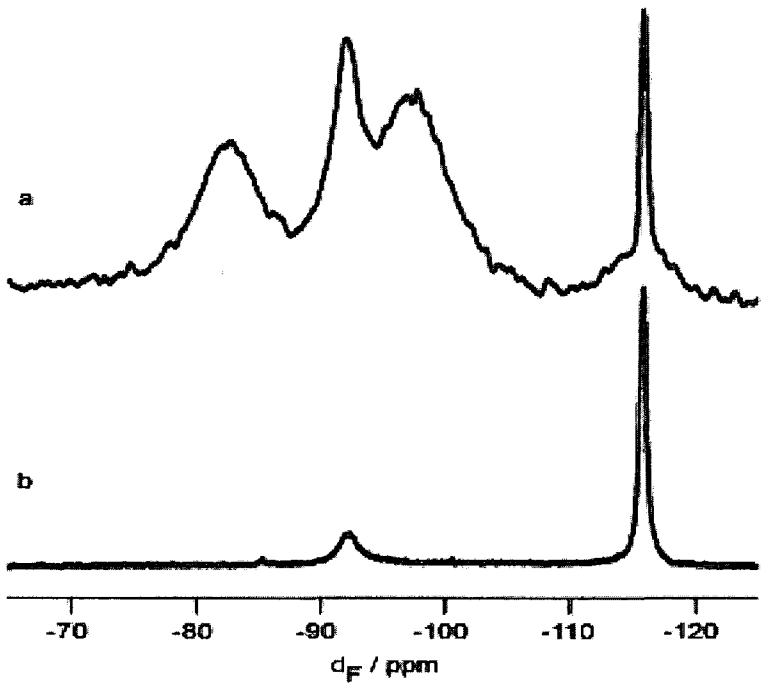

Figure 3.9 The ^{19}F direct polarisation MAS spectrum of PVDF (a) recorded with 25 ms spin lock at 100°C (b) with 4ms delayed acquisition (DPDA) experiment at 60°C.

Even with little or no spin-locking the anomalous R2 signal is more prominent than at 60°C, presumably because it is narrower. More remarkably, this peak has a long $T_{1\rho}(F)$ (6.2 ms, compared to values of 6.2, 2.9 and 5.0 ms for C1, AM and C2 respectively at 100°C), table 2.

This data suggest that the anomalous peak is on the extreme narrowing side of a $T_{1\rho}(F)$ minimum. Thus after 25 ms of spin locking the anomalous band has a peak-height similar

to that of the AM signal (figure 3.9a). In addition, a direct-polarisation delayed-acquisition (DPDA) experiment with a delay time of 4 ms was used to sample signals with long transverse relaxation times. This spectrum (Figure 3.9 b) is dominated by the –115 ppm signal. Variation of the acquisition delay in the DPDA experiment showed approximately exponential decay, with $T_2(F) \sim 1.2$ ms, for this signal.

These experiments suggest that at least part of the R2 signal is associated with very mobile domains, rather than with reversed units in the middle of long chains. Note also that the $T_2(F) \sim 1.2$ ms from the DPDA experiment is in good agreement with the result from the two-component analysis of this signal from the CPMG experiment, which gave one component with a $T_2(F)$ of 1.1 ms. Thus there appears to be a region of super-mobility, which could consist of chain ends, short branches, or perhaps occlusions of relatively small molecules of unknown structure. Whereas chain-ends may appear unlikely as an explanation, given that the molecular weight of the polymer (measured at 1×10^6 D by GPC) implies a maximum of 0.013% for chain-end monomer units, the selectivity of the experiments revealing the relevant signals is very high, and an assignment to $-CF_2H$ chain ends seems to be the most likely explanation since these have been shown by solution-state NMR to give a signal at δ_F = ca. –114.8 ppm [24, 25, 26]. No definitive assignment can be given for the weak signal at ca. –107 ppm which can be seen in spectra at higher temperatures(figure 3.8), though we know that it does not have anomalous mobility. In the solid-state spectrum (figure 3.2a) the fluorines of types A, F and B (chapter 2, figure 2.2) would be unresolved from the major signal centred at –91.2 ppm (AM), whilst peak C is expected to be obscured by the band at –95.6 ppm (C2).

3.8. Spin diffusion

The addition of a mixing time following selection of the crystalline region by the $T_{1\rho}(F)$ filter experiment (figure 1c - a version of the Goldman-Shen experiment [27]) allows the spin-diffusion from crystalline domains to amorphous domains to be monitored. The diffusion coefficients were extracted at 60°C via a plot of the signal intensities (peak heights) against the square root of the mixing time (figure 3.10), both for the main amorphous peak (closed circles) and for the reverse-unit signals (open circles). The dimension of the amorphous domains was calculated [7, 9] using equations 2 and 3

$$\sqrt{D_{eff}} = \frac{\sqrt{D_a} \times \sqrt{D_c}}{\sqrt{Da} + \sqrt{D_c}} \qquad \text{Equation 2}$$

$$d_a = \frac{2\varepsilon}{(1-\chi_c)} \sqrt{D_{eff} t_s^a / \pi} \qquad \text{Equation 3}$$

The effective spin-diffusion coefficient D_{eff} was calculated from the intrinsic spin diffusion coefficients of the crystalline and amorphous phases, equation.2. Here it is assumed that the ratio of spin diffusion coefficients is determined by the ratio of the static proton linewidths [28]. A ratio of $D_a/D_c = 1:6$ has been used [7, 9] and the crystalline value $D_c = 0.6$ nm^2 ms^{-1} [7, 9], giving the amorphous value as $D_a = 0.1$ nm^2 ms^{-1}. The effective spin-diffusion coefficient can then be calculated as $D_{eff} = 0.202$ nm^2 ms^{-1} [7]. The characteristic spin-diffusion time t_s^a of 7.2 ms was measured from the plot of diffusion recovery of the amorphous component with the smaller linewidth (figure 3.10) in the usual way [9]. A dimensionality factor of $\varepsilon = 1$ [5, 9], appropriate to a lamellar morphology, was used. The fractional crystallinity, χ_c was taken to be 30 %, as determined from lineshape analysis and in agreement with the DSC measurement of 28%. The amorphous domain size d_a was then determined according to equation 3.

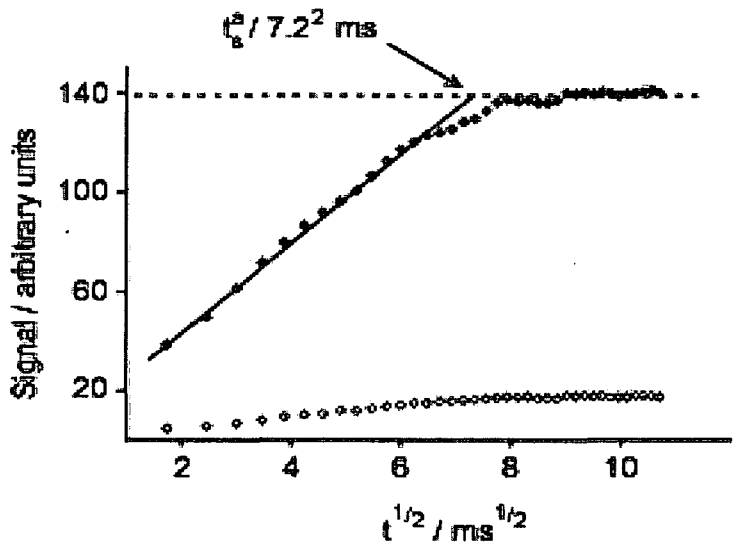

Figure 3.10 Peak heights from the spin diffusion experiment at 60°C for • the amorphous signal (-91.2ppm) and ○ signals for the reverse units. The intersection point t^a_s marks the recovery of 100% intensity used in equation 2.3 for the determination of the domain size.

The value retrieved from this calculation is d_a = 4.9 nm, which is in reasonable agreement with the result given by Holstein [9], namely 5-7 nm, based on a different set of samples with 50% crystallinity. The similarity of the recovery time of the AM and reverse unit signals is consistent with the conclusion that the reverse units are predominantly incorporated into the amorphous region.

3.9. Dipolar Recoupling

The dipole-dipole couplings give important information on molecular structure via distance measurements between spins. Weak dipole-dipole couplings yield data on relatively long-range inter-nuclear distances, but these are often obscured by larger contributions to the spin hamiltonians and are relatively readily removed by MAS. However, they can be reintroduced into an experiment by either rotor-driven 'rotational resonance' or radiofrequency-driven recoupling (RFDR) techniques. For the case where homonuclear recoupling with less sensitivity to the chemical shift than is obtained with rotational resonance is desired, such as correlation spectroscopy of multiple spins over a broad chemical shift range, the coherent averaging of MAS must be disturbed by additional modulation [14,29,30]. In the present work this was achieved by a rotor-synchronised multiple-pulse sequence consisting of a series of π pulses (figure 1a). The introduction of a $T_{1\rho}$(F) relaxation filter before the recoupling period τ_C (figure 1a) suppresses much of the dominant signal from the amorphous material and allows a fuller examination of the correlation between coupled species in immobile regions.

The DP-RFDR [14] spectra (figure 3.11) were recorded with and without a $T_{1\rho}$ (F) relaxation filter at a spin rate of 14 kHz and a τ_C (RFDR mixing time) of 4 ms. It can be seen from figure 2.20 that for short mixing times (of the order of τ_C in the RFDR experiment) spin diffusion from the crystalline to the amorphous domain is limited in extent. The RFDR spectrum (figure 3.11a) shows that there are major recoupling interactions between the amorphous region (–91.2 ppm) and the reverse unit signals. The recoupling between the amorphous region (–91.2 ppm) and the reverse unit signal at –113.8 ppm, seen in figure 3.11 a, is no longer so clearly seen in figure 3.11b due to the selective nature of the experiment. However, weak cross peaks between crystalline and reverse units are clearly seen from the $T_{1\rho}$ (F) filtered experiment (figure 3.11b).

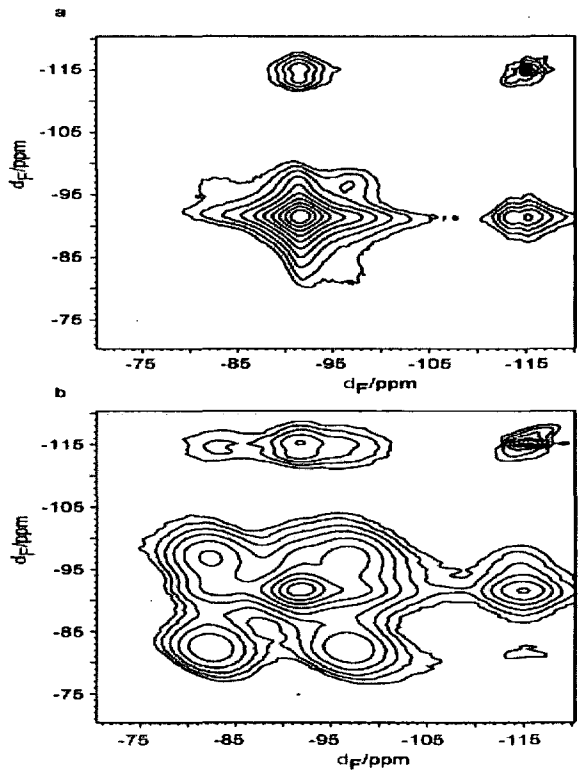

Figure 3.11 The 300MHz ^{19}F RFDR experiment recorded with n=7 at 60°C (a) without spin-lock filter and (b) with spin-lock filter. Note that for (b) the spin-lock time was 18 ms, shorter than for figure 2.13 (c).

This reinforces the conclusion, reached earlier, that some reverse units are intimately associated with crystalline domains (possibly in interface regions). However, the role of the anomalous signal at –115 ppm in this experiment is not clear.

3.10. Summary of solid-state NMR of PVDF

It has been demonstrated that sample temperature greatly influences the spectral linewidth of solid-state ^{19}F NMR high-speed MAS spectra of α-PVDF and that temperature calibration and control is of great importance when evaluating methodologies to achieve line narrowing.

It has been shown by both dipolar-filtered and $T_{1\rho}(F)$-filtered experiments that some reverse units, giving a signal at ca. –113.0 ppm, are associated with the rigid domains, though the majority of reverse units are in the amorphous material. The crystalline-selective RFDR spectrum shows recoupling between the crystalline signals and the signal at –115 ppm. The DPDA spectrum shows a spectrum of highly mobile material with part

of the R2 signal at –115.0 ppm exhibiting long T_2 relaxation. This observation is consistent with the fact that the R1 signal is apparently suppressed to a greater extent than the R2 signal by the dipolar filter experiment. Relaxation studies and lineshape analysis suggest the presence of an array of mobilities in the amorphous signal and are in agreement with the presence of a highly mobile species. The presence of such a highly mobile species renders the reverse unit signals more complicated and therefore difficult to decipher. The assumption that integration provides an estimate of reverse units content in PVDF would therefore seem to constitute an inadequate methodology. This anomalous signal is tentatively assigned to an unidentified signal, but most likely a chain end group. A comparison of our work with that of others [12, 17] shows that $T_{1\rho}$(H) and $T_{1\rho}$ (F) are probably highly dependent on both reverse-unit content and location as well as the degree of crystallinity.

References

[1] Lovinger AJ. Science, 1983,220:1115.

[2] Lando JB, Olf HG, Peterlin A, J Polym Sci 1966;4:941.

[3] Holstein P, Scheler D, Harris RK, Polymer 1998;39:4937.

[4] Greggorio R, Cestari M, J Polym Sci (B) 1994;32:859.

[5] Sajkiewicz P, Wasiak A, Goclowski Z, Eur Polym J 1999, 35, 423.

[6] Lovinger AJ, Davis DD, Cais RE, Kometani JM, Polymer 1987, 28, 612

[7] Schmidt-Rohr K, Spiess HW, Multidimensional solid-state NMR and polymers. New York: Academic Press, 1994. Chapter 13.

[8] Holstein P, Harris RK, Say BJ, Solid State Nucl Magn Reson 1997, 8, 201.

[9] Holstein P, Monti GA, Harris RK, Phys Chem Chem Phys 1999, 1, 3549

[10] Harris RK, Monti G, Holstein P, Ando I, Asakura T, editors, Solid state of NMR polymers, vol. 84. New York, Elsevier, 1998. Chapter 6

[11] Harris RK, Monti GA, Holstein P, Ando I, Asakura T, editors. Solid state of NMR polymers, vol. 84. New York: Elsevier, 1998. Chapter 18.

[12] Ando S, Harris RK, Reinsberg SA, Magn Reson Chem 2002, 40, 97

[13] Scheler U, Bull Magn Reson 1999, 1-4, 19.

[14] Bennet. AE, Rienstra. CM, Griffiths. M, Zhen. W, Landbury. PT, Griffin. RG, Chem Phys 1998, 108, 9463

[15] Egger N, Schmidt-Rohr KL, I Appl Polym Sci, 1992, 44, 289

[16] Ding S, McDowell AC, I Phys. Condens. Mater 1999, 11, L199

[17] McBrierty VI, Douglass Dc, I Polym Sci, Macromol Rev 1981, 16, 295

[18] Shinichi Y, Polym Sci, 1970, A2, 1057

[19] Nabata Y, I Appl Phys 1990, 12, 2782

[20] Nakagawa K, Ishida Y, Polym Sci 1973, 11, 2153

[21] Su TW, Tzou DLM, Polymer 2000, 41, 7289

[22] Bruker Spectrospin, Private communication and mentioned in Ref. [15].

[23] Brus I, Solid State Nucl Magn Reson 2000, 16, 151.

[24] Herman, Toshiyuki U, Astushi K, Susumu U, Takeshi K, Norimasa O, Polymer 1997, 38, 167.

[25] Pianca M, Barchiesi E, Esposto G, Radice S, Fluorine Chem 1999, 95, 71

[26] Ferguson RC, Ovenall DW, Polym Prepr ACS Polym Chern 1984, 25, 340

[27] Goldman M, Shen L, Phys Rev 1966, 144, 321

[28] Spiegel S, Schmidt-Rohr K, Boeffel C, Spiess HW, Polymer 1993, 34, 4566

[29] Ok JH, Spencer RGS, Bennet AE, Griffin RG, Chem Phys Lett 1992, 197, 389

[30] Bennet AE, Ok JH, Griffin RG, Vega S, Chem Phys 1992, 96, 8624

Chapter 4

Studies of a Vinylidenefluoride telomer by solution-state NMR spectroscopy

4.1 Introduction to Vinylidenefluoride.

It is generally accepted that the end groups of a polymer do not greatly influence the macroscopic properties. This is due to their weight being a fraction of the total bulk mass and the bond energies in end groups being usually very similar to those of the main chain. This, however, is not true of fluoropolymers, where hydrogen-containing end groups have an influence on thermal stability due to the difference in C-H and C-F bond energies ~50 kJ/mol. For PVDF, it has been shown that end groups play a vital part in the thermal stability and fire resistance properties due to the type of end group generated. These properties are not solely associated with the difference in C-H and C-F bond energy but also to the degradation mechanism induced by the type of end group formed upon synthesis. Furthermore, the end groups play an important role in the crystallisation kinetics of fluoropolymer-based thermoplastics and thereby processing and end-user properties [1].

Fluorinated derivatives with a hydroxyl end group are of interest for applications such as surfactants, block copolymers, paints and coatings. Although expensive, the market for these polymers is increasing.

The reaction of vinylidenefluoride (VDF) with a chain transfer agent (a telogen) yields short-chained, low molecular weight fluoropolymers. Many different pathways are available for this reaction using different fluorinated alkyls with an array of telogens and initiators. The telomerisation of VDF with hydroxyls as telogens are known to produce fluorinated telomers containing a functional end group. This reaction mechanism has been investigated using varying amounts of VDF, CH_3OH as telogen and di-tert-butyl peroxide ($((CH_3)_3\text{-C-O-})_2$) as the initiator [2]. All telomers in these studies showed the presence of main-chain VDF units and a large amount of reverse units $\text{-}CF_2\text{-}CF_2\text{-}CH_2\text{-}CH_2\text{-}$, up to 19%. This was explained as an effect of the non-regioselectivity of the hydroxyl-methyl radicals on VDF. Furthermore, it was shown that the ratio of reverse tail-to-tail addition decreased from 50%, for the first addition of these adducts, to a limit similar to that of PVDF i.e. 10% when the polymerisation increased [2].

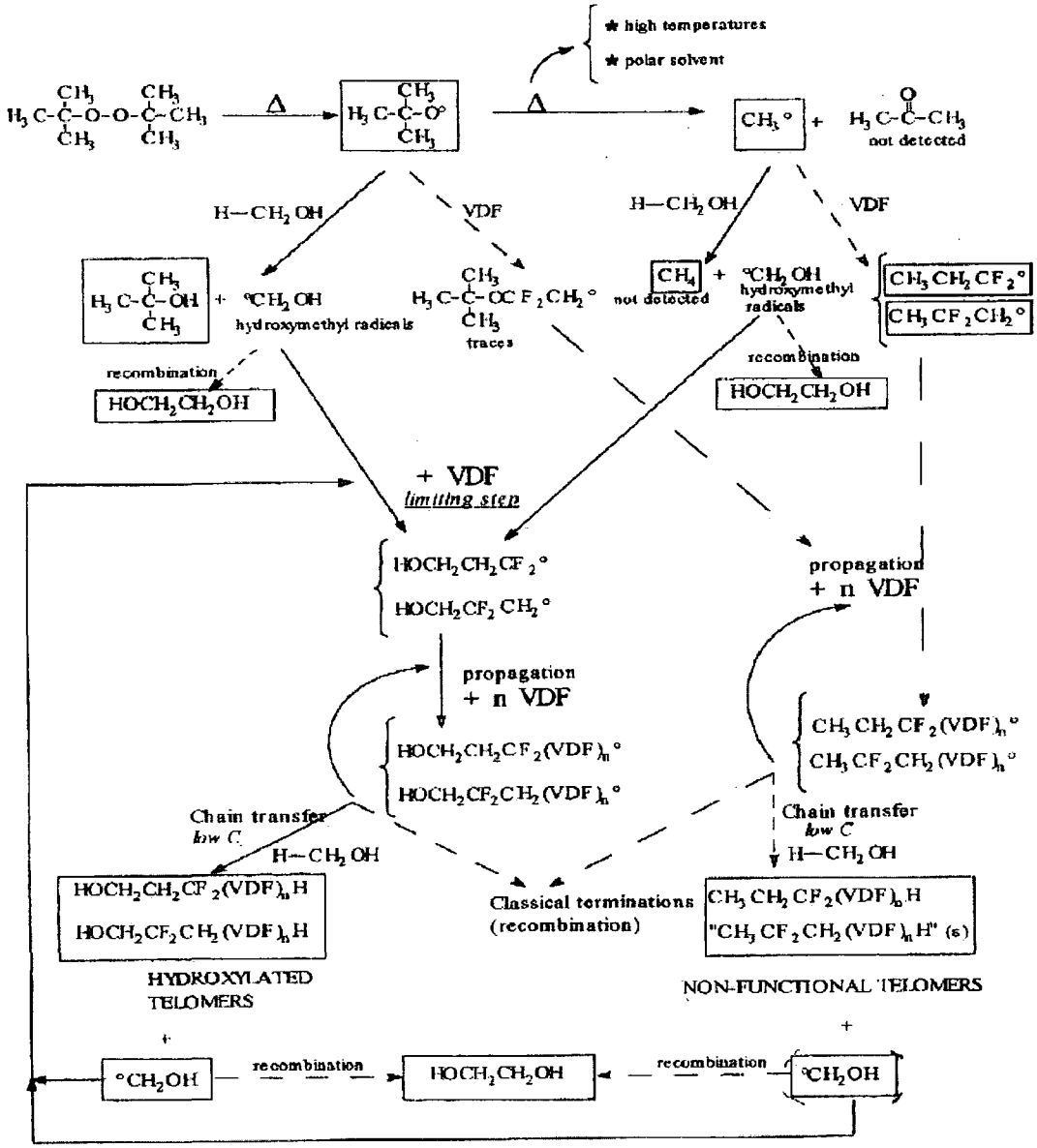

Scheme 1. The synthetic pathway for VDF telomerisation with methanol. Full arrows represent preferred pathways. The scheme is a reprint from reference [2].

Telomerisation with hydroxyl-methyl radicals produces VDF polymers with a molecular weight of ~ 2000, with the possibility of preparing novel macromolecules after chemical modification of the telomers with hydroxylated end groups, see scheme 1 [2].

The results of ^{1}H and ^{19}F solution-state NMR spectroscopy revealed the presence of CH_3, CH_2OH and CF_2H end groups, though the evidence for some of these functional groups is sparse in the literature and in some cases dubious. No thorough investigation pertaining to the association of these end groups with the main chain by modern methods of spectroscopy was found in the literature. However, HMQC and HMBC correlation spectroscopy have been used in the analysis of PVDF copolymers [3,4] and short-chained model compounds. These experiments did not give information on end groups and their functionality. Workers have made assignments using a single pulse experiments or correlation spectroscopy (COSY) [5] often from VDF telomers with

different synthetic background [4,6]. The lack of HETCOR experiments is obvious in the literature and the use of 'accepted' chemical shifts for signal assignment is common. These assignments are often made on the raw synthetic product, which can contain many species, yet experiments such as TOCSY [5] used to assign signals to a specific spin system and therefore the same molecule are not common if done at all.

A major interest in being able to decide this association is to compare the structure of low molecular weight VDF with our high molecular weight PVDF. This should give information of signals that have been difficult to identify in high molecular weight PVDF, both in solution-and solid-state spectra and their origin. The short-chain VDF should give for example a larger degree of chain end groups and reverse units [2].

Also the lack of NMR laboratories with both high field magnets and the ability to observe ^{19}F and decouple ^{1}H simultaneously means that the majority of work in the past has given proton and fluorine spectra of poor resolution from which assignments have been made. This is important for the assignment of signals, especially in spectral regions containing multiple signals, and for structural determination using homo and heteronuclear coupling constants, J_{F-H}, J_{H-H} and J_{F-F}. In general typical coupling constants for fluorine are $^{2}J_{F-H}$ (gem) ~45 Hz, $^{3}J_{F-H}$ (trans) ~17 Hz, $^{3}J_{F-H}$ (cis) ~6 Hz, $^{2}J_{F-F}$ (gem), ~300 Hz and $^{3}J_{F-F}$ ~1-27 Hz [6]. Typical coupling constants found in the literature for VDF telomers are, for the main chain, $^{3}J_{F-H}$ 16 Hz. [7, 8, 9] The reverse unit coupling $^{3}J_{F-H,}$ seen ~2.3 ppm is often not very well resolved [2]. Further couplings of importance are for the end-groups. Here the H-CF_2-CH_2- end-group shows $^{2}J_{F-H}$ = 55.2 Hz and $^{3}J_{H-H}$ = 4.4 Hz. For CH_3-CH_2- groups typical values are $^{3}J_{H-H}$ = 7.5 Hz and CH_3-CF_2- $^{3}J_{F-H}$ = 19.3 Hz [2, 6, 10]. Generally for VDF type structure, couplings are 5Hz $<^{3}J_{F-H}>$ 20Hz and 0 Hz $<^{4}J_{F-H}>$5Hz [3,4]. For small coupling constants the linewidth and resolution of the spectrum are obviously of great importance, which is probably the main reason why these couplings are seldom seen in higher molecular weight PVDF or VDF spectra as mentioned in chapter 2. The reverse unit (-CF_2-CF_2-) is a typical and well-documented feature in the fluorine spectra of both PVDF and VDF telomers, yet $^{3}J_{F-F}$ couplings are not reported [11, 12, 13]. From a model compound of the type CF_2H-CF_2H, the effect of configuration on the magnitude of $^{3}J_{F-F}$ has been determined [3] and a few examples are shown below, however, note that a change in configuration of theses structures will also give a change in the coupling constant.

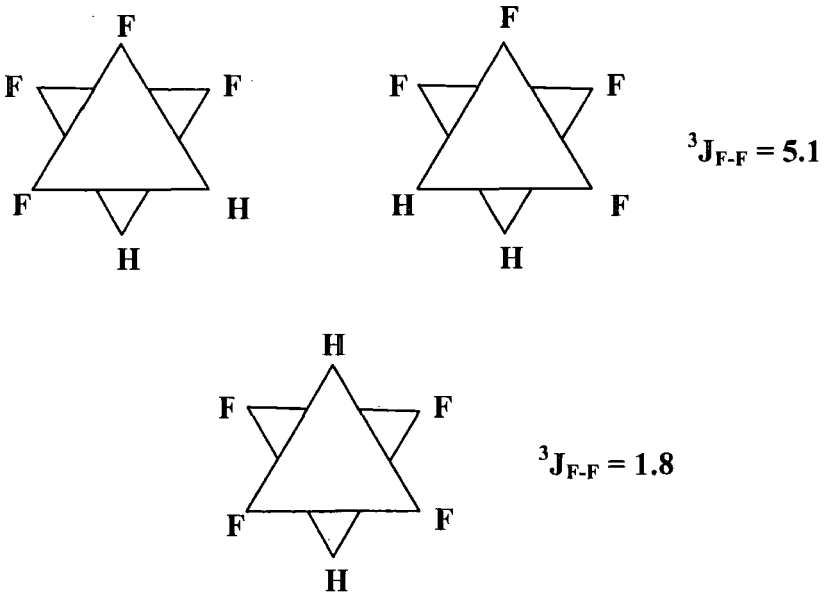

Furthermore, if coupling values become close to zero, off-diagonal peaks in two-dimensional spectroscopy such as COSY spectra are not observed. No $^2J_{H-H}$ or $^2J_{F-F}$ couplings were found in any of the spectra in this thesis. This could be due to small coupling constants combined with a larger linewidth or that the fluorines and protons of the main chain VDF are also chemically equivalent.

As described in chapter 3, the morphology of semi-crystalline PVDF was investigated by acquiring direct polarisation spectra with various relaxation filters and debated in terms of domain selectivity with regard to the reverse units [14]. This showed amongst other things the possibility of a range of mobilities in the amorphous domains. Also, although the signals related to the α crystalline form at -82.1 and –95.6 ppm should be of equal intensity, the signal at –95.6 ppm was larger (chapter 3 figure 3.3a). This discrepancy was explained by the contribution of CF_2 groups in the vicinity of reverse units and verified by solution-state NMR spectroscopy. A contribution to this signal from the β form and /or short-chain VDF molecules showing a range of mobilities is, however, also a possibility.

It was also shown in chapter 2 that the reverse units are mostly associated with the amorphous region and that the dipolar-filtered spectrum, which should equate to the solution-state spectrum, exhibited an anomalous signal at ~-114 ppm [14]. This signal was shown to arise from highly mobile units and can probably be assigned to CF_2H chain end groups. It could not, however, be determined if this end group was part of the

main chain PVDF, a by-product or originated from the reactants. Furthermore, the intensity of this signal in the solid-state spectrum gave a significant contribution to the total reverse unit signal, making any determination of reverse unit content difficult in the solid state.

In the same work [14], a solution-state 2D COSY spectrum allowed further assignment of the reverse unit signals and also showed peaks at ~-107 ppm which were assigned to possible CF sites at chain branching positions as these signals showed no off-diagonal cross peaks. The literature gives assignments to some of these peaks as CF_2-CH_3 end groups and offers chemical shift calculations for the assignments of other peaks in this region to chain branching [1,15,16]. However, no investigation connecting these signals to the same spin system of the PVDF or VDF polymer backbone was found.

In this chapter the reaction products of VDF with methanol as a telogen have been characterized by solution-state NMR spectroscopy. The low molecular weight PVDF may provide an indication to the nature of the minor peaks at ~-106, -107 and -114 ppm in the spectrum of PVDF (see chapter 2). The work in this chapter was made in collaboration with Dr B Ameduri, from the Laboratory of Macromolecular Chemistry, Ecole Nationale de Chimie de Montpellier, UPRESA CNRS 5076, 8 rue de l'Ecole Normale, F 34296 Montpellier Cedex 5, France who synthesized the VDF telomer.

4.2 ^{1}H solution state NMR spectroscopy.

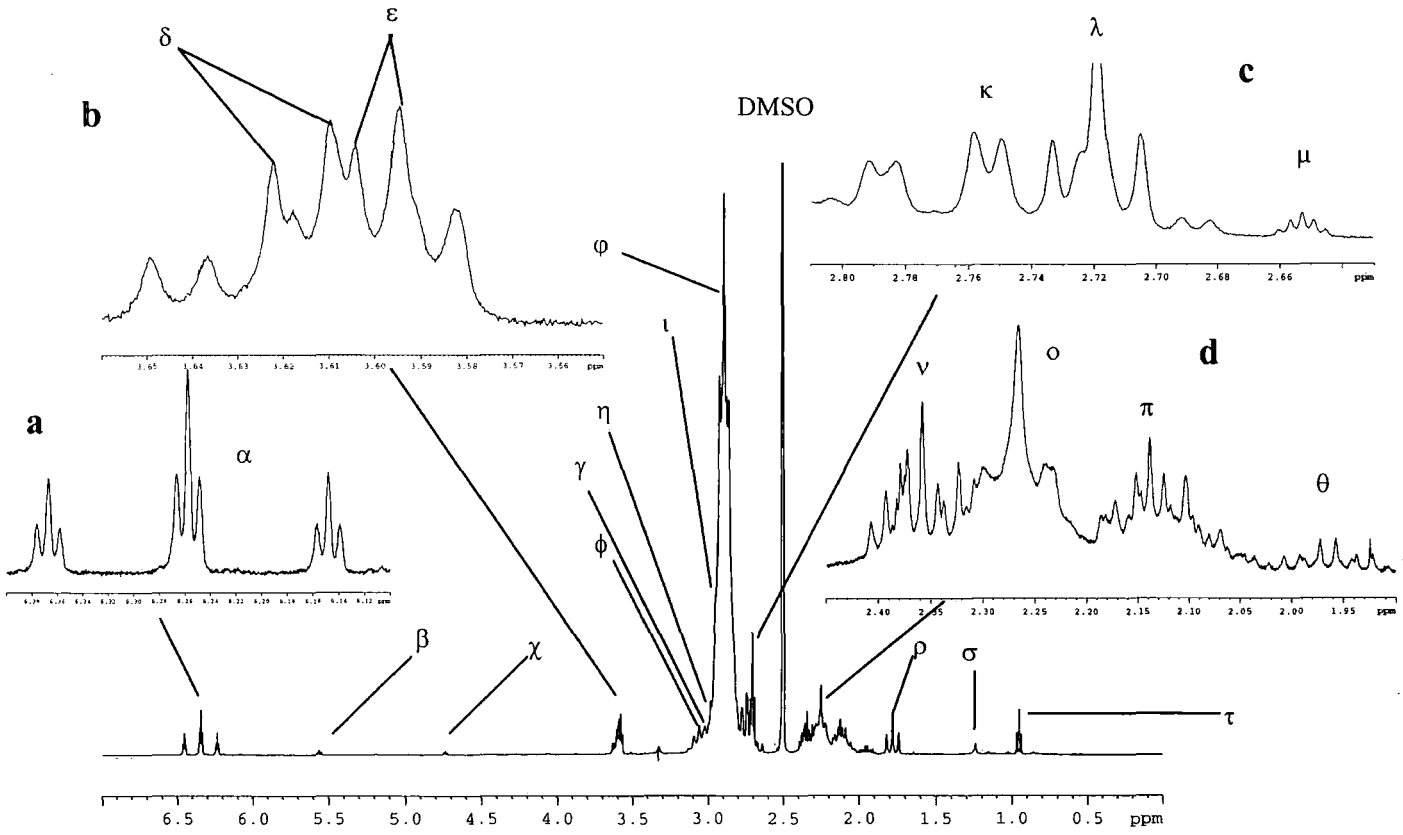

Figure 4.1 The 500 MHz ^{1}H Fluorine-coupled spectrum with H_2O saturation of VDF telomer in DMSO-d_6 at 22°C with expansions a-d. Greek letters are the proton assignments in table 1

Major signals in the proton spectrum with no fluorine decoupling

Figure 4.1 shows the 500 MHz fluorine-coupled proton spectrum of the VDF telomer with expansions (a, b, c and d), and table 1 gives assignments. The signal at 6.360 ppm (α), a triplet of triplets is assigned to the end-chain proton -CH_2-CF_2H (figure 1a) due to its chemical shift and characteristic coupling pattern, which shows both $^3J_{H-H}$ and $^3J_{F-H}$ coupling. The most intense signal in the spectrum is a quintet at 2.905 ppm (φ) with two $^3J_{H-F}$ coupling constants of 16.13 and 8.32 Hz, and assigned to the main chain protons in -CF_2–CH_2-CF_2- structures. A signal at 2.719 ppm (λ) is identified (figure 1c) as a triplet with a $^3J_{H-H}$. At least one more signal is present here as seen in figure 1c. A complex triplet signal, corresponding to both methylene groups of the reverse unit -CF_2–CH_2-CH_2-CF_2–CF_2-CH_2- is present at 2.265 ppm (o). This signal shows one $^3J_{H-F}$ coupling constant of 16 Hz. The relative intensity of this signal is somewhat low with respect to the main chain unit signal, as telomerisation usually produces more reverse

units. Further signals to note are a triplet at 1.793 ppm (ρ) with a 19.5 Hz $^3J_{H-F}$ coupling and assigned to the end group $-CF_2-CH_3$.

H	Signal Intensity	Multiplicity	& Assignments	$^3J_{H-H}$	J_{F-H}	Functionality
360	1	tt	α	4.52	54.71 (^{2}J)	$-CF_2H$
579	0.31	t	β	6.30		$-CF_2-CH_2-OH$
751	0.27	t	χ	5.13		$-CH_2-CH_2-OH$
615		td	δ	6.30	14.57 (^{3}J)	$-CF_2-CH_2-OH$
600	1	td	ε	~6.1and 4.8		$-CH_2-CH_2-OH$
348						H_2O
072	0.58	t	ϕ			
012	0.09	s	γ		17.64(^{3}J)	$-CF_2-CH_2-$
997	0.12	s	η			
963	0.20	s	ι			
905	31.10	q	φ			$-CF_2-CH_2-CF_2-CH_2-$
753	1	qd	κ	4.49		$-CF_2-CH_2-CF_2H$
719	0.52	t	λ	7.27	16.13 & 8.32 (^{3}J)	$-CF_2-CH_2-CH_2-X$
653	0.45	q	μ	1.96	16.56 (^{3}J)	Not identified
358	0.74	t t	ν	7.34		$-CF_2-CH_2-CH_2-$
265	3.42	t	ο			$-CF_2-CH_2-CH_2-CF_2-CF_2-CH_2-$
138	0.84	tt	π	6.30	17.63 (^{3}J)	$-CF_2-CH_2-CH_2-OH$
965	0.32	tqu	θ	7.34	16.67 (^{3}J)	$-CF_2-CH_2-CH_3$
793	1.00	t	ρ		16.56 (^{3}J)	$-CF_2-CF_2-CH_3$
252	0.27	s	σ		17.63 (^{3}J)	$(CH_3)_3COH$
967	0.32	t	τ	7.48	19.77 (^{3}J)	$-CF_2-CH_2-CH_3$

Table 1: Chemical shifts and assignments for the proton spectra of the VDF telomer (figure 1) with no ^{19}F coupling in DMSO-d_6 at 22°C. q=quintet, qu=quartet, t=triplet, d=doublet, s=singlet.

Minor signals in the proton spectrum with no decoupling

In figure 4.1, a triplet at 5.579 (β) is seen with a 6.30 Hz $^3J_{H-H}$ proton coupling constant. This signal is tentatively assigned to a $-CF_2-CH_2-OH$ structure. A signal at 4.751 ppm (χ) with a $^3J_{H-H}$ proton coupling constant of 5.13 Hz is assigned to a hydroxyl end group by reference to the literature. The multiple signals between 3.650 and 3.570 ppm (figure 1.b) showed a complex pattern, but can probably be interpreted as two triplets of doublets at 3.615 ppm (δ) and 3.600 (ε).

There are several signals all at similar chemical shifts to the main chain signal at 2.905 ppm (φ), though the fine structure of individual signals is difficult to interpret due to signal overlap, a triplet at 3.072 (ϕ) ppm is seen. Further signals are 3.012 (γ), 2.997 (η) and 2.963 (ι) ppm. The signal at 2.753 ppm (κ) figure 1(c) is a quintet of doublets with 4.49 Hz $^3J_{H-H}$ and a 16.56 Hz $^3J_{H-F}$ coupling and is the methylene group of the $-CH_2-CF_2H$ end-group. There is a quintet at 2.653 ppm (μ) with a 1.96 Hz $^3J_{H-H}$ coupling, which is not assigned. The signal at 2.358 ppm (ν) could derive from a triplet of triplets

with 7.34 Hz $^3J_{H-H}$ and 16.63 $^3J_{H-F}$ coupling, figure 1d and 7a. The group of signals centered around 2.138 ppm (π) are complex, but a triplet of triplets with a 7.34 $^3J_{H-H}$ and 17.63 $^3J_{H-F}$ coupling can be assigned, giving a $-CF_2-CH_2-CH_2-$ type structure. A triplet of quartets is seen at 1.965 ppm (θ), showing both $^3J_{H-H}$ and $^3J_{H-F}$ coupling. The proton coupling and intensity of this signal is the same as the triplet at 0.967 ppm (τ), These signals are assigned to a $-CF_2-CH_2-CH_3$ end group. A singlet at 1.252 ppm (σ) is assigned to the methyl groups of the *tert*-butyl alcohol $(CH_3)_3$-C-O-H produced from the radical initiator di-tert-butyl peroxide $((CH_3)_3$-C-O-$)_2$ as noted in the literature [2]. It should however be said that no corresponding OH group to the *tert*-butyl alcohol could be identified. A further possibility for this signal is therefore a $(CH_3)_3$-C-O- end group.

The application of fluorine decoupling should give a more resolved proton spectrum, as homonuclear coupling is reduced. Hence it should be possible to assign ^1H and ^{19}F coupling to the individual signals in figure 1. It should be noted that when observing protons and decoupling fluorine it was not possible to do H_2O saturation.

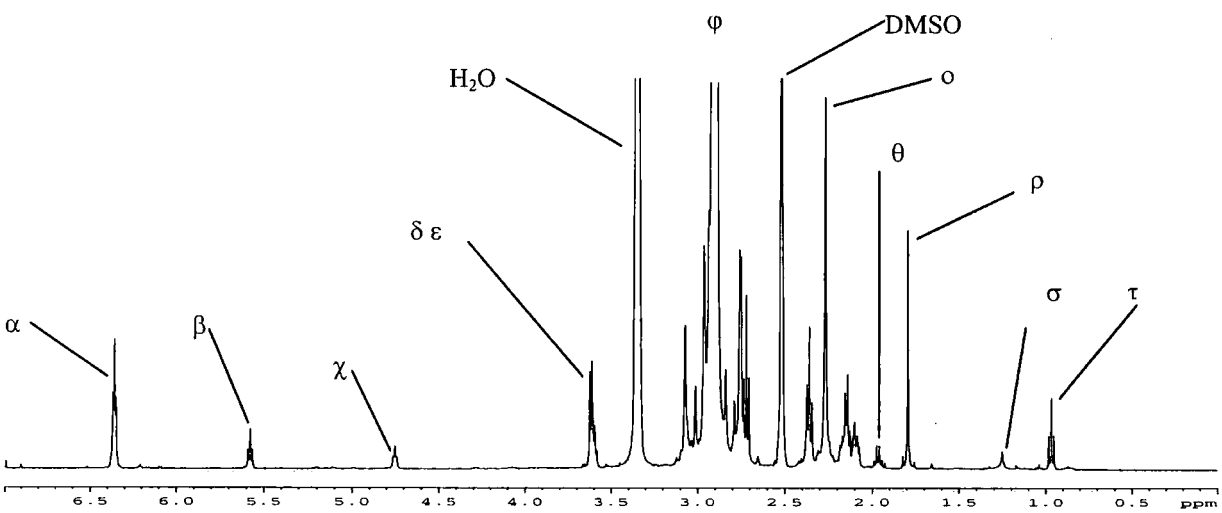

Figure 4.2 The fluorine-decoupled proton spectrum of the VDF telomer in DMSO-d_6 at 22°C, assignments are given in table 2.

Major signals in the proton spectra with fluorine decoupling

Figure 4.2 shows the fluorine decoupled proton spectrum of the VDF telomer and figure 3 shows an expansion of the same. The effect of proton decoupling is seen clearly in the signal at 6.360 ppm (α), which now shows no proton to fluorine coupling as seen in figure 1. This signal is now a signal triplet with a $^3J_{H-H}$ 4.40 Hz. The signals at 3.615 (δ), 3.600 (ε) ppm (figure 4.3) are more resolved with decoupling yet still retain some splittings. A comparison of the proton spectrum with and without fluorine-

decoupling can be seen in figure 4.4a and 4.4b. That the signal at 3.615 ppm (δ) is now a doublet with no fluorine coupling and with an increase in relative intensity. The signal at 3.600 (ε) (figure 4.4b), with a $^{3}J_{H-H}$ ~6.30 Hz coupling, appear to be a triplet of doublets, although they are not well resolved.

δ ^{1}H	Signal Intensity	Multiplicity		$^{3}J_{H-H}$	Assignments
6.360	1.00	t	α	4.40	$-CF_2H$
5.578	0.32	t	β	6.36	$-CF_2-CH_2-OH$
4.751	0.30	t	χ	5.38	$-CH_2-CH_2-OH$
3.622	1	d	δ	6.30	$-CF_2-CH_2-OH$
3.600		d	ε	6.41 and 5.31	$-CH_2-CH_2-OH$
3.348					H_2O
3.072	0.56	s	ϕ		
3.012	0.70	s	γ		
2.963	0.35	s	ι		
2.936	0.21	s	υ		
2.905	24.25	s	φ		$-CH_2-CF_2-CH_2-CF_2-CH_2-$
2.837	0.22	s	ϖ		
2.792	0.18	s	ω		
2.753	1	d	κ	4.40	$-CF_2-CH_2-CF_2H$
2.720	1.22	t	λ	7.34	$-CF_2-CH_2-CH_2-X$
2.653	0.45	q	μ	1.96	Not identified
2.358	0.96	t	ν	7.37	$-CF_2-CH_2-CH_2-$
2.267	1.63	s	ο		$-CF_2-CH_2-CH_2-CF_2-CF_2-CH_2-$
2.138	1.43	t	π	6.30	$-CF_2-CH_2-CH_2-OH$
1.961	0.18	q	θ	7.34	$-CF_2-CH_2-CH_3$
1.794	0.59	s	ρ		$-CF_2-CH_3$
1.252	0.10	s	σ		$(CH_3)_3COH$
0.967	0.27	t	τ	7.34	$-CF_2-CH_2-CH_3$

Table 2: Chemical shifts and assignments for the proton spectra with fluorine-decoupling of the VDF telomer. Multiples are: q = quintet, qu = quartet, t = triplet, d = doublet, s = singlet.

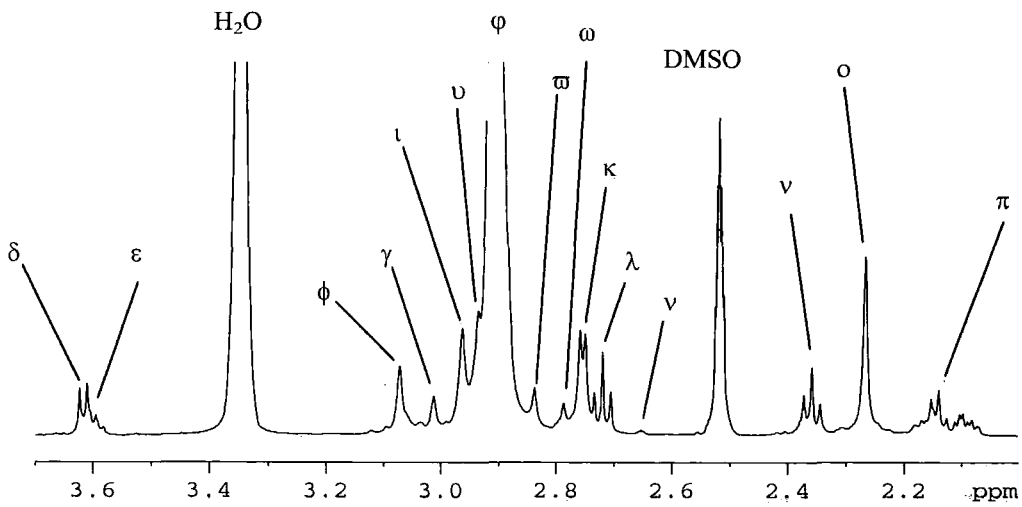

Figure 4.3 Expansion of the fluorine-decoupled proton spectrum of VDF telomer in DMSO-d_6 at 22°C. The proton assignments are given in table 3.

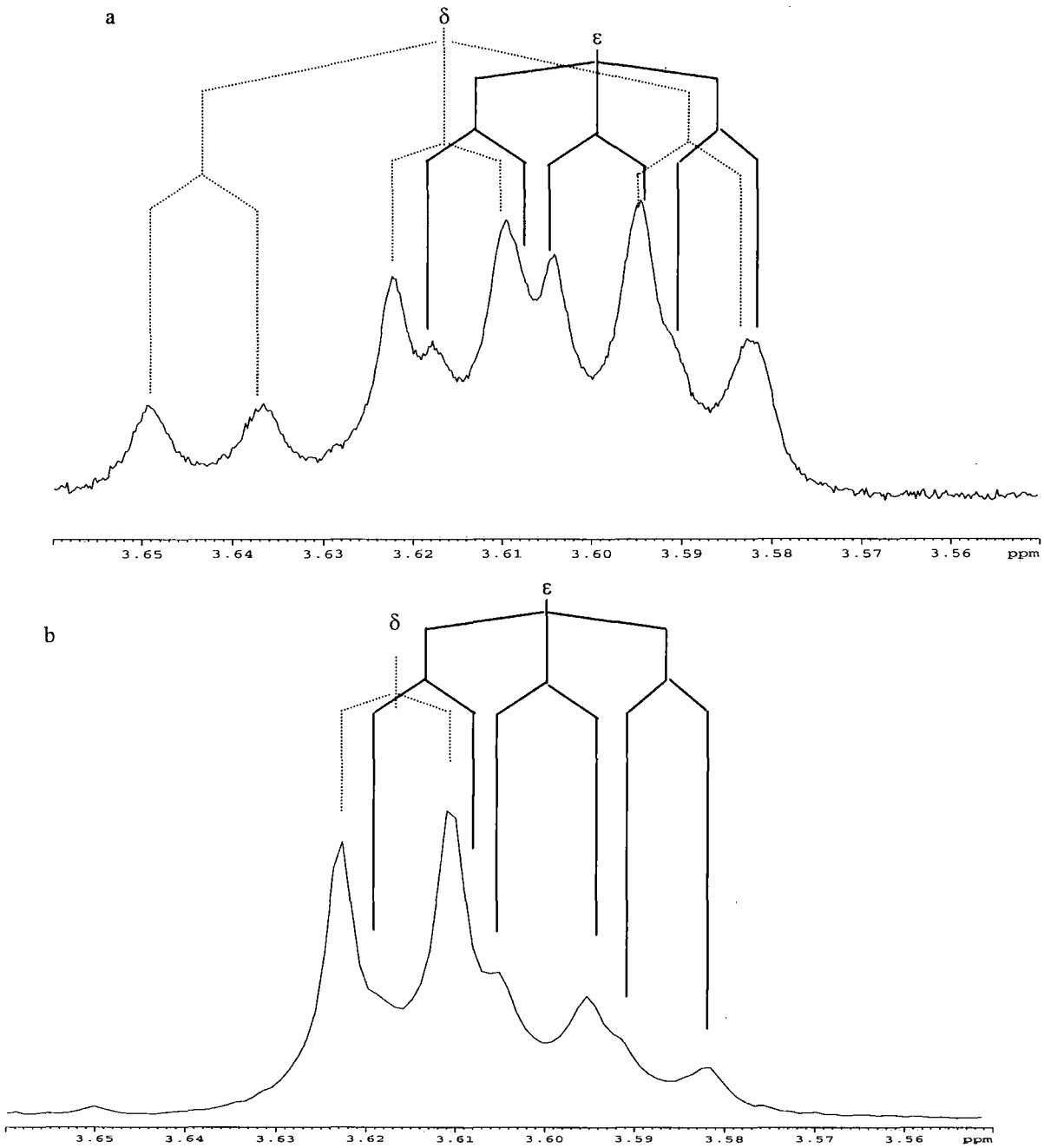

Figure 4.4 Expansion of the ^{1}H spectrum between 3.700 and 3.550 ppm, fluorine coupled (a) and decoupled (b). The proton assignments are in table 2.

Therefore the signal at 3.615 ppm (δ) in the fluorine coupled spectrum figures 4.1 and 4.4a, is a triplet of doublets with the coupling constants, $^{3}J_{H\text{-}H}$ ~6.30 Hz and $^{3}J_{H\text{-}F}$ of 14.57 Hz, corresponding to a -CF_2-C**H**$_2$-OH type structure. The signal at 3.600 (ε) a triplet of doublets could be indicative coupling from a -CF_2-CH_2-C**H**$_2$-OH structure with typical $^{3}J_{H\text{-}H}$ couplings of 4.8 Hz.

The signal at 2.905 ppm (φ) belonging to the main chain -CF_2–CH_2-CF_2- shows a single line in the decoupled spectrum, without any ^{4}J proton coupling, figure 4.5b. This

is due to the proton coupling being smaller than the linewidth ~6 Hz. The geminal proton coupling is not seen probably due to second order nature of the pattern (It should be noted that the digital resolution in these spectra is ~0.4 Hz/pt). A signal at 2.719 ppm (λ) in the fluorine-coupled spectrum is a triplet, with another signal broadening the triplet centre band, figure 6a. This signal in the fluorine-decoupled spectrum (figure 4.6b) shows a resolved triplet void of the any other signal. The signal responsible for the broadening must therefore originate from proton-fluorine coupling of the signal at 2.753 ppm (κ), which was a quintet of doublets in the proton–coupled spectrum but is now a single doublet with an increase in relative intensity, figure 4.6b. This signal has the same proton coupling as the signal at 6.30 ppm (α) and is the signal from the methylene protons of the end-group $-CF_2-C\mathbf{H}_2-CF_2H$. The singlet at 2.267 ppm (o), figure 4.7a, corresponds to reverse unit protons ($-CH_2-CF_2-CH_2-CH_2-CF_2-CF_2-$). As with the main chain signal, no $^4J_{H-H}$ coupling pattern is seen, but only a triplet with a $^3J_{H-F}$ coupling of 16.67 Hz. One would however expect to see two bands of triplets with $^3J_{H-H}$ and $^3J_{H-F}$ coupling for these protons in the fluorine-coupled spectrum and two separate triplets with $^3J_{H-H}$ coupling in the fluorine-decoupled spectrum but this is not the case.

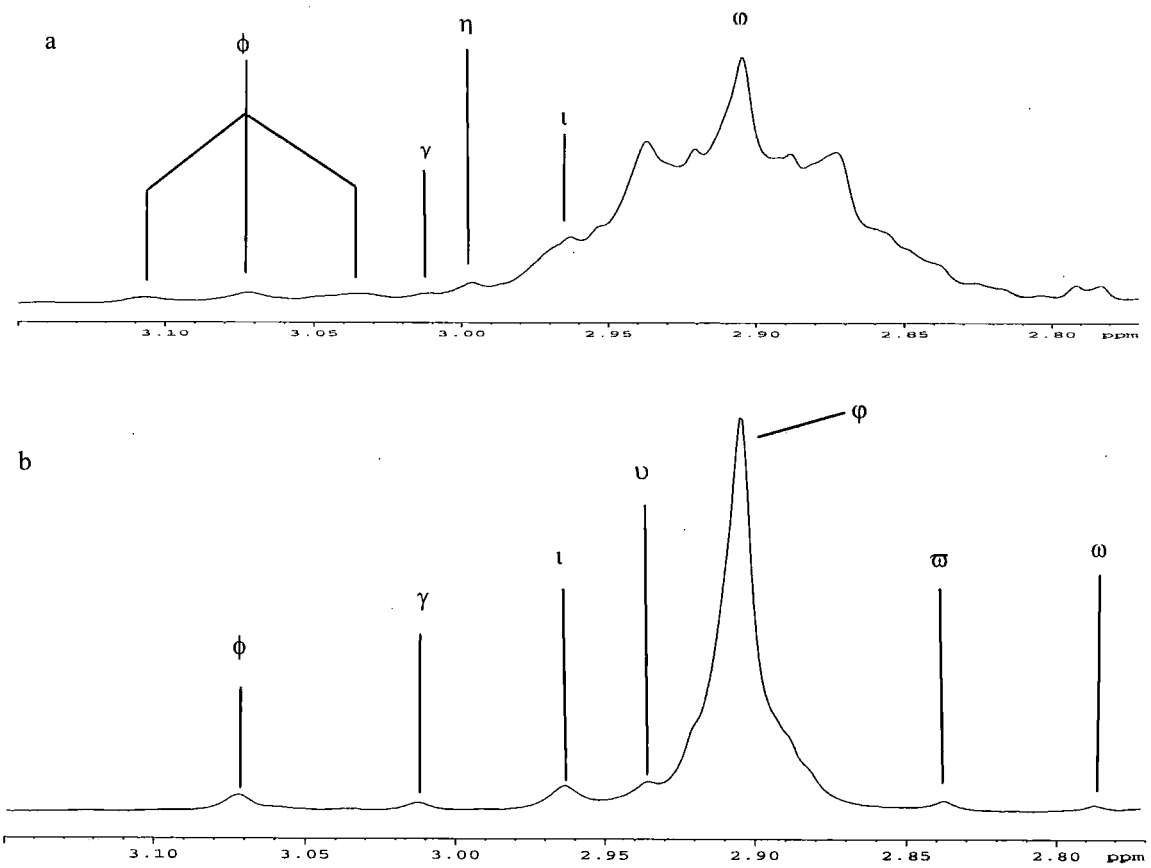

Figure 4.5 Expansion of the fluorine-coupled (a) and decoupled (b) proton spectrum. The proton assignments are shown in tables 2 and 3.

One explanation is that the $^3J_{H-H}$ coupling is smaller than the linewidth of the signal, which is ~4 Hz. A better explanation is that the signal is from both methylene groups of the reverse units, which form a $[AB]_2$ coupled system where the protons have almost exactly the same chemical shift. In this case the lines merge to a singlet.

Minor signals in the proton spectra with fluorine decoupling.

Two triplets, with relative equal intensities at 5.578 (β) and 4.751 ppm (χ), figure 4.2, showed no change with fluorine decoupling. The signal at 4.751 ppm (χ) is assigned to a primary alcohol group from the literature. The signal at 5.578 (β) could not be found in the literature but must also be an OH group. The signal at 3.072 (ϕ), which was a triplet in the spectrum without proton decoupling, is now a singlet with increased intensity. The signals at 3.012 (γ) and 2.936 (ι) ppm are also present but the signal at 2.963 (η) is not suggesting that this signal is part of a $^3J_{H-F}$ coupling pattern, figure 5a. All of these signals have similar linewidths of 6 Hz, to the main chain signal; therefore no proton or fluorine coupling is seen for the same reasons as stated above. The fluorine-decoupled spectrum (figure 4.5b), shows an increase in resolution for these signals. The increase in resolution also reveals the presence of new signals at 2.936 (υ) 2.837 (ϖ) and 2.792 (ω) ppm, figure 4.5b. A doublet is seen at 2.753 ppm (κ), figure 6b, this was a quintet of doublets (figure 4.5a), so it is obviously coupled to two CF_2 groups. Its relative intensity has also increased compared to the triplet at 2.720 ppm (λ). The difference between the fluorine coupled and decoupled spectra in this region, is shown in figure 4.6a and 4.6b. The triplet at 2.720 ppm is now well resolved with no other signal contribution and must be a $-CH_2-C\mathbf{H}_2-$ type structure with the two methylene groups non-equivalent.

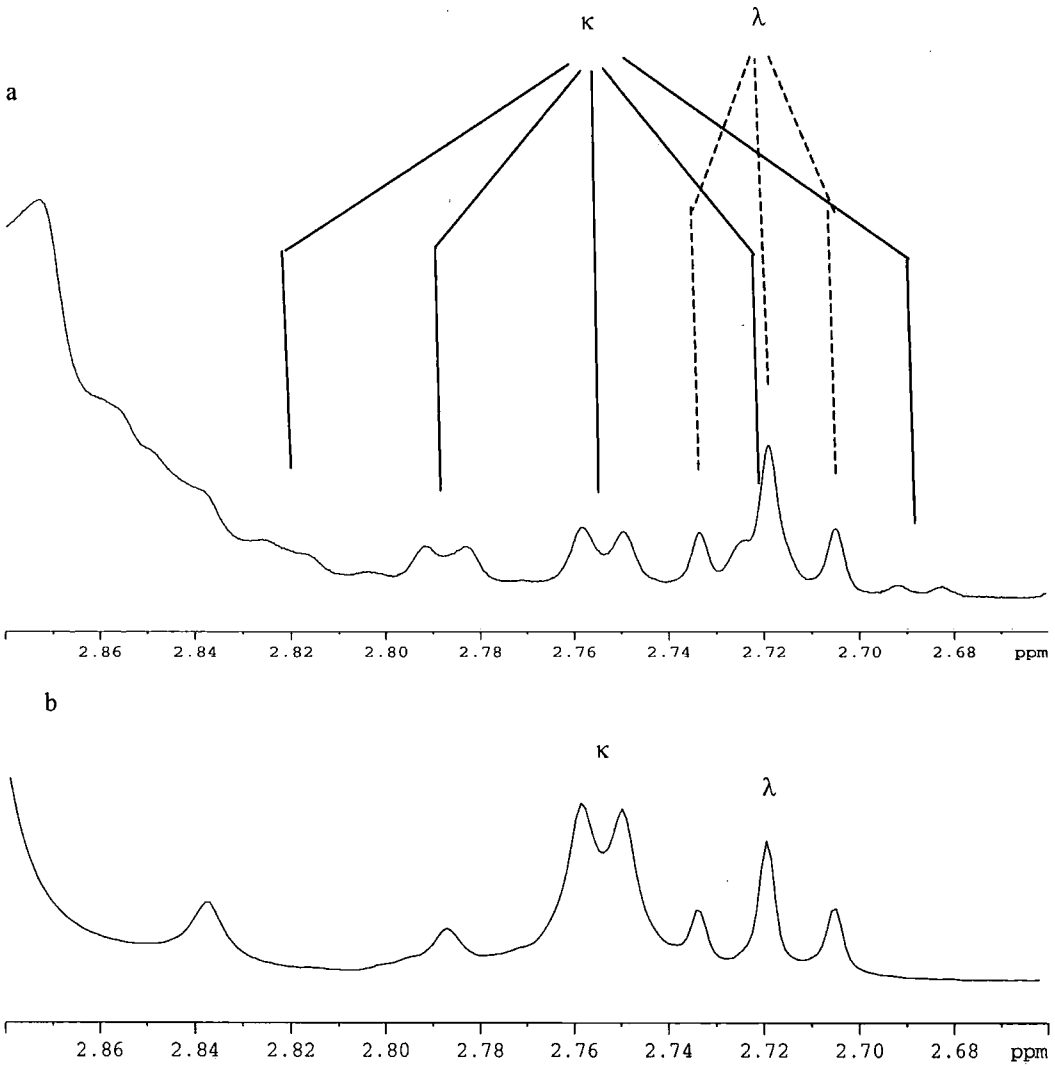

Figure 4.6 Expansion of the ^{1}H spectrum, fluorine coupled (a) and decoupled (b) the proton assignments are shown in tables 2 and 3.

Figure 4.7 shows a comparison between the proton spectra with (4.7b) and without (4.7a) fluorine decoupling for the region between 2.4 and 1.9 ppm. The multiplet signal at ~2.358 ppm (ν) in figure 4.7a is reduced to a triplet when decoupling is applied showing that the multiplet is a triplet of triplets with 7.34 $^{3}J_{H-H}$ and 17.63 $^{3}J_{H-F}$ coupling constants for a CF_2-CH_2-CH_2 unit. The signals at 2.138 ppm (π) are complex, yet a triplet of triplets is identifiable figure 7a.

The multiplet centered at 2.138 ppm (π) changes intensity and is still a complex when decoupled.

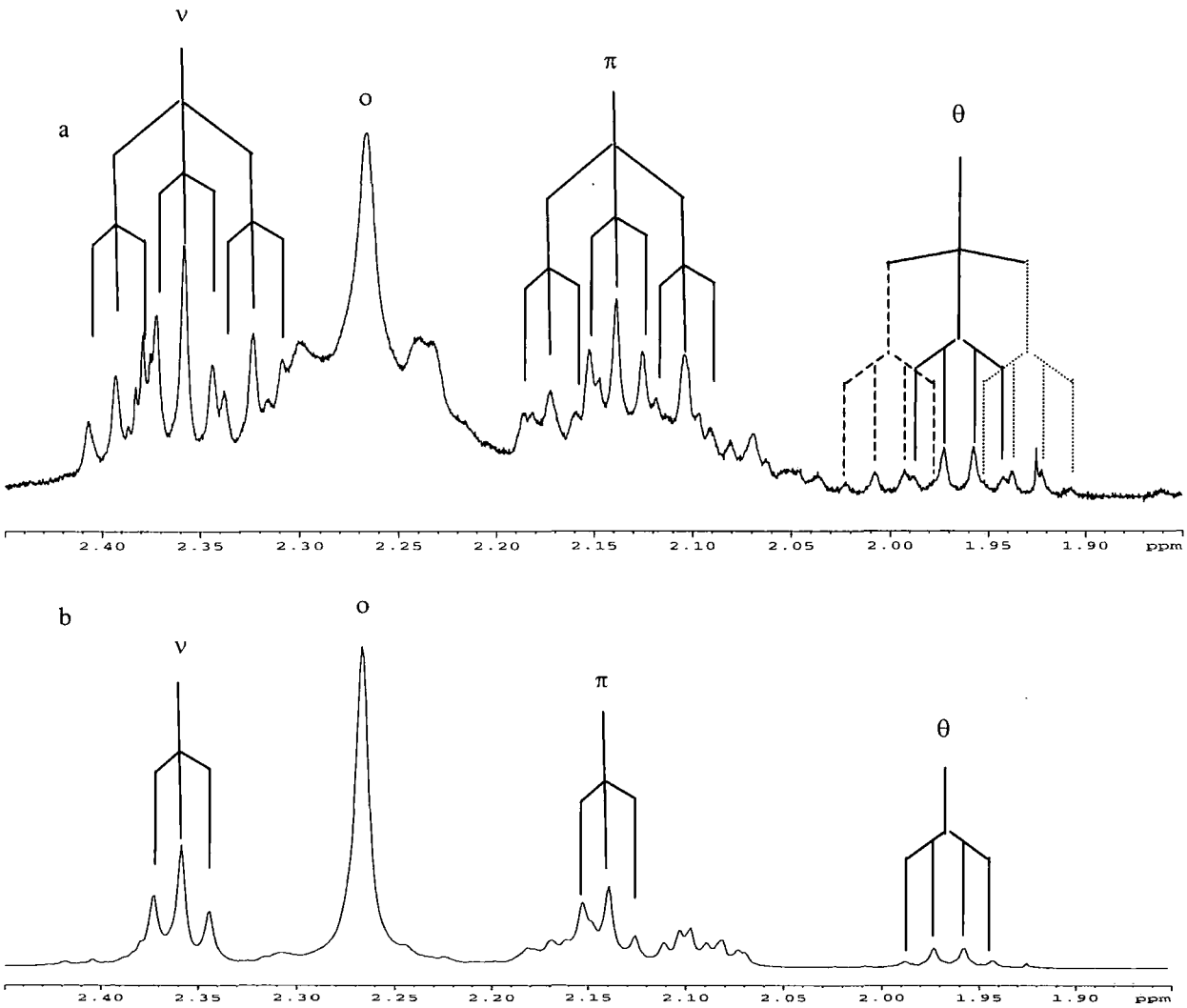

Figure 4.7 Expansion of the proton spectrum, fluorine coupled (a) and decoupled (b) the proton assignments in table 2 and 3.

This signal is assigned to a triplet of triplets $-CF_2-CH_2-CH_2-$ with a $^3J_{H-H}$ of 6.3 Hz and a $^3J_{H-F}$ of 16.56 Hz. There is also a group of signals centred at ~2.109 ppm in the decoupled spectrum figure 4.7 b. No coupling or assignment could be derived for these signals.

A triplet of quartets ~1.961 ppm (θ) is seen, figure 4.7a. With decoupling, figure 4.7b, a quartet is resolved. This signal has similar $^3J_{H-H}$ and $^3J_{H-F}$ to those of signal o and they are assigned to a $CH_3-CH_2-CF_2-$ end-group. The singlet at 1.794 ppm (ρ), which was a triplet in the fluorine-coupled spectrum with a 19.7 Hz coupling constant (figure 4.1) is now a singlet in the decoupled spectrum (figure 2,) which suggests a $-CF_2-CH_3$ end group. The singlet at 1.252 ppm (σ), assigned to tert-butyl alcohol showed no change with decoupling nor did the triplet at 0.967 ppm (τ) indicating a $-CH_2-CH_3$ end group.

4.3 Proton Correlated Spectroscopy.

The proton COSY spectrum was recorded with no ^{19}F decoupling (figure 4.8). The assignments here are made with the chemical shift data in table 1. The connectivities of signals from the COSY experiment are listed in table 3. The proton COSY spectrum, showed the triplet signal at 6.360 ppm (α) to couple with the quintet of doublets at 2.753 ppm (κ) verifying the end-group $-CF_2-CH_2-CF_2H$. No further coupling for these signals was detected. The triplet at 5.579 ppm (β) showed coupling to the triplet of doublets at 3.615 ppm (δ). This coupling suggests a $HO-CH_2-CF_2-$ type structure. The triplet at 4.751 ppm (χ) showed an off-diagonal peak to the signal at 3.600 ppm (ε) which showed further correlation to a triplet of triplets at 2.123 ppm (π). This is indicative of a $-CF_2-CH_2-CH_2-OH$ end-group.

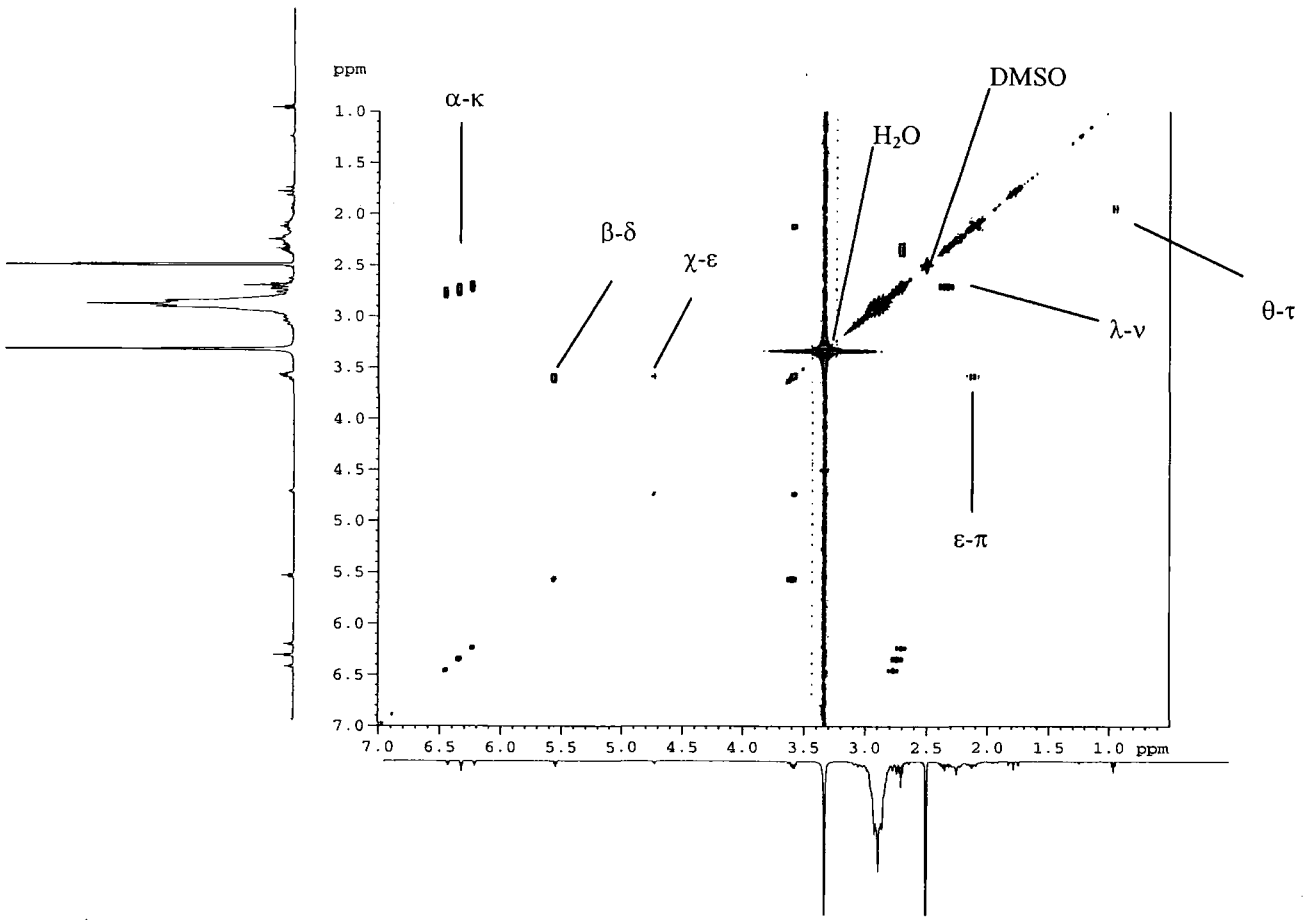

Figure 4.8. The fluorine-coupled proton COSY spectrum of the VDF telomer in DMSO-d_6 at 22°C

δ ^{1}H ppm for correlation's		Assignment
6.360 (tt) to 2.753 (qd)	α-λ	CF_2-CH_2-CF_2H
5.579 (t) to 3.615 (d)	β-δ	-CF_2-CH_2-OH
4.751 (t) to 3.600 (t)	χ-ε	-CH_2-CH_2-OH
3.600 (t) to 2.132 (m)	ε-π	-CF_2-CH_2-CH_2-OH
2.723 (t) to 2.358 (t)	κ-ν	-CH_2-CH_2-CF_2
1.965 (tq)to 0.967 (t)	θ-τ	-CH_2- CH_3

Table 3. The results from the ^{1}H ^{19}F-coupled COSY spectrum (figure 8). The coupling d=doublet, t=triplet and m= multiplet are taken from the fluorine decoupled proton spectrum.

The signal at 2.753 ppm (κ) correlates to a triplet at 2.358 ppm (ν) with a 7.35 $^3J_{H-H}$ coupling. The signal at 2.358 ppm (ν) also shows a 17.63 Hz $^3J_{H-F}$ coupling in the fluorine-coupled spectrum (figure 4.1) giving the structure -CF_2-CH_2-CH_2-X. The signal at 1.965 ppm (θ) a triplet of quartets and 0.965 ppm (τ) have correlation, as seen in table 3 both have a $^3J_{H-H}$ 7.34 Hz coupling and similar intensities and is assigned to – CF_2-C**H**$_2$- C**H**$_3$ structure. The triplet at 1.794 ppm (ρ) with a $^3J_{H-F}$ 19.77 Hz, figure 4.1, shows no correlation in the COSY spectrum and but is seen as a singlet in the proton decoupled spectrum, figure 4.4, showing that this is ^{19}F -^{1}H coupling. This signal is assigned to a methyl group linked to difluoromethylene CH_3-CF_2-CF_2-.

4.4 ^{19}F Solution state NMR spectroscopy.

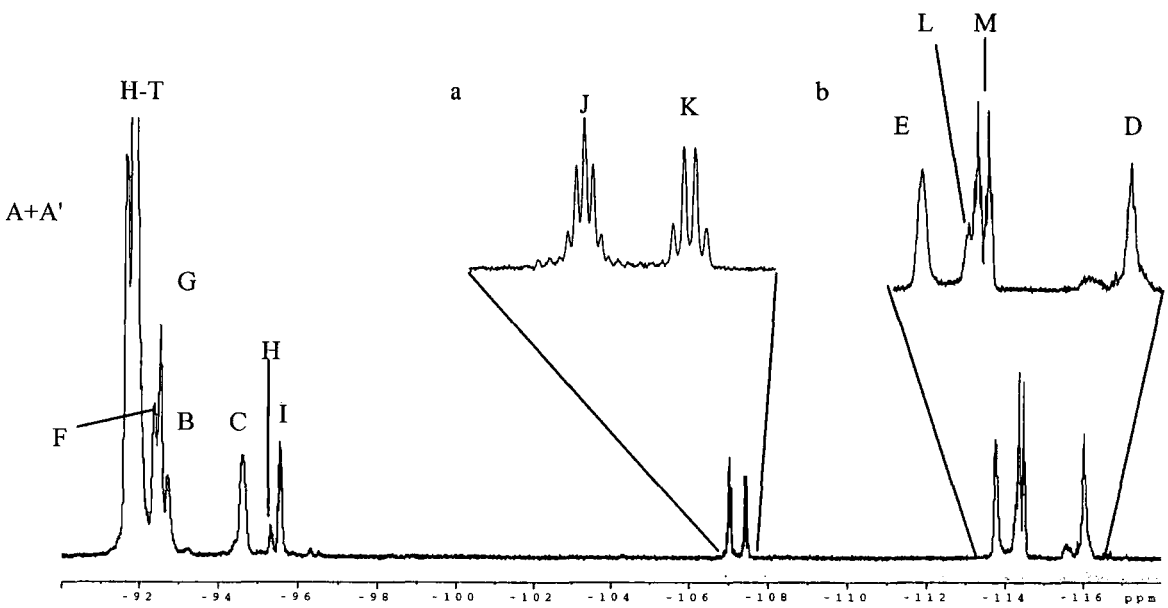

Figure 4.9 ^{19}F spectrum of the VDF telomer in DMSO-d_6 and at 22°C with no proton decoupling.

The proton-coupled fluorine spectrum of the VDF telomer in DMSO at 22°C is illustrated in figure 4.9 and assignments and chemical shift values given in table 4. The most intense peak in the spectrum, -91.878 ppm, arises from CF_2 groups of regular $(CF_2CH_2)_n$ chains remote from any defects. The signals A+A`, F, B, C, D and E are basically the same structural unit as discussed in chapter 2 for PVDF and this will be shown later in this chapter. The spectrum shows two signals at –107.012, a quintet, and –107.413 ppm, a quartet, with $^3J_{F-H}$ coupling of 14.7 and 19.8 Hz respectively. These signals are often assigned to branching and end-group related structures.

δ ^{19}F	Relative Intensities	Signal	Coupling/Hz	Assignment
-91.689	50.12	s		A+A`
-91.878		s		H-T Main Chain
-92.390	7.94	s		F
-92.550		m	9.5	G
-92.737		s		B
-94.632	2.91	s		C
-95.332	0.52	m	9.5	H
-95.568	1.72	m	9.5	I
-107.012	0.96	quintet	14.7	J
-107.413	0.73	q	19.8	K
-113.768	2	s		E
-114.319	4.18	m		L
-114.422		ttd	55.2 16.4, ~4.0	M
-116.027	2.10	s		D

Table 4. Chemical shifts and assignments for the ^{19}F spectrum the VDF telomer with no proton-decoupling. Multiples are: t = triplet, d = doublet, s = singlet.

The signals G, H and I are all multiplets, all showing $^3J_{F-H}$ coupling of 9.5 Hz as seen in figure 13a. The signal M, figures 4.9 and 4.15, assigned to the $-CH_2-CF_2H$ end-group, shows several $^3J_{F-H}$ and $^2J_{F-H}$ couplings and is discussed later in this section. The application of proton-decoupling should simplify the spectrum and allow the assignment of signals with $^3J_{F-H}$ coupling and give signals with $^3J_{F-F}$ coupling pattern only.

Figures 4.10 shows the proton-decoupled fluorine spectrum of the VDF telomer and figures 4.11 and 4.12 are expansions of the area around the main chain signal. The assignments and intensities are shown in table 5. The major difference here is the increase in resolution, as would be expected with proton decoupling. This is seen in the increased resolution in the region of the main chain signal H-T where several signals are now visible; these signals are labeled N, O, and P, figure 4.12.

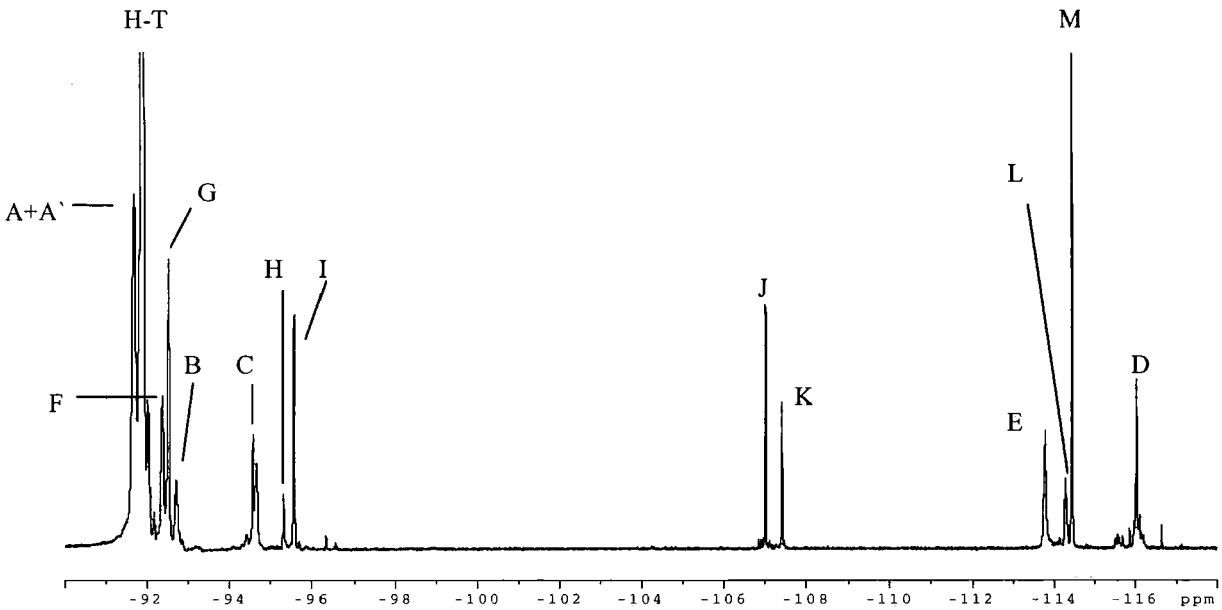

Figure 4.10. The proton-decoupled fluorine spectrum of the VDF telomer in DMSO-d_6 at 22°C.

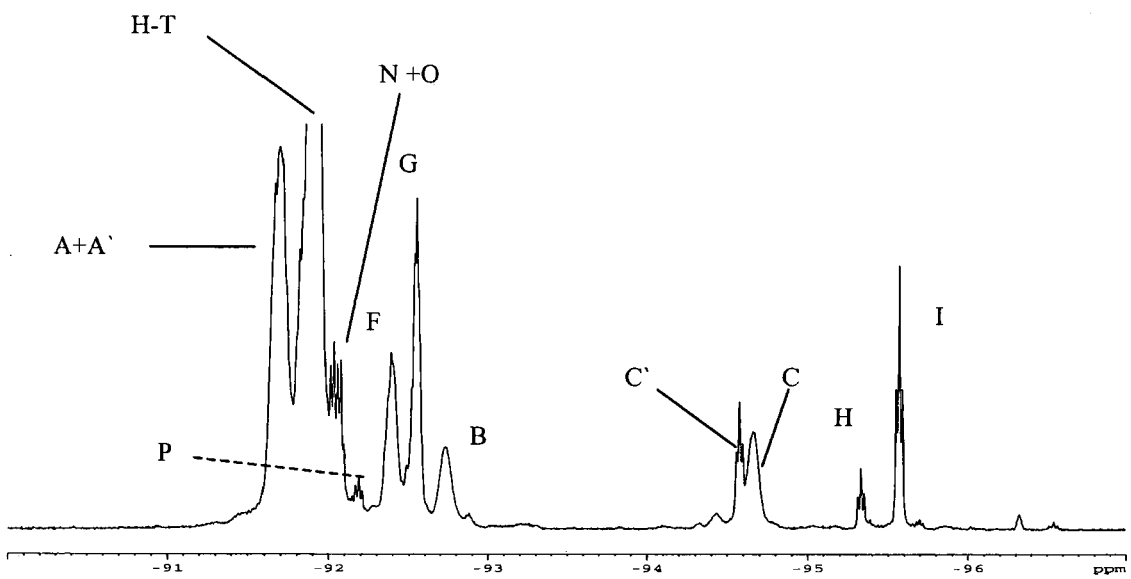

Figure 4.11. ^{19}F proton-decoupled spectrum of the VDF telomer in DMSO-d_6 at 22°C.

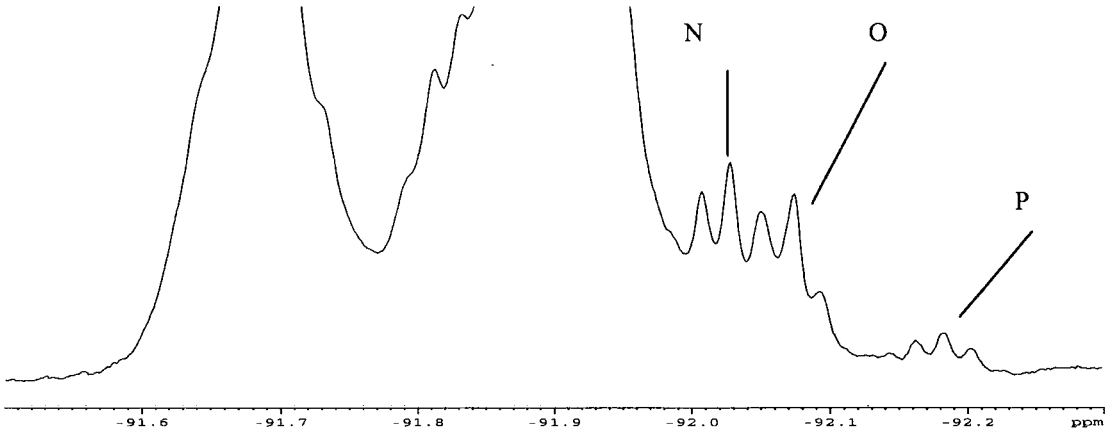

Figure 4.12. The proton-decoupled fluorine spectrum of the VDF telomer in DMSO-d_6 at 22°C. Expansion of the main chain region.

δ ^{19}F	Relative Intensity	Signal	^{19}F coupling	Assignment
-91.690		s		A+A`
-91.897		s		H-T Main Chain
-92.034	50.71			N
-92.078				O
-92.191	0.28	t	9.5	P
-92.390	0.92		9.5	F
-92.550	0.42			G
-92.735	0.21			B
-94.577	1.08	t	9.5	C`
-94.659	0.12	s		C
-95.330	0.43	t	9.5	H
-95.568	1.65	t	9.5	I
-107.010	0.98	s		J
-107.415	0.78	s		K
-113.768	2.00	s		E
-114.319	0.72	t	10.12	L
-114.423	2.93	t	~4	M
-116.226	1.97	s		D

Table 5 Chemical shifts and assignments for the ^{19}F spectra with proton-decoupling, with ^{19}F-^{19}F coupling constants.

The signal C is now resolved into two, now labelled as C` and C, at 9.577 and 94.659 ppm respectively. Together with C`, H and I, all these signals are triplets and have the same $^3J_{F\text{-}F}$ coupling of ~ 9.5 Hz independent of decoupling, except C, which is still broad. This would seem to indicate that the $^3J_{F\text{-}H}$ and $^3J_{F\text{-}F}$ couplings are of very similar magnitude for these signals. However, both the signals H and I (figure 4.13) showing intensities 1:2:5:8:10:12:10:8:5:2:1,could also be from a 4 spin system showing $^4J_{F\text{-}F}$ coupling of ~9 Hz and a $^3J_{F\text{-}H}$ coupling ~19Hz. The signal C` also shows similar

behaviour. The signals J and K are now singlets proving that the splitting seen in figure 9 for these signals was indeed caused by $^{3}J_{F-H}$ coupling. The effect of proton decoupling for the signals G, C, H and I is clearly seen in figures 4.11 and 4.13a-b

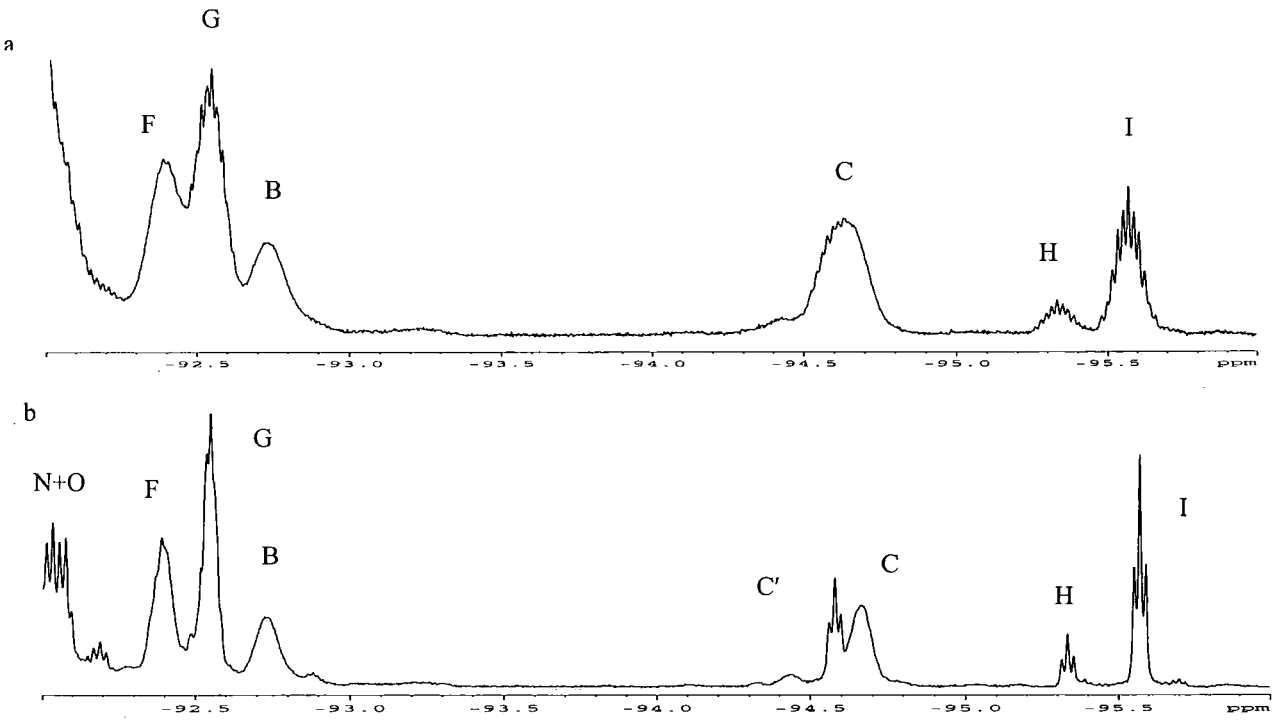

Figure 4.13 Expansion of the ^{19}F spectrum of VDF telomer with no proton decoupling (a) and with proton-decoupling (b).

An expansion of the reverse unit signals E and D, with and without proton-decoupling is shown in figure 4.14(a) and 4.14(b) respectively. The full linewidths of the proton-coupled signals are ~50 Hz (E) and ~44 Hz (D). When proton-decoupling is used this becomes ~33.0 Hz (E) and ~16 Hz (D), so linewidths are reduced by one half. Still none of the signals show any well-resolved $^{3}J_{F-H}$, $^{3}J_{F-F}$ or $^{2}J_{F-F}$ coupling. This again shows that the linewidths of the signals are greater than the coupling or that long range coupling or second-order effects are important. The $^{3}J_{F-F}$ couplings are expected to be 1.8 to 5.1 Hz as discussed in the opening section of this chapter.

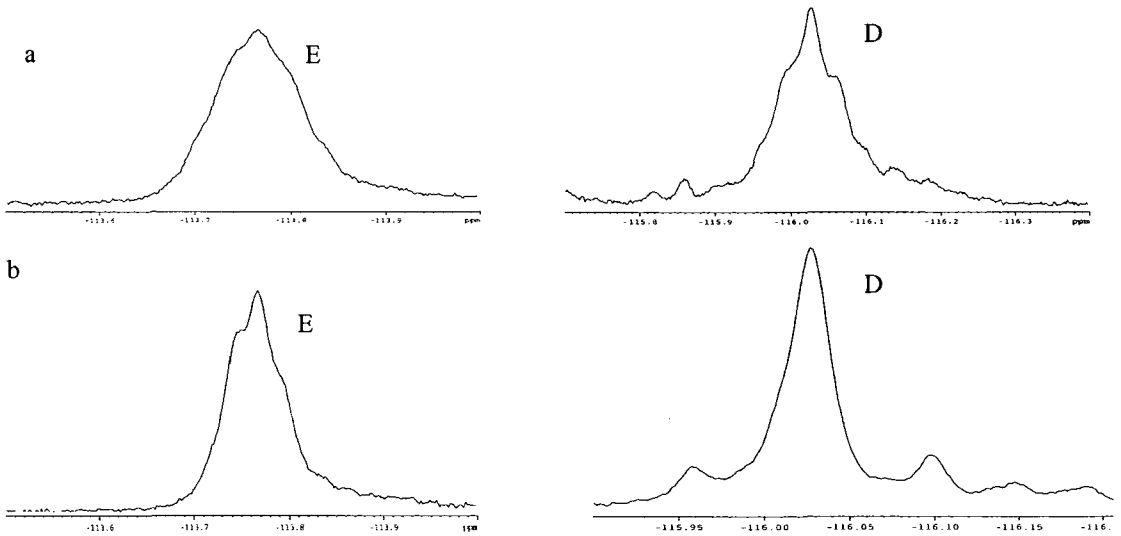

Figure 4.14. Expansion of the proton-coupled (a) and proton-decoupled (b) ^{19}F spectrum showing the CH_2-CH_2-CF_2-CF_2 reverse unit signals, E and D of the VDF telomer.

Perhaps the most striking difference is seen in the -CH_2-CF_2H end-group signal at – 114.372 ppm, figure 4.15a, which is dominated by $^2J_{F-F}$ and $^3J_{H-F}$ coupling. With proton decoupling, the signal now looks like a triplet with a $^4J_{F-F}$ of 4 Hz.

This would be true for an end-group structure of the type -CF_2-CH_2-CF_2H and analogous effects are seen in the proton spectrum, figure 4.1, in the signals at 6.360 (α) and 2.753 ppm (λ). The signal L, which was broad in the proton coupled spectrum, is now a triplet with a ~10.12 Hz $^3J_{F-F}$ coupling.

The geminal $^2J_{F-H}$ coupling of 55 Hz, as seen in the proton spectra at 6.360 ppm (signal α), figure 1, is seen here in the doublet signal M. The latter signal is split further with a vicinal $^3J_{F-H}$ coupling of 16.4 Hz. No further analysis of this signal is made at this stage. The 470.18 MHz fluorine spectra with proton decoupling, shows a great improvement in resolution compared to the majority of work in the literature. The reason for this is that many workers do not have the possibility to do simultaneous high frequency observation with high frequency decoupling. The increase in resolution is clearly seen in the signals N, O and P adjacent to the main chain signal but is obvious in the rest of the signals too, e.g. G, H, M and I. The effect of magnetic field strength, combined with heteronuclear-decoupling is clearly seen at 500 MHz (see also [9, 12]), but not in spectra taken below 300 MHz [2, 5, 6, 7, 10]. Unfortunately, the majority of work in the literature is done below this field strength, giving poor resolution and direct comparison with this work ambiguous.

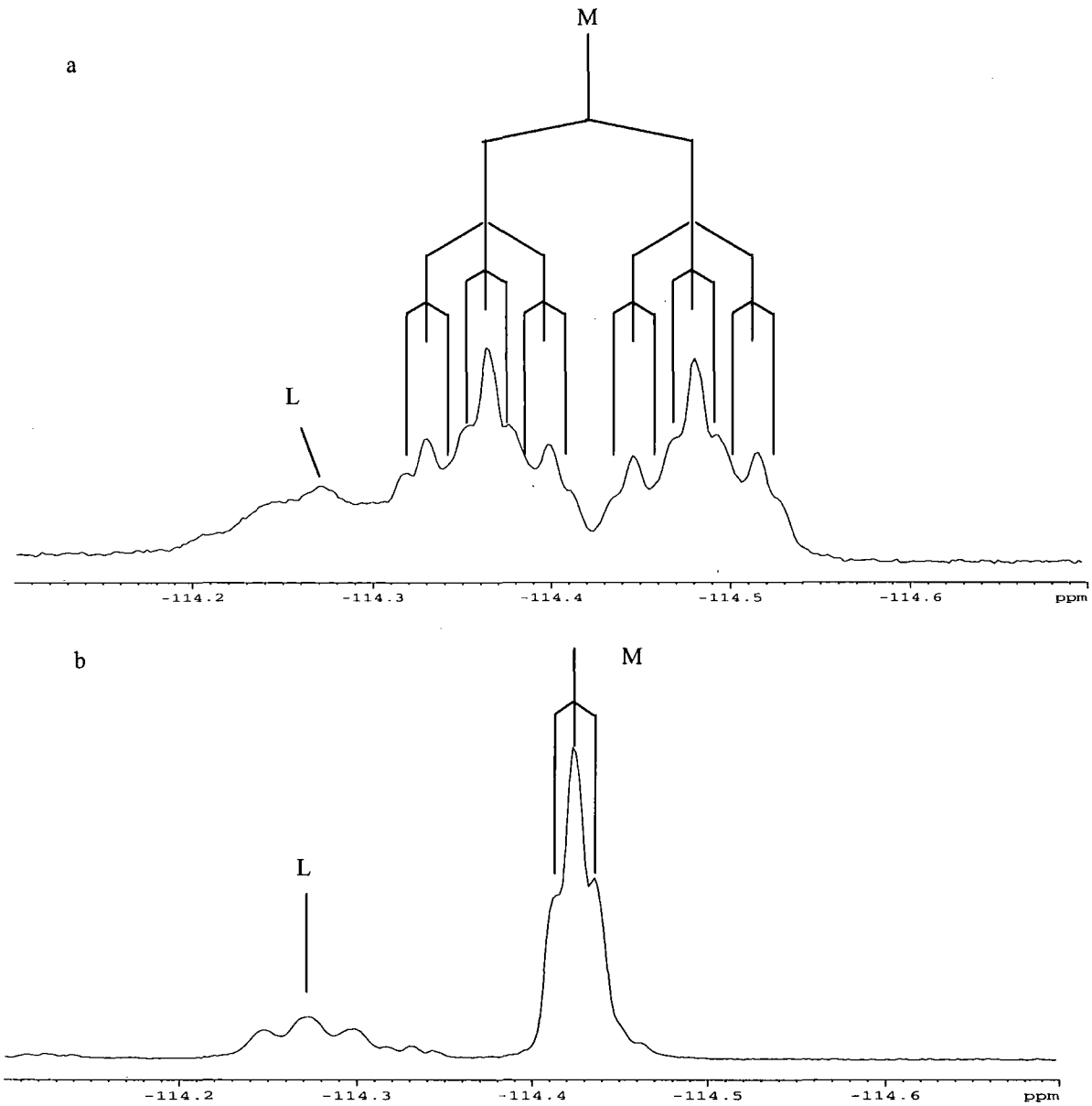

Figure 4.15 Expansion of the proton coupled (a) and decoupled (b) ^{19}F spectrum showing the -CH_2-CF_2H chain end signal M of the VDF telomer. The signal M shows fluorine to proton coupling and four-bond fluorine to fluorine.

Compared to the fluorine spectrum of PVDF discussed in chapter 2, the VDF telomer shows several new signals G, H, I and C` but also some very similar signals of specific interest J, K, and M.

It is therefore of interest to designate these signals to the structure of VDF telomer or to that of other substances possibly formed during polymerisation. The signals between −106 to −107 ppm (figure 4.9), have been attributed to end-groups -CF_2-CH_3, branches

or oligomeric species etc [22, 25, 27, 30, 31]. Therefore, ^{19}F COSY and TOCSY spectroscopy were used to decide homonuclear connectivity.

4.5 Fluorine Correlated Spectroscopy.

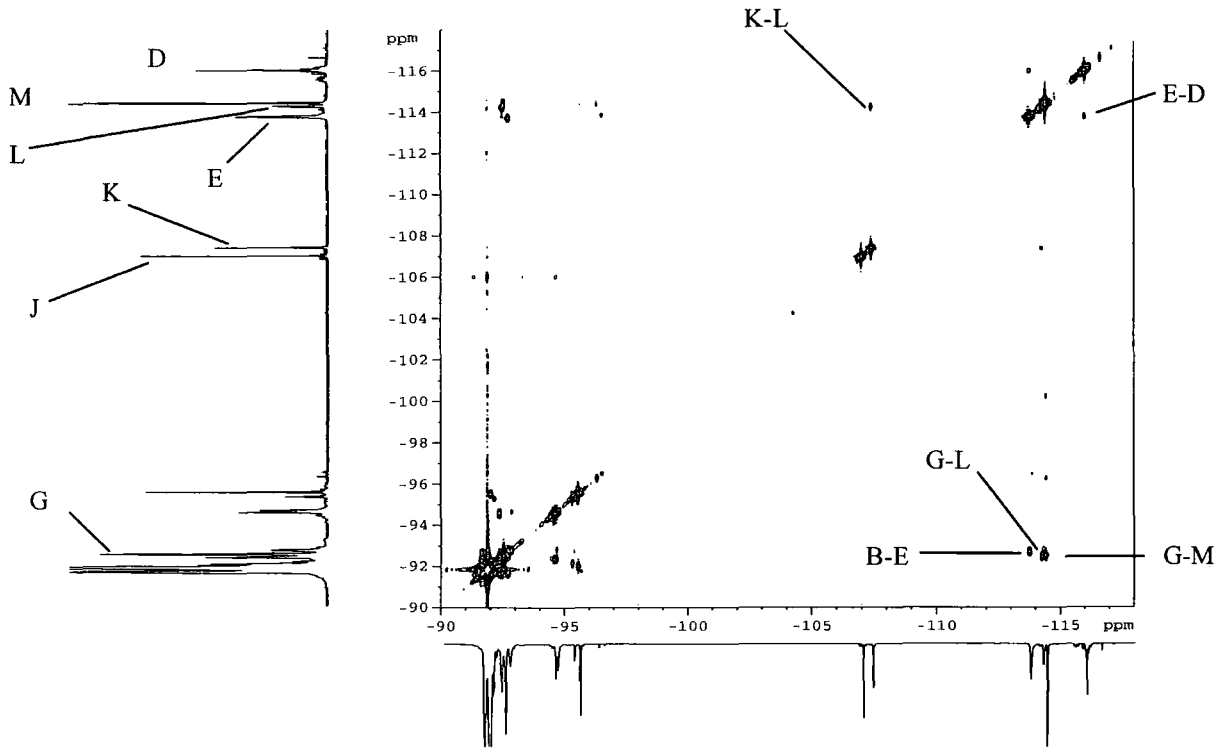

Figure 4.16. The ^{19}F COSY spectrum of the VDF telomer in DMSO-d_6 at 22°C.

Figures 4.16 and 4.17 shows the ^{19}F COSY spectrum of the VDF telomer. Three- and four-bond J-coupling effects are observed but no longer-range (^5J) couplings are detected.

The off diagonal cross peaks show the connectivity of the various fluorine nuclei. The lettering of the signals and their chemical shifts are noted in table 5.

Interesting features to note in the spectrum (figure 4.16) are the signals J and K. The signal J does not show any cross peaks at all, verifying that this site is remote from other fluorine atoms, but does not exclude it from the main chain structure at this point. However, K has cross peaks to the signal L as does G. Furthermore, G shows cross peaks to M, therefore G, K, L and M are coupled. We know that the signal M has a large doublet splitting in the ^{19}F proton coupled spectrum (figure 4.15a). This signal has a $^2J_{F\text{-}H}$ coupling of 55.2 Hz (table 4) and the same coupling constant is seen for the proton signal α at 6.360 ppm in the fluorine coupled proton spectrum (figure 1a, table 1). Therefore the signal M is for the $-CF_2-CH_2-CF_2H$ end-group. The signal K is a quartet with a 19.8 Hz $^3J_{F\text{-}H}$ coupling pattern in figure 9 and must be adjacent to both a CH_3 end group and the signal L which is seen as a triplet in figure 15 (table 5). This

would give a CH_3-CF_2-CF_2- end-group; the proton-decoupled spectrum did not show any $^3J_{F-F}$ coupling as the linewidth for the decoupled signal K was 9.5 Hz. It therefor seems that the signals K and L, which couple to each other in the fluorine COSY spectrum figure 4.16, do so with similar $^3J_{F-F}$ coupling constants. Furthermore, the signal G is associated with these two types of end groups, as discussed above, and therefore composite.

The signals E and D correlate but there is a lack of a strong correlation between D and any other signal, while E couples to another fluorine B. In figure 4.17 the signal G couples to the signal H-T and A´+A to HT. The signals C and F couple to each other and F couples to A. This means that A´ is a composite signal as B and F do not couple, nor do C and B. However, B does shows coupling to A´.

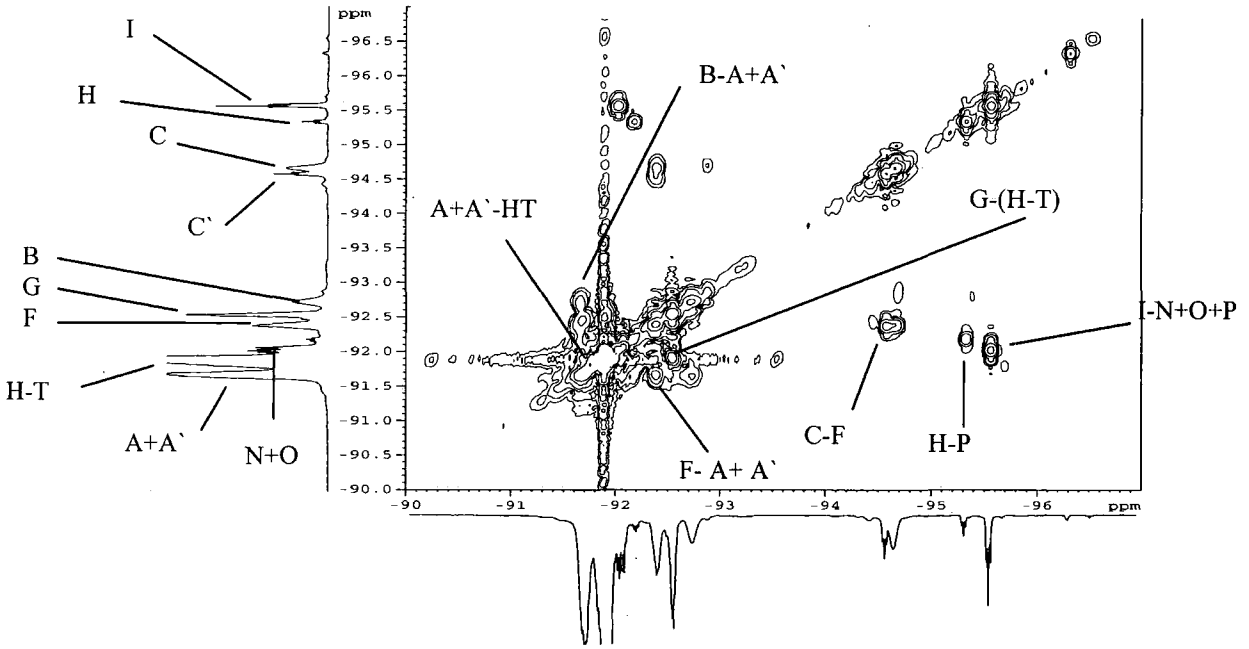

Figure 4.17. The expanded region of the VDF telomer main chain signal of the ^{19}F COSY spectrum.

From the above deductions of the off diagonal cross peaks in the ^{19}F COSY spectrum a structure of the VDF telomer can be deduced, figure 4.18.

K L G H-T A F C D E B A´ H-T G M

CF_2-CF_2-CH_2-CF_2-CH_2-CF_2-CH_2-CF_2-CH_2-CF_2-CH_2-CF_2-CH_2-CF_2-CH_2-CH_2-CF_2-CF_2- CH_2-CF_2- CH_2-CF_2-CH_2-CF_2-CH_2-CF_2-CH_2-CF_2-H

Figure 4.18. The type of structures associated with the VDF telomer assigned from the off diagonal cross peaks in figures 16 and 17, which give the correlation of the individual fluorine nuclei.

Further points to note is that I couples to N, O and P, whereas H couples only to P. Any correlation between the signals N, O and P could not be made due to poor resolution. Furthermore, the peak to high frequency (A+A′) of that for the main-chain units is composite, with cross-peaks to the signals at both –91.689 ppm as recently reported[14].

4.6 ^{19}F Total correlated spectroscopy (TOCSY)

The main principle of COSY experiments is the direct correlation of spins that share the same coupling. Total correlation spectroscopy (TOCSY) is based upon the same principle but reveals homonuclear correlation between nuclei of the same species. If there is a continuous chain of coupled spins by which magnetization can be relayed, cross peaks of nuclei belonging to the same spin system are seen in the spectrum, whether or not they are themselves coupled. The TOCSY experiment has been used here to differentiate between fluorines belonging to the main chain VDF backbone and those that do not.

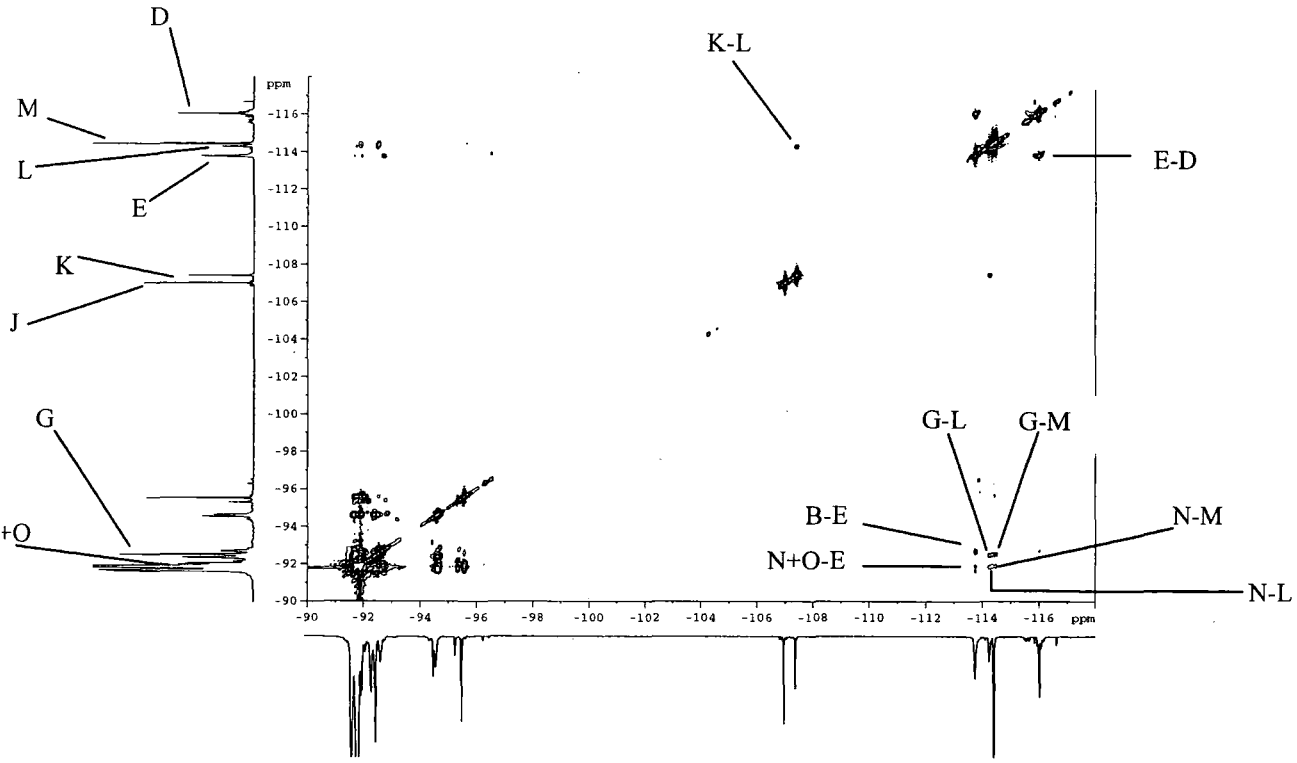

Figure 4.19. The ^{19}F TOCSY spectrum of VDF in DMSO-d_6 at 22°C without proton decoupling.

Figure 4.19 shows the ^{19}F TOCSY spectrum with cross peaks showing the connectivity of the various fluorine nuclei. The lettering of the signals and their chemical shifts are the same as previously given in tables 5 and 6. One interesting point to note is that the

signal J shows no spin correlation in the TOCSY experiment to any other fluorine suggesting, as in the COSY experiment, it is not part of or remote from the main spin system. The signals K and L correlate, as in the COSY experiment, but K shows no further spin coupling to any other fluorine. The reverse unit signals D and E correlate to each other and E correlates further to B. However D does not show any transfer of magnetization though the reverse unit to the fluorine labeled C. Signals L and M both correlate to the signal G, verifying the chain end group assigned from the previous COSY experiment. However, L and M also show correlation to N, and N and O correlate to E in the TOCSY but not in the COSY experiment. This could suggest the presence of varying chains length with similar end-group structures.

Figure 4.20 shows an expanded region of the TOCSY spectrum. Here the correlation of C to A, F and the main chain signal HT is seen, also the correlation of I to O and N. The signal H correlates only to P. The correlation for the signals F, A and HT is seen in figure 4.21 as is B to A′ and HT to A and A′.

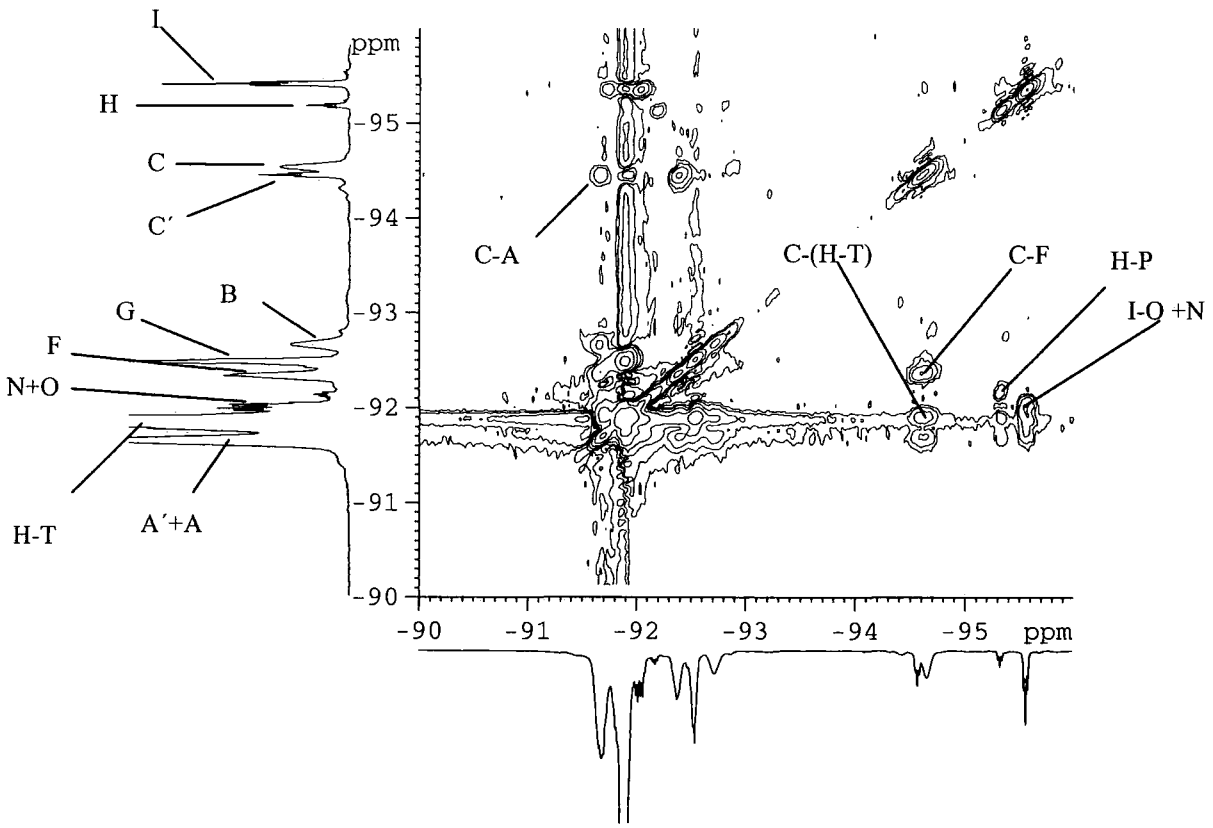

Figure 4.20. Expanded region of the VDF main chain from the ^{19}F TOCSY spectrum of VDF in DMSO-d_6 at 22°C.

The structure presented in figure 18 showing the assignment of the main chain VDF backbone, determined from the COSY experiment and consisting of the fluorine's, A, A′, B, C, D, E, F, G, K, L, M and HT, is also in agreement with the homonuclear spin

correlation seen in the TOCSY experiment. Fluorine signals, which do not correlate with any of these are, J, H. and I. However, H and I show correlation in both COSY and TOCSY experiments to the fluorine signals denoted P and N respectively (figure 4.20). Again, due to poor resolution in this area of the spectrum, further coupling of the fluorine's labelled N, O and P was not achieved. It is therefor not possible to say if these species belong to the main chain fluorine group H-T or originate from another structure.

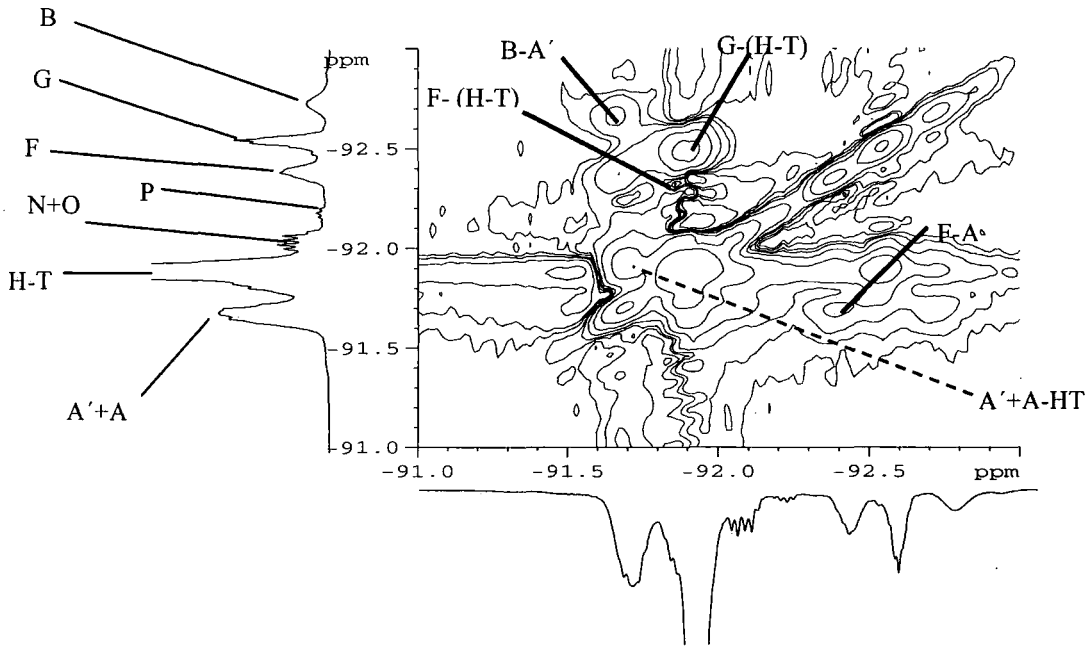

Figure 4.21. Expanded region showing the main chain and adjacent signals from the ^{19}F TOCSY spectrum of the VDF telomer in DMSO-d_6 at 22°C.

From the above information the structure of the VDF backbone has been tentatively assigned, figure 4.18. However, to achieve a full structural assignment we need to know the correlation between the fluorines and the protons. This is done by heteronuclear correlation spectroscopy (HETCOR). This type of experiment will provide us with the information, which will allow us to decide if two fluorines couple to the same proton (see appendix(i)).

4.7 Heteronuclear ^{19}F-^{1}H spectroscopy (HETCOR)

In order to determine the correlation between signals in the proton and fluorine spectra, a basic heteronuclear correlation experiment was made. The figure 4.22 shows the proton correlation for fluorine signals related to chain ends and the reverse unit.

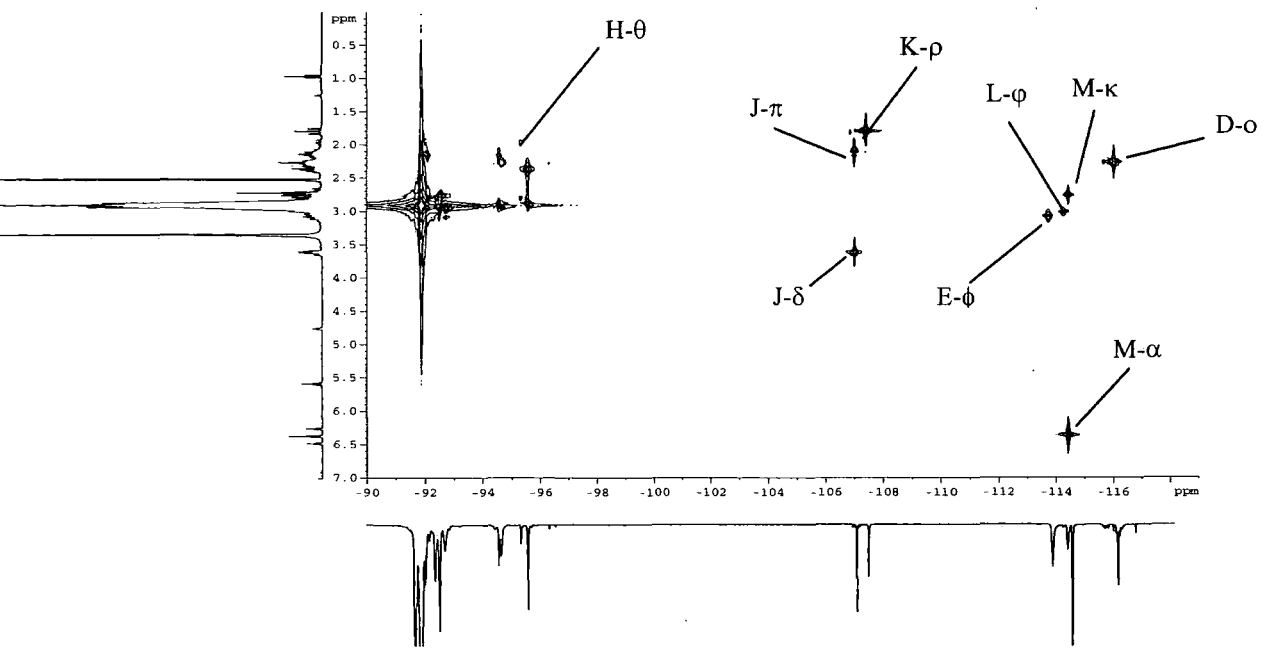

Figure 22. The ^{19}F-^{1}H HETCOR of the VDF telomer, obtained with 30 ms mixing time.

Points to note are: the correlation of the $-CH_2-CF_2H$ end group fluorine M which couples to both proton signals α and λ (figure 4.22). Furthermore K shows correlation to and L (figure 4.16) and L couples to φ. All proton-fluorine correlation is given in table 6.

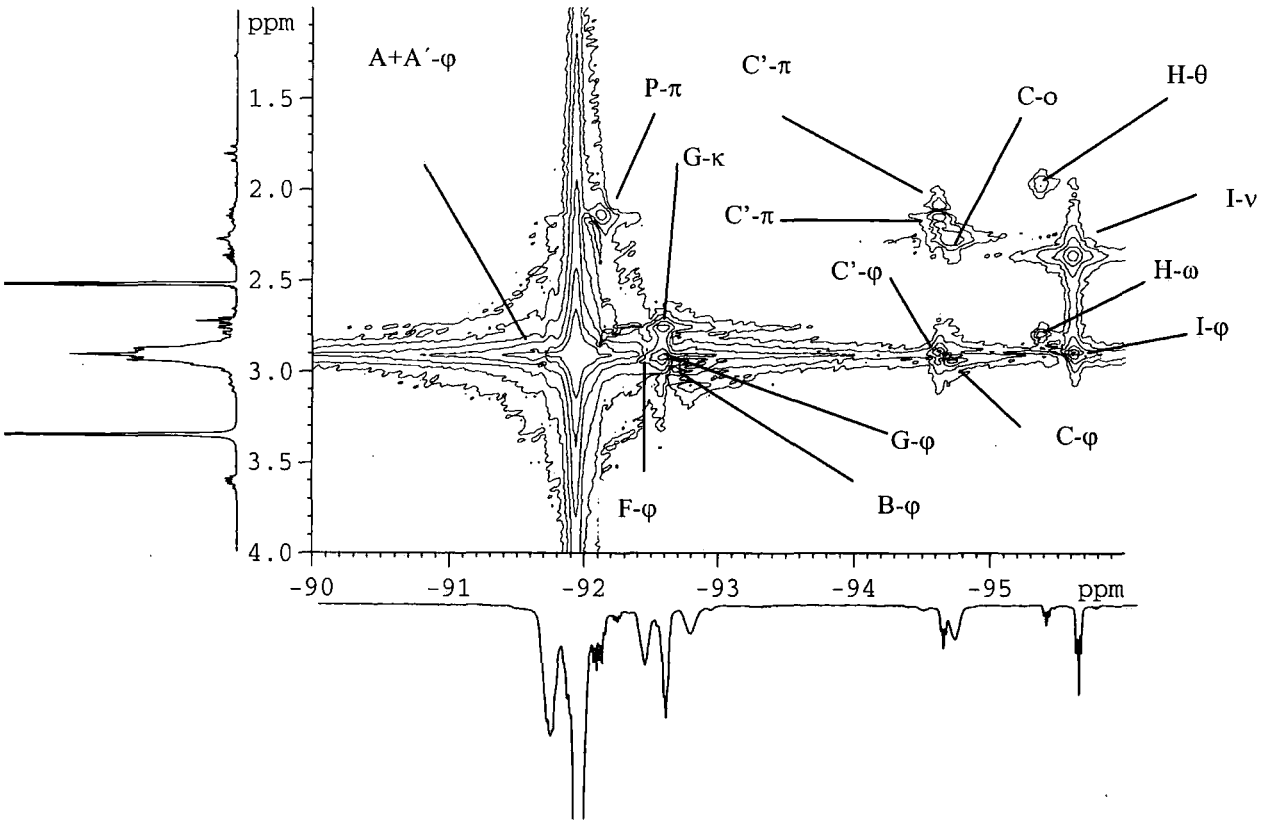

Figure 4.23. The expansion of the ^{19}F-^{1}H correlation spectrum, illustrating the main chain and adjacent signals.

It is seen in figures 4.22 and 4.23 that the fluorines D and C both couple to the reverse unit signal in the proton spectrum. The fluorine signal B showed correlation to both the main chain proton signal φ (as discussed earlier) and the signal ϕ, observed in the fluorine-decoupled proton spectrum figure 4.5 with low intensity. This shows that the intense signals seen in the fluorine spectra can have a dual source and give correlation to signals in the main chain proton signal, showing the presence of smaller structure in the sample. In figure 4.23, the signal G correlates to the proton signal κ as well as the main chain proton signal φ. This suggests an end group of the type φ-G-κ-(M). The signal K correlates to ρ which we know shows no proton to proton correlation, figure 4.3 table 4, but is a triplet with 19.4 Hz $^{3}J_{H\text{-}F}$ coupling to K. However K has fluorine coupling to L yet only L couples to the main chain proton signal φ. From the COSY spectrum, figure 4.16, both the fluorine signals L and G correlate. This is indicative of a second end group, ρ-K-L-φ-G-φ-HT-. A structural proposal for the type of units in the main chain is offered in figure 4.24. The signal J which does not have any ^{19}F-^{19}F coupling in the COSY spectrum nor any ^{19}F-^{19}F spin association in the TOCSY spectrum, does have a $^{3}J_{F\text{-}H}$ coupling of 15 Hz to two proton signals δ and π in the HETCOR experiment. Furthermore, the signal δ shows coupling to β in the proton COSY spectrum figure 4.8, giving a partial structure (A) figure 4.25. In the same COSY spectrum τ couples to θ. From the HETCOR experiment the fluorine signal H correlates to θ and ω.

Furthermore, in the fluorine COSY spectrum H correlates to P (figure 4.17). Though these two nuclei show no common proton correlation. It would therefore seem that smaller molecules are the source of the ^{19}F signal J and the hydroxyl signal β and χ in the proton spectrum. The signal I showed correlation to N, O and P in the ^{19}F COSY spectrum but only to N and O in the TOCSY spectrum. The HETCOR spectrum shows correlation for I to the protons ν and φ. We also know from the proton COSY, figure 4.8, that the protons λ and ν correlate. Furthermore in the TOCSY experiment, N correlated weakly to E, M and L, also O correlates to E, but these were not seen in the COSY experiment. The signals E, M, L and P belong to the same spin system as the signal I, but must be remote from it as these correlation are not seen in the COSY spectrum which shows only $^{3}J_{F\text{-}F}$ coupling. From this information several possibilities arise for structures contain the signal I. It should be remembered that the resolution of the signals N, O, and P are poor and any cross peaks to the proton signals will be unresolved and lost in t1 noise.

δ ^{19}F ppm	δ ^{1}H ppm	Assignment of ^{19}F to ^{1}H
-91.689	2.905	A+A`-φ
-91.897	2.905	HT-φ
-92.034	Unresolved	N θ muliplet
-92.078	Unresolved	O θ muliplet
-92.134	2.138	P-π (tt)
-92.390	2.905	F-φ
-92.550	2.905, 2.753	G-φ-κ
-92.735	3.072, 2.905	B-ϕ-φ
-94.577	2.905, (2.196, 2.148, 2.083)	C′-φ-(π)
-94.659	2.905, 2.265	C-φ-o
-95.330	2.792, 1.965	H-ω-θ
-95.568	2.905, 2.358	I-φ-ν
-107.010	3.620, (2.171, 2.110, 2.068)	J-δ-(π)
-107.415	1.793	K-ρ
-113.768	3.072	E-ϕ
-114.319	2.905	L-φ
-114.47	6.360, 2.753	M-α-κ
-116.027	2.265	D-o

Table 6 ^{19}F chemical shift correlation of PVDF in DMSO-d_6 at 22°C from the heteronuclear correlation spectra figures 22 and 23.

K L φ G φ H-T φ A φ F φ C o o D E ϕ B φ A′ φ H-T φ G κ M α

-CF_2-CF_2-CH_2-CF_2-CH_2-CF_2-CH_2-CF_2-CH_2-CF_2-CH_2-CF_2-CH_2-CF_2-CH_2-CH_2-CF_2-CF_2- CH_2-CF_2- CH_2-CF_2-CH_2-CF_2-CH_2-CF_2-CH_2-CF_2-H

Figure 4.24. Suggested structural units that form the VDF telomer deduced from the ^{19}F and ^{1}H HETCOR correlation spectrum, the ^{19}F -^{19}F COSY and TOCSY spectra.

These results are, however, in partial agreement with the claim by Pianca et al. [31] (implicit in their figure 9, but not actually visible) of correlation between two signals at $\delta_F = -114.3$ and 107.8 ppm, which led these authors to propose end-groups of the type $CH_3CF_2CF_2CH_2$. Our results support the assignment of the peak K and L to this structure, giving the same end group in low molecular weight VDF; this structure is, however, not evident in the spectral data for our PVDF polymer which is of a higher molecular weight. Other signals seen in this region, such as J, have been assigned to branching points, such as -$CH_2CF_2CH(CF_2CH_2$-)CF_2CH_2-, which has been previously deduced [31-33] by use of empirical rules for chemical shifts. No signal is this work

could be assigned to a branch-point type structure. From the above data signal J, (at least in low molecular VDF compounds) results from either a bi-product of the synthetic pathway or a contaminant. It is not associated which the main VDF structure. The signals N, O and P are difficult to assign due to resolution limitations and their chemical shifts, which is similar to the main chain HT. In addition, the signals H and I present problems because they show coupling to protons but no continued correlation could be seen.

4.8 Degree of polymerization, reverse unit and end group content.

The reverse unit content was evaluated by the method of Russo [17, 2], the peaks E and D in the fluorine case and o for the protons, both with and without decoupling. The degree of end groups were calculated by integration of the signals M and K for fluorines and the α, β, χ, ρ and τ proton signals.

$$\text{Reverse units (\%)}=\left[\frac{1}{2}(\text{E+D})/100\times\text{TOTAL}\right]$$

The average cumulative degree of polymerization $\overline{DP}_{ncum}$ was evaluated by integration of the relative proton or fluorine signals representative of the VDF backbone, φ and H-T respectively, and those of the functional ($-CH_2-CF_2H$, α and M) and non-functional ($-CH_2-CH_3$, θ, ρ, and τ) end-groups.

	^1H	^{19}F
Reverse units %	$7.7/3.8^f$	$5.6/5.4^f$
End groups %	$6.6/5.7^f$	$6.7/5.1^f$
$\overline{DP}_{ncum}$	$(38/35^f)^2(23/19^f)^1$	$(37/36^f)^2(19/21^f)^1$

Table 7. The values of the reverse unit end groups and average cumulative degree of polymerization calculated form the integration of proton and fluorine signals. Numbers labeled *f* are decoupled values and values with superscript 2 are values with both functional and non-functional end groups and superscript 1 is functional end-groups only

Table 7 shows the values of $\overline{DP_{ncum}}$, reverse unit, and end group content measured with and without decoupling and functional and non-functional end-groups. Using an average value of 20 from the decoupled NMR spectra for the degree of polymerization and a monomer weight of (-CH_2-CF_2-) 64 Mw the average molecular weight for the VDF telomer is 1280 Dalton. This is in relatively good agreement with the GPC value of 2000 Dalton.

In general the end-group contents derived from protons and fluorines are commensurate, due to good resolution of the signals and are in good agreement with literature[1, 2, 9, 10]. A large difference is seen between the proton and fluorine values for the average degree of polymerization ($\overline{DP_{ncum}}$) depending on whether the spectrum is decoupled or not. This is again due to the resolution of the decoupled spectra where signals are more resolved. The proton main chain signal at 2.905 ppm used to evaluate the degree of polymerization has contributions from adjacent signals not associated with the main chain even in the fluorine-decoupled spectrum. It would seem in light of this information that the decoupled spectra would give a more accurate assessment of these parameters. This is however not the case in the literature where proton spectra without decoupling is often used. The reason for this is that many workers do not have the possibility to do simultaneous high frequency observation with high frequency decoupling.

As stated earlier, the amount of reverse units is usually large in the early stages of polymerization, up to 50%, and decreases with an increase in molecular weight [2]. Although telomerisation should produce short chain oligomers of VDF, in this case the amount of reverse units is low and comparable to values reported for photochemical induced polymerization [13]. The reverse unit values measured form the decoupled fluorine spectra for PVDF and VDF-telomer are very similar ~5.5% in both cases. In light of these results and that the formation of the reverse unit is said to stop with increased polymerization, it would seem that with a molecular weight of 2000 and a $\overline{DP_{ncum}}$ of 20, this limit has already been reached.

4.9 Summary of solution-state NMR of the VDF Telomer

The structure of a VDF fluoropolymer, synthesized with methanol as a hydrogen transfer agent (telomer), has been analyzed by both solution and solid-state NMR spectroscopy.

The solution-state NMR showed that reverse units are formed to a lesser extent than stated in the literature for this method of synthesis and degree of polymerization. Recording fluorine spectra (with proton-decoupling) and proton spectra (with fluorine-

decoupling) using a 500 MHz spectrometer, gave unprecedented resolution for the VDF telomer. Both proton and fluorine linewidths were found to be of great importance for the elucidation of structural units of the VDF telomer. For both proton and fluorine signals associated with the polymer backbone, their linewidths were generally equal to or greater than their homonuclear $^4J_{H-H,}$ and $^4J_{F-F}$ coupling constants. It has been shown that the fluorine linewidths in some cases (~50-30 Hz) were considerably greater than what would be expected for $^4J_{F-F,}$ $^3J_{F-F,}$ $^2J_{F-F}$ and $^3J_{F-H}$ coupling constants. This is the case for the fluorine signals A+A′, H-T, F, C, B, G, D, and E of the proton decoupled spectrum figure 10. This was not found to be true for the signals, N, O, P, H, J, L, K, and I, which probably arise from small molecules or small chain VDF type oligomers. All these signals showed fluorine coupling and increased resolution when proton decoupled. These signals are tentatively assigned to low molecular weight bi-products, with greater mobility, hence the increased resolution. The proton signal φ in figures 1 and 2, assigned to the main chain protons, does not show any coupling. We know a $^4J_{H-H}$ coupling would be ~1.5 Hz and that the linewidth of this signal is ~9 Hz. The application of fluorine decoupling to the 500 MHz proton spectra gave exceptional resolution and made possible the assignment of the proton signal κ at 2.753 ppm (-$C\mathbf{H}_2$-CF_2H), not reported in previous work on VDF telomers, nor in specific work on the end-groups in PVDF polymers. This increase in resolution was also seen for the main chain signal in both the fluorine and proton spectra, where a decrease in linewidth revealed the signals, N, O, P and C', I in the fluorine spectrum, and ϕ, γ, η, ι, ϖ, and ω in the proton spectrum. The degree of polymerization measured with a combination of functional and non-functional end-groups by integration of the VDF backbone signals was high ~20, irrespective of whether decoupling was applied or not (see table 7); literature values varied between 4-7 [2].

The application of homonuclear correlation spectroscopy and has allowed the assignment of the proton and fluorine signals by correlating coupled homonuclear spins (COSY) and spins sharing the same spin system, but not having the same mutual couplings (TOCSY). The proton COSY spectra showed few cross peaks, figure 8. The cross peaks observed mainly belong to well resolved signals, which later were assigned to the end-groups or low molecular weight substances, shown in figure 2. The proton signals β and χ, figures 1 and 2, were of particular interest as they suggest the presence of functional end-groups. The signal χ has been assigned in the literature to hydroxyl groups associated with main chain VDF units. However, this investigation suggests that it is the functional end-group of a smaller molecule. This is an important observation,

as the purpose of the telomerisation of VDF in methanol is to develop a VDF telomer with functional end-groups for further modification. Furthermore, the signal β, which couples to the signal δ, which, in turn showed further coupling to the fluorine signal J in the HETCOR experiment, also suggests a functionalised end-group, which may or may not be in the main chain VDF telomer. The fluorine COSY and TOCSY experiments suggest that the signals N, O, P, L, J and I are from another source than that of the main chain VDF telomer. This is supported by the previous debate in this section on the linewidth and resolution of these signals and the lack of connectivity for these signals to those of the VDF main chain in both the TOCSY and the COSY experiments.

The signal K in the fluorine spectrum was assigned to a $-CF_2-CF_2-CH_3$ chain end-group and is well documented in the literature [1, 2, 3, 17]. However, signals in this region have long been debated and believed to belong to both chain end-groups and branching.

In general, the solution spectra have given structural information on the main polymer chain, including the structure adjacent to the reverse unit, and the presence of signals not related to the VDF telomer. The origins of these signals can be chain ends but also from fluorine nuclei of a different character and origin not reported before. This shows also that caution should be taken when assigning both major and minor peaks in NMR spectra of these types of fluoropolymers from previous works and by the comparison of model compounds, as is often the case in the literature. The application of decoupling is paramount if high resolution and correct assignment is to be achieved. This is especially the case with work on short chained VDF model compounds of the type $C_4F_9-CH_2-CF_2-CH_2-CF_2-CH_2-CF_2H$, where the application of decoupling at higher magnetic field would give increased knowledge of the main chain proton and fluorine $^3J_{H-H}$, $^3J_{F-F}$, $^2J_{H-H}$, and $^2J_{H-H}$ coupling constants. In the literature, many are still documented simply as multiplets due to poor resolution.

4.10 Conclusions

In conclusion the solution-state NMR of the VDF telomer has shown:

1. Unprecedented resolution in both proton and fluorine solution-state spectra permitted a more detailed analysis and assignment of the VDF telomer.
2. The presence of additional signals at similar chemical shifts to those of the main chain proton and fluorine signals, which are not described in the literature. The

intensity of these signals also shows the diversity of the sample in respect to chain variation.

3. Proton and fluorine correlation experiments have increased the ability for assignment of partial structures, verifying existing assignments and giving a more accurate assessment of the end-group content.
4. Solution-state NMR showed the possibility of two oligomers; one with functional end groups and one without.
5. The degree of polymerization obtained was very different, depending on whether the proton or fluorine spectrum was decoupled. Decoupled values were consider to be more accurate due to the elimination of proton-fluorine coupling and agreement with GPC values
6. An inconsistency with the methodologies reflecting the molecular weight of the sample was observed. The DSC showed a high melt transition similar to that of high molecular weight PVDF, yet the GPC and NMR together showed an average molecular weight of 2000 and 1280 Dalton respectively. The high end-group content is commensurate with the estimates of molecular weight calculated by GPC and NMR.

References

1. P. Pianca, E. Barchiesi, G. Esposto, and S. Radice, J. Fluorine. Chem. 95 (1999) 271.
2. M. Duc, B. Ameduri, B. Boutevin, M. Kharroubi, and J-M. Sage, Macromol. Chem. Phys. 199 (1998) 1271.
3. E. Katoh, K. Ogura, and I. Ando, Polym. J. 26 (1994) 1352.
4. J-P. Macheteau, H. Oulyadi, B.Van Hemelryck, M. Bourdonneau, and D. Davoust, J. Fluorine. Chem, 104, 2000, 149/154
5. T.Claridge, High resolution NMR Techniques in Organic Chemistry, Pergamon press. 1999. ISBN 080427987.
6. J.W. Emsley, L. Phillips, and V. Wray, Fluorine coupling constants, Prog. Nucl. Magn. Reson.Spect. 10, 1977, 85,
7. J. Balague, B. Ameduri, B. Boutevin and G. Caporiccio, J. Fluorine. Chem. 102 (2000) 253.
8. J. Balague, B. Ameduri, B. Boutevin and G. Caporiccio, J. Fluorine. Chem. 70 (1995) 215.
9. B. Ameduri, and B. Boutevin, J. Fluorine. Chem. 104 (2000) 52.
10. J. Guiot, B. Ameduri, and B. Boutevin, Macromole. 35 (2002) 8694.

11. R. Saint-Loup, A. Manseri, B. Ameduri, B. Lebret, and P. Vignane, Macromol, 35 (2002) 1524.
12. A. Manséri, B. Ameduri, B. Boutevin, R.D. Chambers, G. Caporiccio, and A.P. Wright, J. Fluorine. Chem. 74 (1995) 59.
13. R. Saint-Loup, B. Ameduri, J. Fluroine. Chem. 166 (2002) 27
14. P. Wormald, D.C. Apperley, F. Beaume, and R.K. Harris, Polymer. 44 (2003) 643.
15. Yu H, Mi J, Ni H.Chin, J. Microwave Radiofreq Spectrosc. 1 (1984) 372.
16. Muracheva YeM, Shashkov AS, Dontsov AA, Polym Si USSR 23 (1981) 711.
17. S. Russo, K. Beharit, and S. Chengji, Polymer. 34 (1993) 4777.
18. G.Teyssedre, A. Bernes and C. Lacabanne, J. Polym. Sci, 31 (1993) 2027.
19. C. Marega and A. Marigo, Euro Poly. J. 39 (2003) 1713.
20. K. Nakagawa and Y. Ishida, J. Polym. Sci, 11 (1973) 2153.
21. R. Greggorio and M. Cestari, J. Polym. Sci. (B), 32 (1994) 859.
22. U. Herman, K.Toshiyuki, U. Astushi, K. Susumu, K. Takeshi and O. Norimasa, Polymer, 38 (1997) 167.
23. P. Holstein, R.K. Harris and B. J. Say, Solid State Nucl. Magn. Reson. 8 (1997) 201
24. K.L. Schmidt-Rohr, Class. J, H.W Spiess, Macromolecules. 25 (1992) 3273.
25. N. Egger, K.L Schmidt-Rohr, J Appl Polym Sci. 44 (1992) 289.
26. R.K. Harris, G.A Monti, and P. Holstein, in I. Ando and T. Asakura (Eds.), Solid State of NMR Polymers, Vol. 84, Elsevier, (1998) chapter 6.
27 R.K. Harris, G.A. Monti and P. Holstein, in I. Ando and T. Asakura (Eds.), Solid State of NMR Polymers, Vol. 84, Elsevier, (1998) chapter 18.
28 P. Holstein, G.A. Monti and R.K. Harris, Phys. Chem. Chem. Phys. 1 (1999) 3549.
29 P. Holstein, U.Scheler and R.K Harris, Polymer, 39 (1998) 4937.
30 Su. TW, Tzou. DLM, Polymer 41. 2000.7289.

Chapter 5

^{19}F solid-state NMR of Vinylidenefluoride and PVDF with variable Magic angle spinning

5.1 Introduction to solid-state NMR spectroscopy of Vinylidenefluoride.

Both solution and solid-state NMR spectroscopy have been widely used to characterise high molecular weight fluoropolymers and co-polymers. However, the products of reaction mixtures of VDF have only been analysed by solution state methodologies. No solid-state NMR study of these substances was found in the literature. The reason for this is probably due to the objectives for these synthetic works, which are mainly targeted at the development of low molecular weight substances with specific end groups and functional groups for further development. It is however of interest for our study. Just as the solution-state NMR spectra of the telomer gave us information related to end-groups and main chain structure, which could be related to the structure of PVDF, solid state NMR spectra could also provide information hitherto not utilized in understanding the spectra of PVDF. The application of relaxation filters and subsequent analysis of relaxation times and lineshape, should give in formation of the range of mobilities of the short chain VDF and thereby a comparison with the long chain PVDF. Also, information with respects to the mode of synthesis, initial crystalline phase, and morphology should be attainable, and comparable to PVDF. The DSC should give an indication as to thermal events and crystallinity of VDF and a comparison of the DSC of VDF and PVDF are given in the discussion to chapter 6.

5.2 Differential Scanning Calorimetry (DSC)

Thermogravimetric analysis (TGA) showed the start of decomposition at 150°C, figure 1.

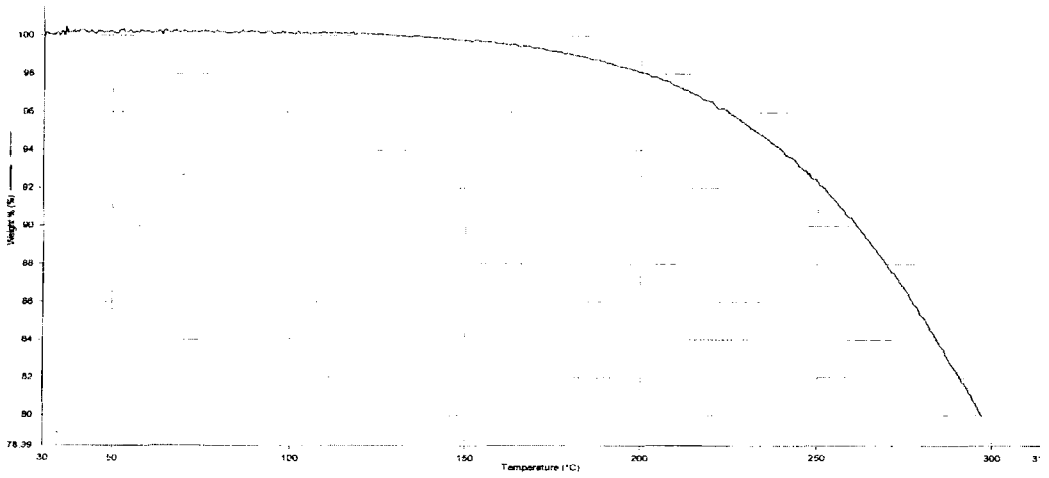

Figure 5.1. The TGA curve of the VDF telomer showing percentage of weight loss as a function of temperature.

Figure 5.2a shows the first heat run, were two endotherms are detected at 100.6 and 150.8 °C. Table 1 shows phase transition values for the telomer from the DSC thermogram. The degree of crystallinity was 27.4%, calculated by dividing the single-crystal heat of fusion value 104.63 J/g of PVDF and the enthalpy value of the endotherm at 150.8 °C, which is the crystalline-melt transition [1, 2]. This is, however, somewhat dubious assumption because of the shape of the transition, which is broad and therefore difficult to assert a correct calculation of the area of the peak. If we, however, accept it this would mean that the low molecular weight VDF (2000 Mw by GPC), has the same degree of crystallinity as the high molecular weight PVDF. As temperature limits of the melt transition were not easy to decipher, this value of crystallinity is probably over estimated. This would seem a reasonable assumption as the high molecular weight PVDF studied in chapter 2 had only 0.013% chain-end monomer units, whereas the VDF telomer has ~6%. As these chain-end monomer units are predominantly in the amorphous region it would seem highly unlikely that such a high crystallinity for the VDF telomer would also give such a large degree of chain-end

monomer units. The broadness of this transition could, however, be related to a wide dispersion of crystallite size and lamellar thickness [2].

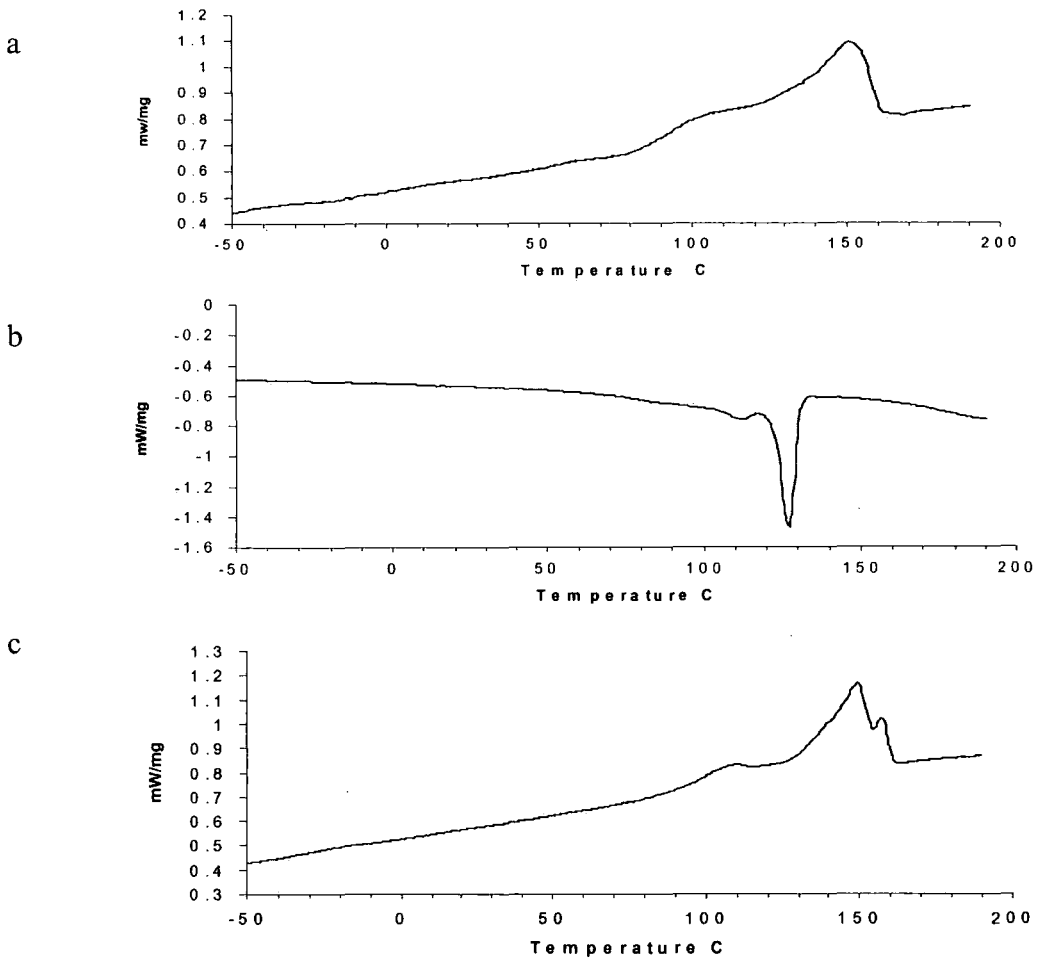

Figure 5.2 The DSC thermogram of VDF telomer (a) First run showing two endotherms, (b) cooling run showing the re-crystallisation peak and a smaller transition at lower temperature, (c) second heating run now showing three heat transition values, as given in table 1.

Rapid cooling gave a recrystallisation peak at 120.0°C; there is also a small recrystallisation peak at 111.6°C. The second heating run shows a broad peak consisting of two melt endotherms at 157.5 and 149.0 °C. A third transition at 107.6 °C is seen and is possibly a pre-melt transition. It would therefore seem that the process of melting and cooling results in the growth of smaller crystallites or lamellar thickness. This effect is seen where the broad transition centred at 150.8°C observed in the first heating run

becomes in the second heat run two peaks at 157.4°C and 149.0°C. The transition at 100.6 °C in the first heat run is now shown to be a possible so called, pre-melt transition at 107.6°C.

T °C	ΔHJ/g
First heat	
100.6	4.0
150.8	28.4
Cooling	
126.9	-26.9
111.6	-1.9
Second heat	
107.6	3.24
149.0	14.8
157.4	1.1

Table 1. The temperature and enthalpy of heats capacities from the DSC of the VDF telomer.

This could also be indicative of a second phase of the VDF telomer not yet fully developed in the sample or correspond to the melting of crystallites formed under non-isothermal conditions and nucleation respectively, as noted in the literature for PVDF and at similar temperatures [3, 4, 5]. However the origin of this double melting phenomenon is controversial and to summarize it could arise from: (1) melting, recrystallisation and re-melting during the DSC heating, (2) variation of morphology and (3) polymorphism. The higher melt temperature peak (157.4°C in the second heating) was associated with recrystallisation during heating; this was the case for high molecular weight PVDF. The endotherm at 107.6°C could indicate the presence of a pre-melt transition also noted for PVDF. It is also important to note that by GPC analysis the average molecular weight calculated was 2000 Dalton (in Polystyrene equivalents), but that the melt temperature of the VDF telomer was close to that of high molecular weight PVDF (160°C). Furthermore, it has been reported that the crystalline melt transition, measured by DSC, of a low molecular weight PVDF (1200 Dalton) was 68 °C compared to that of a commercial high molecular weight PVDF (530.000 Dalton) that was 160°C. Comparing the degree of polymerisation measured by NMR for our

VDF telomer, ~30, with literature values for low molecular weight VDF telomers, 4-7, and the value, calculated from solution-state in chapter 2, for our high molecular weight PVDF = 117. The difference in the melting points here is controversial. The solution state NMR and GPC data both point to a molecular weight value for our VDF telomer ~2000 Dalton.

5.3 Solid-state NMR of VDF telomer

As described in chapter 3, the morphology of semi-crystalline PVDF was investigated by acquiring direct polarisation spectra with various relaxation filters and debated in terms of domain selectivity with regard to the reverse units [6]. These experiments reviled a range of mobilities in the amorphous domains. Though the signals related to the α crystalline form should be of equal intensity, the signal at –95.6 ppm was larger (chapter 3 figure 3.3a). This was explained by the presence of CF_2 groups in the vicinity of reverse units as verified by solution-state NMR spectroscopy. A contribution to this signal from the β form and /or short-chain VDF molecules showing a range of mobilities is also a possibility.

It was also shown in chapter 3 that the reverse units are mostly associated with the amorphous region and that the dipolar-filtered spectrum, reveal an anomalous signal at ~-114 ppm [6]. This signal was shown to arise from highly mobile units and can probably be assigned to CF_2H chain end groups. It could not be determined if this end group was part of the main chain PVDF, a by-product or originated from the reactants. Furthermore, the intensity of this signal in the solid-state spectrum gave a significant contribution to the total reverse unit signal, making any determination of reverse unit content difficult in the solid state.

The direct-polarisation ^{19}F $\{^1H\}$ solid-state NMR spectrum of the VDF telomer is shown in figure 5.3. The chemical shifts and relaxation times are summarised in tables 9 and 10 respectively. Proton decoupling was applied and should remove most, if not all, of the effects from heteronuclear (H, F) coupling [6, 7]. Parameters used were a 90° pulse with a 5-second recycle delay; other parameters are already described in chapter 3.

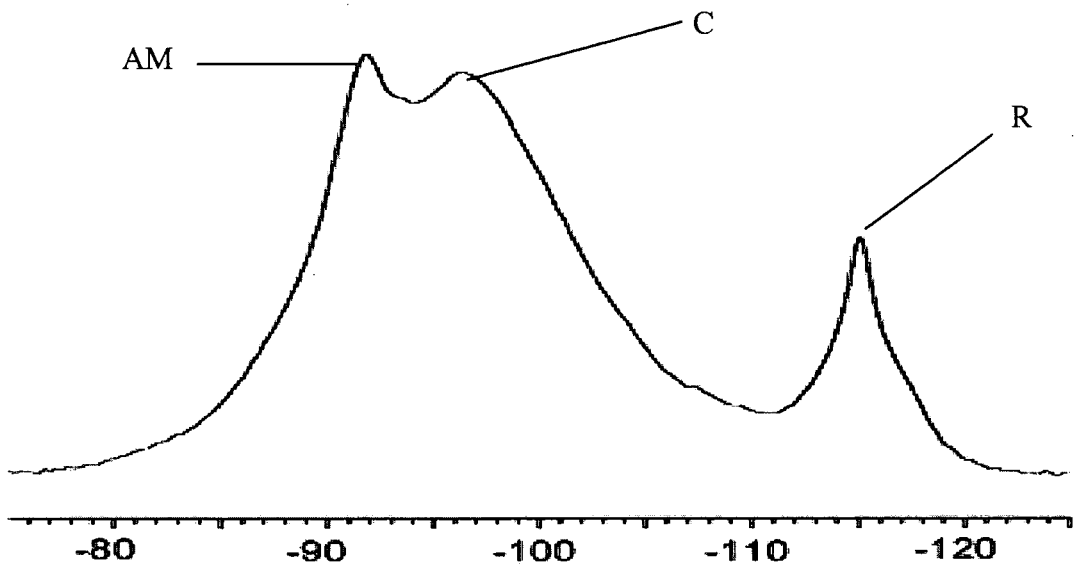

Figure 5.3. The ^{19}F proton-decoupled solid-state spectrum of the VDF telomer at 60 °C and 12 kHz MAS.

Figure 5.3 shows three main peaks at -91.9, –97.1 and –115.0 ppm, labelled AM, C and R respectively. Peak AM at -91.9 ppm corresponds well with the solution-state signal at –91.897 ppm in figure 6 and is therefore assigned to the amorphous main-chain repeat unit structure $-(CH_2-CF_2)_n-$. Remembering that the same signal for PVDF was at –92.2 ppm, these assignments are in relatively good agreement. The signal C at –97.1 ppm is tentatively assigned to the crystalline β form of the VDF telomers and PVDF, which has the all-trans conformation. It is also similar to the crystalline signal, C2 of PVDF seen in chapter 3 figure 3.3c. Furthermore, the absence of a signal at ~ -82.1 ppm shows that no α crystalline form is present. The intensity of this signal at –97.1 ppm is of the same order as that for the amorphous domains though its linewidth is large. It is also probable that this signal has contributions from more mobile entities, which are seen in the solution- state spectrum at similar chemical shifts, the signals F, G, B, G, H, and I chapter 4 figure 4.10. The signal R at –115.0 ppm is the reverse unit $-(CH_2-CH_2-CF_2-CF_2)-$ and the $-CH_2-CF_2H$ end group, of which the latter is the dominating signal. Apart from the obvious difference in resolution compared to the solution-state spectrum shown in chapter 3 figure 3.3a, the solid-state DP spectrum of the VDF telomer shows some similarities, which can be seen as three main groups.

1. A main chain signal AM at -91.9 ppm, similar to the solution state-signal H-T
2. A signal C at –97.1 ppm, similar to the solution-state signals F, G, B, C, H, and I. This signal can also be composite with the crystalline β form of the VDF telomer.

3. Signal R at –115.5 ppm, similar to the solution-state signals D, E, L and M

Integration of the reverse units (R) and spinning side bands, to obtain reverse unit values as for PVDF in chapter 3, was not attempted here due to the obvious overlap of the reverse unit and end group signals.

In order to gain more information on the origin of these signals the NMR experiments can be designed to suppress one selected component from the spectrum, based on differences in the relaxation properties of the components. Two such experiments have been used in this study: a $T_{1\rho}(F)$ filter and a dipolar filter (figures 5.4 and 5.5) respectively [6, 7].

The ^{19}F direct polarisation $T_{1\rho}$ filter experiment was made using a 25 ms spin-lock pulse equivalent to 80 kHz [6]. The result of this experiment is seen in figure 5.4. It should be noted that this spectrum has a very low absolute intensity (of the order of 5% of the total intensity in the direct-polarisation spectrum) because the spin-lock time of 25 ms is substantially longer than the three values of $T_{1\rho}(F)$, table 3. Figure 5.4 shows two groups of signals, one centred at –97.1(C) and a smaller signal at –117.4 ppm (R^1). The signal at –117.4 ppm (R^1) in the $T_{1\rho}$ filtered spectrum suggests the presence of a rigid component in the spectral region associated with reverse units and/or $-CH_2-CF_2H$ end groups. Alternatively, this could be due to a signal on the extreme narrowing side of $T_{1\rho}(F)$ minimum. This has been commented on earlier in chapter 2, where a similar signal was recorded in a $T_{1\rho}(F)$ experiment for PVDF at 100 °C.

By arraying the spin-lock time and monitoring the signal decay in the same manner as described in chapter 2 for PVDF [10, 11], $T_{1\rho}$ values were recorded for the individual signals of VDF and these are shown in table 3. The signal at –97.1 ppm shows a $T_{1\rho}$ value of 9.9 ms, which is similar to the value of 9.5 ms obtained for the crystalline signal of PVDF. The signals at -91.9 (A) and –115.5 ppm (R) gave $T_{1\rho}$ values of 6.1 and 3.5 ms respectively. The $T_{1\rho}$ value (3.5 ms) of the signal at –115.5 ppm was in agreement with the results for reverse unit signals (R1and R2) and the amorphous signal (AM) of PVDF (see chapter 2, table 5). The $T_{1\rho}$ value of A is intermediate between those of signals C and R.

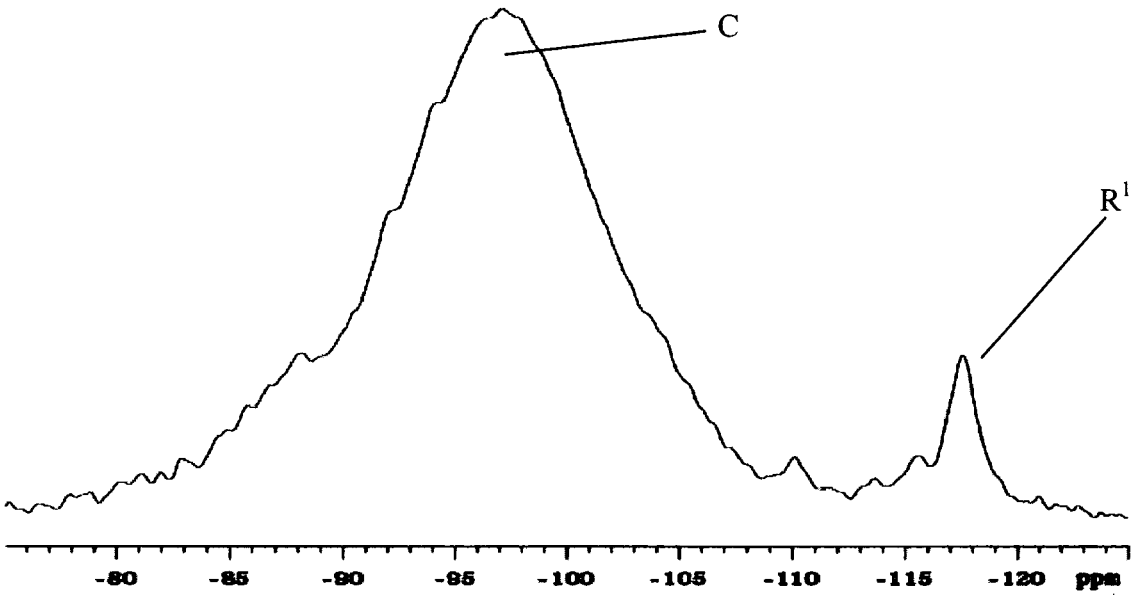

Figure 5.4. The $T_{1\rho}$(F)-filtered solid-state spectrum of the VDF telomer at 60 °C obtained following a 25 ms spin-lock pulse.

A dipolar filter [9] suppresses signals from strongly dipolar-coupled species. It is, therefore, expected to remove signals originating from relatively rigid material i.e. crystalline domains. Figure 5.4 shows the result of such an experiment with the VDF telomer. The signals at -91.9 ppm (A) and –97.1 ppm (C) have decreased in intensity relative to the signal at -115.0 ppm. This indicates that the signals in the DP spectrum (figure 5.5) at -91.9 and –97.1 ppm are a combination of amorphous and rigid material. Also seen in the DP dipolar filtered spectrum, there is a small broad signal between –106.0 and –111.0 ppm (P), which may be indicative of the signals J and K seen in the solution-state spectra (chapter 3 figure 3.3b).

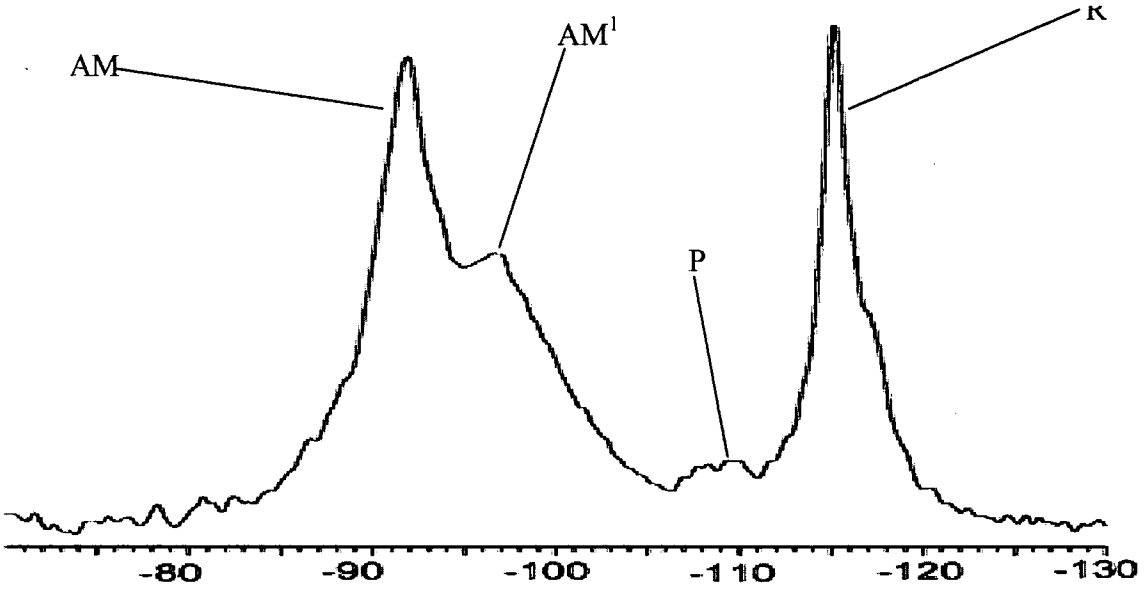

Figure 5.5. The ^{19}F dipolar-filtered solid-state spectrum of the VDF telomer at 60 °C.

The dipolar-filtered spectrum (figure 5) is comparable to the solution-state spectrum (chapter 4 figure 4.9) and four signals can be identified.

1. Signal AM at -91.9 ppm is similar to the solution-state signal H-T and the composite signal A+A`
2. Signal AM^1 at –97.1 ppm is similar to the combined solution-state signals B, C, F, G, H, and I.
3. Signal P between –106.0 and –111.0 ppm corresponds to the solution-state signals J& K.
4. Signal R at –115.5 ppm is similar to the solution-state signals D, E, L and M

δ_F/ppm (solid)		Assignment
-91.9	A	Amorphous domain
–97.1	C +AM^1	Amorphous domain and crystalline domains
-106 to –111	P	End-groups and branching?
~-115.5	R	Reverse units and CH_2CF_2H end groups

Table 2. The ^{19}F chemical shifts of the solid-state spectrum of the VDF telomer. Assignments of the phases are taken from the spectra in figures 3-5.

Although similar to the DP spectrum, the dipolar-filtered spectrum does not contain any substantial contributions from rigid regions and gives us a spectrum of the mobile structure of the VDF telomer. Interestingly, the apparent degree of reverse units and CH_2-CF_2H end groups is high, 30% of the total intensity as measured by integration. The single exponential values of $T_1(F)$ ranged from 1.5-1.4 s for the various fluorine sites, in each case measured at 60°C directly by inversion-recovery (with proton decoupling), see table 3. The T_2 components of the signals were measured by the CPMG experiment, and signal intensities were fitted by a single-component analysis. Fitting to two components did not improve the fit significantly. The results are shown in table 3. The T_2 value of the signal at –115.5 ppm is 11.0 ms and that of the amorphous peak at –91.9 ppm is 0.6 ms.

	-91.9 ppm	-97.1 ppm	-115.5 ppm
$T_1(F)$/s	1.5	1.5	1.4
$T_{1\rho}(F)$/ms	6.1	9.9	3.5
$T_2(F)$/ms	0.6	N/A	11.0

Table 3. Relaxation data of $T_1(F)$ obtained by inversion-recovery with proton decoupling; $T_{1\rho}(F)$ obtained by direct-polarization with varied spin-lock times and proton decoupling during acquisition (only); and $T_2(F)$ obtained by a CPMG experiment. All measurements were recorded at 60 °C.

It has been shown that polymer relaxation properties, as monitored by dielectric spectroscopy and dynamic mechanical analysis [3], are sensitive to reverse-unit content as well as to the degree of crystallinity. It is therefor interesting that the $T_1(F)$ of the VDF telomer, which has a high degree of reverse units and -CH_2-CF_2H end groups and is mainly amorphous, has a $T_1(F)$ three times that of the more crystalline PVDF.

In principle, deconvolution of the direct-polarisation spectrum should give information on the relative intensities of the phases present in the material. However, the apparent complexity of the lineshapes and the number of signals potentially present in the

spectrum (including sidebands) made conclusive data difficult to obtain for the telomer (as for the PVDF in chapter 3). A comparison of line shape analysis is, however, offered in the next section.

5.4 The ^{19}F fast MAS spectra of the VDF telomer and PVDF.

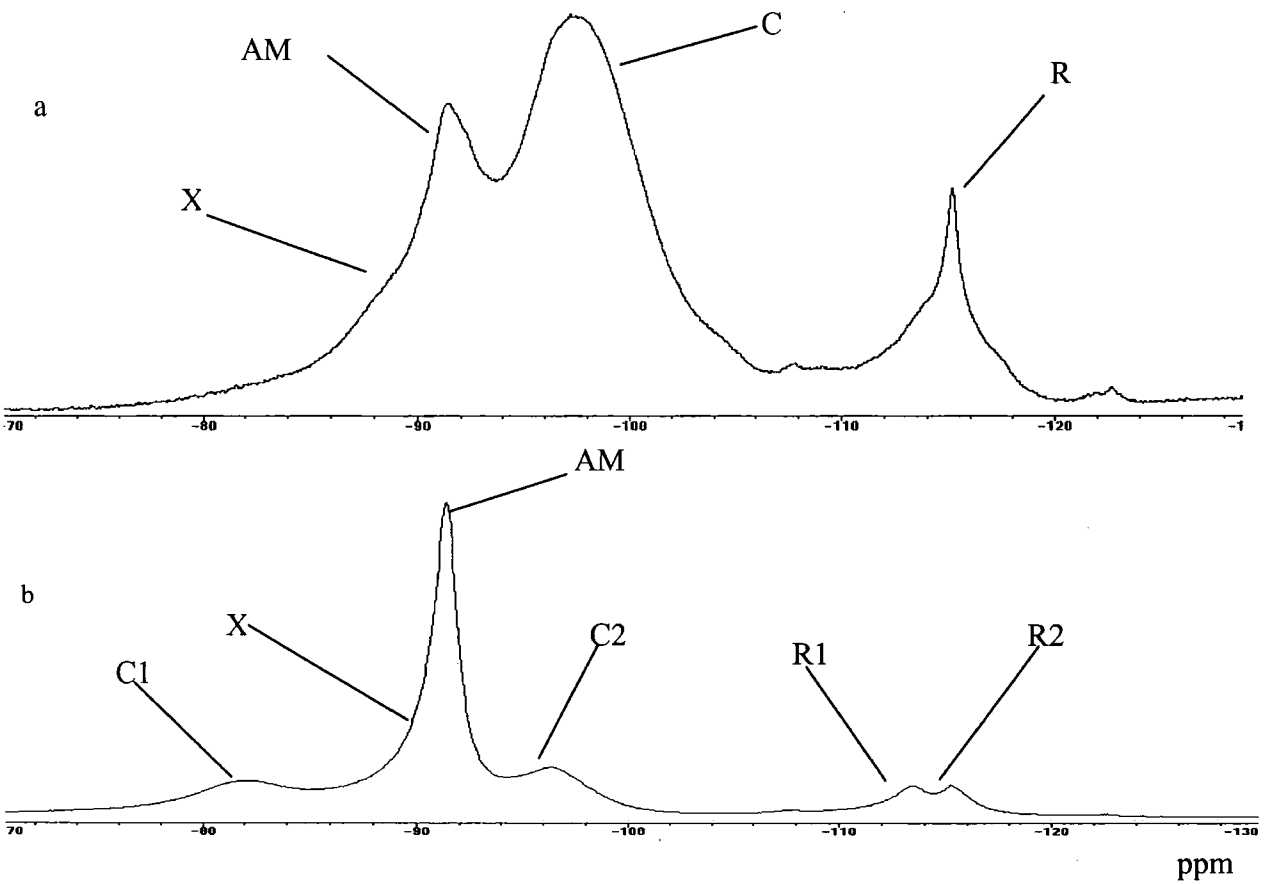

Figure 6. The ^{19}F direct polarisation solid-state spectrum of the VDF telomer (a) and PVDF (b) recorded at 27.5 kHz, without ^{1}H decoupling. Assignments are given in table 4.

The application of magic angle spinning is known to average dipolar interactions resulting in increased resolution in solid-state spectra [12,13,14]. This is achieved when the spinning rate is of the same order in magnitude as the dipolar interactions of the observed spins. Although these spinning speeds would be in the order of ~80 kHz, which not possible at the present time, a reduction in linewidths would be expect with an increase in MAS. The acquisition of a 2.5 mm Chemagnetics HXY probe at Durham,

capable of MAS speeds up to 30 kHz towards the end of this work, made possible the comparison of linewidths for PVDF and the VDF telomer with an increase in spectral resolution.

Figure 5.6a shows the result of a ^{19}F DP experiment with 27.5 kHz MAS for the VDF telomer and figure 5.6b for PVDF. Chemical shift values and assignments are given in table 4. A comparison between the 12 and 27.5 kHz MAS spectra of the VDF telomer, figures 5.3 and 5.6 respectively, shows increased resolution for the signals X, A, and C. Deconvolution values for these two spectra are shown in table 5 and the fitted spectrum showing the assignment are given in figure 5.7. The fitting errors are within 5%.

Chemical shift (ppm) of the VDF telomer	Assignment of the signals	Chemical shift (ppm) of the PVDF	Assignment of the signals
- 115.1	R	-115.4	(R2)
-97.3	C	-113.3	(R1)
-91.3	AM	-96.4	(C2)
-89.6	X	-91.4	(AM)
		-90.8	(X)
		-82.1	(C2)

Table 4. The assignments of the signals from the VDF telomer and the PVDF spectra.

However, the fitting of the reverse unit and end-group signals was not achieved and it proved difficult to apply any sensible analysis to their behaviour. The over representation of the R1 signal could not be successfully dealt with in the fitting parameters. The presence of the signal X as a shoulder to the AM signal is seen at – 89.1 ppm. This signal was discussed in chapter 3 in the spectrum of PVDF. However, the nature of this signal is not fully understood.

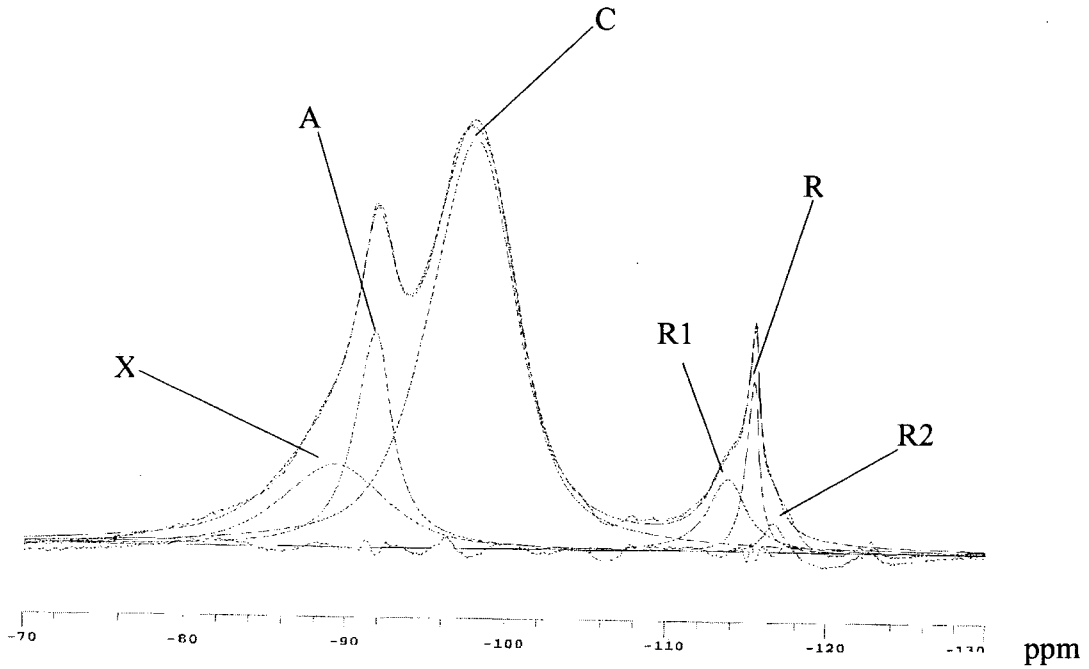

Figure 5.7. Lineshape analysis of the ^{19}F direct polarisation solid-state spectrum of the VDF telomer recorded at 27.5 kHz MAS.

Chemical shift (ppm)	Linewidth/Hz at 27.5 kHz MAS	Linewidth/Hz at 12.0 kHz MAS	Decrease (-) or increase (+) linewidth
-116.5 (R2)	427	676	37%(-)
-115.1(R)	2473	807	300%(+)
-113.6 (R1)	1058	646	60%(+)
-97.5 (C)	2910	3908	25%(-)
-91.5 (A)	1098	2062	53%(-)
-89.1 (X)	2191	2738	20%(-)

Table 5. The lineshape analysis of the VDF telomer at spinning speeds of 27.5 and 12 kHz.

Figure 5.6b shows the ^{19}F DP spectrum of PVDF recorded at 27.5 kHz MAS. Figure 5.8 and table 6 show the results of the lineshape analysis. In general, the main chain signals for both the crystalline and amorphous signals decrease in linewidth by around 20%. However, the line width of the reverse group signals decrease by ~50%. The signal X is also seen in the PVDF spectrum at a similar chemical shift to that of the VDF telomer, verifying earlier observation of a signal of more rigid character

contributing to the AM signal. The fact that this is present in both high and lower molecular weight samples of VDF polymers suggests the presence of two crystalline phases, based on the linewidth, and formed during early stages of polymerisation. This signal has been mentioned in the literature as broadening of the amorphous signal but not analysed to any great extent [14].

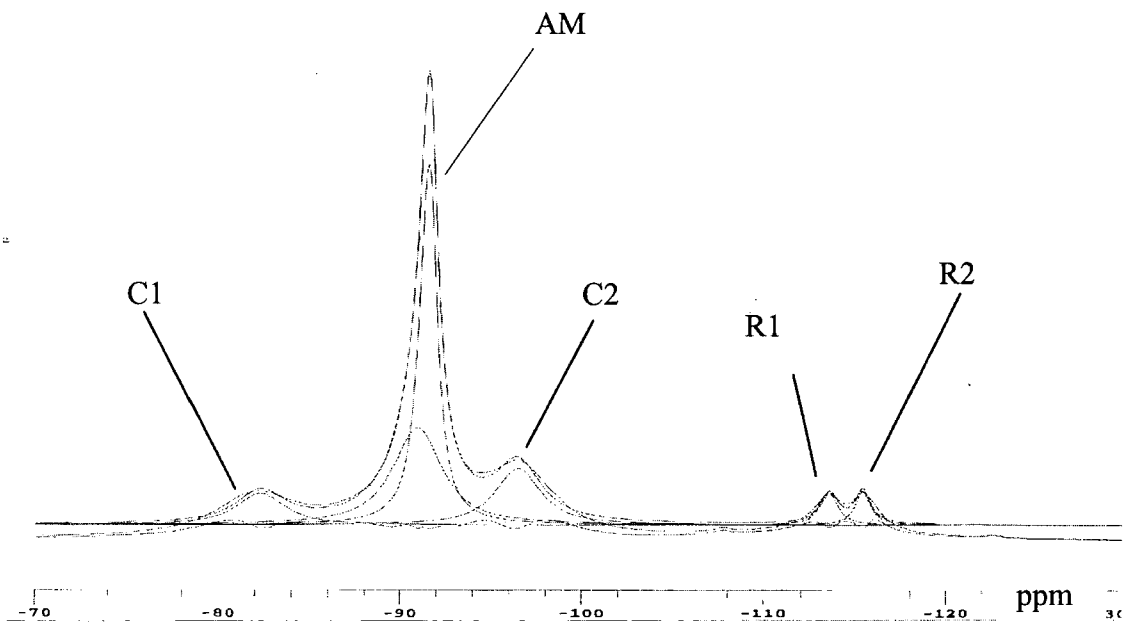

Figure 5.8. The lineshape analysis of the ^{19}F direct polarisation solid-state spectrum of the PVDF recorded at 27.5 kHz MAS.

The application of high speed MAS resulted in a decrease in linewidth for all signals with the exception of the reverse unit and end-group signals of the VDF telomer. High speed MAS reveals the presence of a signal in the spectrum and in the lineshape analysis indicative of a second crystalline phase. The same phase is also seen in the high speed MAS spectrum and line shape analysis of PVDF.

Chemical shift (ppm)	Linewidth/Hz at 27.5 kHz MAS	Linewidth/Hz at 12 kHz MAS	Decrease (-) or increase (+) linewidth
-115.2	471 (R2)	1055 (R2)	56%(-)
-113.1	575 (R1)	429 (R1)	39%(-)
-96.7	1407 (C2)	1917 (C2)	27%(-)
-91.4	552 (AM)	758 (AM)	27%(-)
-91.1	1543 (X)	1876 (X)	18%(-)
-82.2	1491 (C1)	1754 (C1)	15%(-)

Table 8. Results of lineshape analysis of the ^{19}F direct polarisation solid-state spectrum of PVDF at 27.5 and 12 kHz magic angle spinning and comparison with the 12 kHz values. The letters in brackets refer to assignments in figure 6(b) and figure 8 for the 27.5 kHz spinning experiment and figure 3.2a and table 4 for 12 kHz values in chapter 3. Error of fitting is within 5%.

5.5 Summary of the VDF Telomer

The DSC results show the presence of a crystalline phase with a melt transition temperature associated with high molecular weight and a crystallinity of ~28%. No glass transition could be detected though these transitions are in the best cases difficult to detect. Quenching, then heating of the sample, showed a possible pre-melt transition ~107°C. Also two transitions with a higher melting point than previously seen but similar transition temperature to that of high molecular weight PVDF (~156.5°C and ~159°C) were observed. This was interpreted as recrystallisation of the crystals formed during quenching and annealing (149°C) and the transition at 157.4°C to recrystallisation during the heating process.

The signal (R) at –115.5 ppm in the solid-state ^{19}F DP spectrum, figure 5.3 with knowledge of the solution state assignments has been assigned to the end-group $-CH_2-CF_2H$, which due to its intensity dominates this area of the spectrum giving unresolved reverse unit signals. The signal A was assigned to the main chain $-CH_2-CF_2-$ backbone of the VDF telomer and signal C to the fluorine's F, C, B, G, H and I as explained earlier. This signal (C) could have contribution from a crystalline phase and is seen in

the $T_{1\rho}(F)$-filtered spectrum, figure 5.4, which showed a broad signal at -97.1 ppm. It is therefore assigned to the crystalline β phase. The $T_{1\rho}(F)$-filtered spectrum also showed a signal (R^1) at –117.4 ppm normally associated with the reverse units. This signal could be on the extreme narrowing side of the $T_{1\rho}(F)$ minimum or belong to chain end units associated with rigid domains.

The ^{19}F solid-state spectra with a dipolar filter, figure 5.5, gave a spectrum similar to that of the solution-state spectrum of VDF. It showed a high degree of chain ends and reverse units but also verified that the signal at -97.1 ppm is composed of a mobile fluorine species. It is obvious from the solid-state studies that the amorphous signal Am and the signals to high frequency of it in the DP spectrum (figure 5.4) are a combination of both mobile and rigid species. Evaluation of reverse unit content by solid state NMR is not a viable methodology as values are highly distorted by the amount of $-CH_2-CF_2H$ end groups. Rotating frame relaxation times for the different species were found to be in relative good agreement with those of PVDF and in general with the literature. However certain differences should be identified. The spin-lattice relaxation times T_1 for all signals in the DP spectrum of the VDF telomer (~1.5 s) were found to be longer than for PVDF (~0.6 s). This has been shown to be dependent not just on the degree of crystallinity but also on the reverse unit and end group content, which in the latter case is high for the telomer. The $T_{1\rho}(F)$ values for the mobile (A) and rigid (C) signals are in agreement with what would be expected from these domains for the VDF telomer. Furthermore the $T_{1\rho}(F)$ of rigid species for PVDF (C1 and C2 = 9.5 ms) and VDF (C = 9.9 ms), are in good agreement, as are the values for the signals R for both polymers. However, the $T_{1\rho}(F)$ values for signals assigned to mobile entities in PVDF and the VDF telomer, AM and A respectively, do differ substantially. This difference can be an effect of the large amount of reverse units, which are a major structural feature of the amorphous material. Fast MAS ^{19}F DP spectra of the VDF telomer and of PVDF gave a comparison between the increase of resolution, showing a general decrease in linewidth compared to slower MAS rates even without decoupling. The presence of a second crystalline species was also observed in the fast MAS spectra of both polymers and analysed by lineshape analysis.

The ^{19}F solid-state NMR dipolar filter experiment showed that the signal for the $-CH_2-CF_2H$ end group, at –115.5 ppm, was mainly related to the amorphous domain. The presence of branching and other chain-end groups ($-CF_2-CF_2-CH_3$) as seen in the ^{19}F

solution-state NMR at ~107 ppm was also identified. The $T_{1\rho}(F)$ also showed signal for the end-group at –115.5 ppm. This suggests that it may be in some way associated with rigid regions, at least in small part, in contrast to conclusions in the literature [3,10,13] on PVDF samples.

5.6 Conclusions

In conclusion the solution and solid-state NMR of the VDF telomer has shown:

1. The solid-state spectra of VDF showed general similarities with the spectrum of PVDF, with the exception of the crystalline form.
2. The possible presence of a second crystalline form is observed and verified by lineshape analysis. The sample was found to be composed of a varying degree of mobilities for main chain structures.
3. The solid-state NMR highlights the heterogeneous character of the VDF telomer sample with respect to mobility and shows the complexity of the signals historically assigned to amorphous and crystalline structures. Here it is shown that both have contributions from rigid and mobile structures.

References

[1] G.Teyssedre, A. Bernes and C. Lacabanne, J. Polym. Sci, 31 (1993) 2027.

[2] C. Marega and A. Marigo, Euro Poly. J. 39 (2003) 1713.

[3] K. Nakagawa and Y. Ishida, J. Polym. Sci, 11 (1973) 2153.

[4] R. Greggorio and M. Cestari, J. Polym. Sci. (B), 32 (1994) 859.

[5] U. Herman, K.Toshiyuki, U. Astushi, K. Susumu, K. Takeshi and O. Norimasa. Polymer, 38 (1997) 167.

[6] P. Wormald, D.C. Apperley, F. Beaume, and R.K. Harris, Polymer. 44 (2003) 643.

[7] P. Holstein, R.K. Harris and B. J. Say, Solid State Nucl. Magn. Reson. 8 (1997) 201

[8] K.L. Schmidt-Rohr, Class. .J, H.W Spiess. Macromolecules. 25 (1992) 3273.

[9] N. Egger, K.L Schmidt-Rohr. J Appl Polym Sci. 44 (1992) 289.

[10] R.K. Harris, G.A Monti, and P. Holstein, Ando and T. Asakura (Eds.), Solid State of NMR Polymers, Vol. 84, Elsevier, (1998) chapter 6.

[11] R.K. Harris, G.A. Monti and P. Holstein, Ando and T. Asakura (Eds.), Solid State of NMR Polymers, Vol. 84, Elsevier, (1998) chapter 18.

[12] P. Holstein, G.A. Monti and R.K. Harris, Phys. Chem. Chem. Phys. 1 (1999) 3549.

[13] P. Holstein, U.Scheler and R.K Harris, Polymer, 39 (1998) 4937.

[14] Su. TW, Tzou. DLM. Polymer 41. 2000.7289.

Chapter 6

Thermal motion of α poly (vinylidenefluoride): A static ^{1}H solid- state NMR relaxation and Differential Scanning Calorimetry study.

6.1 Introduction to proton relaxation and thermal events of PVDF.

The thermal molecular motion of PVDF has been rigorously studied by various analytical methodologies such as Dynamic Mechanical Analysis (DMA) [1], Dielectric spectroscopy techniques [2], Differential Scanning Calorimetry (DSC) [1, 3, 4, 5, 6], and solid-State Nuclear Magnetic Resonance (SSNMR) [7]. The results of this research have lead to a general understanding of four thermal transitions, one crystalline/rigid (α_c ~120 –100°C) and three amorphous β'(~80°C), β(~ 6°C), and γ (-20°C). From NMR studies the α_c relaxation is believed to have a main-chain axis or the complete rotation of the crystalline chains in the region of defects [8, 9, 10]. The behaviour of the β' transition was rationalised in the terms of co-operative fold motion associated with crystalline domains. The β relaxation is judged to be associated with the glass transition and the onset of general motion in amorphous regions. The γ relaxation is considered to represent the glass transition point/chain rotation in amorphous – non-rigid regions.

The broad glass transition shown in the DSC thermogram of PVDF between –40°C to 100 °C has attracted considerable interest from several investigators. Boyer considered the glass transition of PVDF to consist of a lower [T_g (L)] and an upper [T_g (U)] at –40°C and 42°C respectively [11]. Leonard suggested that the [T_g(U)] at ~ 42°C is related to the solid-state morphology of the polymer and loop length in chain folds [4]. Loufakis [3], however, proposed that no 'rigid amorphous' material could be found above the glass transition temperature at –40°C, and that the influence of the crystalline region on the amorphous region contributes to the broadness of the glass transition. This was explained in terms of conformationally disordered crystals (condis crystals), whereby a change of the trans-gauche chain conformation, tgtg* to tg*tg is induced (Figure 1) [3].

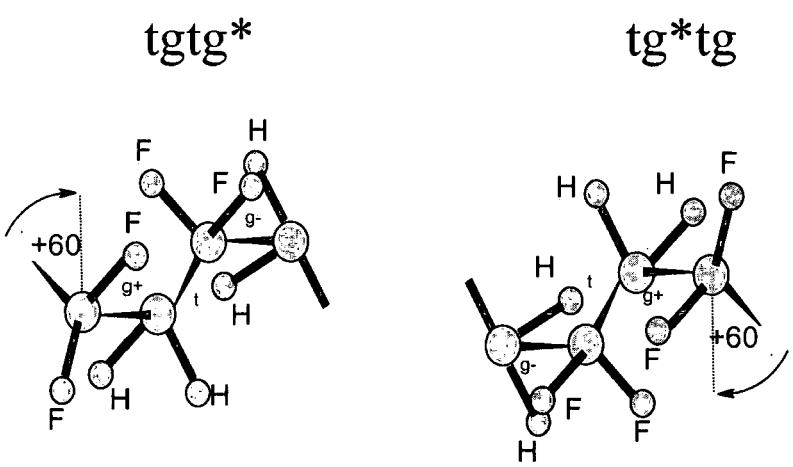

Figure 6.1. The induced change in bond configuration giving conformationally disordered crystals.

Teyssedre [12, 13] using DSC and Thermo-Stimulated Current spectroscopy (TSC) showed similar results and concluded that the α_c transition showed association with the crystalline lamellae, along with a T_g transition comprising two components corresponding to free and restrained amorphous phases for both α and β forms of PVDF [13]. Furthermore, he suggests that the endothermic phenomenon in the DSC curve between 40 °C and 80 °C may be due to conformationally disordered regions – an irreversible condis crystal reorganisation, in agreement with Loufakis [3]. Nakagawa reported two relaxation components corresponding to crystalline and amorphous phases by dielectric relaxation spectroscopy and that the high temperature relaxation was not only attributed to molecular motions in the folds of lamellar crystals but also to motion in the interior of the crystal, suggesting that these processes are coupled [14]. Nabata found similar results by dielectric relaxation spectroscopy, but also showed by Dynamic Mechanical Analysis (DMA) that there are three different relaxation processes above the β transition temperature [1]. These corresponded to the pre-melting of crystalline α PVDF (>127°C), the movement of molecular chains, which are strongly restricted by the neighbouring crystalline regions (80-100°C), and molecular motion of chain moieties at lamellar surfaces (0-30°C). Again, this suggests that the α crystallites and molecular chains strongly restricted by the neighbouring crystalline regions are closely associated. X-ray measurements on β PVDF have shown that complete yet reversible melting of the thinnest crystals and not thermal expansion accounted for the changes in crystallinity between 25°C and 72°C, thereby confirming the role of paracrystalline regions Schultz [15]. Nabata also attributed an endothermic phase transition, observed at ~50 °C in both DMA and DSC experiments, to paracrystallinity [1]. Here, we define

paracrystallinity as a non-crystalline solid, which consists of crystalline, distorted configurations that are preserved during crystal-amorphous or crystal-melt transition and that these configurations can be quasi-aligned in the disordered matrix [16, 17]. Common to all these works was the presence of a transition in the DSC around 40-60°C, which exhibited hysteresis and was found to be highly sensitive to the material's thermal history, hence the variation in reported temperatures of transition. Solid-state NMR can give important information about the molecular motion and structure of polymers [18, 19]. NMR techniques for characterising local motions comparable to DMA, DSC and dielectric relaxation are achieved by the measurement of spin-lattice relaxation (T_1) and spin-lattice relaxation measured in the rotating frame ($T_{1\rho}$). When the spin-lattice relaxation is measured in the rotating frame the relevant sampling frequency is given by the magnitude of the spin-lock field, typically in tens of kHz [7]. It is common to vary the temperature, inducing a change in the nature of molecular motion probed by the spin-lattice experiment. The amplitude and time scale of a given motion is often found to have Arrhenius dependence on temperature; hence activation energies can be derived [20]. Studies of rotating frame spin-lattice relaxation have shown that two characteristic mechanisms are common in polymers: the α_c transition, revealing motion in the crystalline lattice, and the β transition, which takes place at a lower temperature and shows the onset of motion in the amorphous domain. [20, 9, 10]. The role of the α-relaxation in semi-crystalline materials has been defined into two classes [21], firstly a mobile and crystal-fixed transition where the α_c- relaxation provides mobility of chains in the crystallites, and secondly where the α_c relaxation is not present in crystal-fixed structures. The α_c mobility has been found to be an important factor in the ultra-drawability of the polymer, along with low entanglement [21]. Tetrafluoroethylene-hexafluoropropylene copolymer (FEP) and PVDF are two such polymers that exhibit α_c mobility [10]. However, the study of relaxation parameters by solid-state NMR has not been straightforward on such polymers. In a proton relaxation study of FEP fibres it was found that at low temperatures the greater intensity remained with the short $T_{1\rho}$ relaxation time. However at ~10°C a crossover of the relaxation curves and a transfer of intensity to the long component was observed [9]. A model invoking spin diffusion between crystalline and amorphous regions was proposed to explain this transfer of signal intensity and its dependence on the geometry of the interface region [9, 10]. Proton relaxation data have been recorded for α-PVDF and a transfer of signal intensity, in the same manner as for FEP, was observed between

90-120°C [10]. The presence of four relaxation processes were found, one crystalline (α_c ~100°C) and three amorphous β'(~80°C), β(~ 6°C), and γ (-20°C), as described earlier in this text. A difference was seen between the β' relaxation of PVDF 'as received' and PVDF annealed at 160°C; for the latter the β' $T_{1\rho}(H)$ minimum becomes shallow but shows no noticeable shift in temperature. This was interpreted as an indication of morphological rearrangement, which would accompany an annealing process, i.e. the widening of the lamellae. Therefore, the transition at 60°C in the DSC thermogram may have a common source with the β' relaxation, both being related to chain loops associated with crystalline regions. Later work questioned the assignment of the α_c relaxation to chain rotation in the vicinity of defects or rotations of restricted amplitude of all chains about their chain axis by McBrierty [8, 9, 10]. Furthermore, ^2H two-dimensional exchange NMR analysis of the relaxation process α_c concluded that this process is characterised by a electric dipole moment transition along the molecular direction only, with a conformational change tgtg* to g*tgt [22].

Later work of Marand [23, 24] offers an interesting explanation on the melting behaviour of polymers such as poly (arylene Ether Ether Ketone) (PEEK), polyethylene (PET) and ethylene/1-octene co-polymers (EO) using DSC. Of special interest to us were the implications of this work for the behaviour of polymers with α_c relaxation such as poly(vinylidenefluoride) (PVDF). The purpose of this work was to gain information on processes governing the crystal growth after primary crystallisation (nucleation). The primary crystallisation is describe as being mainly the formation of spherulites until growth stops, and that further isothermal lamella growth at least under $T_{\alpha c}$ is not a viable option. However, a secondary crystallisation process is proposed to take place where an increase in crystallinity is seen though the formation of new crystals from short chained amorphous units. These new crystals are formed by a different mechanism and exhibit large differences in melting behaviour. This secondary crystallisation was viewed as a thermo-reversible cross-linking process, which, at temperatures under the onset of primary crystallisation during cooling, involving loops, ties, chains and long cilia and yields interlamellar-fringed micellar structures.

In this chapter differential scanning calorimetry (DSC) and solid-state nuclear magnetic resonance have been used to monitor the changes in thermal motion of nascent and annealed α poly (vinylidenefluoride) (PVDF). Molecular motion was probed, at temperatures between –60°C and 150°C, by monitoring the proton spin-lattice relaxation in the rotating frame. Transitions associated with thermal history, chain-fold

motion, crystallinity and the possibility of para/micro crystallinity are discussed. This was analysed in terms spin populations, and relaxation data, leading to a comparison between molecular motion and thermal events of the nascent and annealed PVDF samples. The results are compared to DSC thermograms, and the effects of annealing are discussed.

6.2 DSC Experimental

The nascent powder sample contained α-PVDF as the crystalline domain (Kynar 301 F), supplied by Atofina, France, with a molecular weight of 1×10^6 D by GPC, reverse unit content of 10% by NMR, crystallinity of 28% and melting point of 158 °C by DSC [17, 21]. The nascent α-PVDF was annealed at 200 °C for 20 hours before DSC and NMR measurements were taken

A Perkin-Elmer Pyris 1 DSC with external nitrogen cryofill and a working temperature range from –180 °C to 260 °C was used for thermal analysis. The calibration was made using cyclohexane (87°C) and indium (156.0°C) and all samples were enclosed in aluminium pans. Measurements were taken with a first heat cycle from –100°C to 200°C with a heating rate of 10°C/min. Then quenching from 200°C to –100°C at 50°C/min was carried out. The temperature was then held at –100°C for 5 minutes before the second heat cycle started from –100°C to 200°C, with a heating rate of 10°C/min. Pyris Thermal Analysis software for Windows version 3.52 was used for instrument control and data analysis.

6.3 Results of DSC

The DSC thermograms of nascent and annealed PVDF are shown in figure 6.2. The values of the heats of fusion for the transitions in the DSC heating and cooling cycles are summarised in table 1. Two types of heat capacities are seen the DSC thermogram showing the heat of transition for thermal relaxation ΔHJ/g for a melt transition and a C_P J/g for a phase transition [25, 26]. The latter is typical of the T_g (glass transition) transition showing the change from a glassy to rubber material. These are easily distinguishable by the shape of the signals: a melt transition has the general form of a rise to a maximum, whilst the T_g transition is a rising of the base line. The first heat cycle of the nascent α PVDF shows two endotherms at ~156 °C (seen as a shoulder in the peak) and ~159 °C, corresponding to the melting of crystallites formed under non-isothermal conditions and nucleation respectively [5] with a crystallinity of ~28 %,

figure 6.2 (a). A broad transition consisting of two peaks at 57 and 88°C was recorded in the nascent

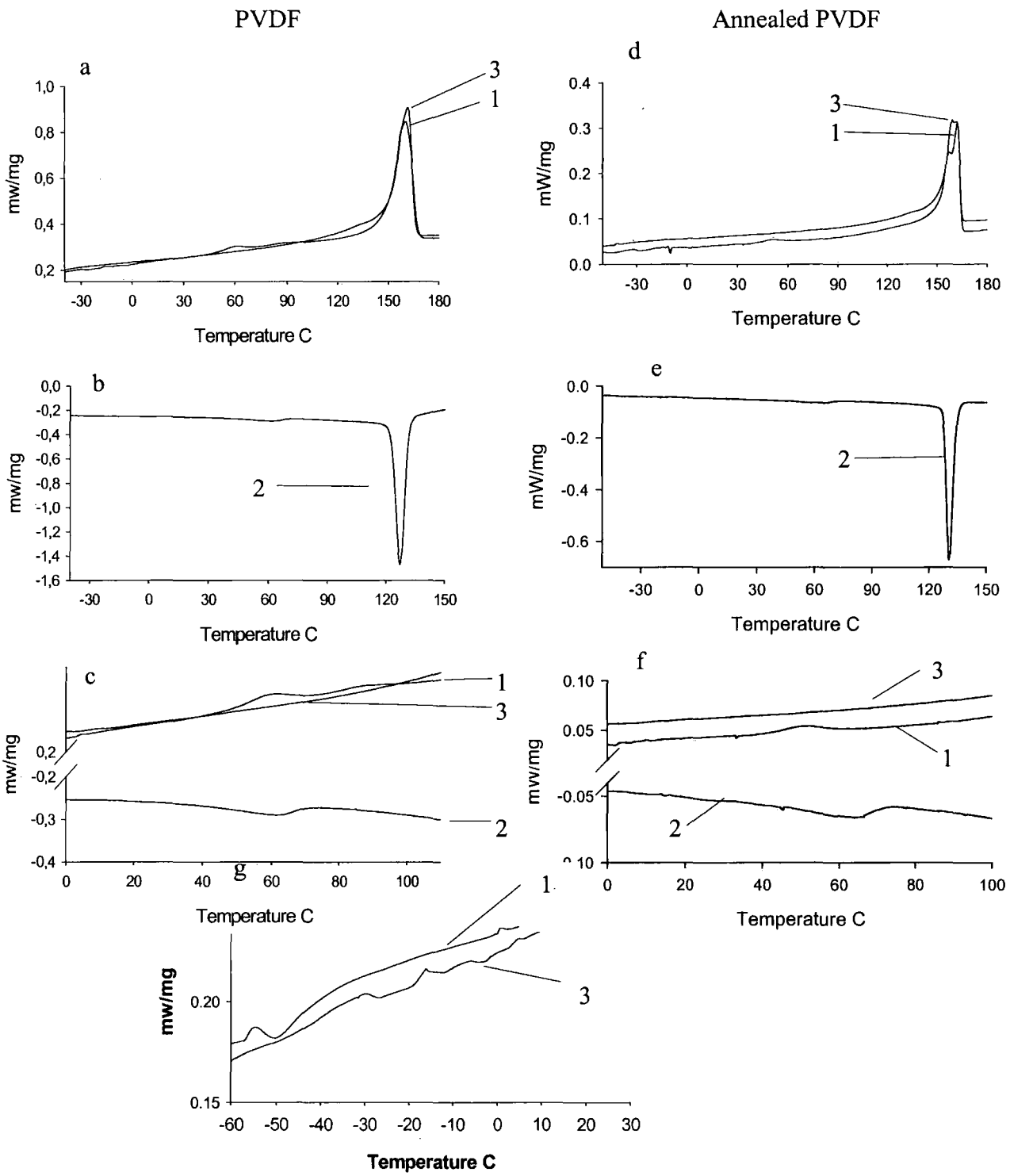

Figure 6.2. The DSC endotherms showing: the first (1) heat run, the cooling run (2) and the second heat run (3) of PVDF (a, b, c and g) and annealed PVDF (d, e, f). Figures (b) and (e) show the cooling runs (2). Figures c and f show an expansion of the 0C to 100 C region for all thermal profiles. Figure g show an expansion of the low temperature region and the problem with assigning the Tg transition.

Sample, (figure 6.2 I). A glass transition (T_g) at –41.4°C was seen in the first heat run of the nascent PVDF but not in the second heat run, figure 6.2 (g). The annealed sample did not show any glass transition. Figure 6.2 (g) also shows the problem in assigning the glass transition T_g due to the effect of the thermal coupling, which is seen in the erratic behaviour of the base line in the first and second heat run. The glass transition proved to be a somewhat elusive event in the thermograms. Although many thermograms were made the glass transition was not always apparent, the reason for this is not understood, but may be due to varying amounts of sample and/or the thermal response of the substance.

Two peaks are seen in the DSC of the annealed sample at 159.9 °C and 156.4 °C at the same temperature as the nascent sample, but now with different intensities, the peak at ~159 °C being the most intense, figure 6.2(d) and (g) and with a crystallinity of 40 %, The annealed sample did not show a T_g transition at –41.4°C or a transition at 88.0°C in the first heat run, but only the peak at 57°C was recorded, figure 6.2(f).

The cooling profile of nascent PVDF figure 6.2 (b) and the annealed sample figure 6.2 e, show two exothermal transitions associated with recrystallisation at 130.3 and 64.1°C for nascent PVDF and 130.6 and 64.0°C for the annealed sample. This indicates a recrystallisation of two components in each sample. The 130°C peaks gave a crystallinity value of 40% and 43% for PVDF and the annealed sample respectively.

The second heat runs of both samples show a peak at ~160°C giving a crystallinity of 41% for PVDF and 42% for the annealed PVDF. In the temperature region –60°C to 100°C of second heat run, no thermal transitions were recorded (figure 6.2c and f).

A comparison of enthalpy values for the endotherm at 64.1°C of the first heat cycle of the annealed sample shows a decrease in enthalpy of 4.2J/g for this transition compared to the broad endotherm of the nascent sample. Also the melt transitions of the annealed sample at 159.9 °C and 156.4°C showed a ~10 J/g increase, which is interpreted as an increase in crystallinity in comparison with the nascent sample. The second heat cycle of the annealed sample showed melt endotherms at 159.9° and 156.4. Again an increase in crystallinity of 8% was recorded compared to its first heat run, seen as an increase in signal intensity of the endotherm at 156.4°C. Calculation of crystallinity was made using the heat of single-crystal fusion 104.64 J/g [1] and equation 1.

$$\frac{\Delta H J/g}{104.63 J/g} \times sample \times 100 = \%Crystallinity. \qquad \text{Equation 1}$$

This calculation should be taken as an estimate of crystallinity as the endotherm is clearly not one single signal. At the low temperature side of the melt endotherms there is a broadening of the signals, this could be indicative of an array of smaller transitions. This also introduces uncertainty in the calculation.

The heat values (J/g) in table 1 from the first and second heat runs of PVDF show an increase in crystallinity of 31% compared to the first heat run. The gravity of the melt endotherm is weighted towards the 159.5°C peak in the second heat run. This was also seen for the annealed sample where an increase in crystallinity of 8 % can be contributed to the 156.4°C signal, as stated earlier, figure 6.2 d. The broad transition of the nascent PVDF, in the second run (-40 to 90°C), is however, only 2% of the melt endotherm. The above results imply that the increase seen in crystallinity does not have its sole source in the broad endotherm, but probably from further development of existing crystallites.

Furthermore, the difference between the first and second heat run of the nascent sample, figures 6.2 (a) and (c), shows that annealing the sample above the melting point does not give back the glass transition, as is also substantiated in the first heat run of the annealed sample. Further comparison of the heat values for the signals at 88.0 and 56.7°C in the nascent PVDF and 64.7°C in the annealed sample shows a decrease of 88% of signal intensity in this region. However this again indicates that the increase in crystallinity seen in the first heat run of the annealed sample of 30%, compared to the nascent sample, cannot only derive from whatever transitions these signals might represent.

Both cooling runs showed the presence of a second rigid component at 64.1°C and 64.7°C for PVDF and the annealed sample, respectively. One could conclude that the origin of this signal is either an artefact of the heating process or an intermittent phase formed between the two heating cycles. It does, however, have the profile one would attribute to a T_g type transition.

SAMPLE	*Crystallinity %*	*T°C*	*J/g*	*CP x J/g x °C*
PVDF	28	159.5		
1st heat		156.3		
		88.0		
		56.7		
		-39.2		0.006
Cooling run	40	130.3	39.558	
		64.1		0.041
2nd heat	41	161.3	40.143	
PVDF	40	159.9		
Annealed		156.4		
1st heat run		64.7	0.073	
Cooling run	42			
		130.6	40.21	0.03
2nd heat run	43	64.0		
		159.3	40.81	

Table 1. Temperatures and energies, of the thermal transitions from the DSC of nascent and annealed PVDF. The sample amount was 10.6 mg for PVDF and 11.0 mg for the annealed sample and crystallinity is measured using equation 1.

6.4 Discussion of Differential Scanning Calorimetry

Thermal transitions monitored by DSC, dielectric spectroscopy and dynamic mechanical analysis which occur between –40°C and 100°C, are generally considered to reflecting the glass transitions, conformational disordered crystal behaviour and /or paracrystallinity of PVDF. Leonard and Boyer related a transition at ~45°C to an upper glass transition using DSC [4, 11]. Loufakis observed hysteresis for this peak and linked it to conformational disorder at crystalline surfaces and proposed that no rigid component existed above the Tg at –41°C [3]. Nabata found the presence of a transition in both DSC and DMA at 57°C and reported this as evidence of paracrystallinity [1]. We have performed annealing at high temperature to eliminate thermal history of PVDF, as annealing at the melt temperature did not result in the elimination of thermal history [9]. The heats of fusion of the transitions in the first heat run of the nascent and 24 hours annealed sample are in agreement with earlier works [1]. The effect of the annealing is seen by the disappearance of 88% of the broad Tg (figure 6.2 a-d). That the crystallinity increased by ~30% after annealing, could support the results of Boyer and

Leonard where this effect was explained as a decrease in the loop length of chains at crystallite surfaces and their incorporation in to the crystalline lamella with elimination of the broad Tg transitions. However, our results suggest that the broad Tg could describe other processes, as the substantial increase in crystallinity cannot be derive solely from this transition, it could only account for a small percentage of the increase in crystallinity. The second DSC cycle of both samples showed similar values of crystallinity and no 57°C or broad Tg transition. Only a small increase in crystallinity is noted for both samples. Thereby, only the process of quenching (cooling cycle) resulted in the elimination of the broad Tg in both samples and gave similar values of crystallinity. These transitions could be linked to different mobilities, or smaller regions of crystallinity, which upon annealing at 200°C and the second heat cycle of both samples, gives an increase in crystallinity. It is clear that annealing and the process of heat cycling by DSC give similar yet not identical results and that the increases in the values of crystallinity do not coincide with the decrease seen in the broad glass transition. However it cannot be determined from these experiments if they contribute or not it the increase. We tentatively assign these to either the release of molecular constraints and/or the presence of micro/paracrystallinity. Also, and most importantly, the 57°C peak or any part of the broad glass transition do not show uniform behaviour with regard to the increase or decrease in crystallinity, as earlier reported by Boyer and Leonard, where their assignment of an upper T_g was related to cilla, loose loops or tie molecules. Wunderlich proposed conformational disorder to be the source of the transition tgtg* to tg*tg. Judged by the behaviour we found after our treatment, we could not associate this transition to either theory except that it was largely independent of any change in crystallinity due to heating or ageing. Furthermore, the transition at 57°C has the characteristics of a phase transition and not that of a C_P jump usually associated with a Tg transition. From the DSC results we speculate that the 'so called' broad glass transition shows the possibility of an array of mobilities above the Tg at – 41°C, intrinsic only to the nascent polymer structure. Yet again this shows the great diversity at the molecular level due to the thermal history of the material. To note here in the fact that DSC is a low frequency experiment and will detect a transition at a lower temperature than a high frequency experiment such as NMR

6.5 Static ^{1}H NMR measurements and technique

A Varian single-channel static probe was use to measure the proton spin-lattice relaxation times T_1, using a saturation recovery pulse sequence [27]. Therefore, it was not possible to apply fluorine decoupling in the following experiments.

The magnetisation M (τ) was recorded for 8 different τ values ranging from 0.2 to 32 seconds and analysed using equation 1 giving the spin lattice relaxation time T_1.

$$M(\tau) = M_0\left\{1 - \exp\left(-\frac{\tau}{T_1}\right)\right\} \qquad \text{Equation 2}$$

To measure the proton spin lattice relaxation in the rotating frame ($T_{1\delta}$) a variable spin-lock pulse was used with a spin-lock power of 2.0 mT, and 49 values of τ were acquired ranging from 40 μs to 40 ms with an increment of 0.8 ms. The measurements were made using a 1.8 μs $\pi/2$ pulse. The $T_{1\delta}$ (H) data (the intensity of the first point of each FID versus the spin-lock time) was analysed in terms of a two-component fit to an exponential decay using equation 3

$$y = y_0 + ae^{-bx} + ce^{-dx} \qquad \text{Equation 3}$$

and Sigma Plot® 4.0 software. The values of $T_{1\rho}$ (H) were obtained by least square fitting of the peak intensities to the Marquardt-Levenberg algorithm, equation 4 [28-32].

$$SS = \sum_{i=1}^{n} w_i (y_i - \hat{y}_i)^2 \qquad \text{Equation 4}$$

Figure 6.3 shows one example of a decay curve from a variable spin-lock experiment at 20 °C and the two-component fitting according to equation 4 (solid line). All relaxation curves were fitted from 1 to 3 components of which the two-component fit gave the best results. The one and three component fitting results are not shown, as these did not contribute significantly to the statistical analysis. The fitting was made using the following parameters, tolerance=1e-6, step size=0.1 and 100 iteration.

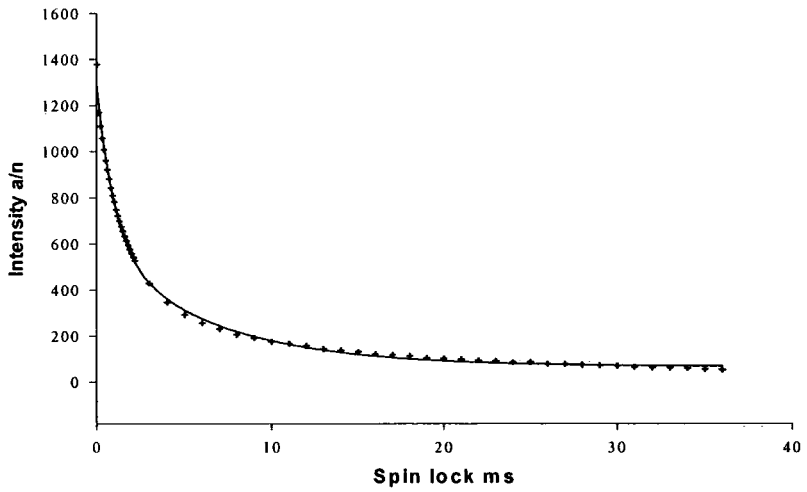

Figure 6.3 Example of a decay curve from a variable spin-lock experiment. The actual fitting, from which relaxation times and populations are calculated, is shown as a solid line.

6.6 Statistical parameters of fit

Statistical results of parameters giving a measure of the 'goodness of fit' are shown for both samples, figures 6.4-6.6. Here Predicted Residual Error Sum of Squares (PRESS) is a gauge of how well a regression model predicts new data. The smaller the PRESS statistic, the better the predictive ability of the model. The PRESS statistic is computed by summing the squares of the prediction errors (the differences between predicted and observed values) for each observation, with that point deleted from the computation of the regression equation.

The standard error of the estimate is a measure of the actual variability about the regression plane of the underlying population. The underlying population generally falls within about two standard errors of the observed sample.

The multiple correlation coefficient R is the measurement of how well the regression model describes the data. R-values near 1 indicate that the equation is a good description of the relation between the independent and dependent variables. The R value equals 0 when the values of the independent variable does not allow any prediction of the dependent variables, and equals 1 when you can perfectly predict the dependent variables from the independent variables.

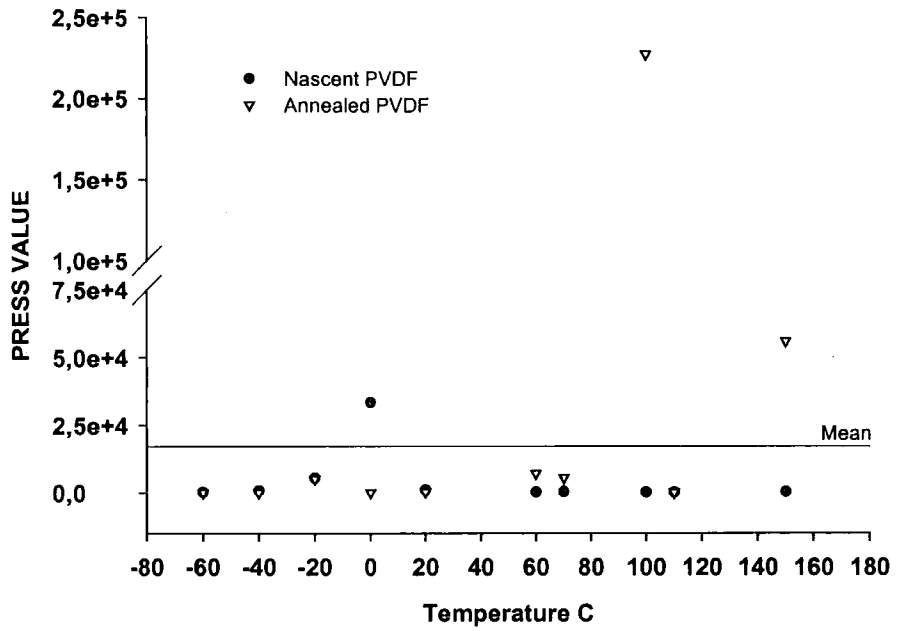

Figure 6.4 The PRESS values of the two-component fitting of relaxation data for nascent and annealed PVDF.

The PRESS value for a few selected temperatures is seen in figure 6.4. For several temperatures the PRESS values of both samples are very similar and show relatively good predictability for the two-component fit, these are –60, –40, –20, 20, and 110 °C. By this we mean the predicted value of the $T_{1\rho}$ decay curve at that temperature, calculated from the forgoing values are in good agreement with actual values, or for the applied model, its prediction is near to actual observed values, a good fit. The annealed sample did, however, give bad values at 100 and 150°C and is probably due to experimental error.

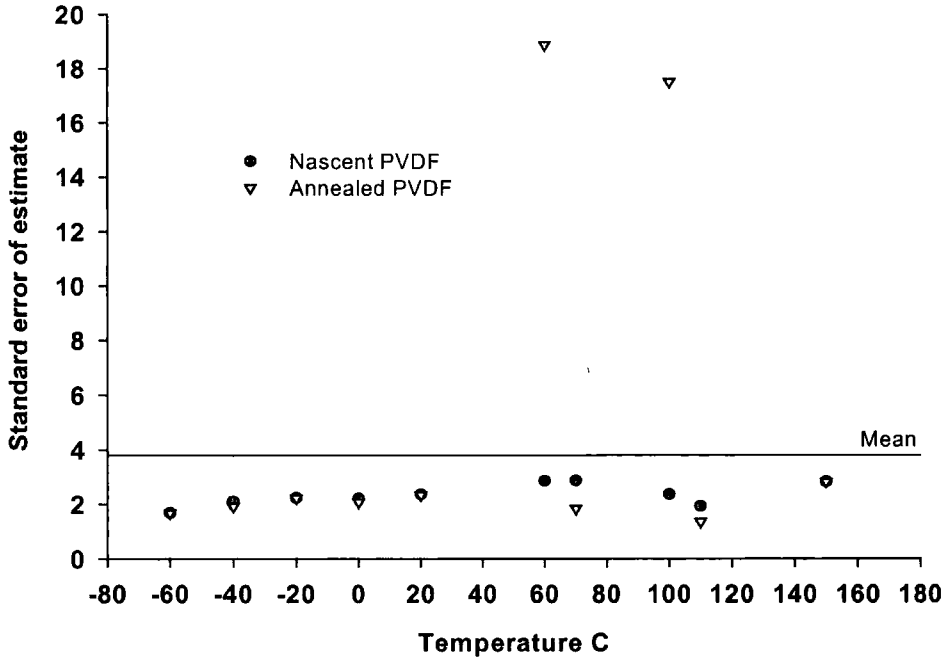

Figure 6.5 The plot of the standard errors of estimate for the two-component fitting of relaxation data for nascent and annealed PVDF.

The standard error of estimate of both samples, figure 6.5, gives similar results at all temperatures, except at 60 and 100°C for the annealed sample. There are two exceptions from the general trend in the data at 60 and 150°C.

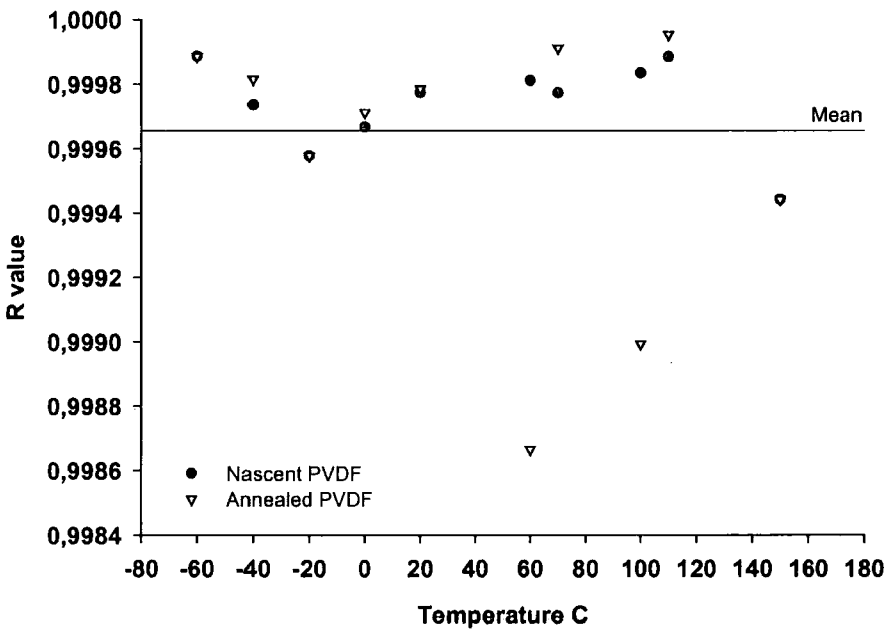

Figure 6.6 The plot of the regression value for the two-component fitting of relaxation data for nascent and annealed PVDF.

The regression value R, describes how well the model fits the data, figure 6.6. The worst fit is seen for temperatures at 60°C, 100 °C for the annealed sample and for both samples at 150 °C. This is in agreement with the PRESS and standard estimates of error values and standard error of estimates for these temperatures. All other data shows relatively good fit with the two-component model.

6.7 Temperature dependent proton spin-lattice relaxation and populations

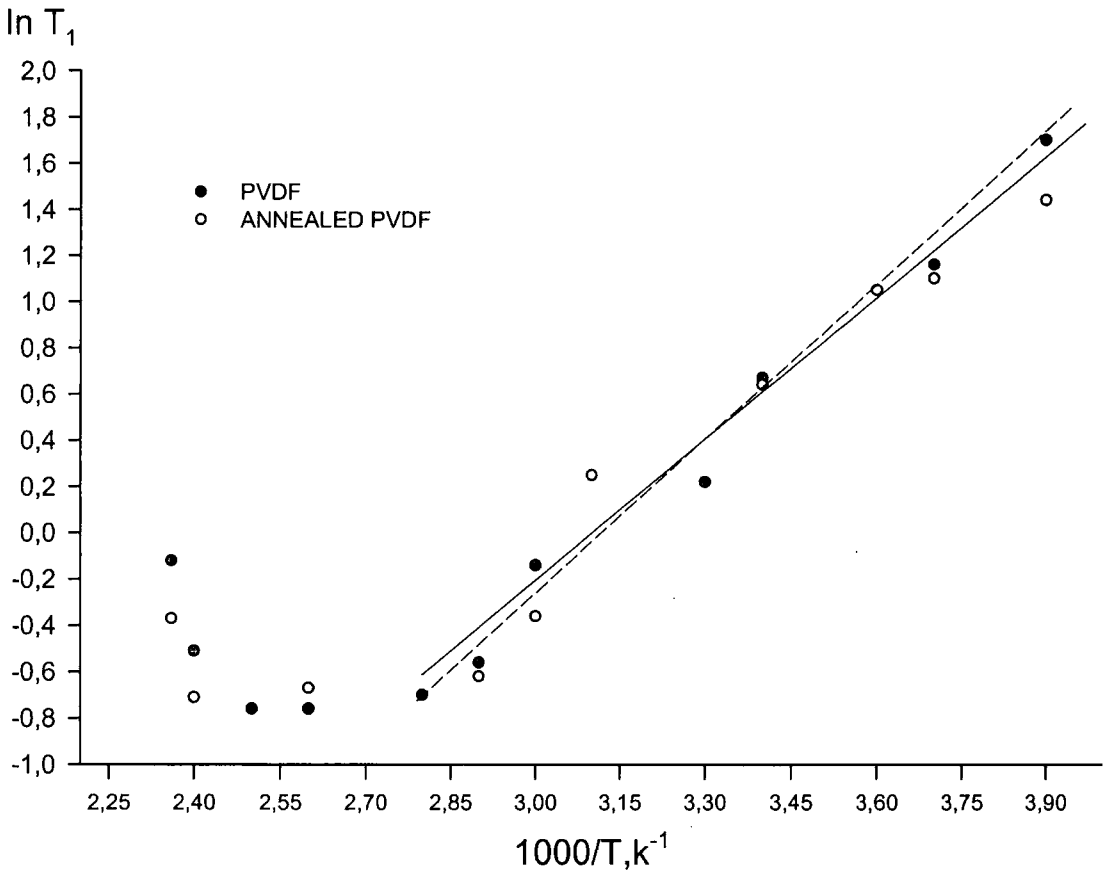

Figure 6.7 Proton T_1 temperature dependency of nascent (solid line) and annealed (dashed line) PVDF.

$$\ln\frac{\tau_1}{\tau_2} = \frac{E_a}{R}\left(\frac{1}{T_1} - \frac{1}{T_2}\right) \qquad \text{Equation 5}$$

Figure 6.7 shows the temperature dependence of the proton T_1 which displays a minimum at ~90°C for both samples. The proton T_1 activation energies calculated from

the Arrhenius equation (equation 5) at the lower temperature (see figure 6) for both the nascent and annealed samples are shown in table 2 where the slope of the line is the activation energy. The differences in energy reflect the increase in crystallinity of the annealed sample indicating a difference in the motion of the bulk material. Note that the values are an average of the crystalline and amorphous domains. This is probably due to effective spin diffusion by strong coupling of one component i.e. the amorphous domain, which, has molecular motion favouring relaxation and can therefore relax resonant nuclei of another component i.e. the crystalline domain [9, 20]. The analysis of T_1 showed only one component behaviour. Spin diffusion is a major interaction in solid polymers and is the cause of reducing T_1 relaxation. This is induced by the motion, such that the dipolar coupling is strong enough to mediate the transfer of relaxation to all protons in the polymer via the so-called flip-flop mechanism.

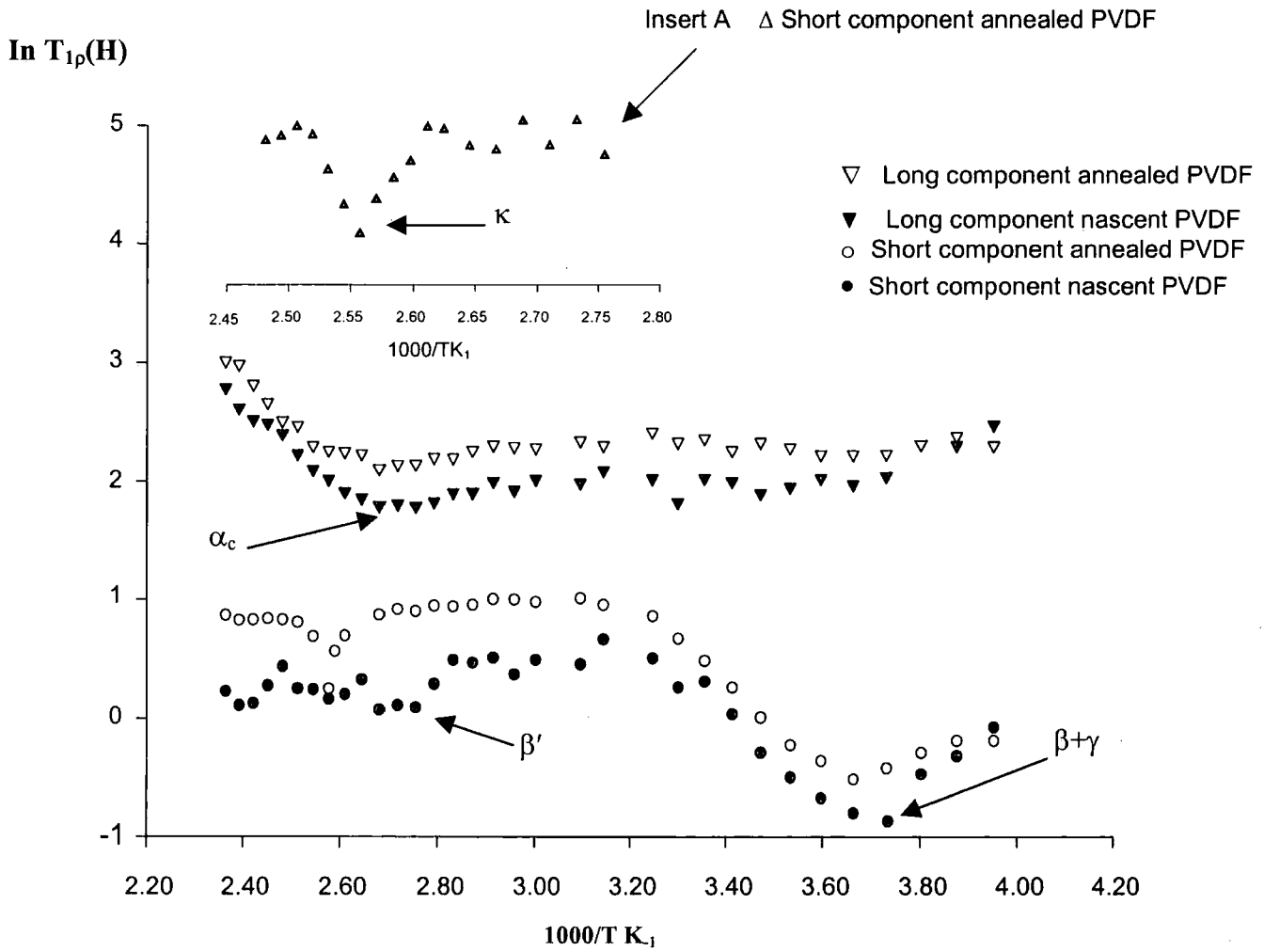

Figure 6.8. The temperature dependence of the $T_{1\delta}(H)$ of nascent and annealed PVDF showing both the long and short components. The insert (A) shows the 118°C transition of the short component for the annealed sample in detail.

Figure 6.8 shows the temperature dependence of the proton $T_{1\rho}$ relaxation for the samples between –60°C and 150°C. A broad local minimum for the long component is seen around 90°C for both samples corresponding to the crystalline α_C relaxation [8, 9, 10].

Major differences in the relaxation behaviour are apparent in the short component behaviour of the two samples. The nascent PVDF shows an irregular behaviour in the temperature region 0 to 150°C with what could be several minima of which one at ~80°C is possibly the β′ transition. However, the annealed sample shows only one sharp and minimum labelled κ, at 118°C. The insert in figure 6.8 (insert A) shows this minimum, which was re-recorded with more data points for clarity. The short component of both samples clearly shows a minimum at –6°C in agreement with β and γ transitions. Although the γ transition should be around –20°C, this might be difficult to separate from the β transition due to the general trend in this region. The β transition shows the general onset of motion in the amorphous domain whereas the γ transition is related to the glass transition point/chain rotation in amorphous domains. It is also worth noting that the irregular behaviour seen between 0°C and 150°C in the nascent sample is no longer present in the annealed sample. All of these transitions and their temperature dependences are in agreement with the literature apart from the 118°C minimum (κ) seen in the short component of the annealed sample, which has not previously been reported. That this amorphous component is only present in the annealed sample (with greater crystallinity) at a relatively high temperature could mean that this transition is for amorphous chains yet associated with more rigid domains.

	Crystallinity	$^{\dagger}H^a$ *kJ/mol* (90°C)	$^{*}H^a$ *kJ/mol* (118°C)	$^{*}H^a\ \alpha_c$ *kJ/mol* (97°C)	$^{*}H^a\ \beta$ *kJ/mol* (80°C)	$^{*}H^a\ \beta+\gamma$ *kJ/mol* (-6°C, -20°C)
PVDF	28.0 %	42	N/A	61.3	40.5	58
PVDF Annealed	39.8 %	60.6	67.0	82.1	N/A	80

Table 2 Spin-lattice relaxation data for thermal events in PVDF: † Calculated from T_1 relaxation data, * Calculate by the Arrhenius equation from the low temperature $T_{1\rho}$ relaxation data for the respective transition. The temperatures of the transitions are given in brackets.

Table 2 show the enthalpies of the transitions seen in the long and short components of the $T_{1\rho}$ H curves, figure 6.8. The transition at 118°C has the greater value of enthalpy. The energy of the α_c transition has increased, as one would expect, for the annealed sample. However, the transition associated with motion in the amorphous domains (β), also showed an increase with annealing, which is perhaps more surprising.

The normalised spin populations, obtained from the two-component proton $T_{1\rho}$ (H) calculation (equation 2), where the coefficients of the decay functions provide a measure of the population of each relaxation time and therefore the amount of material represented by the individual decay terms are seen in figure 6.10. However, it should be noted that here the populations result from the combined effects of relaxation and spin diffusion (magnetisation transport). In the regime where spin diffusion is effective but spin diffusion averaging is not complete, there is no way of associating the observed populations with intrinsic populations of two regions or domains [33, 34] as presented in earlier work of [8, 9, 10]. So, the discussion will be related solely to changes in the observed populations. The model for this will be a two-domain lamellar system consisting of a crystalline and amorphous domain, figure 6.9. Then the observed behaviour can be described by six parameters: the intrinsic relaxation times in both regions, the spin diffusion in both regions and the dimensions both regions. The last two of these parameters are unlikely to change significantly in these experiments, at least at temperatures below the melting point of the crystalline region. The intrinsic relaxation times ($T_{1\rho}$) are related directly to molecular motion at the frequency of the spin-lock power (in this case 40 kHz) in the region in question. However, spin-diffusion coefficients depend on the strength of dipolar coupling in the region and therefore more closely related to changes in the linewidths and T_2. Therefore it is possible that gradual changes in the intrinsic parameters ($T_{1\rho}$ and T_2) with temperature show gradual monotonic changes in the observed populations and sudden changes in relaxation times caused by i.e. the glass transition, could result in a discontinuity in the population plots. This would be seen in the maximums and minima, or a sudden change in the gradient of the plots.

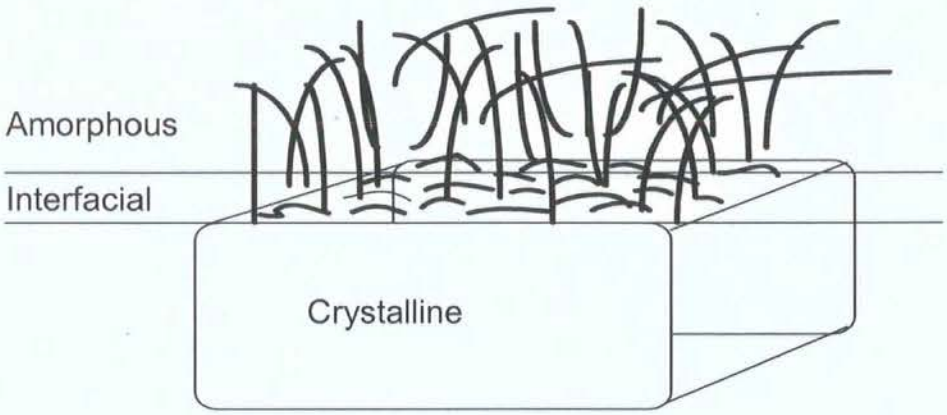

Figure 6.9. Schematic representation of the phases of a semi crystalline polymer.

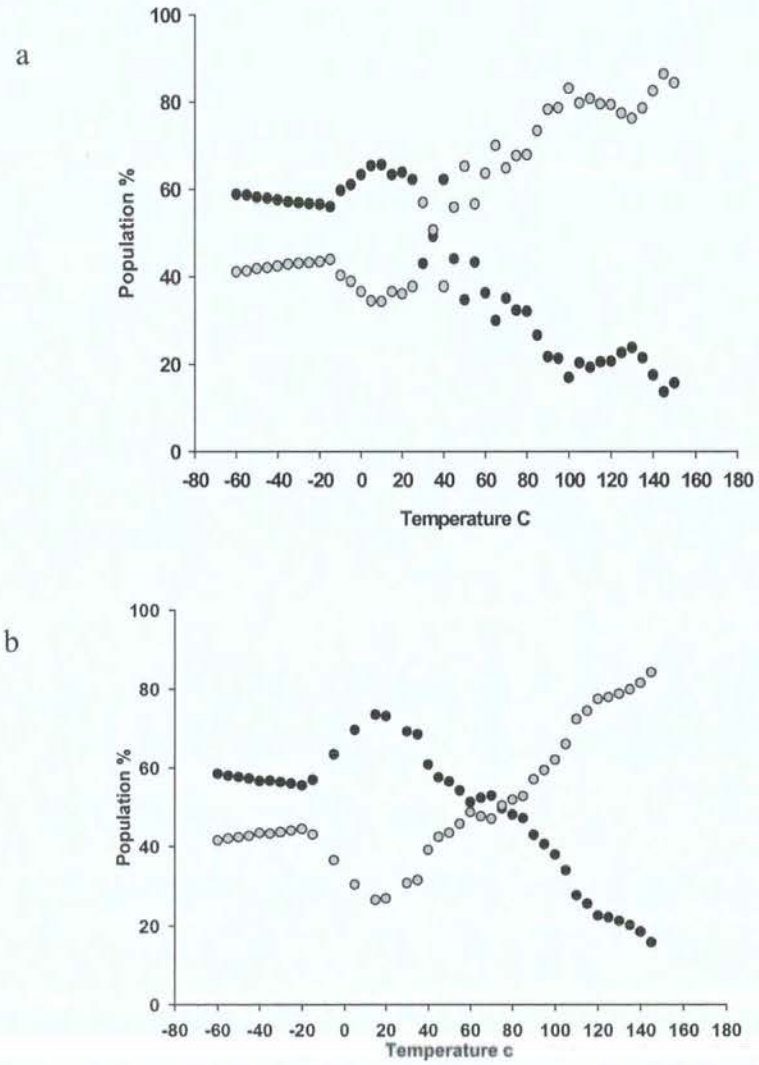

Figure 6.10 The normalised spin populations of PVDF (a) and annealed PVDF (b). Filled circles show the short component, open circles show the long component.

One characteristic feature for both samples is the crossover of the population intensities with increasing temperature. For both samples the short component has the greater magnitude at low temperatures, yet as the temperature increases, its intensity decreases and the long component has the greater magnitude. This happens at ~30°C for the nascent and at ~80°C for the annealed sample.

It would, however, seem strange, as both diagrams show, that an increase in temperature close to the melting point (150°C) would be associated with a continued increase in the amount of crystalline component as shown by the population plots.

This indicates that there is no way of associating the observed populations with intrinsic populations of the two domains [33, 34] and as discussed in paragraph above.

However, discontinuity in the population plot of nascent PVDF (figure 6.10(a)) is seen at –18 °C, +10 °C, +100 °C, and 135 °C. While the annealed PVDF (figure 6.10(b)) we observe the corresponding points -18 °C, +18 °C and +120 °C with a possibility at of a further point at +80 °C.

As the population ratios are not clearly understood the population weighted rate averages were calculated to give information on major transitions from relaxation times and populations,

6.8 Population weighted rate average

The population weighted rate averages (PWRA) of both samples are shown in fig 6.11. The intrinsic relaxation time T is given by the fractional populations, f_a (amorphous) and f_c (crystalline) of the proton $T_{1\rho}$ relaxation times T_a (amorphous) and T_c (crystalline) (equation 5).

$$\frac{1}{T} = \frac{f_a}{T_a} + \frac{f_c}{T_c} \qquad \text{Equation 6}$$

It has been shown that the PWRA of the observed components is equal to that of the intrinsic relaxation rate [35]. Therefore, when motions, which cause relaxation occur at significantly different frequencies, the minimum is dominated by the intrinsic relaxation rate of that motional entity [36]. Here, the inverse of the PWRA represents the $T_{1\rho}$

behaviour, which we would observe if spin-diffusion averaging was effective on the $T_{1\rho}$ timescale. The PWRA for the nascent sample shows minima at 0°C, 80°C and 135°C and the annealed sample exhibits minima at 0°C and 105°C.

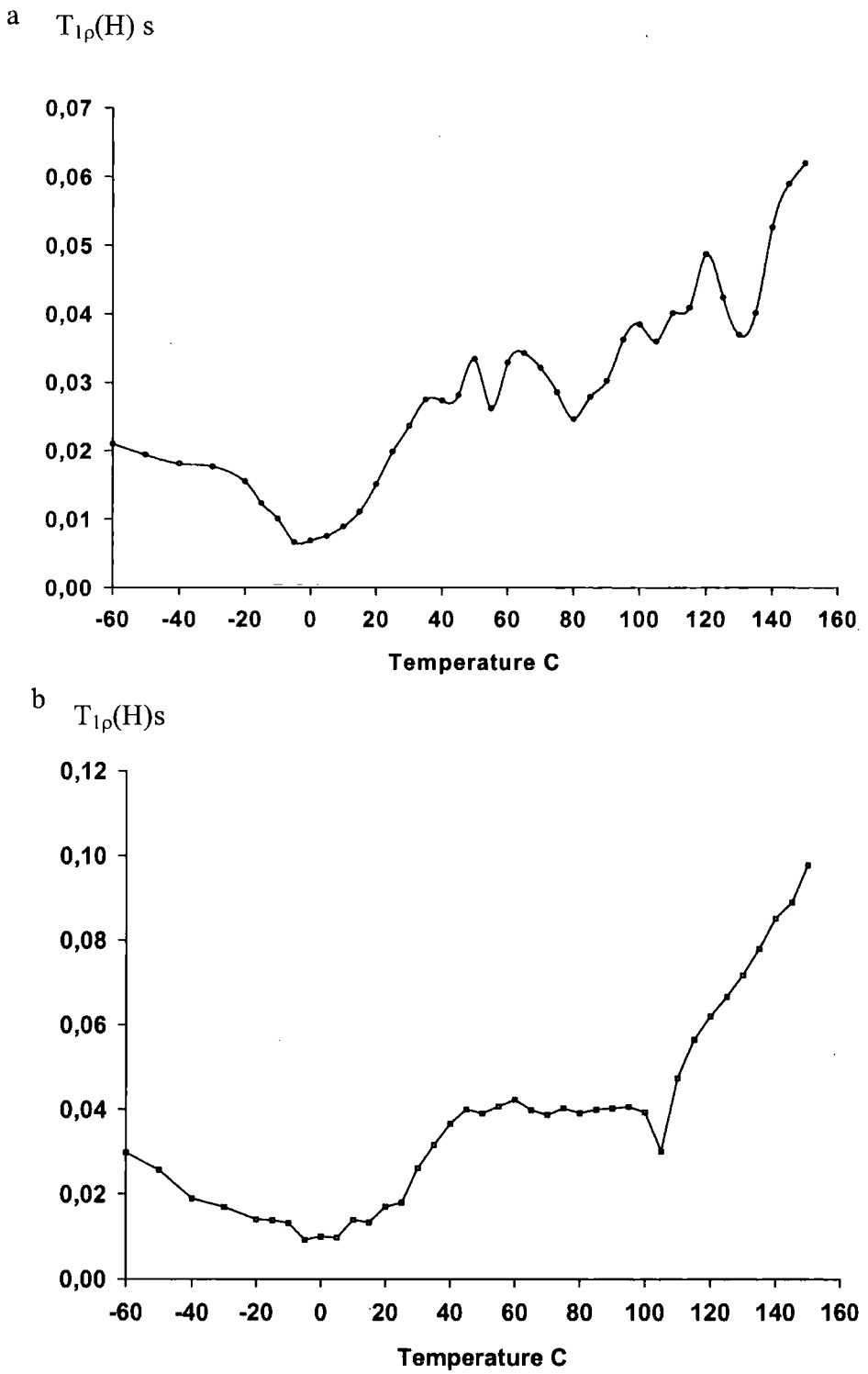

Figure 6.11 The population weighted rate average of nascent (a) and annealed (b) PVDF.

It is therefore obvious that the nascent sample exhibits more major thermal events as monitored by $T_{1\rho}$ than the annealed sample. One major difference seen for the nascent sample is the presence of a transition at 135°C. This is seen in the $T_{1\rho}$ plot for the amorphous component, figure 6.10, but not as obvious. The β (~0°C), β′ (80°C) transitions are also major events. The only transition remaining after annealing is the β (~0°C), and an unknown, high temperature transition (κ) at 110 °C.

6.9 Discussion

The activation energies for bulk motion calculated from the T_1 measurements of each sample, figure 6.3 and table 2, are in agreement with earlier calculations for nascent PVDF. The component analysis of the T_1 data showed all samples to be one component, which is probably due to effective spin diffusion. The DSC thermogram of the nascent PVDF also showed the possibility of phases, previously associated with surface of crystalline domains [1, 3, 4, 11, 12]. This material, near the interface of two different morphological phases will relax more rapidly than material, which is remote [33, 34], or could facilitate rapid relaxation through spin diffusion. Hence the population intensities would bear no resemblance to the quantity of material when spin diffusion is operative. One would also expect greater thermal contact between phases in a semi-crystalline compound resulting in extensive contribution to spin diffusion. This would be a major contributing factor to spin diffusion, resulting in a single T_1 component as was the case in this work. From the temperature dependent rotating frame spin-lattice measurements, the long components of both samples show a broad transition centred at 90°C the α_c transition with activation energies (table 2) in agreement with a change in crystallinity and literature values from dielectric spectroscopy (9, 1). One possible explanation for this transition is the complete rotation of a percentage of the crystalline chains in the region of defects (8, 9). A grain boundary slip process is also feasible [1, 37].

The short component data of both samples show an increase in relaxation values up to ~20°C this is due to the β, and γ minima around –6°C derived from movement of chains in the amorphous region. The nascent sample shows erratic behaviour at temperatures between 20 and 80°C with a possible broad transition at ~80°C (the β' transition). The short component of the annealed sample shows a sharp transition at 118°C. This

component has the highest temperature of transition and a high heat of fusion (table 2). It is tempting to attribute this transition to a pre-melting process or melting of para-crystalline units. It is however dubious to do this, due to the fact that this transition is seen in the short component relaxation data. One of the problems in interpreting the transitions in the relaxation curves is the strange behaviour between relaxation values and their intensities with varying temperature. This has been investigated for both a fibre and powder sample of FEP, and a powder sample of PVDF [10]. The fibre FEP sample showed that at low temperatures the short $T_{1\rho}$ (H) component had the greatest intensity until ~0°C when the intensity transfers to the long $T_{1\rho}$ (H) component. Whereas the powder FEP sample showed that at low temperatures the long $T_{1\rho}$ (H) accounted for the greater intensity until the $T_{1\rho}$ (H) curves cross near –30°C after which the greater intensity still remained with the long $T_{1\rho}$ (H). When a powdered sample of PVDF was investigated it showed similar intensity behaviour to the FEP powder. The results of our investigations on our powder PVDF samples show results similar to the FEP and PVDF fibre sample. It has been suggested that the intensity changes of the relaxation components are due to spin diffusion and explained as a superposition of two relaxation processes through spin diffusion of two domains i.e. crystalline and amorphous, where good thermal contact between the two domains is supplied by the interface material [10].

There is no indication of a crossover of the relaxation components in either of the relaxation data for our samples (figure 6.7). However, a crossover of the population intensities is seen in figure 8. For the nascent sample at temperatures –60°C<T>10°C, one could interpret the behaviour as a transfer of intensity from the crystalline domain to the amorphous domain and that above 10°C this behaviour is reversed. The same type of behaviour is seen for the annealed sample, a difference between the samples is the temperature at which the cross over of the intensity takes place, which is 30°C for the nascent sample and 80°C for the annealed sample. We should, however, remember that the effects of spin diffusion in these experiments are effective through strong dipole-dipole interaction. Furthermore, the longer the time scale of relaxation the more it will be influenced by spin diffusion. Therefore, T_1 will be affected to a greater extent than $T_{1\rho}$, yet the component intensities of such a coupled system have no relevance to the resonant nuclei contributing to the decay terms. Furthermore, motional effects on $T_{1\rho}$ and T_1 rely on motion at the appropriate frequency, 40kHz and 300MHz

respectively, so they tend to be offset from the temperature of the onset of the relevant motion. For this reason the same motion shows up at different temperatures according to which technique used to look at it. For the glass transition this is around -20°C in the $T_{1\rho}$ population plots, at 0°C in the PWRA plots and10°C in the T_1data. What is interesting in the $T_{1\rho}$ population data is the obvious onset of main chain motion above the Tg, which to our knowledge has not been reported earlier. However this does have a problematic consequence in that it is difficult to offer an interpretation for the other discontinuities in the $T_{1\rho}$ population plots, as we are not sure what is contributing each transition. What is evident is that all the major thermal transitions are reflected in these the plots. The difference in the PWRA data, compared to the population plots, is that the nascent sample shows major transitions at 0°C and 80 °C and 135 °C and for the annealed sample at 0°Cand 105° C. It is, however, difficult to assign any of the transitions seen in the PWRA to specific thermal events but changes in relaxation are more apparent.

One explanation for the behaviour of the populations would be that the crystalline $T_{1\rho}$ (H) remains constant but the amorphous $T_{1\rho}$ (H) separates. One part remains amorphous whilst the other increases to the crystalline $T_{1\rho}$ (H) magnitude. This would mean that the population of the long component is the sum of the crystalline and an amorphous long component above the rigid lattice temperature. However, this explanation points to the presence of three components in the $T_{1\rho}$ (H) decay curves, but this was not found in the $T_{1\rho}$ (H) analysis.

From work done on numerical simulation and theoretical analysis it has been stated that no single $T_{1\rho}$ (H) component of the rotating frame relaxation can be equated to a single molecular component. However, for a system with two well-defined regions, a particular $T_{1\rho}$ (H) may be associated with one region more than the other [34, 35]. This would become substantially more difficult with regards to semi-crystalline compounds where it is possible that the amorphous domain could contain a range of mobile to rigid entities along with an interfacial region, which is prolific in propagating spin diffusion form domain to domain. Although the nature of this relaxation and the effects of spin diffusion demands a more specific investigation than here, the fitting of relaxation components to Free Induction Decay (FID) could be approached with other methodologies such as principal component analysis which, may offer a more detailed analysis.

It has also been shown by DSC that heating to ~100 °C results in the disappearance of the transitions from –40°C to 90°C. This has been explained as an annealing effect of regions of higher order such as micro crystallites or para-crystalline regions, perhaps associated with the degree of order in amorphous/interface regions. This also would be in agreement with the findings of Schultz [15] who found by Xray studies that complete melting of the thinnest crystals and not thermal expansion accounted for the changes in crystallinity between 25-72 °C for PVDF, and the findings of Marand [23, 24, 38] where the formation of new crystals via a secondary crystallisation process took place from short- chain amorphous units i.e. loops and long cilia. If this is so, then no rigid structures would exist above the glass transition as argued by Wunderlich. Yet the presence of transitions in the first heat run at 57°C in the DSC and 118°C in the short component of the relaxation data for the annealed sample may oppose this. It has been suggested that the broad β' transition in the short component of the nascent sample at 80°C, due to its tentative assignment to crystallite surfaces, would upon annealing shift to a higher temperature and become narrow [9]. More recently the effect of annealing at different temperature and times on the 57°C peak in the DSC of the annealed sample has been investigated [39]. It was found that varying the annealing time resulted in an increase in intensity, whereas increasing the annealing temperature for the same time period shifted this peak to a higher transition temperature. It was found to obey the kinetic law ruling the secondary crystallisation process as described by Marand [38] and there fore assigned to secondary crystals formed during annealing. This would explain why this transition is not seen in the second heat run.

Indeed this is what we could be observing with the 118°C transition in the short component of the annealed sample. Yet some questions arise from these observations. If the annealing results in the incorporation of chain ends and chain loops into the crystalline matrix leaving only small tight chain loops at it surface, why would the $T_{1\rho}$ (H) of this motion have a value associated with an amorphous component? We would expect it to be more associated at this stage with a more crystalline component? Furthermore the activation energy of the 118°C transition is high and probably associated with a phase change like melting (perhaps of paracrystalline regions, or a pre-melt transition, which would indicate crystalline behaviour.

From the behaviour of the DSC endotherms and the NMR relaxation we suggest that the broad transition, -41°C to 85°C, reflects an array of mobilities in the amorphous / interface region with varying degrees of order, remembering that a purely amorphous state is not be seen in the thermogram. The simultaneous disappearance of the broad Tg in the DSC and the broad β' transition the NMR relaxation data in the annealed sample suggests a common source which could represent an array of mobilities. These events are interpreted as an overall change from random order to increased order and would explain the increase in crystallinity seen for the annealed sample.

In recent work [40, 41, 42] an increase in the amorphous phase was recorded at the expense of the broad Tg and dependent on the annealing temperature. One effect of annealing PVDF was an increase in enthalpy for the β transition; this is also in agreement in our observation, seen in the short relaxation components.

6.10 Conclusion

Temperature-dependent static proton NMR relaxation studies revealed molecular motions in PVDF in general agreement with earlier studies. Deciphering the populations of relaxation values was found to be difficult probably due to spin diffusion, yet NMR revealed a transition at 118°C for the annealed sample which has not been documented earlier, and DSC showed a phase transition at 57°C for the same sample. We believe this is evidence of a rigid unit above the glass transition, contra to earlier work. That the two are the same structural entity cannot be confirmed, as the two methodologies are dependent on different time scales. The broad T_g in the DSC profile of the nascent sample reflects a wide array of mobilities and could not be exclusively related to the increase seen in crystallinity. The proton relaxation and population values and PWRA plots, showed major thermal events and the difference between nascent and annealed PVDF in thermal events, though these could not be attributed to specific molecular motion. This study shows the possibility of influence on the microstructure i.e. interfacial material by annealing and the importance of physico-mechanical properties and its influence on the behaviour of NMR relaxation data.

Comparisons of our NMR data with those of other researchers (8, 9, 10) showed that physical properties associated with morphological structure, fibres and powders are not conclusive and comparisons precarious.

References

[1] Nabata, Y. Jap. J. Appl. Phys. 1990, 12, 2782-2788.

[2] Malecki, J and Hilczer, B. Key Engineering Materials, Vols 92-95, 1994, 81-216.

[3] Loufakis, K.Wunderlich, B. Macromolecules, 1987, 20, 2474-2478.

[4] Leonard, C; Halary, J, L; Monnerie, L; Micheron, F. Polym Bull, 1984.11, 195-202.

[5] Shinichi. Y. J. Polym. Sci. Part A. 1970, 8, 1057-1072.

[6] McGrum. N.G.,Read. B.E.; Williams. G. Anelastic and Dielectric Effects in Polymeric Solids. Dover Publications, New York. 1991.

[7] McCall. DW, Acct. Chem. Res., 4, 1971, 223-232.

[8] McBrierty. J. V, Douglass. D.C, Weber. T. A, J. Polym. Sci. 1976, 14, 1271-1286.

[9] McBrierty. J. V, McCall. D.W, Douglass, D.C, Falcone. D. R, J. Chem. Phys. 1970, 52, (2), 512-520.

[10] Douglass. D.C, Mcbrierty, V. J, J. Chem Phys. 1971. 54, (9), 4085-4089.

[11] Boyer, R.F. J. Polym. Sci. Polym. Sym. 1975 50. 189.

[12] Teyssedre. G, Bernes. A, Lacabanne. C, J.Polym. Sci.: Part B Polym Phys 1993, 31, 2027- 2034.

[13] Wunderlich. B, Thermochimica Acta, 1999, 340, 37-52.

[14] Nakagawa. K, Ishida. Y. J. Polym. Sci, (1973) 11, 2153.

[15] Schultz, J.M. Lin, J.S. Hendricks, R.W. Lagasse, R.R. Kepler, R.G. J. Appl, Phys 51, 10, 1990

[16] Popescu. M, Bradaczek. H. Journal of Optoelectronics and advanced materials, Vol 3, No 2, 2001, 249-254

[17] Hosemann, R. Z.fur Physik 128, 1, 1950, 465.

[18] Schimidt-Rohr. K, Spiess. H.W, Multidimensional Solid-State NMR and Polymers. Academic Press, 1994.

[19] McBrierty. J. V, Douglass. D.C, J. Polymer Science: Macromolecular Reviews.

[20] Komoroski. R.A, High Resolution Spectroscopy of Synthetic Polymers in Bulk, 1986 VCH publishers, ISBN 0-89573-146-0.

[21] Hu, W.G, Schimidt-Rohr. K. Acta Poly. 1999, 50, 271-285

[22] Hirschinger. J, Scheafer. D, Spiess. HW. Macromolecules, 24, 1991, 2428-2433

[23] Marand H, Alizadeh A, Farmer R, Macromolecules, 33, 2000, 3392-3403

[24] Velikov V, Marand H, J Therm Anal 49, 1997, 375-383

[25] Ozawa, T. Kanari, K Thermochimica Acta, 1996, 288, 39-51

[26] Schenker, B. Stäger, F, Thermochimica Acta, 1997, 203/305, 239-228

[27] Experimental Pulse NMR, Fukushima, E and Roeder, B.W.S. Westview Press, 1981, ISBN 0-201-62726-4

[28] Press. W. H, Flannery. B. P, Teukolsky. S. A, and Vetterling. W. T. (1986). Numerical Recipes. Cambridge: Cambridge University Press.

[29] Marquardt, D.W, An Algorithm for Least Squares Estimation of Parameters. Journal of the Society of Industrial and Applied Mathematics, 11, 1963, 431-441

[30] Nash. J.C, Compact Numerical Methods for Computers: Linear Algebra and Function Minimization. New York: John Wiley & Sons, Inc, 1979

[31] Shrager. R.I, Regression with Linear Constraints: An Extension of the Magnified Diagonal Method. Journal of the Association for Computing Machinery
, 17, 446-452, 1970

[32] Shrager. R.I, Quadratic Programming for N. Communications of the ACM, 15, 1972, 41-45

[33] Booth AD, Packer KJ, Colquhoun IJ, Abstr PAP AM Chem s 195 55-Poly part 2 1988

[34] Booth AD, Packer KJ , Mol Phys 62, 1987, 811-828

[35] Kenwright. A.M. and Say. B.J, Solid State Nucl. Magn Reson. 1996, 7, 85- 93.

[36] Kenwright. A.M. and Say. B.J, Solid State Nucl. Magn Reson. 1998, 12, 15-20.

[37] Dosseh. G, Fressigne. C, Fuchs. AH, J. Phys. Chem.Solids, vol 53, No 1, 1992, 203-209.

[38] Marand H, Alizadeh A, Abstr PAP AM Chem S 218, 120-PMSE Part 2 1999

[39] Neidhöfer M, Beaume F, Ibos L, Bernès, A LacabanneC, Polymer, 45, 2004, 1679-1688

[40] Teyssedre. G, Bernes. A. Lacabanne. C. J, Thermal. Anal. 1993, 40, 711- 719.
Appl. Phys. 1980. 51. 5508-5512.

[41] Mohajir. B and Heymans. N, Polymer, vol 42 2001, 5661-5667

[42] Mohajir. B and Heymans. N, Polymer, vol 42 2001, 7017-7023.

General conclusion.

This work has shown the possibilities of using relaxation selective experiments to deduce macroscopic properties of polymers related rigid and mobile domains. The effects of highy mobile groups, i.e. chain-end groups, and groups adjacent to the reverse units, were shown to have a great impact on spectra, making measurement of reverse groups, chain-end groups and estimates of crystallinity unrealieable. Furthermore, it was shown that there is a possibilility of reverse units associated with rigid regions, possibly at interfacial regions. A comparsion between solution-state spectra of PVDF and a VDF telomer showed similar reverse unit content, but a higher degree of chain

end units in the VDF telomer reflecting chain length. The comparision of solution state spectra verified that signals at ~107 ppm in the PVDF sample were related to end groups. These result and were highly dependent on the ability to observe a choosen nuclei with simultainious high power decoupling and at high magnetic field strength. Classical static proton experiments showed to be inadiquate in deducing real data related to the temperature dependenancy of specific motions of the PVDF polymer. Yet, did show a phase related transition in the annealed sample, not present in the nascent sample. Future projects should aim to evaluate small chain VDF type polymers with varing degrees of end groups and reverse groups by solid and solution-state NMR to access structure. Also the contribution to the crystalline fluorine line shape in solid-state NMR should be evaluated .

Appendix (i)

Solution-state pulse sequences

Quantum filtered homonuclear correlation pulse sequence

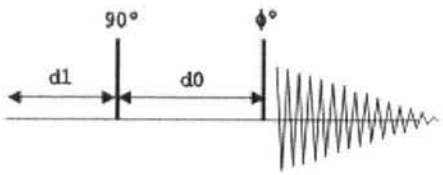


```
;cosyqf
;avance-version (00/04/28)
;2D homonuclear shift correlation
;
;W.P. Aue, E. Bartholdi, R.R. Ernst, J. Chem. Phys. 64, 2229 (1976)
;K. Nagayama et al., J. Magn. Reson. 40, 321 (1980)

#include <Avance.incl>
;;"d0=3u"
1 ze
2 d1
3 p1 ph1
d0
p0 ph2
go=2 ph31
d1 mc #0 to 2 F1QF(id0)
exit
ph1=0 0 0 0 1 1 1 1 2 2 2 2 3 3 3 3
ph2=0 1 2 3
ph31=0 2 0 2 3 1 3 1 2 0 2 0 1 3 1 3

;pl1 : f1 channel - power level for pulse (default)
;p0 : f1 channel - 20 to 90 degree high power pulse
;p1 : f1 channel - 90 degree high power pulse
;d0 : incremented delay (2D) [3 usec]
;d1 : relaxation delay; 1-5 * T1
;in0: 1/(1 * SW) = 2 * DW
;nd0: 1
;NS: 4 * n
;DS: 16
;td1: number of experiments
;FnMODE: QF

;$Id: cosyqf,v 1.3 2002/06/12 09:04:28 ber Exp $
```

Homonuclear Total Correlation pulse sequence

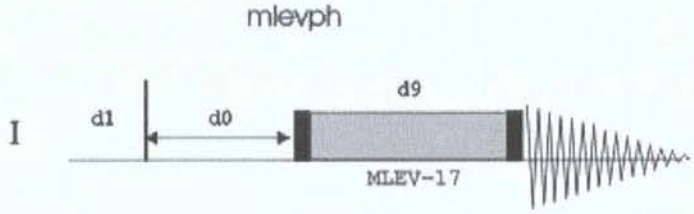


```
;mlevph
;avance-version (00/10/05)
;homonuclear Hartman-Hahn transfer using MLEV17 sequence
; for mixing
;using two power levels for excitation and spinlock
;phase sensitive
;
;A. Bax & D.G. Davis, J. Magn. Reson. 65, 355-360 (1985)

#include <Avance.incl>
#include <Delay.incl>

;;"p5=p6*.667"
;;"p7=p6*2"
;;"d12=20u"

"d0=in0/2-p1*2/3.1416-4u"

"SCALEF=p7*2/p5+0.5"
"FACTOR1=((d9-p17*2)/(p6*64+p5))/SCALEF+0.5"
"l1=FACTOR1*SCALEF"

1 ze
2 d1
3 d12 pl1:f1
p1 ph1
d0
4u pl10:f1
(p17 ph26)
;begin MLEV17
4 (p6 ph22 p7 ph23 p6 ph22)
(p6 ph24 p7 ph25 p6 ph24)
(p6 ph24 p7 ph25 p6 ph24)
(p6 ph22 p7 ph23 p6 ph22)
(p6 ph24 p7 ph25 p6 ph24)
(p6 ph24 p7 ph25 p6 ph24)
(p6 ph22 p7 ph23 p6 ph22)
(p6 ph22 p7 ph23 p6 ph22)
(p6 ph24 p7 ph25 p6 ph24)
(p6 ph22 p7 ph23 p6 ph22)
(p6 ph22 p7 ph23 p6 ph22)
(p6 ph24 p7 ph25 p6 ph24)
(p6 ph22 p7 ph23 p6 ph22)
(p6 ph22 p7 ph23 p6 ph22)
(p6 ph24 p7 ph25 p6 ph24)
```

```
(p6 ph24 p7 ph25 p6 ph24)
(p5 ph23)
lo to 4 times l1
;end MLEV17
(p17 ph26)
go=2 ph31
d1 mc #0 to 2 F1PH(ip1, id0)
exit


ph1=0 2 2 0 1 3 3 1
ph22=3 1 3 1 0 2 0 2
ph23=0 2 0 2 1 3 1 3
ph24=1 3 1 3 2 0 2 0
ph25=2 0 2 0 3 1 3 1
ph26=0 2 0 2 1 3 1 3
ph31=0 2 2 0 1 3 3 1

;pl1 : f1 channel - power level for pulse (default)
;pl10: f1 channel - power level for TOCSY-spinlock
;p1 : f1 channel - 90 degree high power pulse
;p5 : f1 channel - 60 degree low power pulse
;p6 : f1 channel - 90 degree low power pulse
;p7 : f1 channel - 180 degree low power pulse
;p17: f1 channel - trim pulse [2.5 msec]
;d0 : incremented delay (2D)
;d1 : relaxation delay; 1-5 * T1
;d9 : TOCSY mixing time
;d12: delay for power switching [20 usec]
;l1: loop for MLEV cycle: (((p6*64) + p5) * l1) + (p17*2) = mixing time
;in0: 1/(1 * SW) = 2 * DW
;nd0: 1
;NS: 8 * n
;DS: 16
;td1: number of experiments
;FnMODE: States-TPPI, TPPI, States or QSEC
;Processing
;PHC0(F1): 180
;PHC1(F1): -180
;FCOR(F1): 1
;$Id: mlevph,v 1.5.2.1 2002/09/24 09:43:29 ber Exp $
```

Single pulse experiment with pre-saturation pulse for H_2O suppression

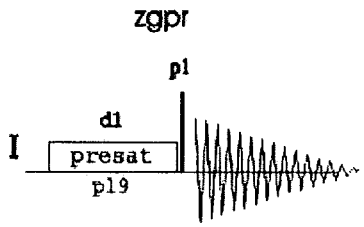


```
;zgpr
;avance-version (02/05/31)
;1D sequence with f1 presaturation
#include <Avance.incl>

;;"d12=20u"

1 ze
2 30m
d12 pl9:f1
d1 cw:f1 ph29
4u do:f1
d12 pl1:f1
p1 ph1
go=2 ph31
30m mc #0 to 2 F0(zd)
exit

ph1=0 2 2 0 1 3 3 1
ph29=0
ph31=0 2 2 0 1 3 3 1

;pl1 : f1 channel - power level for pulse (default)
;pl9 : f1 channel - power level for presaturation
;p1 : f1 channel - 90 degree high power pulse
;d1 : relaxation delay; 1-5 * T1
;d12: delay for power switching [20 usec]
;NS: 1 * n, total number of scans: NS * TD0

;$Id: zgpr,v 1.7 2002/06/12 09:05:24 ber Exp $
```

2D heteronuclear H-1/F-19 shift correlation for F-19 observe with H-1 decoupling

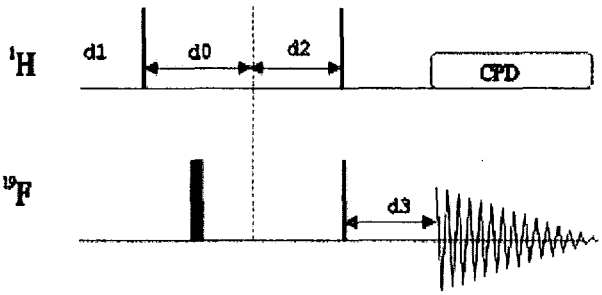


```
;hfcoqf
;avance-version (00/04/28)
;2D heteronuclear H-1/F-19 shift correlation
; for F-19 observe with H-1 decoupling
;for QNP-operation (F-19 via X-QNP output of switchbox)

#include <Avance.incl>

;;"p2=p1*2"
;;"d0=3u"
;;"d2=1s/(cnst2*2)"
;;"d3=1s/(cnst2*cnst11)"
;;"d11=30m"
;;"d12=20u"

d11 QNP_X
1 ze
d12 SWITO_H
2 d11
3 d1 do:f2
d12 pl2:f2
(p3 ph1):f2
d0
d12 SWITO_F
p2 ph3
d0
d2 SWITO_H
(p3 ph2):f2
d12 SWITO_F
p1 ph4
d3 SWITO_H
d12 pl12:f2
go=2 ph31 cpd2:f2
d11 mc #0 to 2 F1QF(id0)
d11 do:f2
exit

ph1=0
ph2=0 2 1 3
```

Appendix (ii)

Solid-state pulse programs

Dipolar filter pulse program.

```
/* dfilter modified xpolar - with "spare line" for F{H}
   includes 12 pulse (x hloop) dipolar filter  Feb 2000
   h90lvl included - May 2002
   filter performed at h90lvl power setting */

/* xpol = 'y' gives cross polarization (cp)
        'n' gives direct polarization (dp)

   pw -    the proton 90 degree pulse (cp)
         the observe 90 degree pulse (dp)
   p1 -    flip-back pulse

   cntct - hartmann-hahn contact time

   toss= 'y'  invokes timed spin-echoes to suppress spinning sidebands
   srate - spin rate (necessary for toss)
   dm - should be set to nny

   includes optional mixing delay

   crossp  - controls fine decoupler power during cross polarization,
   dipolr  - controls fine decoupler power during acquisition time.

*/

#include <standard.h>

static int table1[4] = {0, 1, 2, 3};
static int table2[4] = {1, 1, 3, 3};
static int table3[4] = {3, 0, 3, 0};
static int table4[4] = {1, 2, 1, 2};
static int table5[4] = {3, 3, 1, 1};
static int table6[4] = {2, 3, 0, 1};
static int table7[4] = {0, 1, 0, 1};

pulsesequence()

{

/* declare new variables */

  double       dutycycle,
               cntct,
               pcrho,
               d3,
                     p180,
               pwx,
               at,
               srate,
               crossp,
               h90lvl,
```

```
            mix,
            hloop,
            phshift,
            lvlshft,
            dipolr;
  char        pdp[MAXSTR],
            toss[MAXSTR],
            mixflag[MAXSTR],
            xpol[MAXSTR];
  extern double  getval();

/* set variables */

  cntct = getval("cntct");
  p180 = getval("p180");
  pwx = getval("pwx");
  pcrho = getval("pcrho");
  at = getval("at");
  d3 = getval("d3");
  mix = getval("mix");
  crossp  = getval("crossp");
  h90lvl  = getval("h90lvl");
  dipolr  = getval("dipolr");
  srate = getval("srate");
  hloop = getval("hloop");

  getstr("pdp", pdp);
  getstr("mixflag",mixflag);
  getstr("toss", toss);
  getstr("xpol", xpol);

  initval(hloop,v2);
  phshift = 2.75e-6;
  lvlshft = 4.6e-6;

 /*check dutycycle -
    do not accept dm=y or decoupler duty cycles in excess of 20% */

  dutycycle = (d1 + d2) / (p180 + cntct + pcrho + pw + p1 + d1 + d2 + at);
  if (dm[2] == 'n') dutycycle += at / (p180 + cntct + pcrho + pw + p1 + d1 + d2 + at);

  fprintf(stdout, "Duty cycle is %5.2f%%. Doing ", (1.0 - dutycycle) * 100);

  if ((dutycycle < 0.8) || (dm[0] == 'y'))
  {
    fprintf(stdout, "ABORT! The duty cycle must be less than 20%%.\nPlease adjust d1, at or set dm =
'nny'!\n");
    abort(1);
  }

/* check that a spin rate has been entered where its important */

  if (((toss[0] == 'y') || (pdp[0] == 'y')) && (srate < 50.0))
  {
    fprintf(stdout, "spin rate is too low for toss or dipolar dephasing!\n");
    abort(1);
```

```
}

/*begin pulse sequence*/

  if (xpol[0] == 'n')        /*direct polarization (dp)*/
  {
    fprintf(stdout, "Bloch decay");

    settable(t1,4,table1);
    settable(t3,4,table3);
    settable(t4,4,table4);
    settable(t5,4,table5);
    settable(t7,4,table7);
    setreceiver(t1);

    status(A);
    decpwrf(dipolr);
    delay(d1);
    sp1on();
    delay(rof1);
    starthardloop(v2);
      rgpulse(pw,zero,0.0,0.0);
      delay(d3);
      rgpulse(pw,three,0.0,0.0);
      delay(d3);
      rgpulse(pw,zero,0.0,0.0);
      delay(d3);
      rgpulse(pw,zero,0.0,0.0);
      delay(d3);
      rgpulse(pw,three,0.0,0.0);
      delay(d3);
      rgpulse(pw,zero,0.0,0.0);
      delay(d3);
      rgpulse(pw,two,0.0,0.0);
      delay(d3);
      rgpulse(pw,one,0.0,0.0);
      delay(d3);
      rgpulse(pw,two,0.0,0.0);
      delay(d3);
      rgpulse(pw,two,0.0,0.0);
      delay(d3);
      rgpulse(pw,one,0.0,0.0);
      delay(d3);
      rgpulse(pw,two,0.0,0.0);
      delay(d3);
    endhardloop();

    rgpulse(pw,t1,0.0,0.0);

    if (mixflag[0] == 'y')
    {
      rgpulse(pwx,t7,0.0,0.0);
      delay(mix);
      rgpulse(pwx,t4,0.0,0.0);
    }
```

```
  status(C);
  sp1off();
}

else
{                                   /* cross-polarization (cp)*/

  fprintf(stdout, "Cross polarization");

  settable(t1,4,table1);
  settable(t2,4,table2);
  settable(t3,4,table3);
  settable(t4,4,table4);
  settable(t5,4,table5);
  settable(t6,4,table6);
  settable(t7,4,table7);
  setreceiver(t1);

  status(A);
  decpwrf(h90lvl);
  delay(d1);
  delay(rof1);

  starthardloop(v2);
    decrgpulse(pw,zero,0.0,0.0);
    delay(d3);
    decrgpulse(pw,three,0.0,0.0);
    delay(d3);
    decrgpulse(pw,zero,0.0,0.0);
    delay(d3);
    decrgpulse(pw,zero,0.0,0.0);
    delay(d3);
    decrgpulse(pw,three,0.0,0.0);
    delay(d3);
    decrgpulse(pw,zero,0.0,0.0);
    delay(d3);
    decrgpulse(pw,two,0.0,0.0);
    delay(d3);
    decrgpulse(pw,one,0.0,0.0);
    delay(d3);
    decrgpulse(pw,two,0.0,0.0);
    delay(d3);
    decrgpulse(pw,two,0.0,0.0);
    delay(d3);
    decrgpulse(pw,one,0.0,0.0);
    delay(d3);
    decrgpulse(pw,two,0.0,0.0);
    delay(d3);
  endhardloop();
  decrgpulse(pw, t2, 0.0,0.0);
  decpwrf(crossp);
  status(C);
  decphase(zero);
  sp1on();
  rgpulse(cntct, t3, 0.0, 0.0);
  if (mixflag[0] == 'y')
```

```
    {
      status(A);
      rgpulse(pwx,t7,0.0,0.0);
      delay(mix);
      rgpulse(pwx,t4,0.0,0.0);
    }
    sp1off();
    status(C);
    decpwrf(dipolr);

  }


/*optional interrupted decoupling for protonated carbon dephasing*/

  if (pdp[0] == 'y')
  {
    fprintf(stdout, ", Protonated carbon suppression");
    status(A);
    delay(d2);
    status(C);
    delay(1.0 / srate - pw - d2 - lvlshft);
    sp1on();
    rgpulse(2.0 * pw, t3, 0.0, 0.0);
    sp1off();
    delay(1.0 / srate - pw);
  }
/*optional pi pulses for suppression of sidebands - TOSS*/

  if (toss[0] == 'y')
  {
    fprintf(stdout, ", TOSS");
    delay((0.1226 / srate) - pw - lvlshft);
    sp1on();
    rgpulse(2.0 * pw, t3, 0.0, 0.0);
    sp1off();
    delay((0.0773 / srate) - 2.0 * pw);
    sp1on();
    rgpulse(2.0 * pw, t4, 0.0, 0.0);
    sp1off();
    delay((0.2236 / srate) - 2.0 * pw);
    sp1on();
    rgpulse(2.0 * pw, t3, 0.0, 0.0);
    sp1off();
    delay((1.0433 / srate) - 2.0 * pw);
    sp1on();
    rgpulse(2.0 * pw, t4, 0.0, 0.0);
    sp1off();
    delay((0.7744 / srate) - pw - alfa - rof2);
  }

 fprintf(stdout, ".\n");

/*begin acquisition*/
  delay(rof2);
  acquire(np,1.0/sw);
```

```
/*flip-back pulse*/
  decrgpulse(p1,t5,rof1,rof2);
}
```

RadioFrequency Driven Recoupling (RFDR)

```
/* Fnoesy.c

  solid state x-nucleus 2D exchange spectroscopy with cross-polarization
  or direct polarization preparation and pure-phase quadrature detection
  in the f1 dimension. The mixing period can be synchronized with the rotor
  (sync = 'y') and can contain pi pulses (rfdr ='y') for rotor driven dipolar
  recoupling. Modified with spare line for F and T1rho F filter.
  July 2000.

  xpol = 'y'   cross polarization preparation
  xpol = 'n'   direct polarization preparation

  phase = 0    absolute value cosy
  phase = 1,2  hypercomplex (STATES) pure phase - use wft2da
  phase = 3    TPPI - use wft2d(1,0,0,0)

  pw (xpol = 'y') = proton 90 degree pulse
  pw (xpol = 'n') = x-nucleus 90 degree pulse

*/;

#include <standard.h>

static int tableA[2] ={1,3};
static int tableB[16]={3,3,3,3,3,3,3,3,0,0,0,0,0,0,0,0};
static int tableC[16]={0,2,0,2,0,2,0,2,1,3,1,3,1,3,1,3};
static int tableD[32]={0,0,0,0,0,0,0,0,1,1,1,1,1,1,1,1,
                       2,2,2,2,2,2,2,2,3,3,3,3,3,3,3,3};
static int tableE[32]={0,3,0,3,0,3,0,3,2,3,2,3,2,3,2,
                       1,0,1,0,1,0,1,0,2,1,2,1,2,1,2,1};
static int tableF[16] ={0,0,1,1,2,2,3,3,1,1,2,2,3,3,0,0};
static int tableG[32]={2,0,3,1,0,2,1,3,3,1,0,2,1,3,2,0,
                       0,2,1,3,2,0,3,1,1,3,2,0,3,1,0,2};
static int tableH[16]={1,3,1,3,1,3,1,3,0,2,0,2,0,2,0,2};

/*definition of recoupling sequence*/

xy8(cycles, srate, p180) double cycles, srate, p180;
{
  initval(cycles,v8);
  if (cycles >= 1)
  {
    if (cycles > 1) loop(v8,v9);
      delay((1/(2.0*srate)) - p180/2);
      rgpulse(p180,zero,0.0,0.0);
      delay((1/(srate)) - p180);
      rgpulse(p180,one,0.0,0.0);
      delay((1/(srate)) - p180);
      rgpulse(p180,zero,0.0,0.0);
      delay((1/(srate)) - p180);
      rgpulse(p180,one,0.0,0.0);
```

```
        delay((1/(srate)) - p180);
        rgpulse(p180,one,0.0,0.0);
        delay((1/(srate)) - p180);
        rgpulse(p180,zero,0.0,0.0);
        delay((1/(srate)) - p180);
        rgpulse(p180,one,0.0,0.0);
        delay((1/(srate)) - p180);
        rgpulse(p180,zero,0.0,0.0);
        delay((1/(2.0*srate)) - p180/2);
      if (cycles > 1) endloop(v9);
    }
}

pulsesequence()
{

/*declare variables*/

   double    arraydim,
             ni,
             cntct,
             crossp,
             dipolr,
             mix,
             srate,
             timeon,
             dutycycle,
             at,
             sw1,
             pwx,
             p180,
             pcrho,
             periods,
             cycles,
             lvlshft;
   int       iphase,
             tix;
   char      xpol[MAXSTR],
             rfdr[MAXSTR],
             sync[MAXSTR];


/*assign variables*/

   arraydim = getval("arraydim");
   ni = getval("ni");
   cntct = getval("cntct");
   pcrho = getval("pcrho");
   crossp = getval("crossp");
   dipolr = getval("dipolr");
   mix = getval("mix");
   srate = getval("srate");
   at = getval("at");
   sw1 = getval("sw1");
   pwx = getval("pwx");
   p180 =getval("p180");
```

```
  iphase =  (int) (getval("phase") + 0.5);
  getstr("xpol", xpol);
  getstr("sync",sync);
  getstr("rfdr",rfdr);


  lvlshft = 4.6e-6;

  tix = (int) ((ix - 1) / (arraydim / ni) + 1e-6);

/*set phase tables*/

  if (xpol[0] == 'y')          /*tables for 1Hpw90 and cntct for CP*/
  {
    settable(t1,2,tableA);
    settable(t2,16,tableB);
  }
  else
  {
    settable(t2,16,tableC);    /*alt PULSE1 table for DP*/
    settable(t6,16,tableH);    /*spinlock*/
  }

  if ((iphase == 1) || (iphase == 2) || (iphase == 3))
  {
    settable(t3,32,tableD);    /*PULSE2 table for STATES transform and TPPI*/
  }
  else
  {
    settable(t3,32,tableE);    /*alt PULSE2 table for absvalue*/
  }
  settable(t4,16,tableF);      /*PULSE3 table*/
  settable(t5,32,tableG);      /*receiver phase table*/
  setreceiver(t5);

/*increment t2 table for sine phases of STATES transform*/

  if (iphase == 2)
  {
    tsadd(t2,1,4);
    tsadd(t6,1,4);
  }

/*step table t2 through 4 phases for TPPI*/

  if (iphase == 3)
  {
    tsadd(t2,tix,4);
    tsadd(t6,tix,4);
  }

/*calculate the number of periods during mix*/

  if (sync[0] == 'y')
  {
    periods = (double) ((int)( (mix*srate) + 0.5));
```

```
    if (rfdr[0] == 'y')
    {
      cycles = (double) ((int)(((mix*srate)/8.0) + 0.5));
      periods = cycles*8.0;
    }

    fprintf(stdout,"Will wait %4.0f periods.\nCorrected mix time is %f\n", periods, periods/srate);
  }

/*check the decoupler duty cycle and print messages*/

  if (ix == 1)
  {
    timeon = (pw + (ni/sw1) + 2*pwx + at + 30*pcrho);
    if (xpol[0] == 'y') timeon = timeon + cntct;
    if (sync[0] == 'y')
    {
      timeon = timeon + (periods/srate);
    }
    else
    {
     timeon = timeon + mix;
    }

    dutycycle = (100.0*timeon)/(d1 + timeon);

    if ((dutycycle > 20.0) || dm[0] == 'y')
    {
      fprintf(stdout, "maximum duty cycle is greater than 20%% - abort!\n");
      abort(1);
    }
    else
    {
      fprintf(stdout, "duty cycle is %5.2f%%. Doing ",  dutycycle);
    }

    if (xpol[0] == 'y')
    {
      fprintf(stdout, "cross polarization. \n");
    }
    else
    {
      fprintf(stdout, "direct polarization. \n");
    }
  }

/*begin experiment*/

  if (xpol[0] == 'y')  /*cross polarization*/
  {
    status(A);
    decpwrf(crossp);
    delay(d1);
    delay(rof1);
    spl on();
    decpulse(pw,t1);
```

```
    status(C);
    decphase(zero);
    rgpulse((cntct - lvlshft),t2,0.0,0.0);
    sp1off();
    decpwrf(dipolr);

  }
  else          /*direct polarization*/
  {
    status(A);
    decpwrf(dipolr);
    delay(d1);
    setreceiver(t5);
    sp1on();
    delay(rof1);
    decphase(zero);
    rgpulse(pw,t2,0.0,0.0);
    rgpulse(30.0*pcrho,t6,0.0,0.0);
    sp1off();
    status(B);
  }
  delay(d2);
  sp1on();
  rgpulse(pwx,t3,0.0,0.0);

/*begin mixing period*/

  status(B);
  if (sync[0] == 'y')
  {
    if (rfdr[0] == 'y')
    {
      xy8(cycles, srate, p180);
    }
    else
    {
      initval(periods,v5);
      rotorsync(v5);
    }
  }
  else
  {
    delay(mix);
  }
  status(C);
  rgpulse(pwx,t4,0.0,lvlshft);
  sp1off();

/*acquire data*/

  delay(rof2);

}
```

$T_{1\rho}$ filter with a mixing delay for Goldman-Shen

```
/* Frhofilter - with "spare line" for F{H}
  and including a mixing delay
  UNITY plus version  May 2000*/

/* xpol = 'y' gives cross polarization (cp)
       'n' gives direct polarization (dp)

  pw -    the proton 90 degree pulse (cp)
         the observe 90 degree pulse (dp)
  p1 -    flip-back pulse
  p180 -  preceeding proton pulse (cp)
         preceeding observe pulse (dp)
  cntct - hartmann-hahn contact time
  pcrho - observe spin lock time for T1rho measurement !!!x30!!!

  crossp  - controls fine decoupler power during cross polarization,
  dipolr  - controls fine decoupler power during acquisition time.

 */

#include <standard.h>

static int table1[4] = {0, 1, 2, 3};
static int table2[4] = {1, 1, 3, 3};
static int table3[4] = {3, 0, 3, 0};
static int table4[4] = {1, 2, 1, 2};
static int table5[4] = {0, 1, 0, 1};
static int table6[4] = {2, 3, 0, 1};
static int table7[4] = {0, 1, 0 ,1};

pulsesequence()

{

/* declare new variables */

  double       dutycycle,
               cntct,
               pcrho,
               splock,
               tpwrm,
                     p180,
               pwx,
               at,
               srate,
               crossp,
               dipolr,
               mix,
               lvlshft;
  char          pdp[MAXSTR],
               mixflag[MAXSTR],
```

```
            xpol[MAXSTR];
  extern double  getval();

/* set variables */

  cntct = getval("cntct");
  mix = getval("mix");
  p180 = getval("p180");
  pwx = getval("pwx");
  pcrho = getval("pcrho");
  at = getval("at");
  crossp  = getval("crossp");
  dipolr  = getval("dipolr");
  tpwrm = getval("tpwrm");
  splock = getval("splock");
  srate = getval("srate");
  getstr("pdp", pdp);
  getstr("xpol", xpol);
  getstr("mixflag",mixflag);

  lvlshft = 4.6e-6;
  if (splock == 0)
  {
    splock = tpwrm;
  }

 /*check dutycycle -
    do not accept dm=y or decoupler duty cycles in excess of 20% */

  dutycycle = (d1 + d2) / (p180 + cntct + pcrho + pw + p1 + d1 + d2 + at);
  if (dm[2] == 'n') dutycycle += at / (p180 + cntct + pcrho + pw + p1 + d1 + d2 + at);

  fprintf(stdout, "Duty cycle is %5.2f%%. Doing ", (1.0 - dutycycle) * 100);

  if ((dutycycle < 0.8) || (dm[0] == 'y'))
  {
    fprintf(stdout, "ABORT! The duty cycle must be less than 20%%.\nPlease adjust d1, at or set dm =
'nny'!\n");
    abort(1);
  }

/*begin pulse sequence*/


  if (xpol[0] == 'n')       /*direct polarization (dp)*/
  {
    fprintf(stdout, "Bloch decay");

    settable(t1,4,table1);
    settable(t3,4,table3);
    settable(t4,4,table4);
    settable(t5,4,table5);
    setreceiver(t1);

    status(A);
    decpwrf(dipolr);
```

```
  delay(d1);
  delay(rof1);
  if(p180>0)            /*optional inversion prepulse*/
        {
         sp1on();
         rgpulse(p180, zero, 0.0, 0.0);
         sp1off();
         delay(d2);
        }

  sp1on();
  rgpulse(pw, t1, 0.0 ,lvlshft);

  if (pcrho>0.0)        /*optional spinlock for T1rho*/
  {
    status(A);
    obspwrf(splock);
    sp1on();
        rgpulse(30.0*pcrho, t4, 0.0, 0.0);
        sp1off();
  }
  if (mixflag[0] == 'y')
  {
    status(A);
    sp1on();
    rgpulse(pwx,t5,0.0,0.0);
    delay(mix);
    rgpulse(pwx,t4,0.0,0.0);
    sp1off();
  }

  status(C);
  decpwrf(dipolr);
  sp1off();
}

else
{                               /* cross-polarization (cp)*/

  fprintf(stdout, "Cross polarization");

  settable(t1,4,table1);
  settable(t2,4,table2);
  settable(t3,4,table3);
  settable(t4,4,table4);
  settable(t6,4,table6);
  settable(t7,4,table7);
  setreceiver(t1);

  status(A);
  decpwrf(crossp);
  delay(d1);
  delay(rof1);

  if(p180>0.0)          /*optional proton inversion prepulse*/
  {
```

```
      decpulse(p180, zero);
      delay(d2);
    }
    decrgpulse(pw, t2,rof1,0.0);
    status(C);
    decphase(zero);
    sp1on();
    rgpulse(cntct, t3, 0.0, 0.0);
    sp1off();

    if (pcrho>0.0)          /*optional spinlock for T1rho*/
    {
      status(A);
      sp1on();
          rgpulse(30.0*pcrho, t3, 0.0, 0.0);
          sp1off();
    }
    if (mixflag[0] == 'y')
    {
      status(A);
      sp1on();
      rgpulse(pwx,t7,0.0,0.0);
      delay(mix);
      rgpulse(pwx,t4,0.0,0.0);
      sp1off();
    }
    status(C);
    decpwrf(dipolr);
  }


/*optional interrupted decoupling for protonated carbon dephasing*/

  if (pdp[0] == 'y')
  {
    fprintf(stdout, '', Protonated carbon suppression");
    status(A);
    delay(d2);
    status(C);
    delay(4.0 / srate - pw - d2 - lvlshft);
    sp1on();
    rgpulse(2.0 * pw, t3, 0.0, 0.0);
    sp1off();
    delay(4.0 / srate - pw);
  }

/*begin acquisition*/
  delay(rof2);
  acquire(np,1.0/sw);

}
```

Direct polarisation pulse sequence with optional crosspolarisation

```
/* FH modified xpolar - with "spare line" for F{H}
  UNITY plus version  March 1999 */

/* xpol = 'y' gives cross polarization (cp)
        'n' gives direct polarization (dp)

  pw -    the proton 90 degree pulse (cp)
          the observe 90 degree pulse (dp)
  p1 -    flip-back pulse
  p180 -  preceeding proton pulse (cp)
          preceeding observe pulse (dp)
  cntct - hartmann-hahn contact time
  pcrho - observe spin lock time for T1rho measurement

  toss= 'y'  invokes timed spin-echoes to suppress spinning sidebands
  srate - spin rate (necessary for toss)
  dm - should be set to nny

  h90lvl - controls fine decoupler power for the H 90(s)
  crossp  - controls fine decoupler power during cross polarization,
  dipolr  - controls fine decoupler power during acquisition time.

  modified for pdp/toss order and flip-back January 95
  pwx added July 98 final TOSS delay modified September 98
  modified for status(D) decoupling and independent CP April 2002
 */

#include <standard.h>

static int table1[4] = {0, 1, 2, 3};
static int table2[4] = {1, 1, 3, 3};
static int table3[4] = {3, 0, 3, 0};
static int table4[4] = {1, 2, 1, 2};
static int table5[4] = {3, 3, 1, 1};
static int table6[4] = {2, 3, 0, 1};

pulsesequence()

{

/* declare new variables */

  double       dutycycle,
               cntct,
               pcrho,
                     p180,
               pwx,
               at,
               srate,
               cppwr,
               h90lvl,
```

```
            crossp,
            dipolr,
            lvlshft;
  char        pdp[MAXSTR],
            toss[MAXSTR],
            xpol[MAXSTR],
            dblvl2[MAXSTR];
  extern double  getval();

/* set variables */

  cntct = getval("cntct");
  p180 = getval("p180");
  pwx = getval("pwx");
  pcrho = getval("pcrho");
  at = getval("at");
  cppwr = getval("cppwr");
  h90lvl = getval("h90lvl");
  crossp  = getval("crossp");
  dipolr  = getval("dipolr");
  srate = getval("srate");
  getstr("pdp", pdp);
  getstr("toss", toss);
  getstr("xpol", xpol);
  getstr("dblvl2",dblvl2);

  lvlshft = 4.6e-6;
  if (dblvl2[0] == 'y')
  {
    lvlshft = lvlshft + 2.3e-6;
  }

 /*check dutycycle -
    do not accept dm=y or decoupler duty cycles in excess of 20% */

  dutycycle = (d1 + d2) / (p180 + cntct + pcrho + pw + p1 + d1 + d2 + at);
  if (dm[2] == 'n') dutycycle += at / (p180 + cntct + pcrho + pw + p1 + d1 + d2 + at);

  fprintf(stdout, "Duty cycle is %5.2f%%. Doing ", (1.0 - dutycycle) * 100);

  if ((dutycycle < 0.8) || (dm[0] == 'y'))
  {
    fprintf(stdout, "ABORT! The duty cycle must be less than 20%%.\nPlease adjust d1, at or set dm =
'nny'!\n");
    abort(1);
  }

/* check that a spin rate has been entered where its important */

  if (((toss[0] == 'y') || (pdp[0] == 'y')) && (srate < 50.0))
  {
    fprintf(stdout, "spin rate is too low for toss or dipolar dephasing!\n");
    abort(1);
  }

/*begin pulse sequence*/
```

```
if (xpol[0] == 'n')        /*direct polarization (dp)*/
{
  fprintf(stdout, "Bloch decay");

  settable(t1,4,table1);
  settable(t3,4,table3);
  settable(t4,4,table4);
  settable(t5,4,table5);
  setreceiver(t1);

  status(A);
  decpwrf(dipolr);
  delay(d1);
  delay(rof1);
  if(p180>0)            /*optional inversion prepulse*/
        {
         sp1on();
         rgpulse(p180, zero, 0.0, 0.0);
         sp1off();
         delay(d2);
        }
  status(C);
  sp1on();
  rgpulse(pw, t1, 0.0 ,lvlshft);
  sp1off();
}

else
{                                /* cross-polarization (cp)*/

  fprintf(stdout, "Cross polarization");

  settable(t1,4,table1);
  settable(t2,4,table2);
  settable(t3,4,table3);
  settable(t4,4,table4);
  settable(t5,4,table5);
  settable(t6,4,table6);
  setreceiver(t1);

  status(A);
  decpwrf(h90lvl);
  delay(d1);
  delay(rof1);

  if(p180>0.0)          /*optional proton inversion prepulse*/
  {
    decpulse(p180, zero);
    delay(d2);
  }
  decrgpulse(pw, t2,rof1,0.0);
  decpwrf(crossp);
  status(C);
  decphase(zero);
```

```
    sp1on();
    rgpulse(cntct, t3, 0.0, 0.0);
    sp1off();

    if (pwx>0.0)          /*optional x pulse*/
    {
      sp1on();
      rgpulse(pwx, t6, 0.0, 0.0);
      sp1off();
    }

    if (pcrho>0.0)        /*optional 13C spinlock for 13C T1rho*/
    {
      status(A);
      sp1on();
          rgpulse(pcrho, t3, 0.0, 0.0);
          sp1off();
    }

    decpwrf(dipolr);
    status(D);
  }


/*optional interrupted decoupling for protonated carbon dephasing*/

  if (pdp[0] == 'y')
  {
    fprintf(stdout, ", Protonated carbon suppression");
    status(B);
    delay(d2);
    status(C);
    delay(4.0 / srate - pw - d2);
    sp1on();
    rgpulse(2.0 * pw, t3, 0.0, 0.0);
    sp1off();
    delay(4.0 / srate - pw - alfa - rof2);
  }
/*optional pi pulses for suppression of sidebands - TOSS*/

  if (toss[0] == 'y')
  {
    fprintf(stdout, ", TOSS");
    delay((0.1226 / srate) - pw - lvlshft);
    sp1on();
    rgpulse(2.0 * pw, t3, 0.0, 0.0);
    sp1off();
    delay((0.0773 / srate) - 2.0 * pw);
    sp1on();
    rgpulse(2.0 * pw, t4, 0.0, 0.0);
    sp1off();
    delay((0.2236 / srate) - 2.0 * pw);
    sp1on();
    rgpulse(2.0 * pw, t3, 0.0, 0.0);
    sp1off();
    delay((1.0433 / srate) - 2.0 * pw);
```

```
    sp1on();
    rgpulse(2.0 * pw, t4, 0.0, 0.0);
    sp1off();
    delay((0.7744 / srate) - pw - alfa - rof2);
  }

 fprintf(stdout, ".\n");

/*begin acquisition*/
  delay(rof2);
  delay(alfa);
  acquire(np,1.0/sw);

/*flip-back pulse*/
  decpwrf(h90lvl);
  if (p1>0.0)
  {
    decrgpulse(pw,t5,rof1,rof2);
  }

}
```

APPENDIX (iii)

Courses, conferences and presentations

Ph.D. courses at the University of Durham.

Solid state NMR of condensed matter.

Given by R.K Harris

Solid-state NMR spectroscopy for structural characterisation.

Given by P.Hodgekinson

Publications.

Fluorine-19 solid-state NMR Investigation of Regiodefective Semicrystalline poly(vinylidenefluoride). P. Wormald, D.C. Apperley, F. Beaume and R.K. Harris. Polymer 44, 643-651, 2003.

Selective NMR Pulse Sequences and the Study of Solid Fluoropolymers.
S. Ando, R. k. Harris, P. Hazendonk and P. Wormald. Macromolecul. Rapid. Com. (in press)

Improved Proton Decoupling in NMR Spectroscopy of Crystalline Solids Using The Spinal-64 Sequence. T. Bräuinger, P. Wormald, P. Hodgkinson
Current Developments in solid state NMR Spectroscopy.
Vol VIII, Ed. N. Mueller and P.K. Madhu, Springer-Verlag, Wien, 2003. IBNS 3-211-83894-5.

CONFERENCES

2003 ISMAR and Groupement Ampere. The Alpine Conference on solid state Nuclear Magnetic Resonance. "New concepts and applications"
14-18 September 2003 Chamonix-Mont Blanc France

The 5th Colloque Francophone sur la Chimie du Fluor
May 5-8th 2002 Gaillon, Normandy France.
Presentation: Application of Relaxation filters in Fluorine-19-solid state NMR. A Study of Semicrystalline Fluoropolymers.

43rd ENC (Experimental Nuclear Magnetic Resonance Conference),
April 14 – 19, 2002, The Asilomar Conference Centre, San Francisco, California, USA.

Ismar 14th conference of the International Society of Magnetic Resonance.
August 19-23 2001 Rhodes, Greece.
Poster Presentation: Nuclear Magnetic relaxation and thermal transitions of Semicrystalline α Poly(vinylidenefluoride).

RSC 2001 15th RSC International meeting on NMR Spectroscopy.
8-12 July 2001 University of Durham UK.
Poster presentation: Fluorine-19 solid state NMR Investigation of Regiodefective Semicrystalline α Poly(vinylidenefluoride).

1999 ISMAR and Groupement Ampere. The Alpine Conference on solid state Nuclear Magnetic Resonance. "New concepts and applications"
12-16 September 1999Chamonix-Mont Blanc France

COLLABORATORS.
^{19}F spectroscopy of polymers.
Dr Bruno Ameduri. Laboratory of Macromolecular Chemistry, Ecole Nat. Sup. Chimie de Montpellier
8 rue Ecole Normale. F-34296 Montpellier, France.

Dr Francois Beaume
ATOFINA/Cerdato27470, Serquigny, France

APPENDIX (IV) **GENERAL LITERATURE LIST**

Literature list for PVDF and related subjects

1. NUCLEAR MAGNETICAL RESONANCE IN SOME FLUORINE DERIVATIVES OF POLYETHYLENE
W.P SLICTHER
JOURNAL OF POLY SCI (24) 173-188 (1957).

2. NUCLEAR MAGNETICAL RESONANCE AND XRAY DETERMINATION OF THE STRUCTURE OF POLY(VINYLIDENE FLUORIDE)
J.B LANDO, H.G OLF AND A.PETERLIN
JOURNAL OF POLY SCI, PART A (4) 941- 951 (1966)

3. NUCLEAR MAGNETICAL RESONANCE OF POLYMER FIBERS
V.J MCBRIERTY, D.W.MCCALL, D.C DOUGLASS AND D.R FALCONE
THE JOURNAL OF CHEM PHYS (52) 2 512-520 (1970).

4 DIELECTRIC RELAXATION AND MOLECULAR MOTIONS IN POLY(VINYLIDENE FLUORIDE).
SHINICHI Y.
JOURNAL OF POLY SCI PART A -2 (8) 1057- 1072 (1970).

4. ANOMALOUS INTENSITY BEHAVIOR IN RELAXATION DATA
D.C DOUGLASS AND V.J MCBRIERTY
THE JOURNAL OF CHEM PHYS (54) 9 4085-4089 (1971)

5. POLYMORPHISM OF POLY(VINYLIDENE FLUORIDE): POTENTIAL ENERGY CALCULATIONS OF THE EFFECTS OF HEAD-TO-HEAD UNITS ON THE CHAIN CONFORMATION AND PACKING OF POLY(VINYLIDENE FLUORIDE).
B.L FARMER, A.J HOPFINGER AND J.B LANDO.
JOURNAL OF APPL PHYS. (43) 11 4293-4303 (1972).

6. CRYSTAL STRUCTURES OF THREE CRYSTALLINE FORMS OF POLY(VINYLIDENE FLUORIDE).
R HASAGAWA, Y TAKASHI, Y CHATANI, H TADOKORO.
POLYMER JOURNAL, VOL 3, NO 5 600-610, 1972

7. DIELECTRIC RELAXATION AND MOLECULAR MOTIONS IN POLY(VINYLIDENE FLUORIDE) WITH CRYSTALL FORM II.
NAKAGAWA. K. AND ISHIDA. Y.
JOURNAL OF POLYMER SCIENCE. (11). 1503-1533. (1973).

8. DIELECTRIC BEHAVIOR OF POLY(VINYLIDENE FLUORIDE) IN THE MELT AND IN THE SOLUTION-GROWN CRYSTAL MAT.
OSAKI S. AND ISHIDA H.
JOURNAL OF POLYMER SCIENCE. (12). 1727-1731. (1973).

9. NUCLEAR MAGNETICAL RESONANCE AND MOLECULAR MOTION IN POLY(VINYLIDENE FLUORIDE).
V.J MCBRIERTY, D.C DOUGLASS AND T.A WEBER.
JOURNAL OF POLY SCI (14) 1271-1286 (1976).

10. MULTIPLE PULSE NUCLEAR MAGNETICAL RESONANCE OF SOLID POLYMERS: DYNAMICS OF POLY(TETRAFLUOROETHYLENE).
A.D ENGLISH AND A.J.VEGA
MACROMOLECULES (12) 2 333-334 (1979).

11. MULTIPLE PULSE NUCLEAR MAGNETICAL RESONANCE OF SOLID POLYMERS: DYNAMICS OF POLY(TETRAFLUOROETHYLENE).
A.D ENGLISH AND A.J.VEGA
ACS SYMP (142) 169 (1980).

12. DETERMINATION OF POLYMER CRYSTALLINITY FROM PROTON SOLID-ECHO NMR MEASUREMENTS.
KLAUS BERGMAN
POLY BULL (5) 355-360 (1981)

13. FERROELECTRIC POLYMERS.
A.J LOVINGER
SCIENCE (220) 4602 1115-1121 (1983)

14. DSC STUDIES ON THE TRANSITIONS IN POLY(VINYLIDENE FLUORIDE) AND SOME RELATED COPOLYMERS.
C. LEONARD, J.L. HALARY, L. MONNERIE AND F. MICHERON
POLYMER BULLETIN 11, 195-202 (1984).

15. THE ROLE OF MOLECULAR DEFECTS ON THE STRUCTURE AND PHASE TRANSITION OF POLY(VINYLIDENE FLUORIDE).
A.J LOVINGER, D.D DAVIS, R.E. CAIS AND J.M. KOMETANI
POLYMER (28) 617-626 (1987) APRIL CONFERENCE ISSUE

16. THERMAL ANALYSIS OF THE CONFORMATIONAL DISORDER IN SEMICRYSTALLINE AND POLY(TRIFLUOROETHYLENE).
K. LOUFAKIS AND B. WUNDERLICH.
MACROMOLECULES. (20) 2474-2478 (1987)

17. SOLID STATE NMR INVESTIGATIONS OF PVDF FILMS WITH APPLIED POLING FIELDS.
D. GESCHKE, P. HOLSTIEN AND M. MENDLER
ACTA POLYMERICA (38) 206-207 (1988)

18. MOLECULAR MOTION IN FORM II POLY(VINYLIDENE FLUORIDE).
Y.NABATA.
JAPANISE JOURNAL OF APPLIED PHYSICS (29) 12 2782-2788. 1990.

19. THE SURFACE STRUCTURE AND MORPHOLOGY OF POLY(VINYLIDENE FLUORIDE) MICROFILTRATION MEMBRANS BY ATOMIC FORCE MICROSCOPY.
A.K. FRITZSCHE, A.R. AREVALO, M.D. MOORE, V.B. ELINGS, K. KJOLLER AND C.M. WU.
JOURNAL OF MEMBRANE SCIENCE, (68) 65-79 (1991).

20. INFLUENCE OF THE CRYSTALLINE PHASE ON THE MOLECULAR MOBILITY OF PVDF.
TEYSSEDRE G. BERNES A. LACABANNE C.
JOURNAL OF POLYMER SCIENCE PART B (31) ISS 13 2027-2034 (1993).

21. COOPERATIVE RELAXATIONS/TRANSITIONS IN FERROELECTRIC POLYMERS.
G. TEYSSÈDRE. A. BERNÈS AND C. LACABANNE.
JOURNAL OF THERMAL ANALYSIS (40) 711-719 (1993).

22. POLY(VINYLIDENE FLUORIDE)/CELLULOSE ACETATE-BUTYRATE BLENDS: CHARECTERIZATION BY DSC, WAXS AND FTIR.
H. VÁZQUES-TORRES AND C.A CRUZ-RAMOS.
POLYMER BULLETIN (33) 673-680 (1994).

23. EFFECTS OF CRYSTALLIZATION TEMPERATURE ON THE CRYSTALLINE PHASE CONTENT AND MORPHOLOGY OF POLY(VINYLIDENE FLUORIDE).
R. GREGORIO AND MARCELO CESTARI.
JOURNAL OF POLY SCI, PART B , POLYMER PHYSICS. (32) 859-870 (1994).

24. AN NMR STUDY OF POLY(VINYLIDENE FLUORIDE) STRUCTURE BY ^{1}H, ^{13}C AND ^{19}F TRIPLE RESONANCE METHOD.
E. KATOH, K. OGURA AND I. ANDO.
POLYMER JOURNAL, (26) 12, 1352-1359 (1994).

25. DYNAMIC ANALYSIS OF THE MELTING BEHVIOR OF POLYMERS SHOWING POLYMORPHISM OBSERVED BY SIMULTANEOUS DSC/X-RAY
DIFFRACTION MEASUREMENTS.
H. YOSHIDA
THERMOCHOMICA ACTA (267) 239-248 (1995)

26. LARGE-AMPLITUDE MOTION IN POLYMER CRYSTALLS AND MESOPHASES.
WUNDERLICH. B.
MACROMOL.SYMP. (98). 1069-1084. (1995).

27. SYNTHESIS OF FLUORINATED TELOMERS, PART 4. TELOMERIZATION OF VINYLIDENE FLUORIDE WITH COMMERCIALLY AVAILABLE α,ω DIIODOPERFLUOROALKANES.
A. MANSÉRI, B. AMEDURI, B. BOUTEVIN, R.D CHAMBERS, G. CAPORICCIO AND A. P WRIGHT.
JOURNAL OF FLUORINE CHEMISTRY 74 59-67 (1995).

28. SYNTHESIS OF FLUORINATED TELOMERS, PART 1. TELOMERIZATION OF VINYLIDENE FLUORIDE WITH PERFLUOROALKYLIODIDES.
J. BALAGUE, B. AMEDURI, B. BOUTEVIN AND G. CAPORICCIO.
JOURNAL OF FLUORINE CHEMISTRY 74 59-67 (1995).

29. DIELECTRIC PROPERTIES OF POLY(VINYLIDENE FLUORIDE) FROM MOLECULAR DYNAMICS SIMULATIONS.
N. KARASAWA AND W. A. GODDARD.
MACROMOLECULS (28) 6765-6772, (1995).

30. FLUORINE-19 MAGIC ANGLE SPINNING NMR.
J.M. MILLER.

PROGRESS IN NUCLEAR MAGNETIC RESONANCE SPECTROSCOPY. (28) 255-281 (1996)

31. A METHOD FOR STUDYING CONFORMATIONAL RELAXATION BY MOLECULAR SIMULATION: CONFORMATIONAL DEFECTS IN α- PHASE
POLY(VINYLIDENE FLUORIDE).
J.D CARBECK AND G.C RUTLEDGE.
MACROMOLECULES (29), 5190-5199,(1996)

32. ANALYSIS OF THE EXPERIMENTAL DISTRIBUTION OF RELAXATION TIMES AROUND THE LIQUID-GLASS TRANSITION OF POLY(VINYLIDENE FLUORIDE).
G. TEYSSÈDRE. P. DEMONT AND C. LACABANNE.
JOURNAL OF APPLIED PHYSICS (79), 12, 9258-9267, (1996)

33. FTIR-MICROSCOPY AND DSC STUDIES OF POLY(VINYLIDENE FLUORIDE).
E. BENEDETTI, S. CATANORCHI, A. D' ALESSIO, G. MOGGI, P. VERGAMINI, M. PRACELLA AND F. CIARDELLI.
POLYMER INTERNATIONAL. (41) 35-41 (1996).

34. PROTON-FLUORINE WIDELINE SEPARATION EXPERIMENTS ON POLY(VINYLIDENE FLUORIDE).
U. SCHELER, R.K. HARRIS.
SOLID STATE NUCLEAR MAGNETIC RESONANCE (7) 11-16 (1996).

35. FLUORINE-19 NMR OF SOLIDS WITH BOTH HOMONUCLEAR MULTIPULSE DECOUPLING AND PULSED PROTON DECOUPLING.
U. SCHELER, R.K. HARRIS.
CHEM, PHYS, LETT. (262) 137-141 (1996).

36. PYRO-PIEZOELECTRIC POLYMER MATERIALS - II.
SPHERULITIC GROWTH OF PVDF IN THE PRESENCE OF PMMA AND/OR PVA.
A. LINARES AND J.L. ACOSTA.
EUR. POLYM. J, (32) 9 1127-1130 (1996).

37. REORIENTATIONAL DYNAMICS OF DIPOLES IN POLY(VINYLIDENE FLUORIDE) /POLY(METHYL METHACRYLATE) (PVDF/PMMA) BLENDS BY DIELECTRIC SPECTROSCOPY.
J. MIJOVIC, J-W. SY AND T.K KWEI.
MACROMOLECULES (30) 3042-3050 (1997).

38. STRUCTURAL CORRELATION STUDY OF PULSED PLASMA-POLYMERIZED SOLIDS BY TWO-DIMENSIONAL WIDE LINE SEPARATION SPECTROSCOPY.
K. K. S. LAU AND K. K. GLEASON.
J.PHYS. CHEM. B. (101) 6839-6846 (1997)

39. D.M.A. AND D.S.C. INVESTIGATIONS OF THE β TRANSITION OF POLY(VINYLIDENE FLUORIDE).
ZHEHUI LIU, PHILIPPE MARÉCHAL AND ROBERT JÉRÔME.
POLYMER. (38) 4925-4929 (1997).

40. SOLID-STATE ^{19}F NMR INVESTIGATION OF POLY(VINYLIDENE FLUORIDE) WITH HIGH-POWER PROTON DECOUPLING.
P. HOLSTEIN, R. K. HARRIS AND B. SAY.
SOLID STATE NUCLEAR MAGNETIC RESONANCE (8) 201-206 (1997).

41. STUDYING THE MICROSTRUCTURE OF UNAGED AND AGED PVDF BY SMALL-AND WIDE-ANGLE X-RAY SCATTERING.
N. STRIBECK AND S. BUCHNER
JOURNAL OF APPLIED CRYSTALLOGRAPHY (30) 722-726 (1997).

42. TRIPLE-CHANNEL SOLID-STATE NMR INVESTIGATION OF POLY(VINYLIDENE FLUORIDE) POLYMORPHS.
P. HOLSTEIN, U. SCHELER AND R. K. HARRIS.
MAGNETIC RESONANCE IN CHEMISTRY. (35) 647-649 (1997)

43. HIGH-RESOLUTION VARIABLE-TEMPERATURE ^{19}F MAS NMR SPECTROSCOPY OF VINYLIDENE FLUORIDE BASED FLUOROPOLYMERS
P.K. ISBESTER, J.L. BRANDT, T.A. KESTNER AND E.J. MUNSON
MACROMOLECULES. (31) 8192-8200 (1998)

44. FLUOROPOLYMERS
R.K. HARRIS. G.A. MONTI AND P. HOLSTEIN.
SOLID STATE NMR OF POLYMERS, STUDIES IN PHYSICAL AND THEORETICAL CHEMISTRY: (84) CHAPTER18 667-712, (1998)

45. ATOMIC FORCE MICROSCOPY ON TREE-LIKE CRYSTALS IN POLYVINYLIDENE FLUORIDE BLENDS.
K.CRÄMER. M. FOGLIATO SANTOS LIMA. S. N. MAGONOV
JOURNAL OF MATERIAL SCIENCE (33) 2305-2312 (1998).

46. TELOMERIZATION OF POLY(VINYLIDENE FLUORIDE) WITH METHANOL. ELUCIDATION OF THE REACTION PROCESS AND MECHANISM BY A STRUCTURAL ANALYSIS OF THE TELOMER.
M. DUC, B. AMEDURI, B. BOUTEVIN AND J-M SAGE.
MACROMOL.CHEM.PHYS. (199), 1271-1289 (1998)

47. MOLECULAR ORGANIZATION IN STRUCTURAL PVDF.
D. GLENNON, P.A. COX, R. T. NEVELL, J. R. SMITH. R. J. EWEN, J. TSIBOUKLIS
JOURNAL OF MATERIAL SCIENCE (33) 3511-3517 (1998).

48. ^{19}F NMR
R.K. HARRIS. G.A. MONTI AND P. HOLSTEIN.
SOLID STATE NMR OF POLYMERS, STUDIES IN PHYSICAL AND THEORETICAL CHEMISTRY: (84) CHAPTER 6.6 253-266, (1998)

49. FLUORINE-19 MAS AND $^{1}H \longrightarrow {}^{19}F$ CP/MAS NMR STUDIES OF VITON FLUOROPOLYMERS
G.A.MONTI AND R.K.HARRIS.
MAGNETIC RESONANCE IN CHEMISTRY (36) 892-900 (1998).

50. MISCIBILITY AND SURFACE CRYSTAL MORPHOLOGY OF BLENDS CONTAINING POLY(VINYLIDENE FLUORIDE) BY ATOMIC FORCE MICROSCOPY.
WON-KI LEE AND CHANG-SIK HA.
POLYMER (39) NO 26 7131-7134 (1998).

51. SEMICRYSTALLINITY AND POLYMORPHISM IN PVDF: A SOLID-STATE ^{19}F INVESTIGATION.
P. HOLSTEIN, U. SCHELER AND R.K. HARRIS.
POLYMER (39) NO 20 4937-4941 (1998).

52. THE CRYSTALLINE PHASE OF POLY(VINYLIDENE FLUORIDE)/ POLY(VINYL FLUORIDE) BLEND FILMS.
B.S. KIM, J.Y.LEE AND R.S. PORTER
POLYMER ENGINEERING AND SCIENCE (38) 1359-1365 (1998).

53. THE DIFFERENCE BETWEEN LIQUID CRYSTALS AND CONFORMATIONALLY DISORDERED CRYSTALS.
B. WUNDERLICH AND WEI CHEN.
LIQUID-CRYSTALLINE POLYMER SYSTEMS 233-248 (1996)

54. END GROUPS IN FLUOROPOLYMERS.
M. PIANCA, E. BARCHIESI, G. ESPOSTO AND S. RADICE.
J OF FLUORINE CHEMISTRY. (95) 71-84 (1999)

55. PHASE TRANSITIONS DURING STRETCHING OF POLY(VINYLIDENE FLUORIDE)
P. SAJKIEWICZ, A. WASIAK, Z. GOCLOWSKI.
EUROPEAN POLYMER JOURNAL (35) 423-429 (1999)

56. ANALYSIS OF CROSS-POLARIZATION DYNAMICS BETWEEN ^{1}H AND ^{19}F IN VITON FLUOROELASTOMER USING SOLID-STATE ^{19}F MAGIC ANGLE SPINNING AND $^{1}H \longrightarrow ^{19}F$ CROSS-POLARIZATION MAGIC ANGLE SPINNING NMR.
S. ANDO, R.K. HARRIS, G. A. MONTI AND S. REINSBERG.
MAGNETIC RESONANCE IN CHEMISTRY (37) 709-720 (1999).

57. ANALYSIS OF CROSS-POLARIZATION DYNAMICS BETWEEN TWO ABUNDANT NUCLEI ^{19}F AND ^{1}H, BASED ON SPIN THERMODYNAMICS THEORY.
S. ANDO, R.K. HARRIS AND S. REINSBERG.
JOURNAL OF MAGNETIC RESONANCE (141) 91-103 (1999).

58. STRUCTURE OF STYRENE GRAFTED POLY(VINYLIDENE FLUORIDE) MEMBRANES INVESTIGATED BY SOLID-STATE NMR.
S. HIETALA, S. L. MAUNU,AND F. SUNDHOLM.
MACROMOLECULES.(32) 788-791 (1999).

59. EFFECTS OF CRYSTALLINE PHASE, ORIENTATION AND TEMPERATURE ON THE DIELECTRIC PROPERTIES OF POLY(VINYLIDENE FLUORIDE).
R. GREGORIO, JR.
JOURNAL OF MATERIAL SCIENCE (34) 4489-4500 (1999).

60. A CLASSIFICATION OF MOLECULES. PHASES AND TRANSITIONS AS RECOGNIZED BY THERMAL ANALYSIS.
B. WUNDERLICH.
THERMOCHIMICA ACTA 340-341. (1999). 37-52.

61. CHANGE IN FREE VOLUME OF POLY(VINYLIDENE FLUORIDE).
MURAKAMI H.
RADIATION PHYSICS AND CHEMISTRY. (58) 531-533.(2000)

62. COMFORMATIONAL PROPERTIES IN POLY(VINYLIDENE FLUORIDE).
A QUANTUM CHEMISTRY STUDY OF MODEL COMPOUNDS.
O.G BYUTNER AND G.D.SMITH.
MACROMOLECULES. (32) 8376-8382 (1999).

63. AN EQUILIBRIUM STUDY ON THE DISTRIBUTION OF STRUCTURAL DEFECTS BETWEEN THE LAMELLAR AND AMORPHOUS PORTIONS OF POLY(VINYLIDENE FLUORIDE) AND (VINYLIDENE FLUORIDE-TETRA FLUORO ETHYLENE) COPOLYMER CRYSTALS.
A.K. DIKSHIT AND A.K. NANDI.
J. OF POLYMER SCIENCE. PART B. (38) 297-308. (2000).

64. FLUORINE-19 NMR INVESTIGATION OF POLY(TRIFLUOROETHYLENE)
S. REINSBERG, S. ANDO AND R.K. HARRIS.
POLYMER.(41) 3729-3736 (2000).

65. MORPHOLOGY AND PHASE TRANSITION OF HIGH MELT TEMPERATURE CRYSTALLIZED POLY(VINYLIDENE FLUORIDE).
R. GREGORIO, R.C. CAPITÃO.
JOURNAL OF MATERIALS SCIENCE.(35) 299-306 (2000).

66. SOLID-STATE FAST ANGLE SPINNING ^{19}F NMR STUDIES OF MORPHOLOGY IN POLY(VINYLIDENE FLUORIDE).
TSAO-WEN SUE AND DER-LII M. TZOU.
POLYMER. (41) 7289-7293 (2000)

67. QUANTUM CHEMISTRY BASED FORCE FIELD FOR SIMULATIONS OF POLY(VINYLIDENE FLUORIDE).
O.G BYUTNER AND G.D.SMITH.
MACROMOLECULES. (33) 4264-4270 (2000).

68. MONTE CARLO SIMULATION OF POLARIZATION REVERSAL OF FERROELECTRIC POLYMER POLY(VINYLIDENE FLUORIDE).
T. KODA, K. SHIBASAKI, S. IKEDA
COMPUTATIONAL AND THEORETICAL POLYMER SCIENCE. (10). 335-343. (2000).

69. CORRELATION BETWEEN PYROELECTRIC PROPERTIES AND DIELECTRIC BEHAVIOUR IN FERROELECTRIC POLYMERS.
L IBOS, A BERNES, G TEYSSEDRE, C LACBANNE, S-L WU, AND J-L SCHEINBEIM.
FERROELECTRICS VOL 238, 163-170, 2000.

70. COPOLYMERIZATION OF FLUORINATED MONOMERS: RECENT DEVELOPMENTS AND FUTURE TRENDS.
B. AMEDURI AND B. BOUTEVIN.
JOURNAL OF FLUORINE CHEMISTRY 104 53-62 (2000).

71. CONTROLED STEP-WISE TELOMERIZATION OF POLY(VINYLIDENE FLUORIDE), HEXAFLUOROPROPENE AND TRIFLUOROETHYLENE WITH IODOFLUORINATED TRANSFER AGENTS.
J. BALAGUE, B. AMEDURI, B. BOUTEVIN AND G. CAPORICCIO.
JOURNAL OF FLUORINE CHEMISTRY 102 253-268 (2000).

72. HEATING OF SAMPLES BY FAST MAGIC-ANGLE SPINNING.
J BRUS.
SOLID-STATE NUCLEAR MAGNETIC RESONANCE 16 151-160 2000.

73. QUARTZ CRYSTAL TEMPERATURE SENSOR FOR MAS NMR.
G.SIMON
JOURNAL OF MAGNETIC RESONANCE 128,194-198 1997.

74. HOMONUCLEAR RADIO FREQUENCY-DRIVEN RECOUPLING IN ROTATING SOLIDS
A. E. BENNET,C.M. RIENSTRA, J.M. GRIFFITHS,W. ZHEN,P.T. LANBURY AND R.G.GRIFFIN.
JOURNAL OF CHEMICAL PHYSICS 108, 22 9463 1998.

75. EFFECT OF MOLECULAR WEIGHT AND CHAIN END GROUPS ON CRYSTAL FORMS OF POLY(VINYLIDENE FLUORIDE) OLIGOMERS.
HERMAN,T UNO,A KUBONO,S UMEMOTO,T KIKUTANI AND N OKUI..
POLYMER (38) 167-1683, 1997.

76. ^{19}F SPEDA NMR IN ROTATING SOLIDS
SHANGWU DING, C. A MCDOWELL
CHEMICAL PHYSICS LETTERS 259, 538-544 1996.

77. LONGTIME BEHAVIOUR OF SPIN COHERANCES IN SOLIDS.
SHANGWU DING, C. A MCDOWELL
JOURNAL OF PHYSICS: CONDENSED MATTER 11, L199-L204 1999.

78. CROSS POLARIZATION WITH LONG DELAYED CONTACT IN ROTATING SOLIDS.
SHANGWU DING, C. A MCDOWELL.
CHEMICAL PHYSICS LETTERS 255, 151-155 1996.

79. PROTON SPIN-DIFFUSION IN PVDF : ^{1}H-^{19}F CP/MAS NMR STUDY
P. HOLSTEIN, G.A. MONTI AND R.K. HARRIS.
PHYS. CHEM. CHEM.PHYS. (1), 3549-3555, 1999.

80. FIRST DIRECT MEASURMENT OF THE SPIN DIFFUSION RATE IN A HOMOGENOUS SOLID W, ZHANG AND D.G. CORY
PHYSICAL REVIEW LETTERS. VOL 8. (6). 1324- 1327. 1998.

81. FLUORINE-19 HIGH-SPEED MAS AND SPIN EXCHANGE NMR OF FLUOROPOLYMERS.
U. SCHELER.
BULLETIN OF MAGNETIC RESONANCE. VOL (19). NO 1-4 1999.

82. TEMPERATURE-DEPENDENT SMALL ANGLE X-RAY SCATTERING FROM POLY(VINYLIDENE FLUORIDE.
J.M. SCHULTZ, J.S. LIN, R.W. HENDRICKS,R.R. LAGASSE, AND R.G. KEPLER.
J. APPL. PHYS. 51 (10) 1980.

83. RECENT ADVANCES IN THE NMR OF SOLID POLYMERS.
V. J. MCBRIERTY AND D. C. DOUGLASS
J. POLYM.REV. 16. 295-366 , 1981

84. A METHOD FOR ANALYSING PROTON NMR RELAXATION DATA FROM MOTIONAL HETEROGENEOUS POLYMER SYSTEMS.
M. GEPPI, R. K. HARRIS, A. M KENWRIGHT, B. SAY.
SSNMR , 12, 15-20, 1998.

85. ANALYSIS OF SPIN-DIFFUSION MEASUREMENTS BY ITERATIVE OPTIMIZATION OF NUMERICAL MODELS A. M KENWRIGHT, B. SAY.
SSNMR , 7, 85-93, 1996.

86. INFLUENCE OF THE THERMAL CONDUCTIVITY ON THE CP-DETERMINATION BY DYNAMIC METHODS.
B. SHENKER AND F. STÄGER.
THERMOCHIMICA ACTA, 219-228.1997.

87. DIPOLAR RECOUPLING UNDER MAS CONDITIONS
S. DUSOLD AND A. SEBALD.
ANNUAL REPORTS ON NMR SPECTROSCOPY VOL 41. 185-262 2000.

88. INFLUENCE OF MOLECULAR WEIGHT ON THE CRYSTALLIZATION OF POLY(VINYLIDENE FLUORIDE) .
E. BENEDETTI, A. D' ALESSIO, G. MOGGI, P. VERGAMINI AND M. PIANCA
POLYMER BULLETIN 22 645-651 1989.

89. SYNTHESIS AND MICROSTRUCTURAL CHARECTERIZATION OF LOW-MOL MASS POLY(VINYLIDENE FLUORIDE). M. PIANCA
POLYMER 34.(22) 4777-4781.1993.

90. APPLICATION OF DYNAMIC DSC TO STUDY OF PHASE TRANSITIONS.
I. HATTA. H. ICHIKAWA. M TODOKI
TERMOCHIMICA ACTA 267 83-94 1995.

91. AC CALORIMETRIC ASPECTS OF DDSC.
I. HATTA.
TERMOCHIMICA ACTA. 272 49-52. 1996.

92. HEAT CAPACITY MEASUREMENTS BY DDSC
T. OZAWA. K. KANARI.
TERMOCHIMICA ACTA. 288 39-51. 1996.

93. THE DETERMINATION OF BOND LENGTHS IN SOLIDS USING THE CARR-PURCELL SEQUENCE.
M. ENGELSBERG. C..S. YANNONI
JOURNAL OF MAGNETIC RESONANCE 88 393-400 1990.

94. NEW, COMPENSATED CARR-PURCELL SEQUENCES
T. GULLION, JOURNAL OF MAGNETIC RESONANCE 89 479-484 1990.

95. MEASUREMENT OF LIKE -SPIN DIPOLE COUPLINGS
M. LIZAKT. T.GULLION AND M CONRADI.
JOURNAL OF MAGNETIC RESONANCE 91 254-260 1991.

96. ORIENTATION DEPENDANT 19F DIPOLAR COUPLINGS WITHIN A TRIFLUOROMETHYLGROUP ARE REVEALED BY STATIC MULTIPULSE NMR IN THE SOLID STATE, S. L. GRAGE AND A.S ULRICH.
JOURNAL OF MAGNETIC RESONANCE 146 81-88 2000.

97. STRUCTURAL PARAMETERS FROM 19F DIPOLAR COUPLINGS OBTAINED BY MULTIPULSE SOLID STATE NMR ON STATIC ORIENTED SYSTEMS
S. L. GRAGE AND A.S ULRICH.
JOURNAL OF MAGNETIC RESONANCE 138 98-106 1999.

98. SOLID-STATE 19F CRAMPS, AND19F-13C CP/MAS NMR STUDY OF AN AMORPHOUS PERFLUOROPOLYMER.
S. ANDO, R.K. HARRIS, MACROMOLECULES 34,66-75 2001.

99. DENSITY FUNCTIONAL STUDY OF CHEMICAL SHEILDING TENSORS: A SYSTEMATIC INVESTIGATION WITH RESPECT TP BASIS SETS AND HYBRID FUNCTIONALS, J.C.C. CHAN AND H. ECKERT.
JOURNAL OF MOLECULAR STRUCTURE (THEOCHEM). 535 1-8 2001.

100. FLUORINE SUBSTITUENT EFFECTS (ON BIOACTIVITY)
B.E.SMART, JOURNAL OF FLUORINE CHEMISTRY. 109, 3-11, 2001.

101. INTERMOLECULAR DISTANCE MEASUREMENTS IN SUPRAMOLECULAR SOLIDS: 13C-19F REDORNMR SPECTROSCOPYOF P-TERTBUTYLCALIX[4]ARENE-FLUOROBENZENE.
E.B. BROWER, R. D. M. GOUGEON, J. HIRSCHINGER, K. A. UDACHIN, R. K. HARRIS AND J. A. RIPMEESTER.
PHYS.CHEM.CHEM.PHYS. 1, 4043-4050, 1999.

102. POLYMER ULTRADRAWABILITY: THE ROLE OF α-RELAXATION CHAIN MOBILITY IN CRYSTALLITES.
W-G. HU AND K. SCHMIDT-ROHR.
ACTA POLYM 50,271-285, 1999.

103. FLUORINE-19 SPECTRA AND CHAIN STRUCTURE OF POLYVINYLIDENE FLUORIDE, R. C. FERGUSION AND E. G. BRAME.
J.PHYS. CHEM. 83, 11 1397-1401, 1979.

104. SPIN-SPIN RELAXATION IN LAF_3, M. GOLDMAN AND L. SHEN.
PHYS REV, 144 (1) 321 1966.

105. NUCLEAR DOUBLE RESONANCE IN THE ROTATING FRAME
S. R. HARTMANN AND E. L. HAHN.
PHYS REV, 128, 5, 2042, 1962.

106. NUCLEAR MAGNETICAL RESONANCE STUDIES OF MOLECULAR RELAXATION MECHANISMS IN POLYMERS
D. W. MCCALL, ACC. CHEM. RES. 4, 223, 1971.

107. NUCLEAR MAGNETICAL RELAXATION IN POLYTETRAFLUOROETHYLENE
D. W. MCCALL, D.C. DOUGLAS AND D. R. FALCONE
J.PHYS. CHEM. 71, 4 998-1006, 1967.

108. SOLID STATE NMR INVESTIGATION OF CATIONIC POLYMERIZED EPOXY RESINS, N. EGGER, K. SCHMIDT-ROHR .
J. APP. POLY. SCI. 44. 289-295. 1992

Fluoropolymers

Fluoropolymers: Synthesis & Properties

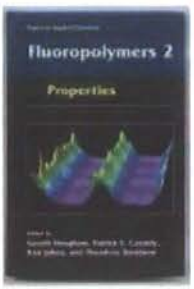

By Gareth Hougham

Plenum Publishing Corporation

1 June 1999

ISBN: 0306460610

Synopsis

Fluoropolymers: Synthesis brings together in one place the chemistry, physics, simulation and applications of fluoropolymers. Internationally known authors from industry, academia and national laboratories address many aspects of fluoropolymers from fundamental scientific principles to engineering applications. Fluoropolymers: Synthesis provides updated information on fluoropolymers to working professionals, academic scholars and graduate students. This will be an essential reference for anyone interested in fluoropolymers or advanced polymer materials in general.

Fluoropolymers - Technology, Markets and Trends (Volume 1)

By J Scheirs

ChemTec Publishing Inc

ISBN 1-85957-273-1

Publication date: 2001

Description of the properties, attributes and limitations of the major fluoropolymer resins. Discussion of the many different types of end-use markets for fluoropolymers. Analysis and estimation of the fluoropolymer industry production figures and trends. Identification and profiles of the major suppliers of fluoropolymers.

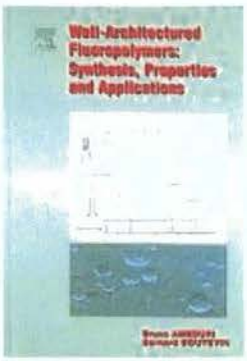

by Bruno Ameduri

Elsevier Science Pub Co

August 2004

ISBN: 0080443885

Because of the increasing need for ever better performing materials endowed with specific properties, macromolecular engineering has become a useful tool for designing well-architectured polymers (telomers, telechelics, stars, dendrimers, alternating, block- and graftcopolymers). These polymers are nowadays seeing an enormous growth. Among them, fluoropolymers are seen as high value added materials in many applications ranging from surfactants, optical fibers, biomaterials, coatings, to membranes for fuel cells. Indeed, the relationship between structure of the monomer to the properties of the polymers is of increasing interest so that these properties are tuned for the most appropriate applications. As most fluoropolymers are prepared from radical synthesis, this book devotes various parts on the use of the controlled radical (or pseudo-living) polymerisation of fluoromonomers leading to discoveries of thermoplastic elastomers or original surfactants for polymerisation in supercritical CO2.

Well-Architectured Fluoropolymers: Synthesis, Properties and Applications, is composed of five chapters starting with a general introduction outlining basic concepts. Emphasis is placed on recent developments, and each chapter describes comprehensive techniques of synthesis of well-defined fluorotelomers or polymers, their properties, characterizations, and their applications, for immediate use by today's engineers, industrial and academic scientists, and researchers.

The book has been arranged to enable self-managed reading and learning. It is both a source of data and a reference.

On the synthesis, properties and applications of fluoropolymers: remarkable, high value added materialsapplied in surfactants, optical fibres, biomaterials, coatings and membranes for fuel cells.

High-resolution NMR Techniques in Organic Chemistry (Tetrahedron Organic Chemistry S.)

Timothy Claridge

Pergamon

December 24, 1999

ISBN: 0080427987

Synopsis

From the initial observation of proton magnetic resonance in water and in paraffin, the discipline of nuclear magnetic resonance has seen unparalleled growth as an analytical method. Modern NMR spectroscopy is a highly developed, yet still evolving, subject which has applications in chemistry, biology, medicine, materials science and geology. In this text, emphasis is on the more recently developed methods of solution-state NMR applicable to chemical research, which are chosen for their wide applicability and robustness. These have, in many cases, already become established techniques in NMR laboratories, in both academic and industrial establishments. A considerable amount of information and guidance is given on the implementation and execution of the techniques described in this book.

Experimental pulse NMR: A nuts and bolts approach

Eiichi Fukushima

Addison-Wesley Publishing Co

1981

ISBN: B0000EGICW

High Resolution NMR Spectroscopy of Synthetic Polymers in Bulk (Methods in Stereochemical Analysis, Vol 7)

R. A Komoroski

Publisher: Wiley-Vch Pub

August 1, 1986

ISBN: 0895731460

Synopsis

Intended primarily for polymer scientists concerned with the structure and morphology of solid polymers, this collection of ten articles offers a comprehensive treatment of the various methods for high-resolution NMR studies of bulk polymers. The book emphasizes the fundamental aspects for both totally amorphous and semicrystalline polymers and 13C NMR studies both above and below Tg. It also treats some analytical applications at various points. This work should be valuable to NMR spectroscopists and others desiring an overview of this important field or a guidepost to future research.

Nuclear Magnetic Resonance and Relaxation

Brian Cowan

Cambridge University Press

Hardcover - April 17, 1997

Cambridge University Press

ISBN: 0521303931

Synopsis

This book provides an introduction to the general principles of nuclear magnetic resonance and relaxation, concentrating on simple models and their application. The concepts of relaxation and the time domain are particularly emphasized. Some relatively advanced topics are treated, but the approach is graduated and all points of potential difficulty are carefully explained. An introductory classical discussion of relaxation is followed by a quantum-mechanical treatment. Only when the principles of relaxation are firmly established is the density operator approach

introduced; and then its power becomes apparent. A selection of case studies is considered in depth, providing applications of the ideas developed in the text. There are a number of appendices, including one on random functions. This treatment of one of the most important experimental techniques in modern science will be of great value to final-year undergraduates, graduate students and researchers using nuclear magnetic resonance, particularly physicists, and especially those involved in the study of condensed matter physics.

Spin Dynamics: Basics of Nuclear Magnetic Resonance

Malcolm H. Levitt

John Wiley and Sons Ltd

September 26, 2001

ISBN: 0471489212

Nuclear Magnetic Resonance

R K Harris

Pitman

April 1983

ISBN: 0273016849

Nuclear Magnetic Resonance (Oxford Chemistry Primers)

P.J. Hore

Oxford University Press

1995

ISBN: 0198556829

Synopsis

Nuclear magnetic resonance spectroscopy is an enormously powerful and versatile physical method for investigating the structure and dynamics of molecules. This book provides a clear, concise introduction to the physical principles of NMR, and the interactions that determine the appearance of NMR spectra. The text describes and explains how nuclear spins interact with a magnetic field (the chemical shift) and with each other (spin-spin coupling); how NMR spectra are affected by chemical equilibria (exchange) and molecular motion (relaxation); and concludes with an outline of the workings of the workings of some simple one- and two-dimensional Fourier transform NMR experiments. The ways in which NMR may be used to study the structures, motions and reactions of molecules are illustrated and discussed. Only essential mathematics and theory are presented. The emphasis throughout is on understanding the basic principles.

Differential Scanning Calorimetry, Dynamic Mechanical and Dielectric spectroscopy.

Anelastic and Dielectric Effects in Polymeric Solids

N.G. McCrum

Dover Publications

November 1991

ISBN: 0486667529

Differential Scanning Calorimetry of Polymers: Physics, Chemistry, Analysis, Technology (Ellis Horwood Series in Polymer Science & Technology)

Vladimir A. Bershtein, et al

Ellis Horwood

February 1994

ISBN: 0132182157

Synopsis

Differential scanning calorimetry (DSC) has played a vital role in materials research, development, manufacturing and processing - especially of polymers - over the last 10 years. This book is the first to provide an in-depth assessment of the applications of DSC in polymer science; technology and analysis, examining the most significant studies that have taken place in this area. The authors show how DSC can be applied to various fields of polymer science where other methods have been unsuccessful. They discuss the ways in which DSC facilitates quantitative studies of the thermodynamic parameters and kinetics of melting, crystallization, liquid-crystallization, different phase and relaxational transition; structural relaxation, estimation of heat capacity, heat conductivity and degree of crystallinity; and also examines the influence of deformation and irradiation on the structure and internal energy of polymers, permits to study the kinetics of their synthesis, and the transformation and degradation of polymers. The book opens up new possibilities for the prediction of relaxation transition parameters as well as the properties and processes in polymers controlled by segmental dynamics.